SERVICE FATIGUE LOADS MONITORING, SIMULATION, AND ANALYSIS

Abelkis/Potter, *editors*

ASTM STP 671

AMERICAN SOCIETY FOR TESTING AND MATERIALS

SERVICE FATIGUE LOADS MONITORING, SIMULATION, AND ANALYSIS

A symposium
sponsored by ASTM
Committee E-9
on Fatigue
AMERICAN SOCIETY FOR
TESTING AND MATERIALS
Atlanta, Ga., 14–15 Nov. 1977

ASTM SPECIAL TECHNICAL PUBLICATION 671
P. R. Abelkis, Douglas Aircraft Company, and
J. M. Potter, Air Force Flight Dynamics
Laboratory, editors

List price $29.50
04-671000-30

AMERICAN SOCIETY FOR TESTING AND MATERIALS
1916 Race Street, Philadelphia, Pa. 19103

Library of Congress Catalog Card Number: 78-74559

NOTE

The Society is not responsible, as a body,
for the statements and opinions
advanced in this publication.

Printed in Baltimore, Md.
April 1979

Foreword

The symposium on Service Fatigue Loads Monitoring, Simulation, and Analysis was presented in Atlanta, Ga., 14-15 Nov. 1977. The symposium was sponsored by the American Society for Testing and Materials, through its Committee E-9 on Fatigue, in cooperation with American Society of Mechanical Engineers, Society of Automotive Engineers, and American Society of Civil Engineers. The symposium was organized by a committee consisting of: P. R. Abelkis, Douglas Aircraft Company, McDonnell Douglas Corp., and J. M. Potter, Air Force Flight Dynamics Laboratory, cochairmen; H. Jaeckel, Ford Motor Company, SAE representative; W. Milestone, University of Wisconsin, ASME representative; B. Hillbery, Purdue University, ASCE representative; and J. Ekvall, Lockheed-California Company; H. Fuchs, Stanford University; D. Bryan, Boeing Company, Wichita.

The symposium introductory paper "Random Load Analysis As Link Between Operational Load Measurement and Fatigue Life Assessment," was given by O. Buxbaum, Laboratorium für Betriebsfestigkeit, West Germany. This presentation was honored by the ASTM Committee E-9 as the best 1977 paper in E-9 sponsored activities.

Related ASTM Publications

Corrosion Fatigue Technology, STP 642 (1978), $32.00, 04-642000-27

Use of Computers in the Fatigue Laboratory, STP 613 (1976), $20.00, 04-613000-30

Fatigue Crack Growth Under Spectrum Loads, STP 595 (1976), $34.50, 04-595000-30

Manual of Statistical Planning and Analysis for Fatigue Experiments, STP 588 (1975), $15.00, 04-588000-30

A Note of Appreciation to Reviewers

This publication is made possible by the authors and, also, the unheralded efforts of the reviewers. This body of technical experts whose dedication, sacrifice of time and effort, and collective wisdom in reviewing the papers must be acknowledged. The quality level of ASTM publications is a direct function of their respected opinions. On behalf of ASTM we acknowledge with appreciation their contribution.

ASTM Committee on Publications

Editorial Staff

Jane B. Wheeler, *Managing Editor*
Helen M. Hoersch, *Associate Editor*
Ellen J. McGlinchey, *Senior Assistant Editor*
Helen Mahy, *Assistant Editor*

Contents

Introduction 1

SERVICE LOADS MONITORING AND ANALYSIS

Random Load Analysis as a Link Between Operational Stress Measurement and Fatigue Life Assessment—OTTO BUXBAUM 5
State of the Art in Aircraft Loads Monitoring—L. E. CLAY, A. P. BERENS, AND R. J. DOMINIC 21
Determination of Sample Size in Flight Loads Programs—A. P. BERENS 36
Use of AIDS Recorded Data for Assessing Service Load Experience—J. B. DE JONGE AND D. J. SPIEKHOUT 48
Overview of the C-5A Service Loads Recording Program—W. J. STONE, A. M. STANLEY, M. J. TYSON, AND W. H. KIMBERLY 67
Highlights of the C-141 Service Life Monitoring Program—D. S. MORCOCK 84
Evaluation of a Crack-Growth Gage for Monitoring Possible Structural Fatigue-Crack Growth—N. E. ASHBAUGH AND A. F. GRANDT, JR. 94

SERVICE SPECTRUM GENERATION AND SIMULATION

Development of a Fatigue Lifetime-Load Spectrum for a Large-Scale Aluminum Ship Model—J. T. BIRMINGHAM, N. V. MARCHICA, F. F. BORRIELLO, AND J. E. BEACH 121
Flight Spectra Development for Fighter Aircraft—N. H. SANDLIN, R. R. LAURIDIA, AND D. J. WHITE 144
Flight-by-Flight Spectrum Development—A. G. DENYER 158
Methods of Gust Spectra Prediction for Fatigue Damage—W. W. WILSON AND J. E. GARRETT 176
Derivation of Flight-by-Flight Spectra for Fighter Aircraft—M. P. KAPLAN, J. A. REIMAN, AND M. A. LANDY 193
Simulation and Monitoring of Loads in Crane Beams—M. P. WEISS 208
Long Life Random Fatigue Behavior of Notched Specimens in Service, in Service Duplication Tests, and in Program Tests—ERNST GASSNER AND WILHELM LIPP 222
Test Simulation of Fighter Aircraft Maneuver Load Spectra—L. L. JEANS AND W. L. TRIBBLE 240
Simulation of Service Fatigue Loads for Short-Span Highway Bridges—PEDRO ALBRECHT AND KENTARO YAMADA 255

Summary 281
Index 285

Introduction

Increasing emphasis on fatigue and fracture control and higher structural reliability in structural design requires, more than ever before, a more precise analytical definition and testing simulation of the fatigue cyclic loading environment. The need for clear understanding and definition of the fatigue loading environment has been emphasized strongly in recent years by developments that clarify the role of fatigue load sequences and interaction in the fatigue failure process. This symposium provided a forum for the exchange of ideas and the presentation of the state-of-the-art papers on fatigue service loads collection and monitoring, data reduction and analysis, and simulation of these loadings for durability, damage tolerance, and residual strength analysis and testing.

The symposium also brought the loads and the fracture mechanics engineers, scientists, and academicians together to better understand each other's work, and how each other's work interacts. Thus, this publication is highly recommended not only to the loads people, but also to the fracture mechanics group in order to fulfill one of the symposium's objectives.

For many years, fatigue loads collection and monitoring has been emphasized strongly in the aircraft world. A major portion of the papers in this publication is from this field. However, in the symposium, an attempt was made to have papers from other fields, for the purpose of exchanging ideas between different fields. This attempt was partly successful. This publication also provides papers of general nature as well as papers dealing with bridges, ships, crane beams, and ground transportation. Many of the ideas and methods developed for aircraft can be applied in other fields.

The seventeen papers contained in this publication represent some of the latest ideas and programs in recording and analyzing service fatigue loads data, monitoring of the loading environment indirectly through crack growth gages and other damage monitoring systems, and the development and implementation of these loading environments in durability and crack growth analyses and testing.

Sincere appreciation is extended to the authors, symposium organizing committee, the reviewers, and Jane B. Wheeler and her ASTM staff for their various contributions in making this publication possible.

P. R. Abelkis

McDonnell Douglas Corp., Douglas Aircraft Co., Long Beach, Calif. 90846; symposium cochairman and coeditor.

J. M. Potter

AFFDL/FBE. Wright-Patterson AFB, Ohio 45433; symposium cochairman and coeditor.

Service Loads Monitoring and Analysis

Otto Buxbaum [1]

Random Load Analysis as a Link Between Operational Stress Measurement and Fatigue Life Assessment

REFERENCE: Buxbaum, Otto, **"Random Load Analysis as a Link Between Operational Stress Measurement and Fatigue Life Assessment,"** *Service Fatigue Loads Monitoring, Simulation, and Analysis, ASTM STP 671,* P. R. Abelkis and J. M. Potter, Eds., American Society for Testing and Materials, 1979, pp. 5-20.

ABSTRACT: All relevant methods for the description of measured stress-time histories in connection with fatigue life assessment are reviewed critically, that is, one- and two-parameter counting methods as well as analyses in the time and frequency domains.

KEY WORDS: counting, random load analysis, power spectra, load spectra, cumulative distributions, fatigue life, fatigue tests

Throughout their service life, machines, equipment, vehicles, and buildings are subjected to loads, the majority of which vary with time. In order to design structures without unnecessary expenditure of material and effort, the operational loads have to be defined, the allowable stresses of the materials have to be investigated, and the ability of the materials to resist the local stress and strain histories at critical points of the structure must be determined.

It follows that structural design criteria are satisfied completely only if, in addition to the information about accurate allowable stresses, the loading environment is defined. The present paper reviews the relevant methods currently in use that describe the loading environment, discusses problems arising from their application using examples from different fields, and shows some guidelines for further research.

[1] Executive director, Laboratorium für Betriebsfestigkeit (LBF), D-6100 Darmstadt, Federal Republic of Germany.

Nature of Stress-Time Histories

According to Newton's first law all bodies, including structures, continue in a state of rest or in uniform motion in a straight line, unless acted upon by an external force. However, the state of rest or of uniform motion is disturbed by loads resulting from one of two sources:

Loads that act upon a structure may originate from the environment, for example, from gusts of wind, sea waves, noise, or road roughness. Loads also may result from the usage of a structure, for example, from the hoisting or lowering of a weight by means of a crane, loading or unloading a container, or steering or accelerating a vehicle. The distinction between these two sources will prove later to be of importance also in the analysis.[2]

As all structures represent more or less complicated elastic systems, time-varying operational loads can excite their natural modes. Therefore, the response, which is in the form of a stress-time history at a point of the structure, that is, far enough away from the point of load introduction, may show differences with regard to amplitudes as well as to frequencies compared with the corresponding load-time history. This means that a stress-time history contains both, the effects of external loadings and the response of the structure to these loadings. These factors should always be kept in mind during analysis, because in general it is not possible to observe the external loads directly; only their reactions at certain points of the structure can be measured.

For simplification a time varying response function as measured at a point of a structure is defined as a stress-time history, whether it be stress, strain, or any other derived quantity like a moment or shear force.

Most stress-time histories that are measured under operational conditions vary at random and are called stochastic (see the examples in Fig. 1). The record of a stochastic signal of any length of time is unique, that is, it is not reproducible in the same way. Therefore, the explicit mathematical relation with which the magnitude of a deterministic (for example, periodic) signal can be predicted with certainty, has to be replaced in the case of stochastic data by statistical functions which only allow the derivation of a probability for the occurrence of a defined magnitude.

Necessity and Aims of an Analysis of Stress-Time Histories

A measured random stress-time history is unique and contains the effects of both external loads and the dynamic response of the structure. This means that the history is not only affected by the structural system but also by the

[2] Besides loadings due to environment and usage a third type of load may occur. These are so-called "rare events" which exceed the normal service loads with respect to their magnitude. Therefore, they must be treated separately, and taken into account primarily to avoid plastic deformation or static fracture rather than fatigue failure. Examples of rare events are severe maneuvering in case of emergency or driving over pot holes of exceptionally large depth.

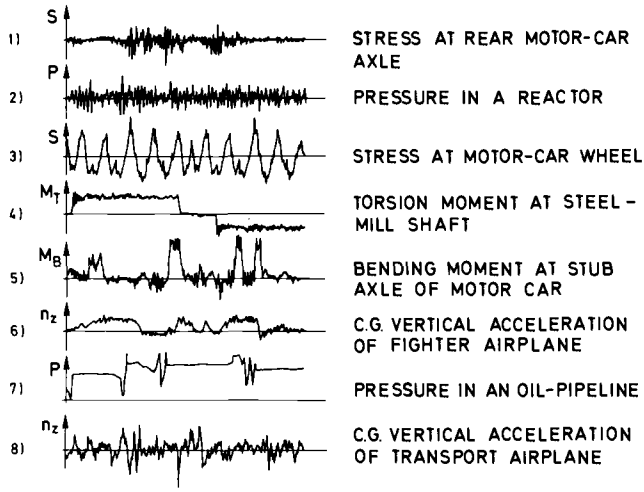

FIG. 1—*Examples of stress-time histories.*

location where the history has been observed. Therefore, it is, impossible to derive criteria for fatigue design from such a measurement without proper analysis. Analyses should be conducted also in connection with fatigue substantiation tests, if testing load sequences are shortened for reason of economy under comparable and defined conditions. However, there are additional reasons for performing analysis that are equally important.

The result of measurements usually must be extrapolated, since field measurements are limited in most cases for technical and economic reasons, whereas the structure must be designed for the required total service life. Therefore, it is important that the field measurements contain all possible loading cases, preferably in the same time proportion as the expected service life. Furthermore, it is desirable that the results of the measurements allow a theoretical fatigue life estimation (by means of an appropriate method) in order to compare different stress-time histories with regard to their relative rate of fatigue damage. The determination of both an economical test sequence and a realistic fatigue life estimation can only be achieved subsequent to an analysis.

Based on the measured stress-time histories, additional information—including information about the external loads—must be derived to be used in the design of other similar structures. An analysis also would be advantageous in separating the stresses resulting from external loads from those resulting from the dynamic response of the structure.

Interconnection of Load Analysis and Fatigue Life Prediction

By definition, an analysis, is always a reduction of the data and, in the case of a stochastic phenomenon, it is the process of extracting statistical func-

tions or values from the data. If analysis is perfect, the complete history can be regenerated statistically from the extracted parameters. However, as will be shown later, information about the original time history is lost with many of the procedures used today. This lost information may influence the fatigue life prediction, which is based upon the result of analysis. Therefore, the selection of the most appropriate method of analysis is essentially a problem of fatigue strength rather than a problem of statistics. This choice cannot be based on fully rational arguments because of our incomplete knowledge of the fatigue process. Consequently, the validity of an analysis method cannot be judged by itself. It must be combined with a subsequent theoretical or experimental method of fatigue life prediction by comparing the life under the original history with that obtained after an analysis and a fatigue test or damage calculation.

The preceding statements refer in principle to all methods aimed at an absolute fatigue life prediction for a component or a complete structure. If the methods of experimental fatigue life assessment are broadly classified according to their purpose (see Fig. 2 (taken from [*1*][3]), we find four categories: (*a*) basic research tests for studying materials behavior, (*b*) control tests for supervising the series-production quality (*c*) development tests for improving the fatigue strength of structural details, and (*d*) proof, substantiation or verification, tests.

Statement *d* yields absolute answers, whereas the others give only relative answers. It should be mentioned here that the counterpart of the relative fatigue tests is the use of a damage accumulation hypothesis for obtaining relative lives [*2,3*].

The three branches—random load analysis, materials fatigue, and fatigue testing technology—have affected each other during their historical development. When the block program test was created by Gassner between 1936 and 1940, it was based, of course, on concepts and knowledge about fatigue damage of the time, which assumed that damage was caused mainly by "cycles" or "ranges" that could be deduced from a stress-history by means of a one-parameter counting method. Likewise, the limitations of existing testing equipment at the time led to the block program tests which are in fact an *S-N* test with varying amplitudes. However, more recent experience has shown that individual stress variations are not the only fatigue criterion and that the sequence of stresses is also of fundamental importance in fatigue life. Although procedures for analysis were already available in the form of two-parameter counting methods and later in the form of characteristic functions obtained in the frequency domain, the proof that the sequence effect must be included could not be determined on a wide basis before servohydraulic testing equipment was available.

[3]The italic numbers in brackets refer to the list of references appended to this paper.

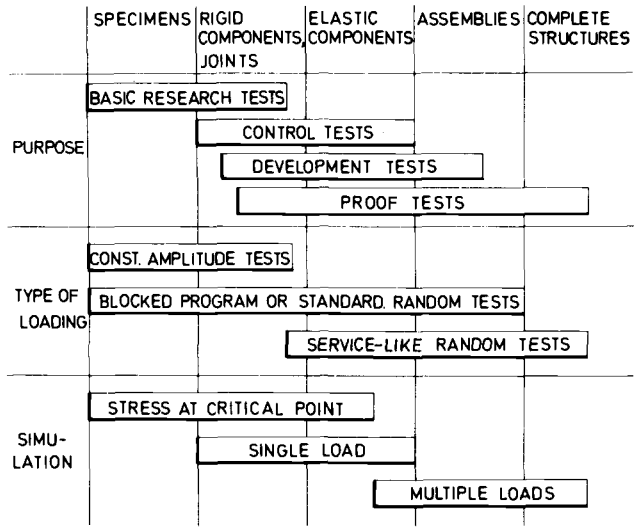

FIG. 2—*A classification of fatigue tests.*

Today, servohydraulic testing equipment in combination with computer techniques is more advanced than our capability in the fields of damage accumulation and load analysis.

One-Parameter Counting Methods

The oldest and simplest method to analyze a random stress-time history is to count how often a defined event has occurred, for example, a peak, a range (as the difference between a subsequent minimum and maximum or vice versa), or a crossing of a given level. It would be beyond the scope of this paper to list all counting methods in detail. This has been done adequately by Schijve [*4*].

It is sufficient for an evaluation of counting methods to keep some of their general features in mind.

It is typical for most one-parameter counting methods (methods which consider only one kind of event) that almost all information about the sequence of individual stress variations is lost during counting because the events are only classified according to magnitude and number of occurrences. This means that the counting result, which is usually presented as a cumulative frequency distribution (see Fig. 3), shows only how often (H_i) maximum and minimum stresses $S_{max,\,i}$ and $S_{min,\,i}$, respectively, have been reached or exceeded. Similar to the result obtained from the analysis of a sinusoidal stress-time history which gives a rectangular distribution (see Fig. 3), the cumulative frequency distribution obtained from a stress-time history can be regarded only as the envelope of maxima and minima of stress varia-

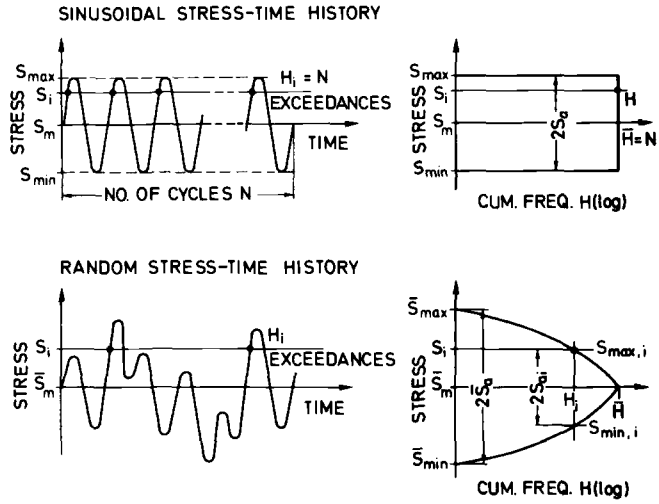

FIG. 3—*Stress-time history and cumulative frequency distribution (schematically).*

tions of a given shape, usually of sine waves. This assumes a damage hypothesis which postulates that the same fatigue life is obtained under the original and the amplitude modulated stress-time history as derived from the counting result, or that at least a constant life ratio is obtained from the two histories. It is evident that this is hardly true for all possible combinations of materials, stress concentrations, stress ratios, surface treatments, etc.

These difficulties increase as we begin to include the sequence of the derived "cycles" or "half cycles." In addition, it must be remembered that, depending on the type of stress-time history, different counting methods will lead to different results (see the example of two stress-time histories as measured on a motor car in Fig. 4). The corresponding power spectra are shown in Fig. 5. The cumulative frequency distributions which were obtained by counting peaks, level crossings, range pairs, and peaks between mean crossings are plotted for matters of comparison in amplitude form in Fig. 6. There is no significant difference in results for the vertical loads (Case A). While for the bending moment due to lateral loads (Case B) the range-pair and peak-between-mean countings are almost equal, the level crossing counting is about one and that for peak counting about two orders of magnitude greater than the other two results except for the region of the highest and smallest amplitudes. Note that the irregularity factor as derived either by calculation from the power spectrum [5] or by counting, which represents the number of crossings of the mean value related to the number of peaks, does not seem to be suited for the choice of an appropriate counting method because the difference between the two values of 0.29 and 0.14, see Fig. 5, is meaningless in this context. This corresponds with test results ob-

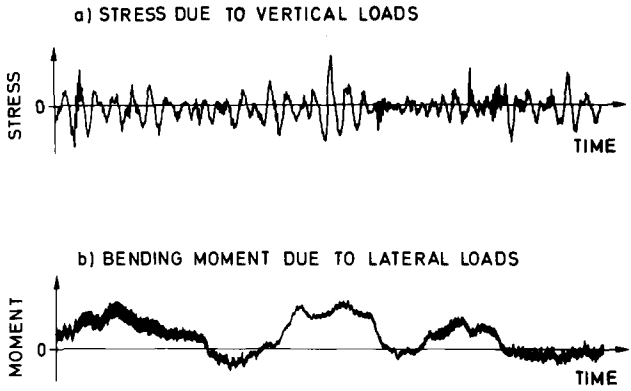

FIG. 4—*Examples of stress-time histories measured at a motor car.*

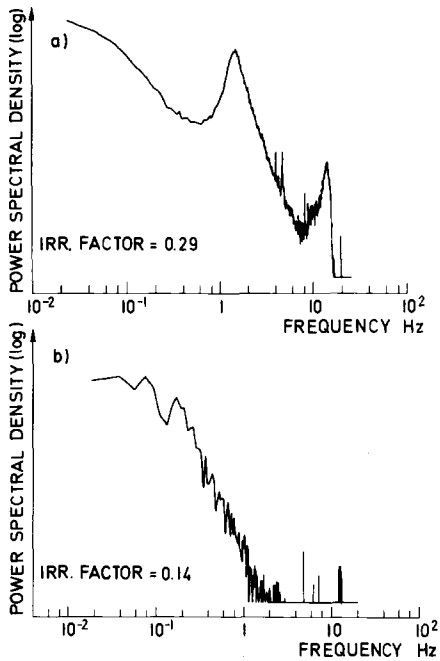

FIG. 5—*Power spectra of stress-time histories as shown in Fig. 4.*

tained under Gaussian load sequences [*6*]. We must conclude that the choice of counting method should be based only on the experience with fatigue test results.

The use of thresholds during counting for reasons other than filtering the stress-time history from noise or for intentionally shortening the history will usually give misleading results and thus should be avoided [*7,8*].

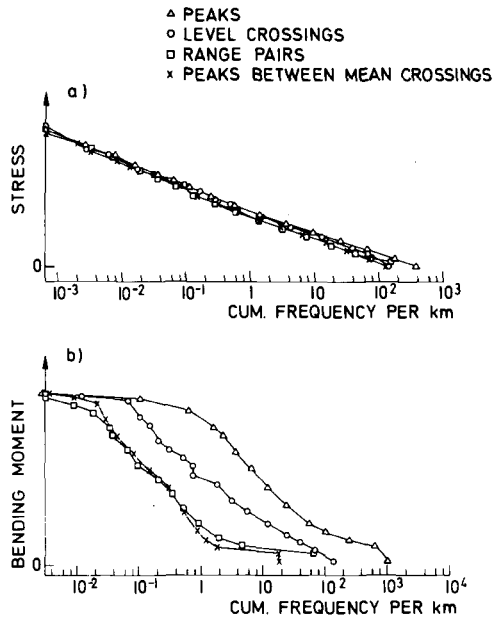

FIG. 6—*Cumulative frequency distributions for stress-time histories as shown in Fig. 4 obtained from four different counting methods (plotted for matters of comparison in the form of amplitudes).*

After sketching the major problems with one-parameter counting methods for fatigue life assessment, some advantageous features shall be mentioned:

First, the cumulative frequency distributions can be extrapolated easily and reliably by means of extreme value distributions [*9,10*], and the probability with which the extrapolated values will be equalled or exceeded also can be found this way.

Secondly, cumulative frequency distributions can be approximated in many cases by standardized distribution functions (see Fig. 7). The introduction of standardized distributions facilitates the establishment of allowable stresses for design and opens the possibility for transfer and interpretation of fatigue test results. Only under the assumption that the system behavior is similar can information about external loads be derived from cumulative frequency distributions of stresses.

Two-Parameter Counting Methods

As mentioned earlier, the sequence of the individual load variations affects the fatigue life significantly. Many years before definitions like material's memory and local elastoplastic behavior became part of our understanding of damage, aircraft engineers realized that the fatigue life of a wing can only be predicted reliably if the actual loading sequence (the so called ground-air-

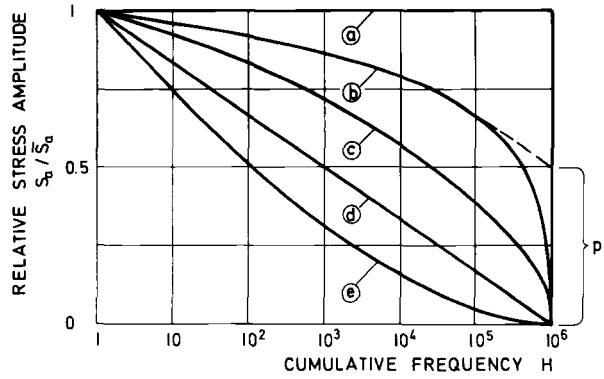

Possible mathematical description:

$$H(S_a) = \mathrm{H}(S_a = 0) \exp\left[-\frac{S_a}{2s}\right]^n$$

a) n: constant amplitude.
b) n 2: approximated as normal distribution with constant part $p = S_{\text{constant}}/S_a$.
c) $n = 2$: Gaussian random process, formerly approximated by a Gaussian normal distribution.
d) $n = 1$: so-called straight-line distribution (Pascal distribution).
e) n 1: formerly approximated by a logarithmic normal distribution.

FIG. 7—*Standardized cumulative frequency distributions.*

ground cycle) is either applied in test or is taken into account specifically in the damage calculations.

The desire for a method of analysis that includes sequence effects is very old. In 1942 Gassner proposed a two-parameter counting method, the peak-trough or range-mean counting [*11*], where the peaks and their subsequent troughs are counted simultaneously, so that the counting result can be presented in the form of a matrix (see Fig. 8). However, nothing is gained unless the joint probability of troughs and peaks is known. Therefore, the two-parameter counting was not used by Gassner. Nevertheless, two-parameter counting methods have become important lately for the generation of standardized load sequences with stationary properties which have been proposed to replace the standardized block program test [*12*].

In addition, two-parameter counting methods were considered recently for damage calculation in combination with damage hypotheses, taking into account the cyclic deformation in the highest stressed volume element of the respective component. The first method, called the rain-flow cycle counting method, was proposed for that purpose in Japan and was reported by Dowling [*13*]. Independently in 1972 Van Dijk published a method called range-pair-range counting [*14*]. Both methods are identical and are called here range-pair-mean counting method (see Fig. 9), because the mean value is identified with each range-pair (consisting of an ascending range and a

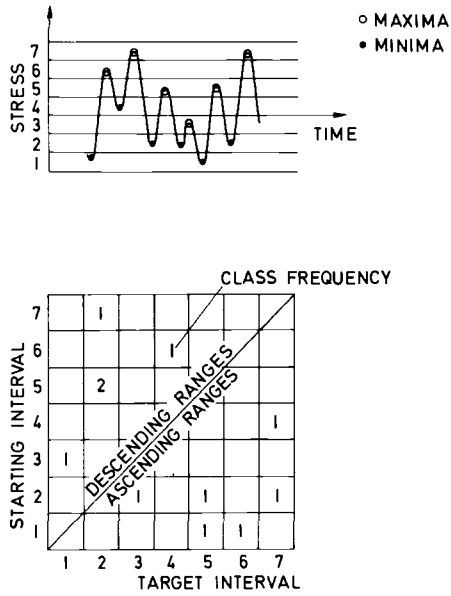

FIG. 8—*Counting of subsequent peaks and troughs.*

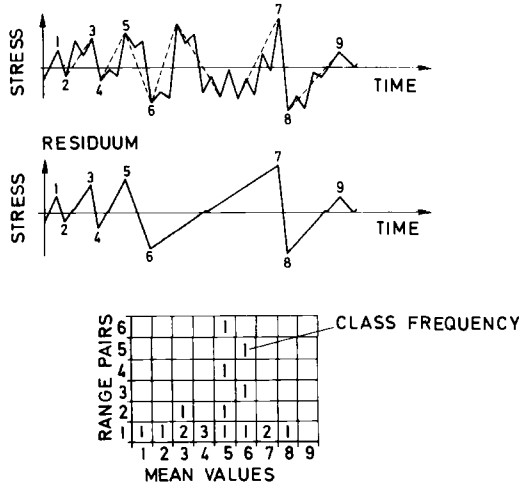

FIG. 9—*Range-pair-mean counting.*

descending range of equal magnitude). Consequently, if the mean values are eliminated, the range-pair counting result is obtained [*15*].

It is not yet clear whether the use of fatigue life calculation methods based on local stress-strain behavior will lead to a general improvement [*16*] in predictions. The general application of two-parameter counting methods as one of its tools is still questionable. Moreover, two-parameter counting

results cannot be extrapolated without further elaborations nor can they be standardized easily.

Some investigators, who apply two-parameter methods for the analysis of measured stress-time histories, derive therefore one-parameter counting results from them for use in fatigue life evaluations. By this procedure, however, no information exceeding that from a one-parameter analysis is being gained.

Analysis in the Time and Frequency Domains

Up to the present time a cumulative frequency distribution was required if a fatigue life calculation was to be performed. For one-parameter counting methods information about sequences and frequencies was lost. Therefore, it seems to be appropriate to check whether the harmonic or time-series analysis may complete the description of a cumulative frequency distribution.

The most common statistical function recommended during the last two decades is the power spectral density. Its mathematical background and especially the theoretical boundary conditions related to its usage are explained in the literature [*17,18*]. An analog scheme illustrated in Fig. 10 demonstrates the physical meaning. Two major items have to be considered. First, the power spectral density is obtained from a continuous time-averaging integration (omission of the band-pass filter in the scheme as shown in Fig. 10 would result in the squared root mean square (RMS) value). Second, only the modulus is obtained, that is, the amplitudes are kept whereas the phase information is lost.

The power spectral presentation of a stress-time history has been receiving more consideration because of the very important results obtained by Rice [5]

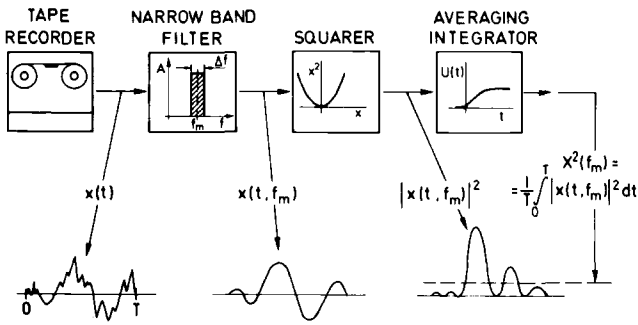

FIG. 10—*Analog scheme for calculating power spectral density from measured stress-time history.*

who has found that for a special type of process, the so-called stationary Gaussian process, the number of crossings of a level x can be calculated from the power spectrum $G(\omega)$ as follows

$$H(x) = H(o) \exp\left[-\frac{x^2}{2\sigma^2} \right]$$

where the number of crossings of the linear mean value ($x = 0$) is given by

$$H(o) = \frac{1}{2\pi} \sqrt{\frac{\int_{-0}^{\infty} G(\omega)\omega^2 \, d\omega}{\int_0^{\infty} G(\omega) \, d\omega}}$$

and

$$\sigma^2 = \frac{1}{2\pi}\int_{-\infty}^{\infty} G(\omega) \, d\omega = \lim_{T-\infty} \frac{1}{2T}\int_{-T}^{T} x^2(t)dt$$

The Gaussian process is stationary (that is, its statistical properties are invariant with time) and ergodic (that is, one record contains all relevant statistical information and thus so-called ensemble averages can be replaced by time averages). Besides it is important that its cumulative frequency distribution of level crossings as defined previously corresponds to that of Fig. 7, Case C. In the field of aeronautics, where Rice's relations were first applied to acceleration-time histories resulting from gust loading, it was observed that the relevant cumulative frequency distributions usually correspond to those of Cases D and E in Fig. 7. Press and his co-workers have proposed the so called quasistationary process as an engineering solution, assuming that the second moment (RMS value) of a Gaussian process varies with time [*19*]. Thus one obtains

$$H(x) = \sum_{i=1}^{n} H(o)_i \exp\left[-\frac{x^2}{2\sigma_i^2} \right]$$

or in infinitesimal form

$$H(x) = H(o) \int_0^{\infty} \exp\left[-\frac{x^2}{2\sigma^2} \right] \cdot f(\sigma) d\sigma$$

where $f(\sigma)$ is the density function of the RMS value σ. Details to be con-

sidered for the application of these relations are reported in Ref *7* and an example for such an analysis is given in Ref *20*. It should be mentioned that for an experimental realisation of $f(\sigma)$ the chosen integration time has a significant effect on the result [*7*].

By means of the model of Press a series of stress-time histories can be described with satisfactory accuracy as necessary for fatigue life evaluation. Stress-time histories can be generated by means of random generators and filters or corresponding digital computer techniques which have the same statistical properties as the original ones. Experience has shown that these stress-time histories are due to the environment, for example, by gusts, sea waves, road roughnesses, etc. Also, if the transfer function of the respective system is linear, the relations between local response and external loads can be derived.

The main reason why this model works is that the stresses resulting from environmental effects usually correspond to random vibrations and can be treated as continuous processes, for which the power spectral presentation seems to be suited (see Fig. 11). The opposite to this represents stresses due to the usage of a structure, for example, due to maneuvers of a vehicle, discontinuous processes for which the time averaging becomes questionable. The difference between a continuous and a discontinuous process may be explained as follows: in the first case, fluctuations of variable magnitude occur continuously about a constant (linear) mean value and the mean value is either crossed or being touched by the signal within very short periods of time. In the second case, the signal returns after one or several deviations from its resting value and may stay there for any period of time until the next deviation occurs.

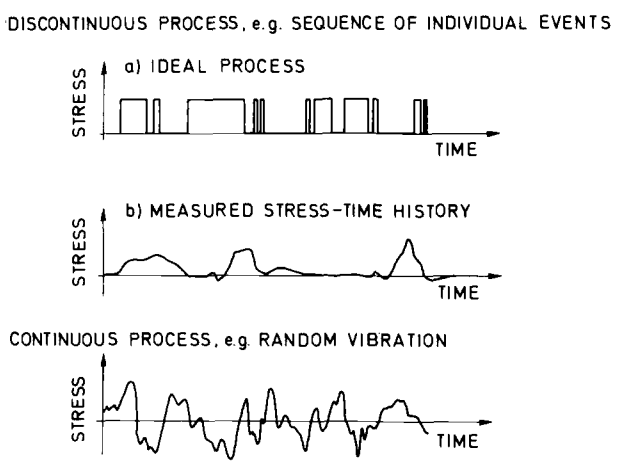

FIG. 11—*Stochastic processes.*

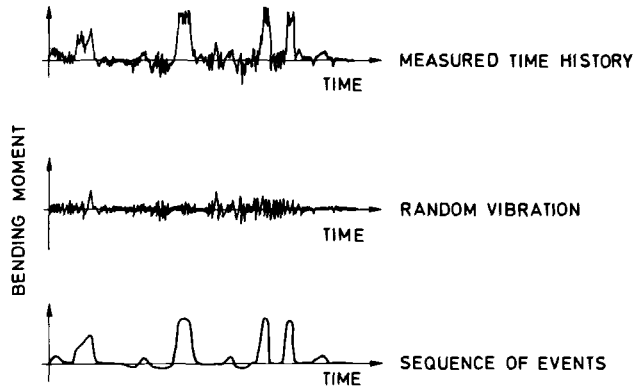

FIG. 12—*Separation of measured axle-spindle bending-moment history into two typical stochastic processes.*

Engineering models that describe discontinuous processes need to be developed. One proposal will be published shortly [*21*]. With this model it will be possible to analyze stress-time histories of discontinuous processes in such a way that not only their cummulative frequency distribution but also the sequence of occurrences will be determined, as well as all statistical properties which may be relevant for fatigue so that the original signal can be regenerated statistically. However, for analysis purposes as well as for deriving design information, it is necessary to separate the two mentioned parts if they are superimposed (see Fig. 12). In order to separate the two portions, frequency filtering in many cases is not sufficient and thus other methods must be developed [*22*]. Finally, for a synthesis of a complex stress-time history, the interactions and correlations between the individual parts must be investigated.

Conclusion

The presented survey about methods of analysis of measured stress-time histories shows the present state and outlines possible further development in this field. The goals are to generate reliable design information, and to utilize modern testing techniques for a safe and economic fatigue life assessment.

References

[*1*] Buxbaum, O. and Haibach, E., "Zur Systematik des Betriebsfestigkeitsversuchs im Fahrzeugbau (About a Classification of Fatigue Tests in Vehicle Engineering)," *Materialprüfung*, Vol. 17, No. 6, VDI-Verlag Düsseldorf, 1975, pp. 173–175 (in German).

[2] Lowak, H. and Schütz, D., "Zur Verwendung von Bemessungsunterlagen aus Versuchen mit betriebsähnlichen Lastfolgen zur Lebensdauerabschätzung (Application of Design Data Derived from Fatigue Tests with Service-Like Load Sequences for Life Prediction),"

LBF Report No. FB-109, Laboratorium für Betriebsfestigkeit, Darmstadt, 1976, (in German).

[3] Schütz, W. in *Symposium on Random Load Fatigue*, AGARD Conference; *Proceedings*, No. 118, Oct. 1972, pp. 7-1 to 7-10.

[4] Schijve, J., "The Analysis of Random Load-Time Histories with Relation to Fatigue Tests and Life Calculations," *NLR Report MP.201*, National Aircraft and Space Laboratory, Amsterdam, 1960.

[5] Rice, S. O., "Mathematical Analysis of Random Noise," *Bell Systems Technical Journal*, Vols. 23-24, 1945.

[6] Gassner, E., Lowak, H., and Schütz, D., "Bedeutung der Unregelmässigkeit Gauss'scher Zufallsfolgen für die Betriebsfestigkeit (Significance of Irregularity of Gaussian Random Sequences on Fatigue Life)," *LBF Report No. FB-124*, Laboratorium für Betriebsfestigkeit, Darmstadt, 1976, (in German).

[7] Buxbaum, O. in *Fatigue Life Prediction for Aircraft Structures and Materials, AGARD Lecture Series No. 62*, May 1973, pp. 2-1 to 2-19.

[8] Buxbaum, O. and Ladda, V., "An Experimental Study About the Effect of Thresholds on C. G. Acceleration Countings Obtained from a Military Airplane," *LBF Report No. TB-123*, Laboratorium für Betriebsfestigkeit, Darmstadt, 1975.

[9] Buxbaum, O., "Bestimmung von Bemessungslasten schwingbruchgefährdeter Bauteile aus Extremwerten von Häufigkeitsverteilungen (Determination of Maximum Loads of Fatigue Critical Components by Means of Extreme Values Taken from Measured Distributions of Exceedances)," *Konstruktion*, Vol. 20, No. 11, Springer Verlag, Berlin, 1968, pp. 425-430 (in German).

[10] Buxbaum, O., "Extreme Value Analysis and its Application to C. G. Vertical Accelerations Measured on Transport Airplanes of Type C-130," *AGARD Report No. 579*, March 1971.

[11] Gassner, E., "Ergebnisse aus Betriebsfestigkeitsversuchen mit Stahl- und Leichtmetallbauteilen (Results from Blocked Program Tests with Steel- and Aluminium-Components)," *Report No. 152*, Lilienthal-Gesellschaft für Luftfahrtforschung, Berlin, 1942, pp. 13-23 (in German).

[12] Haibach, E., Fischer, R., Schütz, W., and Hück, M. in *Fatigue Testing and Design; Proceedings*, International Conference Society of Environment Engineers, Vol. 2, London, pp. 29.1-29.21.

[13] Dowling, N. E., "Fatigue Failure Predictions for Complicated Stress-Strain Histories," *Journal of Materials*, Vol. 7, No. 1, March 1972, pp. 71-87.

[14] Van Dijk, G. M. in *Advanced Approaches to Fatigue Evaluation, NASA Special Publication 309*, 1972, pp. 565-598.

[15] Zaschel, J. M., "Zur Analyse einer im Fahrbetrieb gemessenen Schwingwegzeit-Funktion mit Hilfe von ein- und zweiparametrigen Zählverfahren (About the Analysis of a Time History Measured Under Operational Conditions by Means of One- and Two-Parametric Counting Methods)," *LBF Technical Note No. 78*, Laboratorium für Betriebsfestigkeit, Darmstadt, 1977, (in German).

[16] Schütz, D. and Gerharz, J. J. in *Problems with Fatigue in Aircraft; Proceedings*, 8th ICAF Symposium, Swiss Federal Aircraft Company (F + W), Emmen/Switzerland, 1975, pp. 3.3/1-3.3/22.

[17] Papoulis, A., *Probability, Random Variables, and Stochastic Processes*, McGraw-Hill, New York, 1965.

[18] Bendat, J. S. and Piersol, A. G., *Random Data: Analysis and Measurement Procedures*, Wiley, New York, 1971.

[19] Press, H., Meadows, M. T., and Hadlock, J., "A Reevaluation of Data on Atmospheric Turbulence and Airplane Gust Loads for Application in Spectral Calculations," *NACA Report 1272*, 1956.

[20] Buxbaum, O., "Beschreibung einer im Fahrbetrieb gemessenen Beanspruchungs-Zeit-Funktion mit Hilfe der Spektralen Leistungsdichte (Analysis of a Stress-Time History Measured Under Operational Conditions by Means of Power Spectral Density)," *LBF Report No. TB-102*, Laboratorium für Betriebsfestigkeit, Darmstadt, 1972, (in German).

[21] Zaschel, J. M., "Ein Verfahren zur Ableitung statistischer Kenngrössen für die Bemessung gegen Zufallsartige, aus Arbeitsvorgängen entstandene Beanspruchungen (A Method for Deriving Statistical Parameters for the Design Against Random Stresses

Resulting from Working Operations)," *LBF Report No. FB-135*, Laboratorium für Betriebsfestigkeit, Darmstadt, 1978, (in German).

[22] Buxbaum, O. and Zaschel, J. M., "Verfahren zur Trennung von Beanspruchungs-Zeit-Funktionen nach ihrem Ursprung (Methods for Separation of Stress-Time Histories According to Their Origin)," to be published in 1978 (in German).

L. E. Clay,[1] *A. P. Berens,*[1] *and R. J. Dominic*[1]

State of the Art in Aircraft Loads Monitoring

REFERENCE: Clay, L. E., Berens, A. P., and Dominic, R. J., **"State of the Art in Aircraft Loads Monitoring,"** *Service Fatigue Loads Monitoring, Simulation, and Analysis, ASTM STP 671,* P. R. Abelkis and J. M. Potter, Eds., American Society for Testing and Materials, 1979, pp. 21-35.

ABSTRACT: The paper summarizes current state-of-the-art equipment and techniques for the monitoring of loads during military aircraft operation. Monitoring systems are discussed which record strain, center-of-gravity motions, and control deflections, or the occurrence of selected load conditions. The raw data are reduced to sequences of stress peaks and troughs or to tabulations of peaks and coincident values of the recorded parameters. Finally, monitoring system cost estimates are provided for typical applications to individual aircraft tracking and loads and environmental spectra survey problems.

KEY WORDS: aircraft loads, aircraft structural integrity, data recording, fatigue tests

Aircraft Loads Monitoring—Why?

As the requirements for aircraft performance have increased, the conservatism in structural design has decreased to the extent that design limit loads often are reached in service. In addition, the use of high-strength materials has reduced fatigue tolerance to repeated loads below the design limit load. At the same time, there has been an increased emphasis on the reduction of aircraft costs by extending the service life and by extending inspection intervals. All of these factors make it very critical that the actual service repeated load spectra be measured and compared with the design repeated load spectra. Thus, the monitoring of in-flight aircraft loads has become a critical part of the aircraft structural integrity program.

Flight data collection programs can be considered generally in two categories: (1) flight tests, and (2) operational loads programs. Flight tests are used to verify analytically derived airload and stress distributions,

[1]Research engineer, research statistician, and research engineer, respectively, University of Dayton Research Institute, Dayton, Ohio 45469.

while operational loads programs monitor actual aircraft usage for comparison with specified intended usage and computation of expected service life.

Design Analysis Verification

The prime objective of flight loads data is to verify that the aircraft structural design analysis computed the correct values for limit loads and for the frequency and level of repeated loads.

Design limit loads are derived from the most severe of a series of specified flight conditions. During flight test, these flight conditions are flown and the measured stresses are compared with the stresses predicted from the loads and stress analyses. To minimize the cost of flight test, the flight-test recorders are designed to record several hundred channels of data so that stresses at many structural points can be measured simultaneously during the small flight test conditions.

The exceedance of the design limit load of an aircraft during its service life is a random event which occurs infrequently. Therefore, it is not practical to attempt to record this event. The probability of exceeding the design limit load is projected by extrapolating the distribution of loads recorded during a representative operational data sample to the design load levels as shown in Fig. 1. This use of loads data has diminished over the years

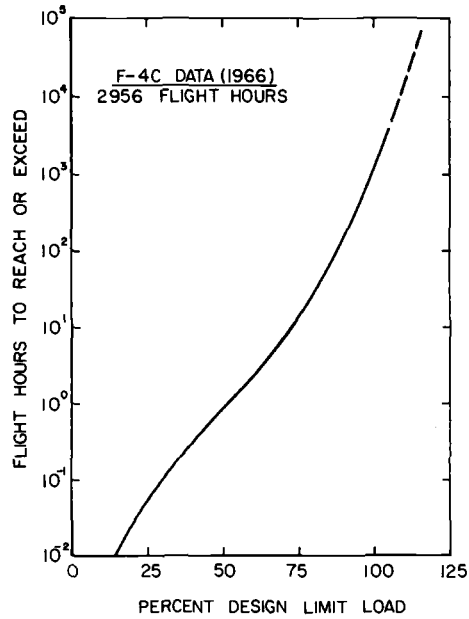

FIG. 1—*Typical curve of flight hours to exceed a given percentage of design limit load.*

because the occurrence of failures due to overload is rare compared to the occurrence of fatigue failures.

The Air Force specifies a required service life for each new aircraft design. The actual service life for a fleet of aircraft is recognized generally to be a function of the airframe's fatigue tolerance to repeated loads. Therefore, it is important that a reasonably accurate estimate of the anticipated service repeated load spectra be substantiated as quickly as possible after the aircraft enters service by recording actual service loads spectra. These spectra data are recorded during a loads/environmental spectra survey program (L/ESS). These spectra data are presented in the form shown in Fig. 2 and are combined with the durability test results to estimate actual service life. The accurate estimation of aircraft service life keys the planning for airframe modification and replacement aircraft procurement.

Structural Maintenance Resource Allocation

System life cycle costs are driven, to a large extent, by maintenance costs. Some maintenance costs are fixed well in advance by projected maintenance requirements such as major airframe inspections and overhaul. Using these projected requirements, the Air Force develops a phased inspection plan and a programmed depot maintenance (PDM) schedule for a period of several years which, in turn, determines the spares and airframe maintenance personnel resource allocations for this period. Once these resource levels are fixed, they are very difficult to adjust and tend

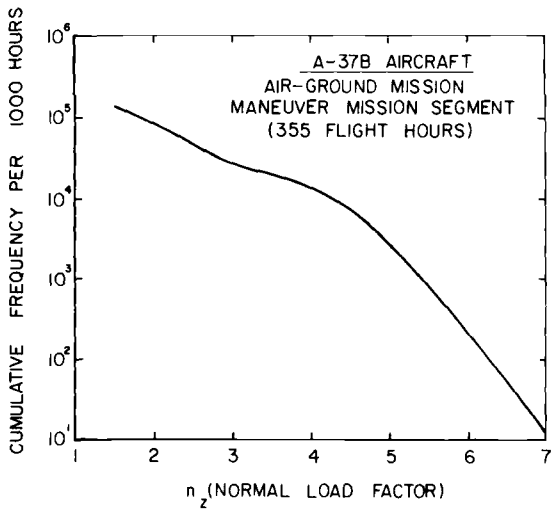

FIG. 2—*Typical curve of peaks per 1000 h exceeding each level of load factor.*

to be relatively insensitive to actual field experiences in structural reliability, particularly if the reliability is better than predicted. Thus, the early monitoring of structural loads is important in maintenance resource allocation.

Structural Inspection and Maintenance Scheduling

To provide more cost-effective structural maintenance, there is a current trend to abandon the use of aircraft hours for scheduling major structural inspections and modifications and to schedule instead according to a damage index that is related to the severity of structural usage. The objective of this scheduling is to determine the priority or sequence in which individual aircraft are scheduled for major structural maintenance (not to vary the overall scheduled structural maintenance resource requirements). To set this priority, it is necessary to determine, on an individual aircraft tail number basis, how each aircraft is operated and thus how long it can safely (and economically) operate between major structural inspections or before a specific structural modification. The process by which this operational usage data is gathered and utilized is called an individual aircraft tracking program (IAT).

Aircraft Loads Monitoring—When?

The key to an intelligent projection of structural maintenance requirements is a representative service loads spectrum sample. Data samples are gathered as soon as possible after an aircraft reaches full operational status. For each category of operation, such as a mission type, a sample of 50 to 500 flights is required to form a stabilized distribution of load occurrences. For a reasonably stable distribution, 200 flight hours of flight data recorded over a 12-month period has been recommended for each mission type. This sample should provide a stable spectrum sample but not necessarily a representative sample. To be representative, the aircraft selected for monitoring should be a cross section of the fleet. The fleet cross section is defined by geographic and climatological deployment, special or peculiar mission requirements, and special operational requirements. Because of cost and operational constraints on the aircraft to be monitored, the selection of representative aircraft usually is not given the priority it deserves. However, an attempt is made to select aircraft from bases in different geographical locations and with the most significant mission variations. As a hedge against likely variations in the overall loads spectrum, the recorded data are processed generally by mission segment so that various mission profiles may be "constructed" by piecing together appropriate mission segment samples to obtain a complete spectrum. This technique is used also to generate flight-by-flight durability tests and analysis sequences for new aircraft.

Another problem in sampling is that the overall population of service loads is likely to change over a period of years as operational requirements and usage change. Thus, it may be necessary to repeat the sample data collection after a period of time. The indication that a new sample is required is called "detection of a change in usage." There are three sources of information on usage changes: (1) the operational requirements obtained from the operating command; (2) the recorded data from usage monitors such as counting accelerometers or usage forms; and (3) the feedback of structural failure data from inspection results. The best procedure for detecting usage change is through an analysis by the aircraft operator of upcoming requirements. The operator's recommendations can then be verified by observing the data from the usage monitor. Normally, the feedback of structural failure data is too late to detect a change in usage in time to avoid major operational curtailment.

When loads data are collected as usage data under an individual aircraft tracking program, it is critical that the entire aircraft operational lifetime be accounted for. For these programs, data collection should be started when the aircraft is delivered and continued for the life of the aircraft.

Aircraft Loads Monitoring—How?

This discussion of techniques for aircraft loads monitoring is limited to operational loads programs which can be conducted on a noninterference basis during normal aircraft operations. These programs are grouped into three types: (1) strain monitoring, (2) center-of-gravity (cg) motion/control deflection monitoring, and (3) load condition monitoring. A fourth subsection describes the processing of recorded data into loads.

Strain Monitoring

Strain monitoring programs provide data for direct conversion to stress at specific points in the airframe. These programs are an accurate measure of operational effects on the monitored structure but tend to provide little useful mission information for design criteria on other aircraft.

Strain data have been recorded for years on oscillograph recorders. The oscillograph galvanometers are matched to output levels of strain gage bridges and the assembly of such a recording system is a relatively simple task for an experienced instrumentation engineer. Although this type of system is not, by any means, state of the art, it is still used frequently because it is extremely cost effective for short-duration programs with small quantities of data. The major disadvantage of the oscillograph system is the high cost of the manual procedure necessary to edit and measure the recorded data on the film.

The mechanical strain recorder (MSR) shows promise as a low-cost device

for recording a continuous time history of strain at any location in an airframe. The recorded data are in the form of a scratch on a stainless steel tape. The advantages of this device are: (1) it requires no electrical power and operates continuously during ground handling and flight operations, (2) it has no "drift" problems associated with electrical strain gages; (3) installation is easy with no wiring required; (4) the recording media has the capacity to store up to six months of data; and (5) operation is simple and does not require skilled personnel. Disadvantages are: (1) the MSR is relatively large—25 by 20 by 200 mm (1 by 0.8 by 8 in.)—and cannot be mounted on small or sharply curved surfaces; (2) the MSR must be protected from weather and the airstream and requires a cover when mounted externally; (3) the MSR must be serviced to change the recording media and suitable access must be provided for the installed device; and (4) a special optical device is required to extract the data from the steel tape. The Air Force Aeronautical Systems Division is procuring MSR's from Leigh Instruments Limited Avionics Division. A MSR of a different design is available from Prewitt Associates.

A strain counter device has been tested but never produced in quantity. This device uses an electrical strain gage circuit and four or eight mechanical counters. When the aircraft power is on, the device increments one of the counters each time the output of the strain gage circuit passes from below to above a specific level. The counter will not count successive level crossings unless the gage output falls below a specific reset level corresponding to each counter. The advantage of the device is that no special data playback or processing is required. The major disadvantages are: (1) the electrical strain gage circuit is difficult to install and can have some drift problems, and (2) the interpretation of level-crossing strain data is much less precise than for strain time-history data. Development programs for strain counters have been conducted by NASA-Langley and by the Naval Air Development Center (NADC).

Digital microprocessor devices for recording strain data are currently in the development stage. The microprocessor provides a large amount of processing capability and data storage capacity in a very small space with high-speed access so that input signals can be digitized and processed to reduced form before they are recorded in permanent storage. The advantage of the microprocessor recorders is that they can reduce by an order of magnitude or even eliminate the cost of processing on a central ground-based computer. It is within the capability of these recorders to detect strain peaks and troughs in real time and to compute a damage index or a potential crack length growth within the airborne unit. Permanent storage can be provided in solid-state memory or by a cassette-type tape recorder. The NADC currently is sponsoring a microprocessor strain recorder development, and several instrument and airframe manufacturers have similar designs in the prototype stage.

Strain data also have been recorded by digital and analog magnetic tape systems. The MXU-553 digital recording set currently is used by the Air Force to record strains on several types of aircraft. These programs monitor strains instead of cg motion because the flexibility of the structure of these aircraft types does not allow an accurate determination of loads from the cg response. Analog FM tape recorders have been used for strain monitoring programs, but the development of advanced digital recording techniques has made analog systems obsolete.

Table 1 lists recent and current strain monitoring systems.

CG Motion Control Deflection Monitoring

The monitoring of aircraft cg motion and control deflection permits the deduction of the corresponding airloads and inertia loads followed by the calculation of stress time histories at various airframe locations. Since control inputs and motion are a direct result of mission requirements and pilot reactions, these data can be used as design criteria for other aircraft types which fly the same missions.

Acceleration time histories were recorded on film by an airborne accelerometer before 1925 as reported by the National Advisory Committee for Aeronautics (NACA). Since that time a variety of equipment has been used to monitor aircraft motion.

Digital recorders currently represent the most advanced systems for monitoring motion and control deflections. From 3 to 26 channels are recorded on magnetic tape which can be removed from the recorder for processing at a central computer facility. Because they are in digital form, the data are well suited for automatic processing with a minimum of handling operations. The most common system currently in use is the Aircraft Structural Integrity Program (ASIP) recorder designated the MXU-553/A. Depending on the multiplexer configuration, the recorder will monitor from 16 to 26 channels at various sampling frequencies for up to 15 h of operation. The recorded data from Air Force Programs are

TABLE 1—*Representative operational monitoring systems.*

Recorder	No. of Applications	No. of Strain Channels	Approximate Hours Recorded
Strain level counter	1(A-37)	1	70
MSR-Prewitt	2	1	2600
MSR-Leigh	4	1	7000+
Oscillograph	many	2 to 4	5000+
MXU-553	6	4 to 8	6500
Garrett digital recorder	1(F-106)	2	1000
Parson's FM analog recorder	1(B-58)	8	6500

processed at the ASIMIS facility at Tinker Air Force Base, Oklahoma. Table 2 presents a typical list of recorded parameters as arranged for F-100 aircraft. Other digital recorders with similar capabilities are the A/A24U-6 used on the Air Force F-111 aircraft and the ASH-28 used on the F-15 aircraft.

Previous generation digital recorders had some features which warrant mention here. The Air Force A/A24U-10 VGH recorder is still in use on F-4 aircraft. This recorder employs an integral computer to preprocess the data to detect and count acceleration peaks in specific ranges and elapsed time in corresponding ranges of airspeed and altitude. An event monitor records the status of external stores released and gunfire sample and hold circuits at each record output. A 12-channel Digital Adaptive Recording Set (DARS) was utilized on the F-111 aircraft to record motion data. This recorder "compressed" the data by omitting repeated samples of identical values of a parameter. By eliminating these redundant samples, the tape data storage capacity was increased significantly.

Analog tape recorders have been used for a few recording efforts, but the extensive analog-to-digital processing equipment required has limited the application of this type of recorder in operational loads programs. The only advantage of this equipment is the ability to record relatively high frequency data and then to decide on the digital sampling frequency after examining the data.

The use of oscillograph recorders to monitor loads has declined during the last ten years with the deployment of large quantities of the digital recorders. The oscillograph allows a relatively flexible quick-response system because preliminary data reduction can be performed by the technician-operator using an engineers' scale. The problem with the oscillograph data system is that, to process large quantities of recorded data, the data had to be measured manually and converted to digital form suitable for input into a computer system. Even with semiautomatic measurement equipment, this was an expensive task. The oscillograph recorder varied in size and capacity from the 70 mm-wide, 3-channel NASA VGH (velocity-acceleration-altitude) recorder to the 12-in. wide, 50-channel CEC recorder.

TABLE 2—*Recorded parameters F-100 aircraft.*

Airspeed	Elevator deflection
Altitude	Rudder deflection
Vertical acceleration	Aileron deflection
Lateral acceleration	Fuel quantity
Roll rate	Wing strain
Pitch rate	Store drop events
Yaw rate	Touchdown event
Elapsed time	Refueling event

The most common oscillograph for operational loads recording is the 3⅝-in. wide, 14-channel Century Model 409 recorder. The recording speed varied from 1 in./min to approximately 30 in./min with recording capacities of up to 30 h at the low speed using a 150-ft magazine and up to 2.3 h at the high speed using a 400-ft magazine.

Common uses of the oscillograph include gathering VGH data (airspeed, acceleration, and altitude); 8-channel data (airspeed, altitude, 3-axis cg accelerations, roll rate, pitch rate, and yaw rate); and other combinations of motion and strain measurement channels.

The most widely used cg motion monitor is the counting accelerometer which is installed by the manufacturer on several types of aircraft. These devices count the number of exceedances of four specific acceleration levels. The advantage of the counting accelerometer is its high reliability and the simplicity of the output. The disadvantages are: (1) the limited number of counters does not provide an accurate description of the distribution of exceedances; (2) the lack of sequence of peaks does not allow application of the fracture mechanics data analysis except by making gross assumptions; and (3) the value of acceleration without corresponding airspeeds, altitudes, and weight distribution does not allow an accurate calculation of loads.

Older recording systems included the NACA VG (velocity-acceleration) recorder, the Willy's Flight Recorder, and the Hathaway Flight Recorder. The NACA VG recorder had a stylus which scratched carbon from a smoked-glass with a horizontal motion proportional to airspeed and a vertical motion proportional to normal acceleration. Since the stylus retraced many times over the same airspeed-acceleration coordinates, the recorder was capable only of detecting the extreme values and provided no sequencing of the recorded data. The Willy's Flight Recorder produced a continuous record of airspeed, altitude, and acceleration in specific ranges of the three parameters as defined by a set of fixed styli which burned a trace in the paper by an electric arc. The Hathway Flight Recorder had three styli which deflected in proportion to the value of airspeed, altitude, and acceleration. The recording paper was preprinted with a set of three vertical scales for calibrating the trace deflections into engineering units. The NACA VG recorder still is used to record loads on general aviation aircraft. The Willy's and Hathaway recorders are no longer in service.

Table 3 lists cg motion/control deflection monitoring systems which have seen recent use.

Load Condition Monitoring

Load condition monitoring, as used in this paper, refers to the technique of preprocessing the monitored data, before recording, into occur-

TABLE 3—*Representative cg motion/control deflection monitoring systems.*

Recorder	No. of Applications	No. of Channels	Approximate Hours Recorded
Counting accelerometer	many	1	500 000+
Oscillograph	many	3	100 000+
A/A24U-10	10	4	100 000+
Oscillograph	3	8	1 000+
MADARS	1(C-5A)	8(loads)[b]	10 000
DICOR[a]	1(A-37B)	14	4 000
DARS[a]	1(FAA)	24	2 500
ASH-28	1(F-15)	22	1 000
A/A24U-6	1(F-111)	24	4 000
MXU-553	10	8-26	16 000

[a] First generation multichannel digital tape recorders.
[b] Other channels record maintenance data.

rences of, or elapsed time in, defined load conditions. The defined load condition can be a flight condition, such as climb or cruise at a given airspeed, a maneuver type, such as a turn or a pullup, or a mission event, such as a weapon delivery or refueling. The advantage of using load conditions in the data processing is that this information can be correlated directly back to the design conditions specified for the aircraft. Another advantage is the reduction in the quantity of recorded data which reduces the subsequent processing costs. Two types of recording systems lend themselves to this type of monitoring: (1) the microprocessor-based system, and (2) crew forms.

The microprocessor provides the speed and processing capability in a small package necessary to monitor recorded response parameters, detect characteristic patterns or combinations of parameter values, and recognize the occurrence of predefined load condition events. The resultant data can be stored on magnetic tape or in a solid-state memory for retrieval during ground servicing of the recorder. A recording system of this type is being developed by the Army for application to rotary wing aircraft and by the Air Force for application to engine monitoring. As of this writing, a load condition monitoring microprocessor system has not been used operationally.

A simple existing load condition monitoring system is the crew forms used for the C-130, C-141, C-5, T-37, and other aircraft. In this case, the crew member is the preprocessor who monitors the aircraft motion parameters and detects and records the occurrence of the load conditions. For low-frequency events that are defined accurately by the normal aircraft indicator readings, the forms are a simple, reliable system. Where the number of events or crew workload forces the crew member to commit part of the data to memory for later entry on the form, the data reliability rapidly disappears.

Loads Data Processing

In general, the processing of recorded data into loads can be categorized as those which preserve the recorded sequence and those which do not.

To preserve the recorded sequence requires a cycle-by-cycle transformation of the recorded strain or motion data into values of load at the peak and trough of each cycle. For the motion data, this is performed by computing a set of external and inertia loads which "balance" the aircraft according to the vehicle equations of motion. For the strain data, loads are computed for nearby structural locations by using a direct empirical (or analytical) relation between strain and load. The advantage of the sequenced data is that they account for large cycle retardation effects in crack growth calculations. The primary disadvantage is the cost of processing this type of data, particularly when many points in the structure must be considered. This disadvantage could be overcome partially by using a microcomputer to process the data in real time aboard the aircraft or during playback so that the time for computation can be absorbed into time already committed for other required functions.

The systems that do not preserve sequence during processing generally reduce the data to distributions of peaks or cycles in joint intervals of two or more parameters. The recorded data are transformed to load cycles by a statistical approach to define combinations of parameter values for input into the equations of motion. The computational cost is controlled by a judicious choice of parameter intervals to retain the most significant variations while limiting the total number of input parameter value combinations. Pseudosequence is constructed from the reduced data by randomly ordering missions, and load cycles within a mission, to obtain a representative sequence of load cycles. There is some evidence to indicate that errors in crack growth rates computed by this technique are within the accuracy limits of analytical crack growth rate predictions. The advantages of nonsequenced data are: (1) they can be presented in summary parametric curves which permit easy comparison with other data samples, and (2) they can be adjusted readily for use as design criteria on new aircraft types with improved capabilities. The primary disadvantages are the more complicated procedures required to calculate loads and the reduction in accuracy of the resultant load values.

Aircraft Loads Monitoring—Cost?

The cost of monitoring aircraft loads is part of the total structural integrity program costs. Although it is difficult to judge the worth of the structural integrity program, it is important to provide the essential elements of the program at the minimum cost. Since the budget constraints are established very early, the problem often is worked in reverse; that is,

to provide the best possible loads monitoring program within the available funding. This approach tends to discourage development of new techniques and equipment as the system managers opt for lower risk current techniques. In spite of this effect, several new recording systems have been introduced during the last 10 years and others appear imminent.

Table 4 presents cost estimates for several types of load monitoring systems. The setup costs include all one-time costs which can be allocated to a specific aircraft system such as data reduction software, central data playback devices (apportioned among the user systems), and depot level ground support equipment. Systems hardware costs include the airborne equipment, any flight line support equipment, and the cost of installation. For L/ESS applications, the airborne recorder, signal conditioners, and ground support equipment are included only to the extent of the proportion of equipment life used; while the transducers are assumed to be expended entirely with each system installation. Recurring costs include system overhaul and maintenance, recording system operation, data handling and transmittal, and data reduction to strain or load values in cycle counts or peak-trough sequences. Analysis costs for fatigue damage or crack growth calculations were considered but were found to have little effect on the relative system costs and were not included in the tabulated results. Analysis costs generally range from $50 000 to $150 000 per year depending on analytical complexity. Computer costs for analysis can be very high because of the $1500 per hour rate for many large commercial computer systems.

Four IAT systems (crew forms, mechanical strain recorders, microprocessor strain cycle counters, and acceleration level counters) were considered for individual aircraft tracking (IAT), but the cost information appeared too premature to make comparisons between these systems. The values presented in Table 4 for IAT systems are good preliminary estimates for a microprocessor strain counter system. The estimates for other fleet monitoring systems vary up to 50 percent above and below these numbers and the particular application will determine which system is the most economical. Since neither the mechanical strain recorders nor the microprocessor strain cycle counters have seen fleetwide use, the recurring cost estimates for these systems are still tentative.

For loads/environmental spectra surveys, Table 4 presents cost estimates for five representative recording systems. Because of the expected low recurring cost of the microprocessor load condition recorder, this system appears to offer significant cost advantages for L/ESS applications. The A/A24U-10 VGH digital magnetic tape system is the most economical among the current systems. The MXU-553 multichannel digital tape system is the next most economical system particularly because of the information content in this type of data. Finally, the two oscillograph systems, VGH and multichannel, are the least economical for the two L/ESS problems

TABLE 4—*Load monitoring system estimated costs.*

Cost Element	IAT Systems	L/ESS VGH Oscillograph	L/ESS VGH A/A24U-10	L/ESS Multichannel Oscillograph	L/ESS Multichannel MXU-553	L/ESS Micro-processor
Setup costs	$100 000	$15 000	$172 000	$40 000	$214 000	$100 000
System hardware costs	3 600	5 600	21 300	14 800	45 500	5 300
Recurring O&M[a] and data costs (per hour)	1.25	93.00	38.00	300.00	54.00	3.12
Analysis (not included)	...	...	...	...	...	...
Fighter fleet:[b]						
Total cost	$4.0 × 10^6	$2.5 × 10^6	$1.9 × 10^6	$7.8 × 10^6	$3.3 × 10^6	$0.4 × 10^6
(per hour)	(2.00)	(103.00)	(81.00)	(326.00)	(139.00)	(16.00)
Transport fleet:[c]						
Total cost	$7.1 × 10^6	$2.9 × 10^6	$1.7 × 10^6	$9.3 × 10^6	$2.7 × 10^6	$0.3 × 10^6
(per hour)	(1.40)	(97.00)	(58.00)	(311.00)	(91.00)	(10.00)

[a]Operating and maintenance.
[b]IAT fleet: 400 aircraft, 500 h per year, 10 years.
L/ESS sample: 40 aircraft, 300 h per year, 2 years.
[c]IAT fleet: 200 aircraft, 1000 h per year, 25 years.
L/ESS sample: 20 aircraft, 750 h per year, 2 years.

selected but for sample sizes up to about 1000 h, the low setup and equipment costs of the oscillograph systems can make them cost effective.

Acknowledgments

We wish to thank D. S. Morcock of Lockheed-Georgia Company, H. Hostetter of the Air Force Oklahoma City Air Materiel Area, C. G. Peckham of the Air Force Aeronautical Systems Division, and R. I. Rockafellow of CONRAC Corporation, for supplying recording system information for preparation of this paper.

Bibliography

Oscillograph Systems

Clay, L. E. et al, "C-130 Life History Recording Program (1970-1972)," *Report No. WRAMA-72-MME-011*, Service Engineering Division, Warner Robins Air Materiel Area, Robins Air Force Base, Ga., 1973.

Coy, R. G., "OV-10A Flight Loads Recording Program," *URDI-TR-76-16*, University of Dayton Research Institute, Dayton, Ohio, 1976.

Doolittle, J. H., "Accelerations in Flight," *NACA Report No. 203*, National Advisory Committee for Aeronautics, 1925.

Militello, J., "F-105F Combat Statistical Flight Loads Program," *Report (EFR) 82.4.1*, Service Engineering Division, Sacramento Air Materiel Area, McClellan Air Force Base, Calif., 1969.

Strain Counter

Clay, L. E. and Buehler, S. K., "Evaluation of the NASA Electronic Strain-Level Counter as a Fatigue Damage Monitor," *Report AFFDL-TR-72-135*, Air Force Flight Dynamics Laboratory, Wright-Patterson Air Force Base, Ohio, 1973.

A/A24U-10 System

Peckham, C. G. and Morton, W. W., "F-4C Flight Loads Data From A/A24U-10 Magnetic Tape Recorders," *Report SEG-TR-67-21*, Systems Engineering Group, Aeronautical Systems Division, Wright-Patterson Air Force Base, Ohio, 1967.

DICOR and DARS Systems

Clay, L. E. and Nash, J. F., "Flight and Taxi Data from A-37B Aircraft During Combat and Training Operations," *Report ASD-TR-72-1*, Deputy

for Engineering, Aeronautical Systems Division, Wright-Patterson Air Force Base, Ohio, 1972.

MXU-553 System

"CONRAC Data Acquisition System," brochure, CONRAC Corporation, P.O. Box 32, Caldwell, N.J. "Recorder, Signal Data MXU-553A, *Military Specification MIL-R-83165A (USAF)*, 26 Aug. 1969.

MSR-Prewitt Associates

Clay, L. E. et al, "C-130 Scratch Strain Gage Recording Program," *Report WRAMA-72-MME-014*, Service Engineering Division, Warner Robins Air Materiel Area, Robins Air Force Base, Georgia, 1974.

Loads Analysis

Clay, L. E. et al, "Statistically Predicting Maneuver Loads from Eight-Channel Flight Data," *Report TI 166-68-1*, Technology Incorporated, Dayton, Ohio, 1968.

Clements, R. F., "Parametric Fatigue Cost Comparison Study A-37B," *Report 318E-7505-083*, Cessna Aircraft Co., Military Aircraft Division, Wichita, Kan., 1975.

Landy, M. A. et al, "Derivation and Analysis of Loading Spectra for USAF Aircraft," *Report ASD-TR-76-1*, Aeronautical Systems Division, Wright-Patterson Air Force Base, Ohio, 1976.

Parker, G. S., "Generalized Procedures for Tracking Crack Growth in Fighter Aircraft," *Report AFFDL-TR-76-133*, Air Force Flight Dynamics Laboratory, Wright-Patterson Air Force Base, Ohio, 1977.

Roth, G. J., "Development of Flight-by-Flight Fatigue Test Data from Statistical Distributions of Aircraft Stress Data," *Report AFFDL-TR-75-16*, Air Force Flight Dynamics Laboratory, Wright-Patterson Air Force Base, Ohio, 1975.

White, D. J. et al, "A-7D ASIP Part I Damage Tolerance and Fatigue Assessment Program," *Report 2-53440/7R-5928*, Vought Corporation, Dallas, Tex., 1977.

A. P. Berens[1]

Determination of Sample Size in Flight Loads Programs

REFERENCE: Berens, A. P., "**Determination of Sample Size in Flight Loads Programs,**" *Service Fatigue Loads Monitoring, Simulation, and Analysis, ASTM STP 671,* P. R. Abelkis and J. M. Potter, Eds., American Society for Testing and Materials, 1979, pp. 36-48.

ABSTRACT: This paper describes the application of a statistical model of a cumulative damage index to the problem of determining the number of flights to be monitored in aircraft operational usage programs based on samples of flights. The method can be used to calculate the optimum number of flights to achieve given precision and confidence under stratified sampling. It also provides a method for determining precision at any level of confidence given a sample size. Examples of the use of the techniques are provided using data from the operational usage programs of three aircraft types.

KEY WORDS: fatigue damage, operational usage, sample size, flight loads, cumulative damage, fatigue tests.

In assessing the operational loading environment for a given aircraft type, economical and practical considerations often dictate that only a sample of all operational flights will be monitored. The loads/environment spectra survey task of Military Standard MIL-STD-1530A, for example, envisions instrumenting 10 to 20 percent of the operational airplanes with no firm guidelines for ending the survey. In this approach, the observed loading environment depends on the usage of the instrumented aircraft and the resulting environmental description is subject to a possible sampling error.

If aircraft usage across the fleet is stable, it is reasonable to assume that increasing the number of monitored flights decreases the chance of an erroneous description due to an adverse sample. However, increased confidence must be balanced against the increased cost of the larger data sample. The complex nature of the description of the loading environment obscures the relationship between measures of possible sampling errors and the sample size. This paper presents a relatively simple statistical approach for evaluating the sampling error in a given set of flight history

[1]Research statistician, University of Dayton Research Institute, Dayton, Ohio 45469.

data, and for estimating the amount of data required to achieve a given degree of precision.

Background and Assumptions

From the statistical viewpoint, the question of sample size is answered by trading off the cost of the sample with the resulting level of precision of an estimate or degree of confidence in the statistical inference to be drawn from the sample. This procedure implies that: (1) the objective of the program can be defined in terms of parameters which are calculable from the sample, (2) the sampling distribution of these parameters can be determined so that levels of confidence can be quantified in terms of probability statements, and (3) the effect of sample size on the "goodness" of statistical inferences about the parameters can be evaluated.

An operational loads recording program is a highly complex "experiment." In a typical program, center of gravity loads data, strain data, and supplementary data are recorded, reduced in accordance with some peak-valley definitions, and processed into distributions and joint distributions of relevant combinations of the recorded parameters. They also are preserved in time history form for some currently unknown problem or analysis method. The processed data are subjected to various analyses to obtain estimates of damage, structural life, crack growth, or inspection intervals. Ideally, the sample size determination would be made on the basis of the recorded parameters. However, due to the relatively large number of parameters and their diverse applications, the sample size problem cannot be resolved in terms of precision of the estimates of the distributions and joint distributions of the recorded data. Therefore, it is necessary to make assumptions limiting the objective of these programs in order to make tractable the problem of evaluating sample size.

Assume the objective of the recording program is to obtain estimates of parameters from which a damage index at critical points of a typical aircraft of the fleet can be calculated as a function of aircraft age. Assume that the damage index accumulates additively across flights and that the incremental damage due to a flight is independent of the previous damage accumulation. The accumulation of fatigue damage according to the Palmgren-Miner theory is an example of a damage index that satisfies these assumptions. Since crack length as a function of service time is relatively linear in the early stages of structural life, it may be feasible to use crack length or normalized crack length as the damage index for sample size evaluation in some applications. Although there may be many critical points of interest in the structure, no generality is lost by considering only one in the description which follows.

It is also necessary to assume that the particular sample of monitored flights is a random sample for some population of interest. The economics

of data collection for sampling operational usage dictates that the data sample will be obtained from the flights of a fixed set of instrumented aircraft. If the recorded flights are reasonably representative of total fleet operations, then the sample will be called completely random and will be used to make statistical inferences without stratifying the data into subpopulations. However, it is common for certain mission types to be disproportionately represented in the sample. In this case the recorded flights will be a random sample of stratifications of the population of all flights and the statistical inferences will be drawn by combining results at the individual stratification levels. This latter situation will be called stratified sampling in the following paragraphs. Note that stratifications can be defined in terms other than mission types; for example, mission by base combinations or specific cross country routes. The stratifications (if any) must be defined by an analysis of the operations to be sampled and the desired extent of the statistical inferences to be drawn from the sample.

Statistical Model

Under the above assumptions, the amount of damage accumulated at a critical location in N flights is given by

$$D(N) = \sum_{i=1}^{N} D_i \tag{1}$$

where D_i is the incremental damage due to flight i. By the Central Limit Theorem of probability theory, when N is large and all N flights are from the same population, the random variable $D(N)$ can be modeled by a normal distribution with mean and standard deviation given by

$$\begin{aligned} \mu_{D(N)} &= N\mu_D \\ \sigma_{D(N)} &= \sqrt{N}\sigma_D \end{aligned} \tag{2}$$

where μ_D and σ_D are the mean and standard deviation of damage per flight, respectively.

Since damage accumulation in operational aircraft will occur relatively slowly, it can be assumed that N will be sufficiently large to use the normal distribution to describe the damage after N flights. It is not being assumed that incremental damage per flight has a normal distribution. In fact, the distribution of damage per flight is typically J-shaped, highly skewed, with a nonzero probability of having no discernible damage in a flight. However, it is important to note that the mean and standard deviation of the damage per flight random variable are the key parameters in the distribution of cumulative damage in N flights.

Under the assumptions of this paper, the damage accumulated by a specific aircraft during a fixed number of flights is not known. However, given the mean and standard deviation of the incremental damage per flight, probable ranges of damage can be calculated. This is illustrated in Fig. 1 which displays the distributions of damage values after N_1 and N_2 flights. The center of the distributions, $N\mu_D$, represents the damage that would be experienced by the "typical" airplane of the fleet. (Note that this is the value that has been calculated traditionally in parametric fatigue analyses. There is an algebraic equivalence between average damage values calculated from damage per hour and damage per flight parameters.) However, the standard deviations can be used to indicate possible differences between individual aircraft and the "typical" aircraft. Note that as N increases, the entire distribution shifts to greater damage values and the individual aircraft are more dispersed from the mean. However, the coefficient of variation decreases as $1/\sqrt{N}$.

The preceding model can be generalized easily to permit a description of the damage distribution in terms of parameters derived from stratifications (for example, missions) of the total population. Let $N(\alpha)$, $\alpha = 1, \ldots, m$, represent the number of flights in stratification α and $D_{\alpha i}$ represent the incremental damage from flight i in stratificaton α. Then the total damage in N flights is given by

$$D(N) = \sum_{\alpha=1}^{m} \sum_{i=1}^{N(\alpha)} D_{\alpha i} \tag{3}$$

For larger $N(\alpha)$, the damage for each stratification can be modeled by the normal distribution. The sum of m normally distributed random variables also has a normal distribution. Therefore, $D(N)$ will have a normal distribution with mean and standard deviation given by

$$\mu_{D(N)} = \sum_{\alpha=1}^{m} N(\alpha)\, \mu_{D\alpha} \tag{4a}$$

$$\sigma_{D(N)} = \left[\sum_{\alpha=1}^{m} N(\alpha)\, (\sigma_{D\alpha})^2 \right]^{1/2} \tag{4b}$$

Again, the damage distribution at N flights can be modeled in terms of means and standard deviations of the damage per flight values. Here, however, these statistical parameters must be available for each stratification level.

Sample Size Objectives

Assuming that the objective of the data collection program is to obtain

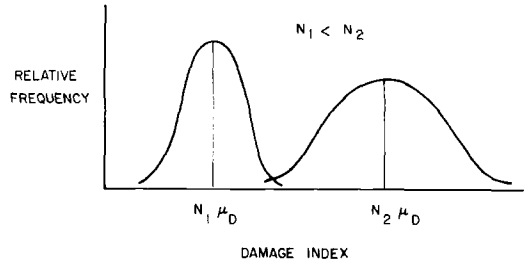

FIG. 1—*Damage distributions after* N_1 *and* N_2 *flights.*

damage estimates for the fleet aircraft, Eq 4 permits interpretation of the objective in terms of the random variable of damage per flight. The true mean and standard deviation of damage per flight become the key parameters and sample size evaluations can be formulated in terms of precision of the estimates of these parameters. However, since primary interest is centered on cumulative damage after many flights, the precision must be evaluated for $\mu_{D(N)}$ and $\sigma_{D(N)}$.

Sample estimates, $\overline{D}$ and S_D, of the true mean and standard deviation of damage per flight reflect the specific flights that were monitored and are subject to a sampling error. To evaluate the relative magnitude of the sampling errors of $\overline{D}$ and S_D on the estimated distribution of damage at N flights, a sensitivity analysis was performed. The sampling distributions of both $\overline{D}$ and S_D were introduced into the estimate of the distribution of $D(N)$, assuming different sample sizes.[2] The analysis indicated that the effect of sampling error on the estimate of the standard deviation was small in comparison with the effect of sampling error on the estimate of the mean. Therefore, it can be assumed that if a sample size is sufficient for the mean damage per flight then it is also sufficient for the standard deviation of damage per flight. This result was anticipated since mean damage in N flights increases linearly with N whereas the standard deviation increases as $\sqrt{N}$.

Sample Size Evaluation

The preceding defined objectives imply that sample size evaluations can be performed by analyzing the sampling properties of the sample mean. Furthermore, since it can be assumed that at least 30 flights will be sampled for each mission type, it is reasonable to assume that the sample means will have a normal distribution. Therefore, well known statistical methods can be used in the evaluation of the precision which results from a particular

[2]Berens, A. P., "The Determination of Sample Size in Flight Loads Programs," *Technical Report ASD-TR-74-17,* Aeronautical Systems Division, Dayton, Ohio, 1974.

sample size or for determining the number of flights that would need to be monitored to obtain a given degree of confidence and precision.

Completely Random Sample

The completely random sample case is resolved quite simply. When the observed flights are assumed to be representative of the total fleet operation, all statistical inferences are made in terms of the mean and standard deviation of the average damage per flight sampling distribution. If k represents the number of sampled flights and k is greater than 30, then $\overline{D}$ has a normal distribution with

$$\mu_{\overline{D}} = \mu_D$$

$$\sigma_{\overline{D}} = \frac{\sigma_D}{\sqrt{k}} \tag{5}$$

For the distribution of damage in N flights, these sampling statistics must be transformed by multiplying by N. $\mu_{D(N)}$ is estimated by $N\overline{D}$ and $N\overline{D}$ has a normal distribution with mean and standard deviation given by

$$\mu_{N\overline{D}} = N\mu_D$$

$$\sigma_{N\overline{D}} = \frac{N\sigma_D}{\sqrt{k}} \tag{6}$$

Thus, normal distribution theory can be used to place confidence limits on the location of the damage distribution after N flights, where the width of the confidence interval depends on the degree of confidence, the standard deviation of damage per flight, and the sample size. Tests of hypotheses for detecting changes in usage can also be formulated and probabilities of Type I and Type II errors can be evaluated for different sample sizes and different magnitudes of usage changes.

An upper confidence limit, UCL, on the true mean of the distribution of damage after N flights is given by

$$\text{UCL} = N\overline{D} + \frac{Z_p N S_D}{\sqrt{k}} \tag{7}$$

where Z_p is the p^{th} percentile of the standard normal distribution. The best estimate of the distribution of damage at N flights and the upper confidence limit distribution is illustrated in Fig. 2.

It is apparent from Eq 7 that increasing the sample size, k, will provide greater precision in the estimate of the location of $\mu_{D(N)}$. The degree of pre-

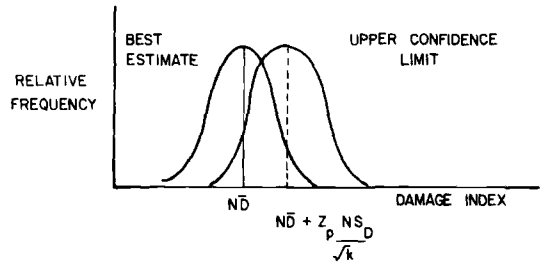

FIG. 2—*Estimate of damage distribution with confidence limit.*

cision as a function of sample size can be expressed in terms of absolute damage or in terms of percent difference of the confidence limit from the mean. For precision expressed in absolute damage units, let

$$\epsilon = \frac{Z_p N S_D}{\sqrt{k}} \tag{8}$$

Given a sample, the magnitude of ϵ can be calculated. Conversely, to be p percent confident that the mean of the damage distribution will not be more than ϵ damage units less than the true location will require a sample size given by

$$k \geq \left[\frac{Z_p N S_D}{\epsilon}\right]^2 \tag{9}$$

To express the precision in terms of percent error, the right hand side of Eq 7 is divided by $N\bar{D}$ and the percentage error, denoted by 100δ, is calculated from

$$\delta = \frac{C Z_p}{\sqrt{k}} \tag{10}$$

where $C = S_D/D$ is the coefficient of variation. Note that the precision expressed in terms of percent error is independent of N, the age of the aircraft at time of damage evaluation. To be within 100δ percent of the true mean will require a sample size given by

$$k \geq \left(\frac{C Z_p}{\delta}\right)^2 \tag{11}$$

Stratified Sampling

Consider now the more complex case for which the sample of flights is random only at levels of stratification of the total population of all flights.

There are three major reasons for considering the sampling to be done on subpopulations. First, due to the data collection system, the recorded flights may contain a nonrepresentative mixture of mission types. Second, an administrative decision may be anticipated which changes past mission mixes and, if the effect of the change is to be evaluated, it is necessary to have damage data available at the stratified levels. Third, from the statistical standpoint, it is more efficient to have a larger proportion of samples from the subpopulations with greater variances. Therefore, formulas will be presented for evaluating sample sizes and for determining required sample sizes in the various levels of stratification to achieve a given precision.

As previously noted, the damage in N flights ($N = \Sigma N_\alpha$) will have a normal distribution with mean and standard deviation given by Eq 4*a* and *b*. Again assuming sampling variation in the estimate of $\sigma_{D(N)}$ is negligible compared to sampling variation in the estimate of $\mu_{D(N)}$, interest is centered on the precise estimation of $\mu_{D(N)}$. Now $\mu_{D(N)}$ is estimated by

$$\overline{D(N)} = \sum_{\alpha=1}^{m} N_\alpha \overline{D}_\alpha \tag{12}$$

where $\overline{D}_\alpha$ is the observed average damage per flight for stratification α. If each $\overline{D}_\alpha$ is based on a sample size, k, greater than 30, $\overline{D(N)}$ is the sum of m normally distributed random variables and, thus, is distributed normally. Since the mean and standard deviation of each $\overline{D}_\alpha$ is given by $N_\alpha \mu_{D\alpha}$ and $N_\alpha S_{D\alpha}/\sqrt{k}_\alpha$, respectively, the mean and standard deviation of $\overline{D(N)}$ are

$$\mu_{\overline{D(N)}} = \sum_{\alpha=1}^{m} N_\alpha \mu_{D\alpha} \tag{13a}$$

$$\sigma_{D(N)} = \left[\sum_{\alpha=1}^{m} \frac{N_\alpha^2 \sigma_{D\alpha}^2}{k_\alpha} \right]^{1/2} \tag{13b}$$

Again letting ϵ represent the increment to be added to the observed mean to obtain an upper p percent confidence limit, then

$$\epsilon = Z_p \left[\sum_{\alpha=1}^{m} \frac{N_\alpha^2 S_{D\alpha}^2}{k_\alpha} \right]^{1/2} \tag{14}$$

Given a data set, $S_{D\alpha}$ and k_α can be determined and the precision in the estimate of the location of the damage distribution for N flights can be calculated from Eq 14. The precision cannot be interpreted readily in terms of percent error for this case due to the more complex expression for average damage per flight.

Given estimates of the $S_{D\alpha}$ and a fixed ϵ, any set of k_α for which the right hand side of Eq 14 is less than ϵ will provide the desired precision. If there is a choice for the flights to be monitored, it is apparent that selecting a large percentage of flights for those stratification levels with the large $N_\alpha S_{D\alpha}$ values would be a more efficient strategy. The efficiency could be realized either in terms of greater precision for fixed total sample size or reduced sample size for fixed precision. The optimum allocation of the total sample, k, to achieve the minimum variance of the total projected mean life is given by Cochran.[3]

$$k_\alpha = k \cdot \frac{N_\alpha S_{D\alpha}}{\sum N_\alpha S_{D\alpha}} \tag{15}$$

Note that every k_α must be at least 30 for the assumption of normality of the $\overline{D}_\alpha$ to apply. After determining the optimum allocation by use of Eq 15 and 14, it may be necessary to increase the number of flights for some levels of stratification to this minimum value.

Examples

The formulas for evaluating sample sizes are expressed in terms of parameters calculated from damage per flight values. In the past, damage per flight has not been calculated routinely and, hence, little experience has been gained with the parameters of mean and standard deviation of damage per flight. Data from three aircraft types have been processed in this form, and these summary statistics will indicate the range of variation that can be expected and also will be used to demonstrate example applications of the theoretical results.

Miner's damage per flight values at a critical point were obtained for F-105D, C-135, and T-38 aircraft. The F-105D data consisted of 1317 flights from 15 aircraft operating out of two bases in Southeast Asia. These combat data were of one mission type, and, since no base-to-base variation was observed, the data were treated as a totally random sample. The C-135 data consisted of 1169 flights of 13 aircraft performing three missions out of four bases. These data were treated as stratified by mission types since the proportion of observed missions was biased by the deliberate collection of data in a "Weather" mission. The damage values for the C-135 aircraft critical point reflected only the damage due to gusts and maneuvers and did not contain the more significant contribution of the ground-air-ground cycle. The T-38 data comprised 3848 flights which were stratified into four types of missions. In the T-38 data collection program, the data were processed by the mission types even though the sample was considered to be totally random for the fleet operations.

[3]Cochran, W. G., *Sampling Techniques*, 2nd Ed., Wiley, New York, 1953.

Table 1 presents the pertinent summary statistics from the three programs. The coefficients of variation (the ratio of the standard deviation to the average) indicate the large degree of variability that can be expected in the damage per flight values. The smallest coefficient of variation for any of the aircraft-mission type combinations occurred in the training mission of the T-38, and for this mission the standard deviation was equal to the mean.

The sample sizes of these data collection programs can be evaluated in terms of percent error by substituting the observed parameter values in Eq 10. For the F-105D combat mission, the upper 95 percent confidence limit on the mean is 10 percent greater than the best estimate as provided by the observed average damage per flight. For the composite of all T-38 flights, the 95 percent confidence limit was only 3.4 percent greater than the best estimate. The greater precision in the T-38 data resulted from a reduction in the coefficient of variation and a sample size three times greater. The 148 weather flights, on the other hand, provide a 95 percent confidence limit that was 23 percent greater than the observed average.

Figure 3 presents sample size as a function of percent increase in mean for 95 percent confidence limits for the range of coefficients of variation observed in the three data collection programs. This figure provides a rapid evaluation of the sample size required to obtain a given percent precision if an estimate of the coefficient of variation is available. Caution is necessary if sample sizes for individual missions are evaluated in terms of percent error. If the total damage contribution of a particular mission is small compared to other missions, a larger percent error in the estimate of mean damage per flight for the mission can be tolerated.

In the T-38 data, the navigation and general mission type has a large coefficient of variation, a high percentage of flights, but a low average damage per flight. On the other hand, the training mission has a relatively

TABLE 1—*Damage per flight statistics for three aircraft types.*

Aircraft Type	Mission Type	Per Flight Average, $\overline{D}$	Coefficient of Variation,[a] C	Sample Size, k
F-105D	combat	2.9×10^{-4}	2.3	1317
C-135	cargo	5.8×10^{-6}	1.9	822
	training	16.3×10^{-6}	1.1	199
	weather	27.3×10^{-6}	1.7	148
T-38	training	31.2×10^{-6}	1.0	1941
	formation	19.0×10^{-6}	1.3	234
	navigation and general	2.8×10^{-6}	3.0	1529
	administration	11.0×10^{-6}	1.6	144
	composite	18.4×10^{-6}	1.3	3848

[a] Coefficient of variation, $C = S_D/\overline{D}$.

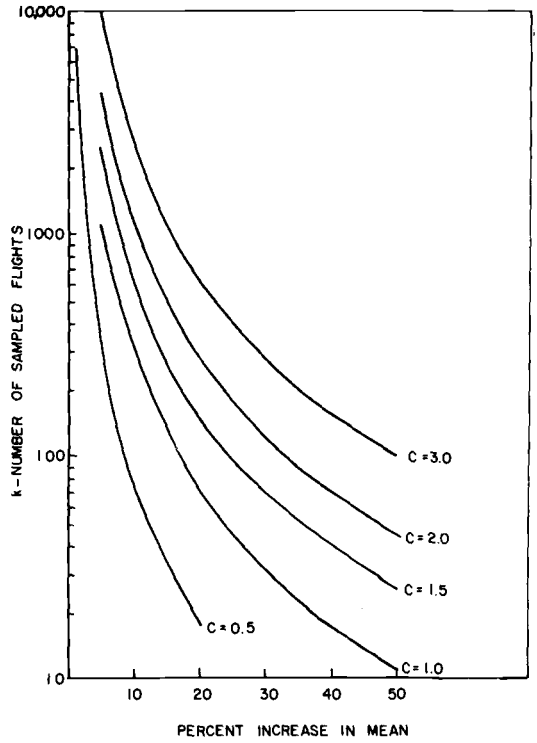

FIG. 3—*Sample size as function of percent increase in mean for upper 95 percent confidence limit.*

small coefficient of variation, a high percentage of flights, and a large average damage per flight. Under these conditions it may be of interest to determine the optimum mix of mission types if another program were to be conducted for the T-38 aircraft.

Since the T-38 observed data were used to estimate the mission mix to be applied to damage computations it is reasonable to assume that

$$\frac{N_\alpha}{N} = \frac{k_\alpha}{k} = p_\alpha \tag{16}$$

where p_α is the observed proportion of flights in mission α. Substituting in Eq 15 to obtain the optimum proportion of flights in mission α yields

$$p_\alpha' = \frac{k_\alpha'}{k'} = \frac{p_\alpha S_{D\alpha}}{\Sigma p_\alpha S_{D\alpha}} \tag{17}$$

where p_α' is the optimum ratio of flights of mission α to obtain greatest

TABLE 2—*Comparison of observed mission mix with optimum of T-38 data.*

Mission Type	Observed Mission Mix, percent	Optimum Mission Mix, percent
Training	50	74
Formation	6	7
Navigation and general	40	16
Administrative	4	3

precision for a fixed total sample size of k'. Table 2 presents a comparison of the observed mission mix with the optimum for the T-38 data. Note that the larger contribution of the training mission to the damage calculation results in an increased percentage of flights in this mission type.

Summary

A statistical framework was presented for evaluating the quantity of operational usage data when the usage is monitored by a random sample of flights. It was assumed that the objective of the data collection program was to obtain a precise estimate of the distribution of a damage index at a critical point. It was assumed that the damage index increases additively by flights and that the incremental damage for a flight is independent of previous history. Under these assumptions, it was shown that the objective of usage monitoring can be interpreted in terms of obtaining precise estimates of the average damage per flight. Due to the large sample sizes of flight loads programs, normal distribution theory can be used for making statistical inferences. Formulas were presented for some example applications when the sampled flights are considered representative of the total operations and also when considered representative of mission types.

Damage per flight summary statistics were presented for three aircraft types and these values were used in sample applications of the formulas. For the range of variability observed in the damage per flight values of these aircraft, at least 280 flights would have to be recorded to be 95 percent confident that the true distribution of damage per flight does not exceed the estimated distribution by 10 percent.

Acknowledgment

This work was supported by contracts with the San Antonio Air Logistics Command and the Aeronautical Systems Division of the United States Air Force.

J. B. de Jonge[1] *and D. J. Spiekhout*[1]

Use of AIDS Recorded Data for Assessing Service Load Experience

REFERENCE: de Jonge, J. B., and Spiekhout, D. J., **"Use of AIDS Recorded Data for Assessing Service Load Experience,"** *Service Fatigue Loads Monitoring, Simulation, and Analysis, ASTM STP 671,* P. R. Abelkis and J. M. Potter, Eds., American Society for Testing and Materials, 1979, pp. 48-66.

ABSTRACT: Inspection periods and safe service lives of transport aircraft are based on an assumed average design load experience. Actual service loads may deviate appreciably from these assumptions.

Fatigue related load data may be obtained on a routine basis from AIDS-recordings. The importance of careful data quality checking is stressed.

Examples illustrate the highly relevant information with regard to aircraft usage and loading environment that may be obtained.

KEY WORDS: load monitoring, aircraft integrated data systems, atmospheric turbulence, service load experience, data management, fatigue tests

Modern aircraft structures are subject to fatigue. Fortunately, fatigue has been overcome as a safety problem, since very few accidents are caused by fatigue. However, this favorable situation could only be obtained by a careful consideration of fatigue aspects both in the design and during the maintenance and operation of aircraft. Specifically, all primary structure must be inspected at regular intervals for fatigue cracking. In cases where a part is considered noninspectable, it must be replaced after a certain period.

Usually, the inspection periods and replacement times are determined by means of calculations and tests that are based on an assumed "design load experience," corresponding with an expected "average" airplane usage under average environmental conditions.

However, the actual load experience encountered by a specific operator may deviate appreciably from these design assumptions. First, his usage may be completely different. For example, a specific operator may serve a network associated with flight lengths deviating from the fleet average. Also, differences in fuel policy of different companies are known to have

[1]Aerospace research engineers, National Aerospace Laboratory NLR, Amsterdam, The Netherlands.

resulted in appreciable differences in take off weights and cruising speeds. Moreover, it should be noted that often the usage of aircraft changes with time; the transatlantic liners of a decade ago are still being used, but on short stretches.

Secondly, different operators may meet a different loading environment. For example, the operator flying largely overseas routes will encounter a milder gust environment than the company serving a network over mountainous areas. Also, the loading environment may change with time. The introduction of efficient avoidance-radar systems has reduced noticeably the number of gust encounters.

Clearly, it would be very interesting to an airline operator if he could show that the load experience of his aircraft is less severe than the design assumption so that he could ask the airworthiness authority to apply a relaxation factor on replacement times and inspection intervals. On the other hand, if the load experience is more severe, it is a matter of safety to shorten the inspection intervals.

Consequently, monitoring actual service load experience is considered desirable with respect to aircraft safety and operational economy.

Unfortunately, the installation, operation, and maintenance of specific load monitoring equipment such as velocity-acceleration-altitude (VGH) recorders is relatively expensive.

However, current transport aircraft are often equipped with fairly complex so-called Aircraft Integrated Data System (AIDS) recorder systems.

It will be shown in the present paper how AIDS recorded data may be used to yield, at very little cost, highly relevant information with regard to fatigue load experience.

A few years ago, the airlines within the KLM-SAS-Swissair-UTA (KSSU) group operating Boeing 747 aircraft, namely KLM, SAS, and Swissair, decided to develop a system to extract on a routine basis fatigue load related data from their 747 AIDS recordings. These data were to be stored at National Aerospace Laboratory (NLR) for further processing and future analysis.

This system has now been operative since 1974, and a considerable amount of data has been obtained already.

After a brief survey of the KSSU-747-AIDS-system principles, the present paper starts with a description of the methods used for extracting fatigue load related data. Special attention will be given to the checking of the reliability of the obtained data. The importance of an accurate data quality control will be stressed.

Recently, the NLR developed under contract with the Netherlands Civil Airworthiness Authorities a program for the analysis of AIDS recorded load data.

This program consists of two parts, the first part providing aircraft mission profile data, the second part providing information with regard

to the loading environment. Results obtained with these programs will be presented and discussed as an illustration of the type of information that can be made available.

Finally, a number of conclusions are offered.

Brief Description of the KSSU-747 AIDS System

The AIDS system used for KSSU-747's performs a continuous scanning of about 350 parameters, including speed, altitude, cabin pressure, instantaneous weight, center of gravity (cg) acceleration, engine pressures, etc.

This data stream is divided into data frames, each frame covering 4 s of data scanning.

However, not all data frames are recorded. A number of criteria are maintained that determine whether a data frame is to be recorded or not. These criteria are:

Time Interval—At *least* once per 400 s a data frame is to be recorded.

Flight Mode—During specific flight modes, namely, take-off, initial climb, approach, landing and roll-out, all data are recorded.

Limit exceedance—Whenever certain parameters exceed preset limits, a data frame is recorded.

These limits may be either "fixed" or "floating."

The cg acceleration, which is scanned eight times per second, is one of the parameters for which a floating limit exists. The criterion is explained in Fig. 1.

The ultimate effect is that all patches of turbulence exceeding a certain strength will be recorded.

To summarize, the following properties of the AIDS records may be observed: (*a*) basic flight parameters are recorded at least once per 400 s, (*b*) periods of turbulence, leading to cg accelerations of certain magnitude are recorded continuously.

Acquisition of Fatigue-Relevant Load Data

The AIDS recordings obtained by the various KSSU-747 operators are processed in their respective computer facilities on a routine basis through a number of application programs. After this processing, the original AIDS data are thrown away.

A few years ago, it was decided to establish a system for the extraction and storage of a limited number of fatigue-load related data from the AIDS recordings. Basic requirements were that the existing AIDS recording systems should not be changed and that the cost associated with the system should be kept low.

As shown in Fig. 2 the resulting data acquisition system consists of a number of successive steps that will be described separately.

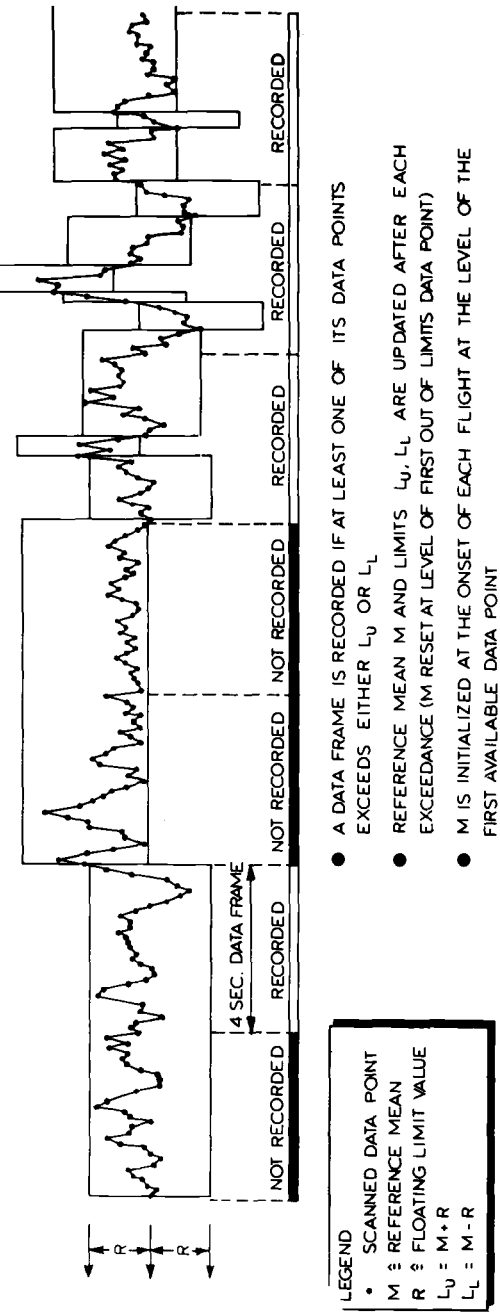

FIG. 1—*Illustration of floating limit recording criterion.*

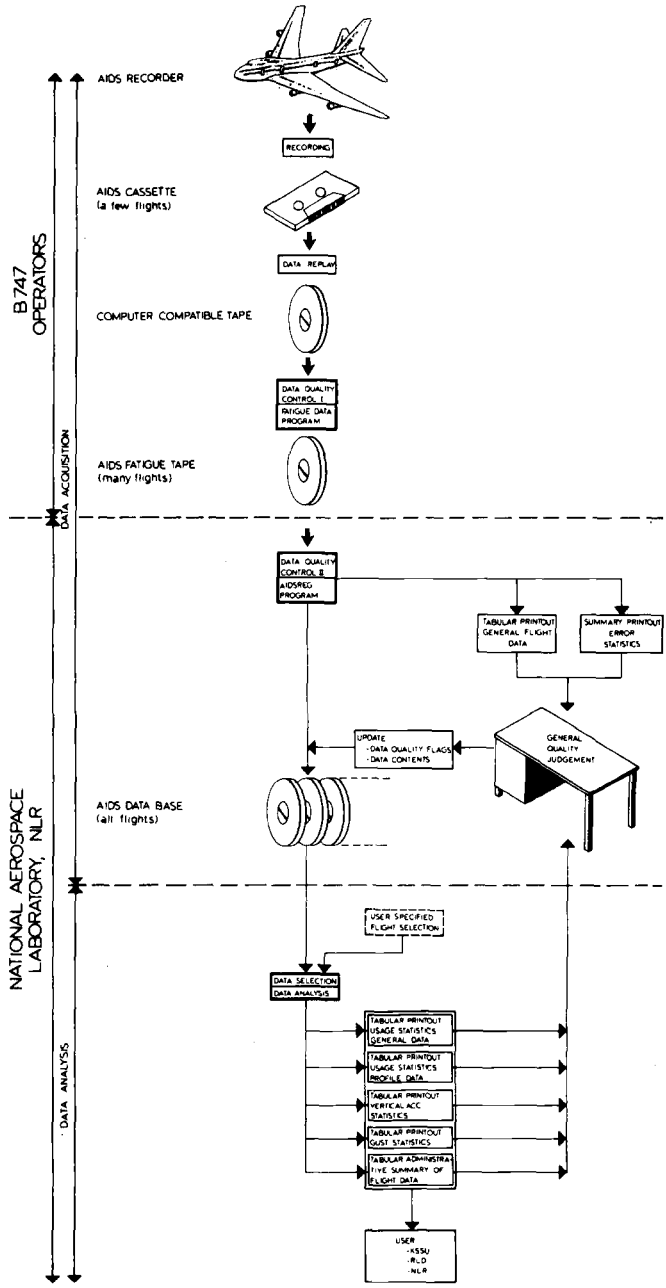

FIG. 2—*Summary of B747 AIDS fatigue data processing.*

Load Data Extraction

The application program used by the KSSU operators for the extraction of load data is called Fatigue Data Program. It was developed by the Swissair Software Group on specifications provided by NLR.

The main features of the applied data extraction procedure may be summarized as follows: (*a*) the AIDS data are analyzed on a flight-by-flight basis. (*b*) each recorded flight is split up in a number of flight segments.

A flight segment ends (and the next one starts): (*a*) if the flight altitude has changed 2000 ft within 400 s (in climb and descent), or (*b*) after 4000 s since the start of a segment (predominantly at cruise altitude).

AIDS recorded acceleration data are searched for peak values (maxima and minima), maintaining a certain range-filter width (see Fig. 3).

Data selected in this way are stored on the AIDS fatigue tape which constitutes the output of the Fatigue Data Program. For a better understanding of the subsequent error-detection procedures, the structure of the AIDS fatigue tape must be explained in some detail.

The data are stored in blocks each consisting of 75 individual data positions. Four different block types are being distinguished:

"100" Block or Begin Block—This block contains documentary data related with the start of the flight, such as take-off weight, time and date of departure, departure airport, etc.

"200" Block or Segment Block—This block contains data describing the flight conditions at the end of a flight segment, plus acceleration peak data related to peaks that occurred during that segment.

"250" Block or Overflow Block—This block type is used as an overflow for acceleration peak data if more than ten acceleration peaks did occur in one flight segment.

"300" Block or End Block—This block contains documentary data related with the end of a flight.

The blocks are recognized by the presence of the figures 100, 200, 250, or 300 at a certain position in the block.

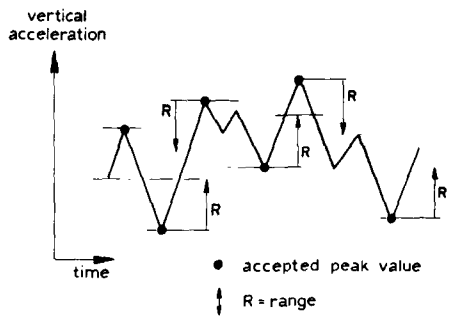

FIG. 3—*Illustration of peak-search with range-filter R.*

Depending on the flight duration, one flight will provide between 8 and 35 data blocks. The complete string of blocks pertaining to one flight must start with a "100" block and end with a "300" block.

Data Quality Assurance

The AIDS fatigue tapes produced by the KSSU operators are sent to NLR for additional processing and final storage.

It should be realized that AIDS recordings will include a certain percentage of erroneous data, either due to recorder malfunctioning or because of sensor failures, inaccuracies, etc. In order to allow a meaningful statistical analysis of AIDS data, it is of vital importance that the reliability of the data be checked and erroneous data deleted.

For this reason, the AIDS fatigue data are subjected to an extensive data quality check. The checking program consists of a large number of error detection tests.

These tests can be divided into two groups, the so-called Blocktests or B-tests and Flighttests or F-tests.

In the B-tests, individual parameter values contained in a block are checked, either on proper value or proper range.

Examples are: (*a*) the parameter value at the block code-data position must be 100, 200, 250, or 300, (*b*) the recorded value for aircraft weight must be between 169 996 and 352 893 kg, and (*c*) the value of the c.g. vertical acceleration must be between -3.2 and $+6$ g.

In the F-tests corresponding quantities in successive data blocks are compared. The tests refer to:

(1) *Proper Sequence of Block-Types*—It may be recalled that a complete flight consists of a "100" block, a number of "200" blocks and possibly "250" blocks, and finally a "300" block.
(2) *Consistency of Variations*—For example the aircraft weight must decrease during flight, time must increase, flight modes like take-off, initial climb and approach/landing must occur in proper sequence.
(3) *Uniqueness*—Sometimes data pertaining to one and the same flight appear more than once on one tape. The checking program memorizes key-data of flights that have been checked.

The data blocks are checked in the same order in which they are read from the AIDS fatigue tapes.

As soon as a "300" block has been tested, it is decided whether the preceding data blocks, starting with a "100" block, do constitute an "accepted" flight.

In principle this is only the case if all these blocks have passed all tests. Exceptions were made for a few tests, where a restoration or limited acceptance was performed:

(1) *Data Restoration and Subsequent Flight Acceptance*—For example, sometimes the take off weight, which has to be entered before the flight by the pilot on the AIDS data entry panel was recorded as zero. Take-off weight can then be estimated from aircraft weight at end of the first flight segment and time elapsed since take off.

(2) *Limited Flight Acceptance*—Sometimes one of the recorded parameters turns out to be continuously erroneous. For example, this happened with the cabin pressure indications of one aircraft. Instead of rejecting all data pertaining to these flights, data may be accepted in a limited sense. A "flag" is added indicating how and where data are incomplete.

Otherwise, occurrence of an error in one data block will result in "flight rejection," that is, rejection of all blocks pertaining to that flight. In the same way, "loose" data blocks are rejected.

Currently, approximately 45 percent of all data offered have to be rejected.

The present data-checking program is rather extensive and it is felt that the accepted flight data are sufficiently accurate to allow a reliable analysis. However, it must be stressed that no computerized checking procedure can ever be foolproof.

A careful survey of all accepted and rejected data by an intelligent human eye remains necessary to detect new error sources and to guarantee the reliability of the accepted data.

Data Storage

As a final step in the data processing procedure the accepted flight load data are rearranged according to a format most suitable for future analysis.

Moreover, some administrative data are added, including: (*a*) a flight identification number, (*b*) a "flag" identification, indicating possible incompleteness of data as described previously, and (*c*) a "level" indication, describing the status of the computer programs used for extracting the load data and for checking the load data.

The data are written on magnetic tapes on a per flight basis, using three types of data arrays. These are: (*a*) the Flight Data Array (FLDA Array), containing basic data pertaining to the flight such as, the date of flight, take-off weight, etc., plus flag and level indications (see Table 1), (*b*) the Segment Data Array (SEDA Array), containing data pertaining to one specific flight segment (see Table 2) (the number of SEDA Arrays pertaining to one flight is equal to the number of segments in that flight), and (*c*) the Peak Data Array (PEDA Array), containing information related to one specific acceleration peak (see Table 3).

The number of PEDA Arrays pertaining to one flight is equal to the number of recorded acceleration peaks.

The ensemble of all accepted flights load data stored at NLR will be further indicated as AIDS-DATA-BASE.

TABLE 1—*Contents FLDA array.*

Item No.	Description	Remarks
1	identification number	
2	A/C number + operator	
3	flight type	...[a]
4	departure/arrival location	
5	flight no.	
6	year/day/GMT	...[b]
7	flight duration	...[c]
8	block time	...[d]
9	take-off weight	
10	end of flight weight	
11	Δn extreme positive	
12	Δn extreme negative	
13	1 g − reference initial/final	
14	turbulence mode envelop	
15	flags/level identification	
16	number of segments	
17	number of peaks	
18	spare	
19	spare	
20	spare	

[a] *Types of flight*— A, scheduled commercial flight—B, charter flight—C, test flight—D, training flight—X, miscellaneous flight.
[b] GMT at activation of AIDS system.
[c] Defined as time elapsed between take-off and touch-down.
[d] Block time defined as time elapsed between AIDS system activation and system shut down.

Analysis of Fatigue Load Data

The data stored in the AIDS-DATA-BASE may be analyzed statistically in a variety of ways, depending upon the specific property of interest. Probably, all that these programs have in common is that the analysis is carried out on data pertaining to groups of flights that are selected from the population of recorded flights, that is, the AIDS-DATA-BASE, using various selection criteria.

The analysis program developed for the Netherlands Civil Aviation Department RLD offers the possibility to apply a wide variety of different selective constraints. The actual program consists of two parts, namely, the "Usage Statistics" part and the "Load Statistics" part. The main features will be briefly described. Details are presented by Spiekhout et al [*1*].[2]

The Usage Statistics Program performs a mission profile analysis. A number of flight duration intervals and altitude intervals are defined. The program counts the number of flights within each duration interval

[2] The italic numbers in brackets refer to the list of references appended to this paper.

TABLE 2—*Contents SEDA array.*

Item No.	Description	Remarks
1	segment number	
2	flight mode	...[a]
3	Δ time	...[b]
4	A/C weight	
5	pressure altitude	at end of segment
6	cabine pressure	
7	true air speed	
8	mach number	
9	number of peaks in segment	
10	spare	
11	spare	

[a] *Flight modes*—1, preflight check—2, engine start—3, taxi—4, take-off—5, climb—6, enroute—7, approach-landing—8, rollout.

[b] Δ time is defined as time elapsed since AIDS system activation.

TABLE 3—*Contents PEDA array.*

Item No.	Description	Remarks
1	segment number	
2	Δn — value of peak	
3	Δ time	see Table 2
4	flap position	
5	left hand spoiler position	at instant of Δn-peak
6	right hand spoiler position	
7	turbulence mode setting	
8	spare	

and calculates for each flight duration the average flight-time, average take-off weight, average fuel consumption plus the standard deviation of these last two quantities. Moreover, the program calculates for each flight duration the average times spent in the various altitude bands plus the average weight, speed, Mach-number, and altitude when flying in these bands.

The Load Statistics program makes an analysis of recorded acceleration peak data. First, recorded peak values are "filtered" according to the "peak between means" counting techniques. Remaining peak values are classified according to magnitude interval and altitude interval.

Additionally, these incremental load factors are reduced to "derived gust velocities," using two different formulas. One is the well-known National Advisory Committee for Aeronautics (NACA) formula [*2*] referring to a "(1 − cos)"-discrete gust. The other factor is based on a power spectrum density PSD gust approach, assuming a rigid aircraft and plunge freedom only, but accounting for finite-span effects and sweep back [*3*].

Analysis Results

On 1 April 1977 the "AIDS-DATA-BASE" contained 2496 accepted flights, covering 12 450 flight hours and a total flight distance of 9 483 706 km. Some additional information is presented in Table 4.

These data were subjected to the previously described analysis program using the following selection of groups of flights:

(1) All flights
(2) KLM-flights only
(3) Swissair flights only
(4) SAS flights only
(5) Flights shorter than 2 h
(6) Flights longer than 2 h but shorter than 5 h
(7) Flights longer than 5 h
(8) Transatlantic flights (from Western Europe to North America or vice versa)
(9) Transatlantic flights in summer (between April 1 and October 1)
(10) Transatlantic flights in winter (between October 1 and April 1)
(11) All flights between Zürich, Basel, and Geneva.

Complete analysis of all these cases together took 1 h and 10 min on the CDC Cyber 72 Computer system of the NLR.

The following discussion of the results of the analysis is intended primarily to illustrate the type of information that may be obtained.

Aircraft Usage

Figure 4 gives a bar-chart of the distribution of flight durations for the three airlines.

It is interesting to note the differences between these three airlines. Both SAS and Swissair fly mainly the transatlantic route plus a specific "domestic" stretch, namely, Stockholm-Copenhagen and Zürich-Geneva, respectively. The KLM 747 network includes flights of intermediate duration, for example to the Middle and Far East and over the American continent.

However, for all three companies the average flight duration is considerably longer than the design assumption of 3.0 h [*4*].

It is clear that for those parts like the pressure cabin, the landing flaps, and the landing gear for which the number of fatigue load cycles is proportional to the number of flights, this implies a considerable reduction in load experience "per hour" as compared to the design assumptions.

Figure 5 illustrates the variation of take-off weight, landing weight, and fuel consumption as a function of flight duration.

The "design usage" considered three "typical" flights with a duration of 1 h (50 percent), 3 h (25 percent), and 7 h (25 percent), respectively.

TABLE 4—*Example of tabular output format: general flight data.*

Run Identification: Date 77/03/11
Time 11.12.27
Run No.

General Heading: ***SUMMARY ALL-FLIGHTS, PERIOD JULY 1974-JAN. 1977***

Usage-Statistics Results, General Data

	Flight Type Legend	Flight Duration Intervals (h)													All Flight Durations
		0.0–0.5	0.5–1	1–1.5	1.5–2	2–3	3–4	4–5	5–6	6–7	7–8	8–9	9–10	>10	
Number of flights of indicated flight type	A	173	266	64	126	81	191	29	121	566	481	253	12	1	2364
	B	2	3	3	8	12	5	2	0	7	7	11	2	0	62
	C	0	0	0	1	0	0	0	0	0	0	0	0	0	1
	D	0	0	2	1	3	1	0	0	0	0	0	0	0	7
	X	1	7	3	4	2	1	1	0	32	6	5	0	0	62
	all	176	276	72	140	98	198	32	121	605	494	269	14	1	2496
Average flight duration (h)		0.44	0.77	1.17	1.71	2.65	3.43	4.56	5.52	6.59	7.55	8.30	9.15	10.08	4.99
Average block time (h)		0.78	1.16	1.57	2.16	3.10	3.89	5.11	5.98	7.10	8.05	8.75	9.59	10.53	5.45
Average tow (× 1000 kg)		220.01	223.15	228.12	227.98	246.60	259.02	277.79	280.87	299.03	309.60	317.34	317.28	327.90	276.83
Standard deviation tow (× 1000 kg)		12.29	20.18	24.04	17.51	13.74	19.18	21.21	15.19	14.65	16.86	17.40	19.37	...	40.18
Average fuel consumption (× 1000 kg)		7.15	10.64	14.38	19.85	30.26	39.26	55.07	61.54	77.23	89.09	98.39	102.90	118.80	58.78
Standard deviation fuel consumption (× 1000 kg)		5.97	6.71	1.70	2.86	5.46	5.05	10.86	5.50	6.30	7.43	7.36	11.27	...	33.70

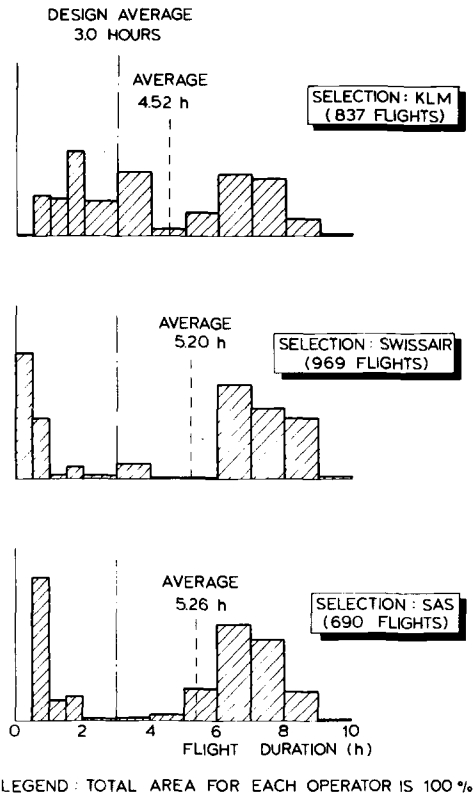

FIG. 4—*Flight duration distribution for different operators.*

As indicated in Fig. 5, the assumed take-off weight and landing weight for these "typical" flights are approximately 15 to 20 000 kg higher than the actually observed values, due to an overestimation of the payload.

Again, the actual usage turns out to be favorable with regard to loading as compared to the design assumptions.

Information concerning the time spent within various altitude bands is depicted in Figs. 6 and 7, respectively.

Figure 6 shows that about 80 percent of all flight-time is spent within the typical cruise band between 10 000 and 13 500 m (30 000 and 40 000 ft); the figure indicates a rather constant rate of climb and descent during the climb and descent phases of flight.

Figure 7 shows that for a wide range of flight durations, say between 1 and 7 h, the time spent below 10 000 m (30 000 ft) is practically constant. For shorter flights there is no "cruise" phase, climb is immediately followed by descent.

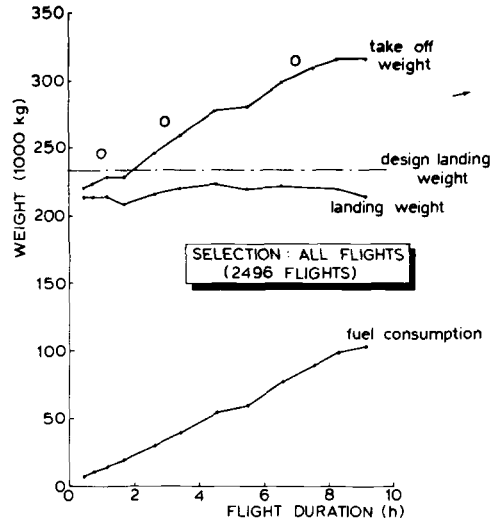

LEGEND: O DESIGN ASSUMPTION FOR 1-, 3- AND 7-HOUR FLIGHT (REF. 4)

FIG. 5—*Take-off weight, landing weight and fuel consumption as a function of flight duration.*

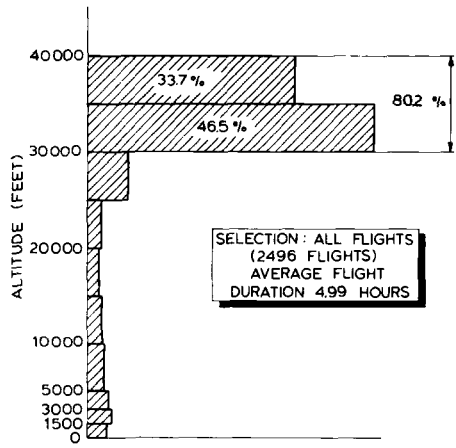

LEGEND: AREA OF ALL BARS IS 100 %

FIG. 6—*Time spent at various altitudes for the average flight duration (1 ft = 0.305 m).*

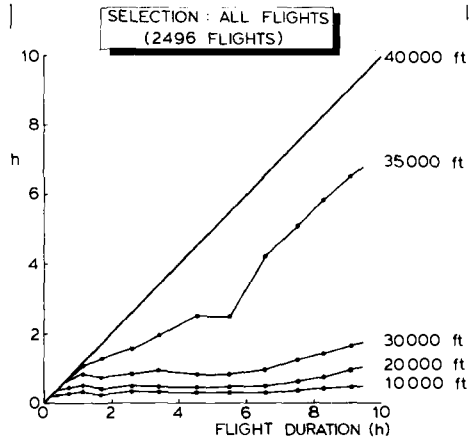

FIG. 7—*Time spent below different altitude levels as function of flight duration (1 ft ≈ 0.305 m).*

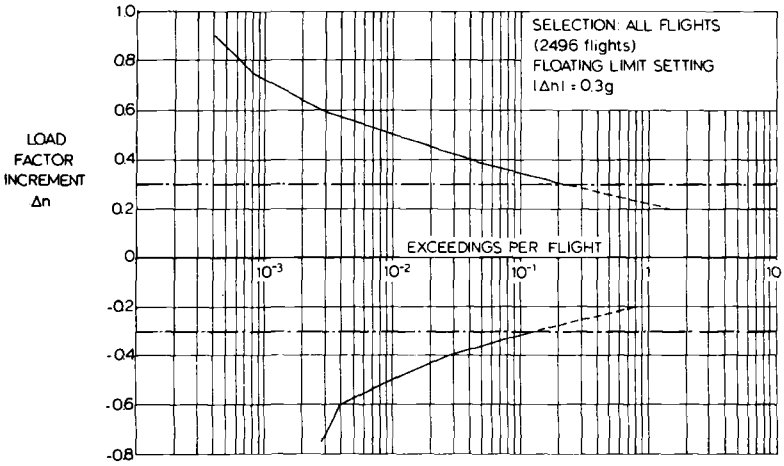

FIG. 8—*Load factor spectrum.*

Load Experience

The load factor spectrum pertaining to all recorded flights is depicted in Fig. 8. It should be kept in mind that because of the "floating limit" of 0.3 g which was maintained in the AIDS system, the spectrum below 0.3 g is unreliable. The floating limit has been recently reduced to 0.18 g.

Figure 9 illustrates how the load peaks encountered are distributed over various altitude bands.

It may be noted that, although about 80 percent of flight time is spent at "cruise altitudes above 10 000 m (30 000 ft), only 17 percent of all

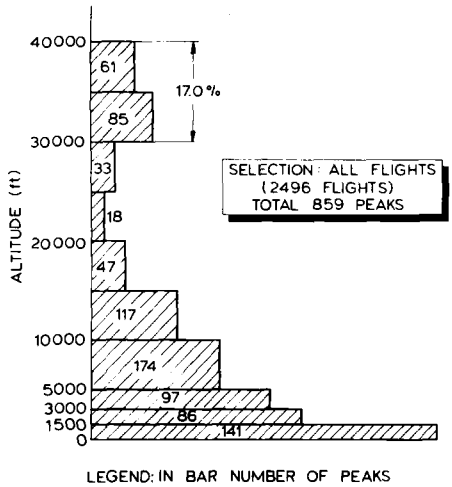

FIG. 9—*Load peaks larger than 0.3 g encountered at various altitudes (1 ft = 0.305 m).*

loads are encountered above that altitude. Considering that, as discussed previously, climb and descent are largely independent of flight duration, one would expect that the load experience per flight tends to increase slightly with flight duration.

Figure 10 shows that this expectation does not come true. Considering the groups of flights with a duration of less than 2 h, between 2 and 5 h and of more than 5 h, respectively, it turns out that the latter group has the lowest load experience.

This effect can be explained partly by differences in weight; the average weight increases with flight duration. One and the same gust gives a smaller Δn on a heavier aircraft.

More important, however, is the influence of route on the loading environment. It should be noted that the flights longer than 5 h consist largely of transatlantic flights, hence overseas flights.

Figure 10 shows that the average load experience of transatlantic flights is 0.278 peaks per flight, whereas flights of the same duration which are not transatlantic experience 0.364 peaks per flight.

To investigate the possible influence of season on load experience, the transatlantic flights were divided into "summerflights" and "winterflights." As shown in Fig. 10, the environment was found to be more severe during the summer period.

Finally, Fig. 10 shows the load experience in flights between Zürich and Geneva. In these very short flights in which an altitude of 7 000 m (20 000 ft) is never reached, the load factor experience is equal to that of a 7-h transatlantic flight.

TABLE 5—*"Derived gust velocity"—experience (discrete "1 − cos" − gust).*

Gust velocity (m/s EAS) / Altitude band	Number of Gusts per N.M. Exceeding Indicated Magnitude													Sample Size, nm
	Downward Gusts							Upward Gusts						
	−11	−9	−7	−5	−4	−3	−2	+2	+3	+4	+5	+7	+9	+11
< 1500 ft	4.7-4[a]	2.3-3	7.8-3	4.0-2	7.8-2	...	...	...	...	1.1-1	8.4-2	1.8-2	3.8-3	1.2-3	14 646
1 500 to 3 000 ft	...	5.4-5	4.9-4	8.4-3	2.3-2	...	...	...	...	3.6-2	1.6-2	1.9-3	3.2-4	...	18 441
3 000 to 5 000 ft	...	8.0-5	2.4-4	2.3-3	7.0-3	1.7-2	...	...	2.7-2	1.5-2	5.4-3	5.6-4	4.0-5	...	24 988
5 000 to 10 000 ft	...	5.2-5	1.0-4	6.6-4	2.1-3	5.6-3	7.8-3	...	7.5-3	3.3-3	1.4-3	2.5-4	...	...	57 208
10 000 to 15 000 ft	...	...	...	1.4-4	3.8-4	1.2-3	2.9-3	3.6-3	2.3-3	7.3-4	3.4-4	3.6-5	...	...	55 840
15 000 to 20 000 ft	...	...	...	...	1.8-4	5.3-4	1.8-3	1.5-3	7.6-4	3.2-4	1.5-4	...	...	...	62 629
20 000 to 25 000 ft	...	...	...	2.6-5	9.0-5	3.5-4	9.2-4	1.1-3	4.2-4	1.0-4	4.1-5	...	...	...	76 853
25 000 to 30 000 ft	...	...	4.4-6	3.1-5	4.8-5	1.5-4	4.4-4	5.1-4	1.1-4	3.1-5	8.8-6	...	...	...	228 116
30 000 to 35 000 ft	...	2.2-6	3.6-6	1.2-5	2.7-5	9.3-5	2.7-4	2.4-4	9.0-5	2.4-5	1.1-5	...	...	...	1 397 700
35 000 to 40 000 ft	...	...	2.0-6	5.3-6	1.7-5	5.5-5	1.6-4	1.2-4	4.1-5	1.0-5	4.7-6	...	...	...	1 504 266

[a] Legend: 4.7-4 means 4.7×10^{-4}. Selection: SAS + KLM (1527 flights). 1 ft = 0.305 m.

FLIGHT GROUP	AVERAGE DURATION (h)	PEAKS
ALL FLIGHTS	4.99	0.344
KLM	4.52	0.346
SWISSAIR	5.20	0.314
SAS	5.26	0.384
< 2 HOURS	0.92	0.413
2 TO 5 HOURS	3.31	0.433
> 5 HOURS	7.15	0.295
TRANSATLANTIC	7.27	0.278
. SUMMER	7.24	0.311
. WINTER	7.29	0.241
> 5 HOURS, NOT TRANSATLANTIC	6.75	0.364
ZURICH-GENEVA	0.47	0.271

FIG. 10—*Number of loadpeaks $\Delta n > 0.3$ g per flight.*

It may be recalled that in the analysis program load factor peaks also are reduced to derived gust velocities. Table 5 illustrates the "discrete gust" distribution derived from the present AIDS-DATA-BASE.

Conclusions

Fatigue related load data may be extracted on a routine-basis from AIDS recordings.

The procedures described in this paper incurred only very limited extra cost and did not require any change in existing AIDS systems.

However, it must be stressed that careful data checking is vitally important in order to guarantee adequate reliability of subsequent data analysis.

Examples illustrated the highly relevant information that may be obtained with regard to aircraft usage and load experience. Moreover, it was shown that the possibility of obtaining very large data samples offers the opportunity to investigate specific influences like the effects of season and geographical location on the loading of aircraft.

Acknowledgments

The authors wish to thank KLM, SAS, and Swissair for their permission to publish the data presented in this paper. The kind permission of the Netherlands Civil Aviation Department RLD to use their programs in preparing this paper is acknowledged also.

References

[*1*] Spiekhout, D. J., de Jonge, J. B., and Keuter, G., "Description of the NLR ANALY Computer Program for the Analysis of B-747 Flight Load Data," *NLR TR 77047 L*, National Aerospace Laboratory.

[2] Pratt, K. G. and Walker, W. G., "A Revised Gust-Load Formula and a Reevaluation of V-G Data Taken on Civil Transport Airplanes from 1933 to 1950," *Report No. 1206,* National Advisory Committee for Aeronautics.

[3] Kaynes, I. W., "Aircraft Center of Gravity Response to Two-Dimensional Spectra of Turbulence," *Aeronautical Research Council R and M 3665,* 1971.

[4] "Boeing 747 Fatigue Integrity Plan," *Document D6-13050-773,* Boeing Aircraft, Feb. 1970.

W. J. Stone,[1] *A. M. Stanley,*[1] *M. J. Tyson,*[1] *and W. H. Kimberly*[1]

Overview of the C-5A Service Loads Recording Program

REFERENCE: Stone, W. J., Stanley, A. M., Tyson, M. J., and Kimberly, W. H., **"Overview of the C-5A Service Loads Recording Program,"** *Service Fatigue Loads Monitoring, Simulation, and Analysis, ASTM STP 671*, P. R. Abelkis and J. M. Potter, Eds., American Society for Testing and Materials, 1979, pp. 67-83.

ABSTRACT: The United States Air Force (USAF) C-5A Service Loads Recording Program (SLRP) was initiated in the early 1970s to acquire in-service data in sufficient quantity to define the operational environment of an "average" C-5A and to develop repeated loads (stress) spectra for applications in loads and fatigue analyses. Instrumentation was installed on 26 airplanes to record up to 53 different data parameters on magnetic tape by means of the C-5A MADARS recorder. Over 9000 h of usable operational data were acquired in the course of the program. Using these measured data along with current analytical data for wing stresses, airplane vertical acceleration, and other responses, analyses were conducted for 13 different load sources. The results were new criteria and modified analytical wing loads which were used in the design phase of the C-5A Wing Modification Program and in the updating of service life predictions made by the C-5A Individual Aircraft Service Life Monitoring Program.

KEY WORDS: airplanes, data recording, service life, fatigue tests

Nomenclature

ASIP	Aircraft Structural Integrity Program
CDB	Central data bank
CMA	Central multiplexer adapter
CSU	Control and sequencer unit
DAE	Data analysis and evaluation
D/COMP	Digital computer
IASLMP	Individual Aircraft Service Life Monitoring Program
MADARS	Malfunction Detection, Analysis, and Recording Subsystem
MDR	Maintenance data recorder
OC-ALC	Oklahoma City Air Logistics Center

[1] Aircraft development engineer specialist, structures engineer, structures engineer, and aircraft development engineer specialist, respectively, Lockheed-Georgia Co., Marietta, Ga. 30063.

SAR-A Signal acquisition remote—automatic
SC/M Signal conditioner/multiplexer
SLRP Service Loads Recording Program

As a result of structural fatigue problems that developed on first-line USAF airplanes in the late 1950s, the Air Force established general requirements for a Structural Integrity Program to ensure adequate service life of future aircraft. These requirements concerned primarily the fatigue characteristics of structures [*1*].[2] As a result of an intensive review in 1961 by engineering and weapons systems personnel of Aeronautical Systems Divisions, the program requirements were expanded to cover the entire structural integrity effort, that is, strength in addition to service life [*2*]. These requirements were consolidated into five phases as follows: I, Design Information; II, Initial Design Analysis; III, Testing; IV, Final Structural Integrity Analysis; and V, Actual Operational Usage. In 1968, Technical Report ASD-TR-66-57 was issued to update and clarify further the requirements of the Aircraft Structural Integrity Program (ASIP). This report added a sixth phase, Inspections, to ensure that periodic and as-needed special inspections are conducted. This six-phase program, in addressing airplane requirements, is described in Ref *3* as "a systematic procedure applied to a particular airplane system to enhance design, diagnose potential or impending failure, provide a basis for corrective action, and predict operational life expectancy of the airframe." Additional information on the airplane requirements of the ASIP can be found in Refs *4* and *5*.

As diagrammed in Fig. 1, the requirements for a Service Loads Recording Program (SLRP) are covered in the Operational Loads Recording Program in Phase V. According to Ref *3*, the objective of SLRP is "to provide loads spectra of operational airborne and ground loading experience on all the major structural components of the airplane." The SLRP and a follow-on program, Life History Recording Program, have been implemented to gather information on structural loads encountered by operational C-5A airplanes. This information forms the basis for the establishment or reevaluation of fatigue spectra, service life expectancy, inspection schedules, modification and maintenance schedules, new mission techniques, and operational limitations. The resulting operational data also are available for the development of improved structural design criteria for future cargo-type aircraft.

C-5A Service Loads Recording Program

Planning and preliminary discussions between the Lockheed-Georgia Company and the C-5A System Program Office for the purpose of imple-

[2]The italic numbers in brackets refer to the list of references appended to this paper.

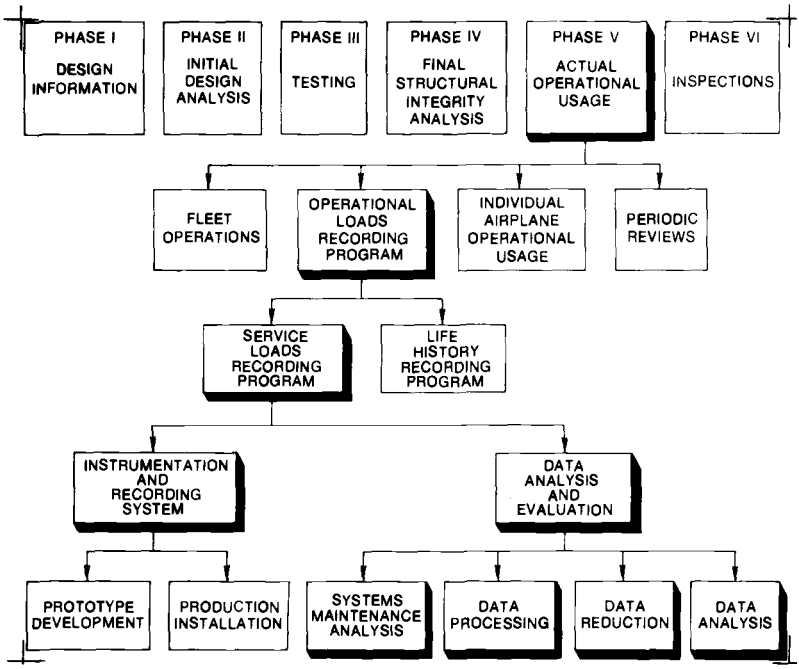

FIG. 1—*Relationship of SLRP elements to ASIP Phase V.*

menting the C-5A SLRP were initiated in the late 1960s shortly after the first flight. Based on consideration of many factors including quantity of data required and time table for data acquisition, it was decided that 26 C-5A airplanes would be instrumented for the SLRP. As illustrated in Fig. 1, there were essentially two phases in the development of this program. The first phase involved defining the instrumentation requirements, designing the system to meet those requirements, flight testing and development of a prototype system on one airplane and finally, the procurement and installation of "SLRP Kits" on the 26 airplanes. These kits consisted of basic instrumentation (transducers, wiring, etc.) and electronic components for the modification of the onboard C-5A Malfunction Detection, Analysis, and Recording Subsystem (MADARS) to record SLRP data. The second phase of SLRP, referred to as Data Analysis and Evaluation (DAE), involved the development of procedures and digital computer programs to operate on the recorded data followed by the actual work of processing, reducing, and analyzing the data. Goals of the DAE were the establishment of environmental descriptions for an "average C-5A," the evaluation of assumptions and criteria currently in use in analytical load/stress calculation methods, and the verification of airplane operating techniques as related to design and parametric loads considerations.

The data and information resulting from SLRP analyses were used to

refine analytical loads and criteria contained in the C-5A Parametric and Service Missions Fatigue Analysis, a program of Phase IV of the ASIP. In updating these analytical loads and criteria, SLRP ultimately improved the fatigue life calculations of each C-5A by means of the Individual Aircraft Service Life Monitoring Program, an ASIP Phase V program which continuously tracks the service life of each airplane.

This paper presents the highlights of the DAE phase of SLRP including a brief description of the onboard data recording system.

SLRP Data Recording System

The system utilized in the C-5A SLRP to record operational data is a modified version of the Lockheed-Georgia Company designed MADARS which is installed on all C-5A airplanes. The purpose of MADARS, by design, is to assist flight crews and ground crews in inspecting the operational characteristics of airplane line replaceable units and systems for either degradation of performance or failure while inflight or on the ground. Some key features of the system are data compression, large data storage capacity, automatic system self-test and malfunction reporting, recording resolution and sampling revisions by onboard computer program changes, plug-in type signal conditioning, and flexibility in modification of ground data computer programs. Upon modification for SLRP applications, the MADARS continued to perform its primary function (that is, malfunction detection and analysis) while simultaneously recording the additional data required for SLRP. The modifications consisted of hardware and software additions and revisions which resulted in increased capabilities in terms of signal sensing, conditioning and multiplexing, digitizing, sampling, formatting, buffering, and recording speed.

Principle of Operation

Figure 2 illustrates the functional relationships of the component parts of the SLRP data acquisition/recording system. As seen in this diagram, analog signals are input to the signal acquisition remote-automatic (SAR-A) and signal conditioner/multiplexer (SC/M). In these units the raw signals are filtered, amplified, and multiplexed. The SAR-A, capable of handling 32 channels of information, is a standard component of the MADARS. The SC/M, a 64-channel unit with two outputs, is an add-on unit to the basic MADARS designed to handle the additional signals required by SLRP.

The conditioned signals next enter the central multiplexer adapter (CMA), a unit that functions as a central point for transfer of information from the SAR-As and the SC/M to the recorder. The CMA interrogates or samples the conditioned analog signals according to an order or sequence

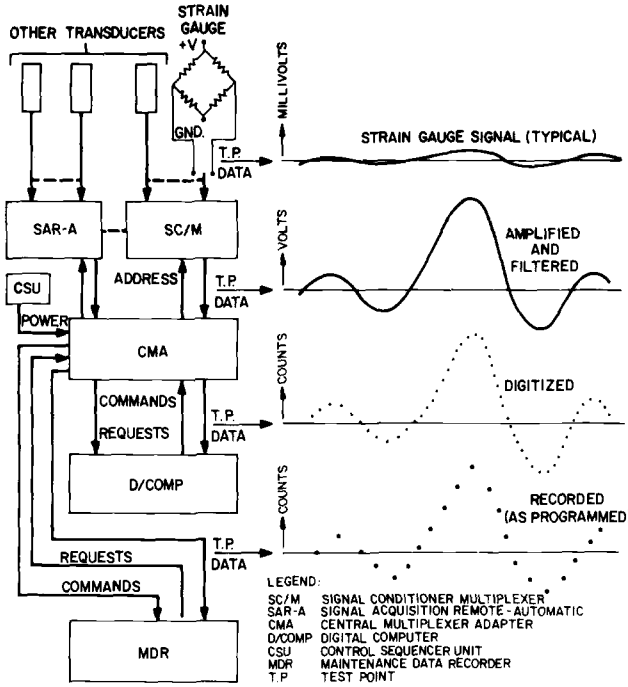

FIG. 2—*Schematic of C-5A SLRP data recording system.*

controlled by a digital computer (D/COMP). The number of times per second that a particular channel is sampled is called the sample rate; typical values are 1, 2, 5, 10, or 20. In the process of data sampling, the instantaneous analog voltage of the sampled data channel is digitized and compared to the last recorded value of the same channel. If the new value differs from its previous recording by as much as a specified "resolution" value, then the new value and its corresponding time of occurrence are recorded; otherwise, it is not recorded. This data sampling concept is often called a "moving window" recording technique. The unique benefit of this system is, of course, data compression; that is, large quantities of relatively constant data are reduced to a very few recordings. Typically, one standard 2400-ft magnetic tape can contain the information from about 30 h of airplane operations.

The digital computer is a general purpose, internally programmed, single address, fixed point fractional binary arithmetic machine. It utilizes a random access magnetic core memory and parallel transfer techniques. As modified for the SLRP, it has a 16 384 28-bit word core memory capacity. Data required to program the computer are stored on two punched mylar tapes known as the data (or parameter) tape and the program tape. The data tape is peculiar to a particular airplane in that it contains unique

routines and constants for that airplane alone, including SLRP test point selection schedule, data channel sampling rate, recording resolution, and fault isolation logic. The program tape, applicable to all C-5A aircraft, contains generalized software routines including logic for data sampling.

The computer contains two buffers that act as temporary data storage devices. The purpose of the smaller buffer, which has a 280-word capacity, is to hold all SLRP-generated messages as they are acquired during sequential twentieths of a second and then transfer the formatted messages to the larger buffer during the course of the second. This second buffer, which has a 4000-word capacity, receives all recordable messages during each second and temporarily stores them until commanded by the CMA to transfer the messages to the recorder. Since the maximum effective recording rate for the recorder is about 47 messages per second, it often happens that the data acquisition rate exceeds the recording rate capability of the recorder. In periods of high activity when this occurs, that is, acquisition rate exceeds recording rate capability, the larger buffer begins accumulating data. In periods of lesser activity, when the acquisition rate is less than the maximum recording rate, any accumulation of messages will begin decreasing. Under ideal circumstances all messages entering the recorder buffer would be recorded on tape with effectively no accumulation within the buffer. As illustrated in Fig. 2, the digital computer interfaces with the CMA for test point data acquisition from the signal conditioning units and with the recorder for output of processed data.

The maintenance data recorder (MDR) is an incremental digital seven-track magnetic tape recorder that writes test point data onto magnetic tape for later playback on a compatible magnetic tape transport. Data are recorded at a SLRP-boosted rate of 400 steps (or characters) per second. The 2400-ft tape utilized by the recorder is contained in cassette form for ease of loading.

The control and sequencer unit (CSU) provides a manual interface between the automatic portion of MADARS and the operator. Push-button controls are used for functions such as power on/off, clock time update, or test point interrogation for visual monitoring of signal performance on an oscilloscope, the printout unit, or both.

Data Measurements

The implementation of SLRP required not only the modification of the MADARS, but also the specification/design, acquisition, and installation of numerous transducers and associated wiring to transmit data measurements to the signal conditioning units. A list of SLRP data parameters (channels) is presented in Fig. 3 with a sketch of the C-5A showing approximate sensor locations. These data parameters were selected so as to define airplane configuration, flight and ground operating conditions, certain air-

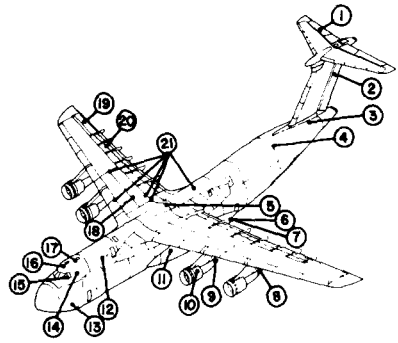

MOTION PARAMETERS:
- (5)- VERTICAL ACCELERATION, FS 1383
- (5)- LATERAL ACCELERATION, FS 1383
- (3)- LATERAL ACCELERATION, FS 2494
- (12)- PITCH ACCELERATION

CONTROL SURFACE PARAMETERS:
- (1)- RIGHT OUTBOARD ELEVATOR
- (2)- UPPER RUDDER
- (19)- RIGHT AILERON
- (20)- FLAPS

DISCRETE EVENT PARAMETERS:
- (4)- AIR DROP
- (6)- TAKEOFF/LANDING
- (8)- OUTBOARD THRUST REVERSER
- (9)- INBOARD THRUST REVERSER
- (14)- TERRAIN FOLLOWING
- (15)- PITCH AUTOPILOT ENGAGEMENT
- (16)- AERIAL REFUELING
- (17)- KNEELINGS
- (18)- GROUND SPOILER ACTUATION

DOCUMENTARY PARAMETERS:
- (7)- GROUND SPEED
- (12)- MACH NUMBER
- (12)- ALTITUDE
- (12)- RADAR ALTITUDE
- (16)- FUEL WEIGHT

STRESS PARAMETERS:
- (21)- RIGHT WING, 6 LOCATIONS
- (21)- AFT FUSELAGE

LANDING GEAR VERTICAL LOADS:
- (6)&(11)- 4 MAIN GEAR
- (13)- NOSE GEAR

LANDING GEAR TURN ANGLES:
- (6)- LEFT AFT MAIN GEAR
- (13)- NOSE GEAR

PROPULSION PARAMETERS:
- (10)- 4 ENGINE PRESSURE RATIOS
- (10)- 4 ENGINE COMPRESSOR SPEEDS
- (10)- 4 ENGINE FUEL FLOW RATES

FIG. 3—*C-5A SLRP instrumentation.*

plane rigid body motions, key control surface deflections, landing gear angles, and either landing gear vertical loads (on 13 of the 26 airplanes) or wing and fuselage stresses (other 13 airplanes). Reference *6* describes the instrumentation verification tests.

Organization of Data Analysis and Evaluation Phase

To define requirements and develop necessary procedures and computer programs, this phase of SLRP was organized into four distinct efforts: systems analysis/maintenance, data processing, data reduction, and data analysis. As their names imply, these functions were directed toward maintaining instrumentation and the recording system, testing and organizing the data, reducing it to the significant points needed for analysis, and finally performing the analyses and reporting the results for application in other ASIP programs. These four areas of work are briefly described as follows.

Systems Analysis/Maintenance

The purpose of this function was to maintain the C-5A SLRP instrumentation and data recording system so that a maximum amount of usable data could be acquired during the programs. Responsibilities for maintaining the system were divided between the U. S. Air Force and the Lockheed-Georgia Company. Lockheed, having designed and installed the recording system, was designated to investigate data problems and determine their most expeditious solution. Specific responsibilities of Lockheed were the development of computer programs and procedures for identifying instrumentation related problems in the data, periodic acquisition and evaluation of representative data from each SLRP airplane, and identification of maintenance procedures to the U. S. Air Force to fix airplane hardware/software as required to correct data problems. Air Force maintenance personnel were responsible for performing the required maintenance. As a result of this cooperation, data acquisition was very successful.

In the course of this work, a number of computer programs were developed and transferred, for operation, to the computer facilities at the Oklahoma City Air Logistics Center (OC-ALC). These programs could be activated, however, by inputs on the U.S. Air Force's ground processing system computer terminal installed at Lockheed. Using this terminal, Lockheed engineers acquired data periodically for each SLRP airplane, analyzed the data for indications of system malfunctions, and transmitted maintenance action requests to the Air Force by means of the computer terminal. This manual inspection of data was supported by the investigative features of the MADARS itself as it systematically interrogated its own components for proper functioning. Data identifying specific malfunctions were recorded automatically on the MDR tape and also on the onboard printout unit, which provided an immediate hard copy record for the airplane crew. In the normal routine of processing the computer tapes, programs at the OC-ALC facility generated maintenance action requests which were automatically sent to Air Force maintenance organizations for implementation. Lockheed tracked each maintenance action required and inspected data continually to determine whether the action had been completed and the malfunction corrected.

Data Processing

The data processing function is concerned primarily with the acquisition of recorded data, the determination of its completeness and quality, and the elimination of spurious recordings that could detract from the final analyses. To this end, data processing was organized into four distinctive operations: data extraction, editing, correlation, and monitoring. Figures 4 and 5 illustrate the flow of data to and through data processing operations.

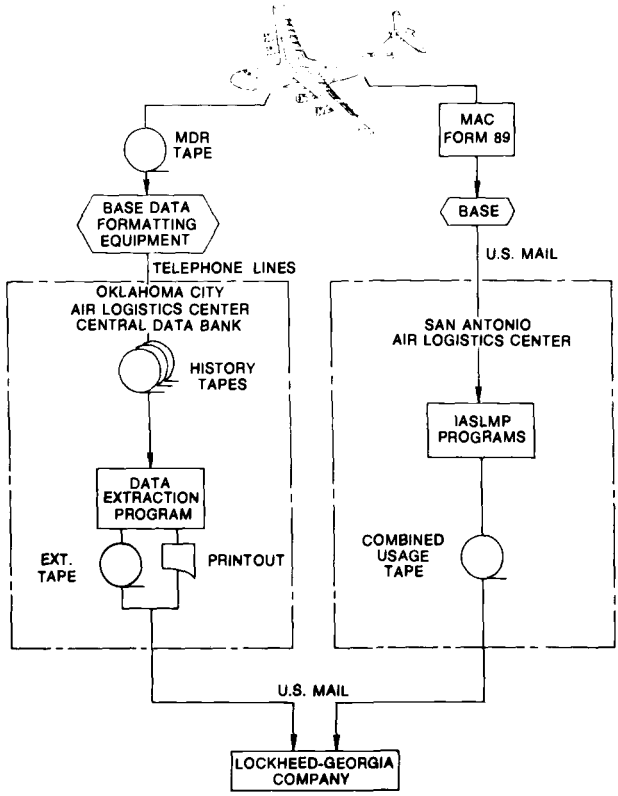

FIG. 4—*Data flow from airplane to contractor.*

Data extraction, Fig. 4, was concerned with the acquisition of recorded data. As illustrated in this figure, two forms of data are recorded onboard the airplane during each flight: MDR tape and a MAC Form 89. The MDR tape, when full, is removed from the airplane and processed through data formatting equipment at the C-5A bases which transmit the data by means of telephone lines to the central data bank (CDB) at OC-ALC to be merged onto files called "history tapes" containing similar data from other C-5As. These history tapes are maintained in the data bank awaiting computer operations that extract data needed for the SLRP or other applications. A Lockheed-developed computer program, transferred to OC-ALC for the purpose of extracting potentially usable data onto magnetic tapes, was operated against every C-5A history tape generated during the SLRP period. This program searched for SLRP airplane recordings, separated data into logical flights (missions), accepted only "whole flights," applied validity checks to key data channels, and checked for operational SC/Ms. If all checks were satisfactory, the SLRP flight was extracted onto magnetic

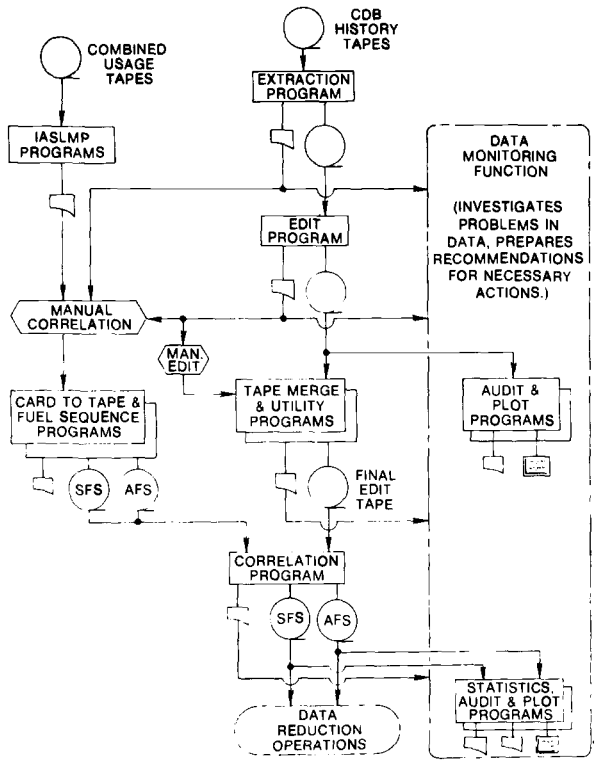

FIG. 5—*Data processing operations.*

tape. Approximately 25 extracted flights could be merged together on a single tape prior to transmittal to Lockheed.

The second type of data, the MAC Form 89, is a handwritten form prepared by the flight crew which basically defines the ground and flight operations of each mission in terms of time, fuel weight, cargo weight, Mach number, altitude, and occurrences of particular events such as touch-and-go landings. The MAC Form 89s are accumulated at each home base and mailed periodically to the San Antonio Air Logistics Center for sorting, editing, and transfer to magnetic tape. The resulting tapes, "C-5A Combined Usage Tapes," are mailed to the Lockheed-Georgia Company for use in the SLRP and in subsequent fatigue damage calculations for individual airplanes.

The primary purpose of data editing is to detect and eliminate spurious recordings found on the extracted tapes. As shown in Fig. 5, editing is accomplished in two stages: automatically by comprehensive tests within a computer program, and manually by engineering review of detailed areas of data pinpointed by the computer. In addition to checking for errors in the recorded data, the edit computer program generates a flight segment profile listing the start time of successive ground and air segments (for

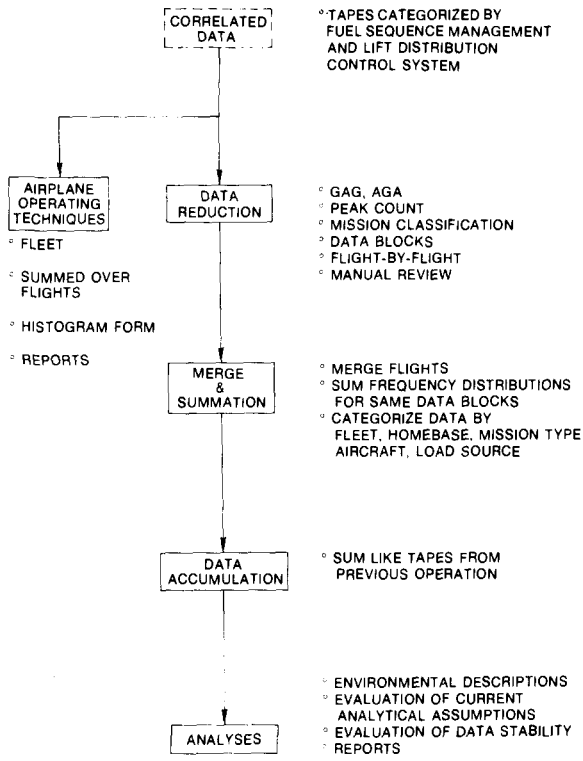

FIG. 6—*Data reduction and analyses operations.*

example, taxi, takeoff, traffic, climb, etc.). This flight profile serves as a road map to subsequent computer operations. On the edited tape, data values and their time of occurrence are output by channel and in chronological order in proper engineering units. If manual edit procedures indicate the need to eliminate a marginal channel previously passed by the edit program, provision is made in a utility computer program to make such alterations on the edit tape.

Data correlation, as shown in Fig. 5, is performed by matching the MADARS recorded flight with its proper MAC Form 89 recorded flight. The match is accomplished manually based on airplane serial number, flight log number, date of takeoff, length of flight, characteristics of the mission, and sometimes the number and timing of multiple touch-and-go landings. This procedure resulted in correlating 99.7 percent of all flights passed by the edit operations. Further computer operations resulted in adding the combined usage (that is, MAC Form 89) data to its corresponding MADARS flight and separating these data onto two different tapes according to whether the mission had been flown by the standard fuel sequence or alternate fuel sequence management procedures. Data

were maintained in these fuel categories through subsequent reduction and analysis operations.

The data monitoring function consisted of in-depth investigations of extracted, edited, or correlated data using any of a number of "audit" type computer programs designed to produce plotted time histories or statistical charts and tables which aid in the evaluation of specific data points or whole areas of multiple-channel recordings. This monitoring effort is brought into play at any time that data become suspect. The end result can be recommendations for the deletion or acceptance of data, or even the modification of hardware or software.

Data Reduction

The purpose of this function was to reduce the many recorded values found on the correlated tapes to the fewer points pertinent to the required analyses. In accomplishing this, reduction took two approaches. The primary effort was directed toward peak counting the motion, loads, stress and control surface data time histories. Peak counting was performed using a mean crossing peak count technique which counted only the single largest peak between each crossing of a threshold constructed on either side of a local mean value. The raw peaks were adjusted by adding an incremental value equivalent to half the recording resolution of the channel to account for the fact that the sampling technique did not always pick up the true peak value. Adjusted peaks were accumulated in magnitude bands (16 to 26 bands per channel) spanning the range of the channel and output on computer tape as frequency distributions. Each frequency distribution was identified by a code number called the "data block" which identified the range of conditions in which the airplane was operating at the time the peak was recorded. A total of 16 242 different data blocks were used to define the measured data. Considering the number of peak counted data channels, number of bands per channel, and number of data blocks, a simple computation shows that an individual peak could be put into any one of more than 6 million different data slots during reduction operations. For the purpose of computing analytical spectra to be compared with the measured spectra, the increment of time during which the data were peak counted also was determined for each frequency distribution. As depicted in Fig. 6, further computer operations summed the frequency distributions over flights, ultimately combining them to form cumulative exceedance (peak or cycle) spectra categorized by data channel, airplane, home base, fleet, mission type, and load source. These spectra were output on computer tape for use in analysis operations. In addition to peak counting, provision was made to extract data applicable to the definition of the mean-to-mean and peak-to-peak cycles of the ground-air-ground and air-ground-air load sources.

The second area of data reduction work was concerned with the extraction and organization of operational data to support studies aimed at evaluating various analytical criteria and verifying typical C-5A operating techniques. For these purposes, data were obtained for eight categories: turning, inflight thrust reverser usage, landing gear movements, air-ground-air cycles, takeoff, landing impact, landing rollout, and flap movement.

Data Analyses

The analysis phase of the SLRP has as major objectives the evaluation of current C-5A environmental descriptions/criteria, assumptions, and analytical methods, the development or derivation of new criteria and methods as required, and the evaluation of the statistical stability of the recorded data. The analyses were organized and performed on a load source basis for gust, maneuver, ground-air-ground, air-ground-air, aerial refueling, taxi, takeoff, landing impact, landing rollout, touch-and-go roll, turning, braking, and alignment. Where applicable, analytical exceedance spectra were calculated and compared with measured spectra as illustrated in Fig. 7. Where significant differences were noted, investigations were undertaken to determine the reason and if necessary, derive new criteria or methods of analysis. The results of these analyses are reported in Ref *7*.

Program Scope

Data Statistics

Data were collected over a period of 40 months of C-5A operations during which 43 459 h were logged on the SLRP C-5As. Of that total, a large percent of the data were not extractable for one reason or another. One study of a 6-month period of data recorded in 1974–1975 revealed that data for approximately 40 percent of all flights made during that timespan could not be located in the CDB. The data were not recorded or were lost during the transmission from base to CDB or were lost in CDB operations. In any event, a substantial number of flights were unavailable for extraction. Other flights failed extraction criteria on the basis of missing or faulty "key" data parameters, an inoperable SC/M, or missing takeoff or landing. In spite of these losses, a total of 11 948 h of data were extracted during the program. This represents a data yield of 27.5 percent based on flights "flown," approximately 46 percent based on flights available in the CDB. This is considered excellent for an operational data recorder program. Statistics for the 13 strain gage instrumented airplanes show that from a relatively low figure of 20 percent for the first 6 months of the program, the data yield (based on flights "flown") increased steadily until during the last 9 months the average data yield per airplane was 50 percent with

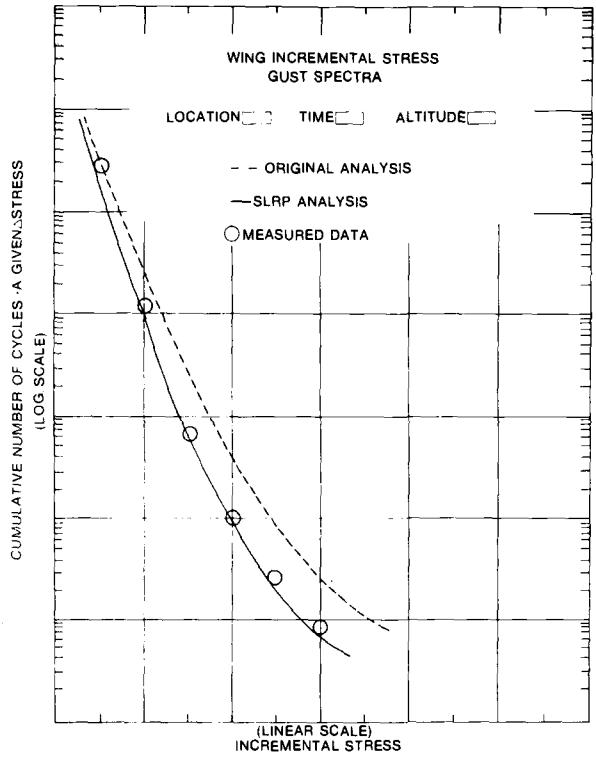

FIG. 7—*Typical format of spectra comparisons.*

2 airplanes reporting 70 percent or better. This steady increase in performance is attributable to improvements in maintaining the instrumentation system coupled with increasing experience in detecting problems. Of the 11 948 h extracted, approximately 24 percent failed edit checks or was deleted in peak count operations because of inactivity, that is, the airplane was not moving. The remaining 9104 h of data constituted the database for final analyses.

While 9104 h of data would appear to be a great quantity of data, one must remember that this "total" must be broken into many parts for analysis. Figure 8 illustrates the problem. In this figure, the total data are divided first according to stress or gear loads airplane groups. Considering only the stress airplane data, note the division into active and passive lift distribution control system configurations which are then subdivided according to standard and alternate fuel sequence management plans. These data are then divided into air and ground parts which, in turn, are divided into load sources and further divided as indicated. Thus, a large quantity of data input to the top of the program becomes a relatively small quantity at the point of analysis. However, this is not to say

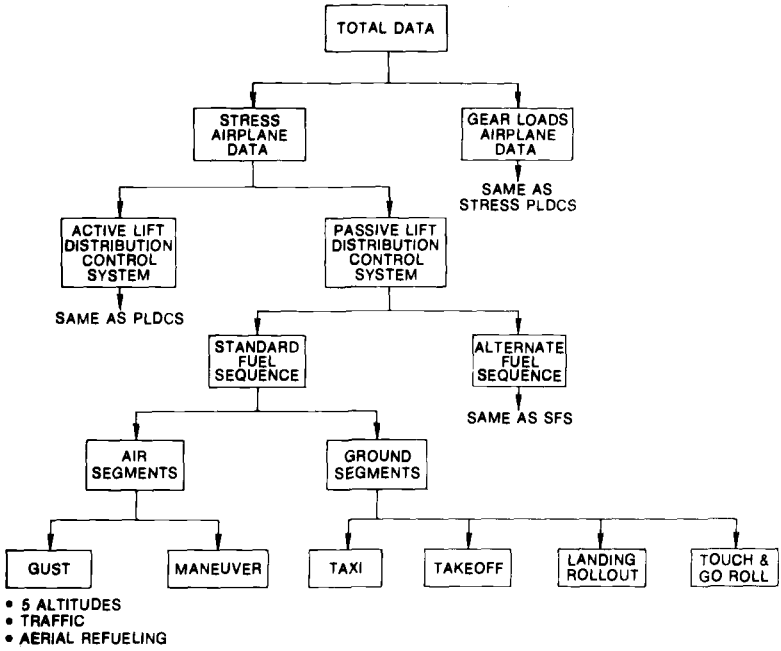

FIG. 8—*Divisions of SLRP data for analysis purposes.*

that the results of SLRP are negated by lack of data. To the contrary, studies of data stability as a function of data quantity indicated that, with minor exceptions, sufficient data were acquired to support valid analyses.

Stress Data

The successful acquisition of a large quantity of measured stress data from 13 operational Air Force airplanes over a period of several years of service is considered one of the outstanding achievements of the SLRP. Considered at first to be little more than an experiment to see what could be obtained, the measurement of stresses became a vital element of the program and contributed greatly to the final analyses. Overall performance of the instrumentation was good. The automatic procedure of comparing measured stresses to analytical stresses for ground and air operations on every mission convincingly demonstrated that measurements from all airplanes were very comparable and, therefore, that the data could be combined legitimately to represent an "average" airplane.

Computer Operations

The 11 948 h of data extracted from the CDB were estimated to com-

prise almost a quarter of a billion individual data recordings. These recordings, in various assortments and formats, were operated upon by an array of computer programs developed during the course of the SLRP. These programs sorted and organized data, produced plots and tables, performed repetitious calculations, made rapid comparative analyses, and in general made the SLRP a viable program. Far from being a push-button operation, however, SLRP required the constant vigil of many engineers in managing the flow of data and in the evaluation of day-to-day results.

Conclusion

The C-5A Service Loads Recording Program successfully accomplished its objectives. As a result of analyses performed with SLRP-measured data and current analytical data, a total of 52 conclusions and recommendations were presented in the final analysis report [*7*]. The environmental criteria and methodology for ground-air-ground, air-ground-air, landing impact, and taxi turning load sources were not changed as a result of SLRP investigations. However, for other load sources, specifically gust (turbulence), maneuver, aerial refueling, taxi, takeoff, landing rollout, braking, and alignment, SLRP did recommend changes in criteria or analysis methodology or both. Many of these recommendations were adopted immediately for use during the design phase of the C-5A Wing Modification Program. The SLRP results also have been incorporated in the most recent update of the service life predictions made by the C-5A Individual Aircraft Service Life Monitoring Program. Finally, the SLRP results will be incorporated in a formal revision of the loads and criteria volume of the C-5A Parametric and Service Missions Fatigue Analysis report [*8*].

As a further testimony to the success of the C-5A SLRP, the C-5A Life History Recording Program has been initiated. This long term operational data recording program, a reduced form of the SLRP, will continue gathering data to detect any changes in SLRP-derived operating environmental descriptions. Should significant changes be found, the SLRP can be reactivated to investigate thoroughly and recommend actions as required.

References

[*1*] "Detail Requirements For Structural Fatigue Certification Programs," *Technical Memorandum WCLS-TM-58-4*, Aircraft Laboratory Directorate of Laboratories, Wright Air Development Center, Air Research and Development Command, U.S. Air Force, June, 1958.

[*2*] Bachman, R. W. and Wells, H. M., Jr., "Detail Requirements and Status Air Force Structural Integrity Program, Part 1: Background and Requirements," Structures and Air Environment Division, Aeronautical Systems Division, Air Force Systems Command, U.S. Air Force, Sept. 1961.

[*3*] Wells, H. M., Jr., and King, T. T., "Air Force Aircraft Structural Integrity Program: Airplane Requirements," *Technical Report ASD-TR-66-57*. Aeronautical Systems Division, Air Force Systems Command, U.S. Air Force, May 1970.

[4] "Aircraft Structural Integrity Program (ASIP)," *AF Regulation 80-13*, Department of the Air Force, June 1969.

[5] "Aircraft Structural Integrity Program, Airplane Requirements," *Military Standard MIL-STD-1530A*(11), Department of Defense, Sept. 1972.

[6] "SLRP Production Recording System Verification Final Report," *Contractor Data Document No. LG1DI-T-3718/T-119-2*, Lockheed-Georgia Company, Marietta, Ga., May 1973.

[7] "C-5A SLRP-DAE Data Analyses Results Report," *Report No. LG1DI-S-3570-4*, Lockheed-Georgia Company, Marietta, Ga., Aug. 1977.

[8] "C-5A Parametric and Service Missions Fatigue Analysis, Volume 2, Loads and Criteria," Lockheed-Georgia Company, Marietta, Ga., May 1973.

D. S. Morcock[1]

Highlights of the C-141 Service Life Monitoring Program

REFERENCE: Morcock, D. S., **"Highlights of the C-141 Service Life Monitoring Program,"** *Service Fatigue Loads Monitoring, Simulation, and Analysis, ASTM STP 671,* P. R. Abelkis and J. M. Potter, Eds., American Society for Testing and Materials, 1979, pp. 84-93.

ABSTRACT: 271 C-141A and 1 YC-141B Lockheed Starlifter cargo transport airplanes are presently in the United States Air Force (USAF) Military Airlift Command (MAC) inventory. The C-141A program includes all elements of the Aircraft Structural Integrity Program (ASIP) defined in Military Standard MIL-STD-1530 (USAF), "Aircraft Structural Integrity Program, Airplane Requirements," 1 Sept. 1972. The purpose of this paper is to present highlights of the C-141A service life monitoring program.

KEY WORDS: service life, monitoring, fatigue mechanics, fracture mechanics, fatigue tests

The C-141A is a long-range logistics transport manufactured by the Lockheed-Georgia Company. Figure 1 shows the configuration of the airplane which features drive-in loading through a full-width rear opening. During the period from 1963-1968, 285 of these airplanes were manufactured. The C-141A has been in continuous service with the United States Air Force (USAF) Military Airlift Command (MAC) providing rapid delivery of military supplies throughout the world.

The C-141A program began in 1961 and subsequently incorporated all elements of the USAF Aircraft Structural Integrity Program (ASIP) requirements. This paper presents highlights of the structural integrity program, with emphasis on the Service Life Monitoring and Life History Recording Program activities.

C-141A Aircraft Structural Integrity Program Description

The original C-141A structural design and verification program conformed to the Air Force Aircraft Structural Integrity Program requirements

[1] A/C development engineer specialist, Lockheed-Georgia Co., Manetta, Ga. 30063.

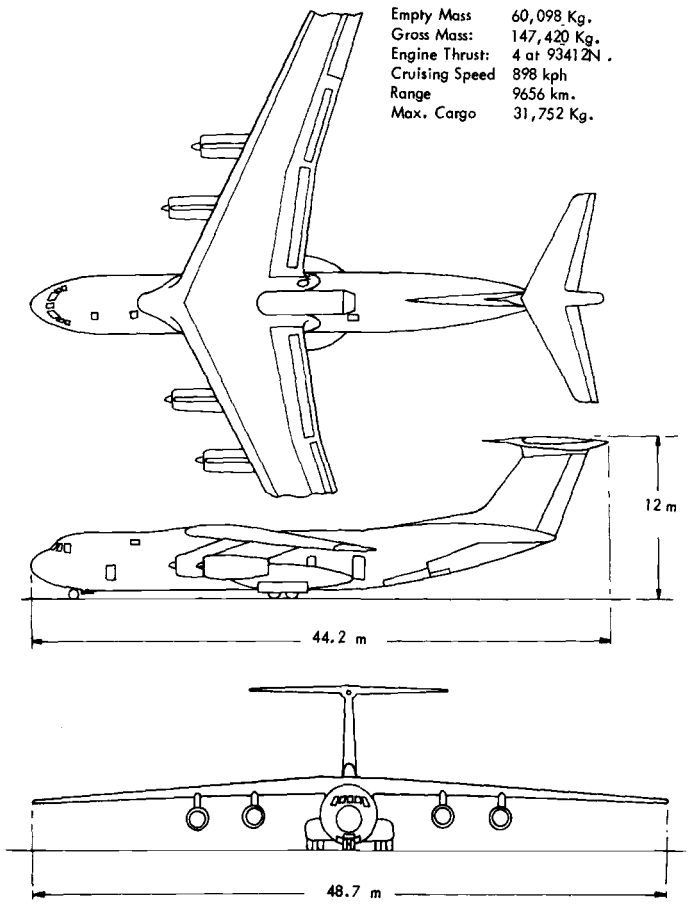

Fig. 1—*C-141 general arrangement.*

which were developed concurrently with the C-141A development. Table 1 shows these requirements. Design changes based on the results of the component tests, full-scale static tests, flight tests, in-service loads data, and early full-scale fatigue tests were incorporated during production or by retrofit modifications to the C-141A. Revisions to the static strength analyses and fatigue analyses, and the development of the Service Life Monitoring Program, also were based on these elements. Fatigue testing of a full-scale wing/fuselage incorporating all the structural and loads changes resulting from tests and 2 years of service experience was begun in late 1969. This test has been updated at intervals to reflect changes in service aircraft usage and criteria and is still in process toward a goal of 130 000 simulated flight hours.

TABLE 1—*USAF aircraft structural integrity program tasks.*

TASK I	TASK II	TASK III	TASK IV	TASK V
Design Information	Design Analysis and Development Tests	Full Scale Testing	Fleet Management Data Package	Fleet Management
ASIP master plan	Material and joint allowables	Static	Final analyses	Loads/environment spectra survey support
Structural design criteria	Analyses:	Damage tolerance	Strength summary	Service monitoring program
Fracture and fatigue control plan	—Loads	Fatigue	Parametric analysis	Service inspection Maintenance and repair
Selection of Materials, processes and joining methods	—Temperature	Sonic fatigue	Instrumentation and data recording provisions	Structural performance records
Planned operational usage	—Stress	Flight and ground loads survey	Service inspection and maintenance control	
	—Damage Tolerance	Flutter		
	—Fatigue	Flight flutter		
	—Sonic Fatigue	Loads environment spectra survey		
	—Vibration			
	—Flutter			
	—Nuclear Weapons Effects			
	—Nonnuclear Weap. Effects			
	—Design Dev. & Preprod. Design Verification Tests			

TABLE 2—*C-141A service life analysis VGH and ground loads data base.*

Time Period	Data		
	Flight, h	Ground, h	Landings
1966	10 671	359	2 861
1968-1969	9 556	751	7 782
1969-1971	6 797	854	6 268
Totals	27 024	1 964	16 911

The service life monitoring program is being updated when needed as indicated by service and test experience or by state-of-the-art changes. A life history recording program is in process, and updating is being considered to obtain more useful output from the program. These activities are discussed in more detail in the following sections.

C-141A Service Life Monitoring Program

The initial data base for the C-141A service life analysis was the projected utilization of the airplane and the analytical and flight test verified loadings. Subsequently, updated service life analyses were performed, utilizing velocity-acceleration-altitude (VGH) and ground loads data obtained from oscillographic recordings on service aircraft. Table 2 summarizes the data base for these analyses. The service life analyses also used information from the individual aircraft flight crew data sheets shown in Fig. 2. Fatigue endurance (flight hours to crack initiation) was estimated at fatigue-susceptible locations on the airframe by combining cyclic stress calculations with standardized coupon fatigue data in accordance with Miner's cumulative damage hypothesis.

The present C-141A Individual Aircraft Service Life Monitoring Program (IASLMP) is based on these data and on the individual flight crew data sheets. Data have been acquired since 1968 for individual flights of each airplane. The crew data sheet information is transcribed optically to magnetic tape and input to a computer program which reduces the usage data into 3204 data blocks based on bands of speed, altitude, cargo weight, fuel weight, and runway roughness. Not all of the total flying hours produce usable data. Therefore, the data are edited and factored quarterly to 100 percent usage, as indicated by a separately compiled MAC Airframe Report which records the number of flight hours, full-stop landings, and total landings for each airplane per quarter. Additional programmed logic is used to classify the flights into 14 previously defined basic missions and determine utilization by base by mission, to compute quarterly and

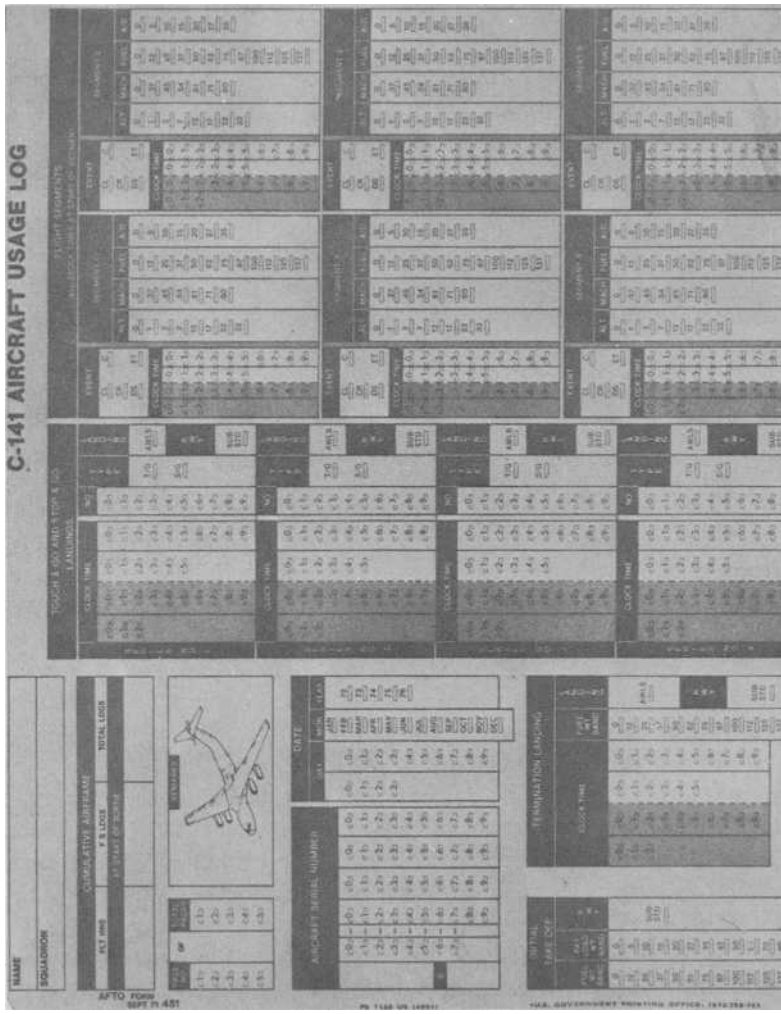

FIG. 2—*USAF flight crew form.*

cumulative analytical fatigue damage for twelve monitor locations per airplane, and to predict the number of months and flight hours to crack initiation. These data are ordered also by number of flight hours, full-stop and total landings, and fatigue damage severity, reviewed statistically, and classified into other forms for future analyses. The data are stored quarterly and cumulatively, and reported for use in the structural integrity program management.

In 1973, the Lockheed-developed IASLMP computer programs were assimilated into the Air Force Aircraft Structural Integrity Management Information System (ASIMIS) center at Oklahoma City Air Logistics Command (OC-ALC). Currently, the data are reduced by ASIMIS and are used by Warner Robins Air Logistics Center (WR-ALC) force management personnel in determining inspection or modification requirements, or both, overall service aircraft status, likely operational usage, and other force management information.

C-141A Life History Recording Program (LHRP)

In addition to the individual airplane tracking activity just described, the structural integrity effort for the C-141 involves a Life History Recording Program (LHRP). The LHRP is regarded as a means of continuously monitoring the actual operational environment and response, so that the corresponding descriptions used in the IASLMP analyses may be kept up to date. The data are measured by onboard recorders which read airplane speed, normal load factor at the center of gravity, altitude (VGH), and strain level as a function of time. Twenty-six C-141A aircraft are instrumented with the Conrac MXU 553/A digital multichannel recorder developed under Air Force sponsorship for use in fighter and cargo/transport aircraft. Twenty parameters, listed in Table 3, are recorded in sequence at a scanning rate of 240 samples per second in a dense format on a 9-track cassette tape having approximately 15 h (four average flights, or almost 5 days) capacity. The cassette tapes are transcribed and reformatted to computer tapes at the Oklahoma City ALC ASIMIS center and then erased and reused. Figure 3 shows the data flow.

The computer tapes obtained from the cassette tapes are input to data reduction computer programs developed and initially checked out by Lockheed. The computer first performs reasonability and completeness checks to see that the data are usable. Figure 4 shows the data reduction process. Acceptable flight parameter data then are processed through logic decisions which sort the information into the same data blocks on which the IASLMP crew data sheet computer programs are based. The remainder of the LHRP computer program is compatible to the IASLMP computer program. Therefore, the output from the LHRP analysis can be compared directly with the output from the IASLMP analysis. This provides a means

TABLE 3—*C-141 LHRP measured parameters.*

Parameter	Samples/s	Range	Units
Pitot static pressure	1	31.02 to 3.42	in. hg.
Pitot total pressure	1	0 to 13.78	in. hg.
Ground Speed	2	0 to 103	knots
Normal acceleration	30	−1 to +4	g
Cabin pressure	1	0 to 9.77	psi
Pitch rate	20	−30 to +30	deg/s
Yaw rate	20	−30 to +30	deg/s
Rudder position	10	72 r to 72 l	deg
Elevator position	10	41 up to 42 down	deg
Flap position	5	16 up to 106 down	percent
Nose gear angle	5	94 r to 93 l	deg
Lateral acceleration	30	−2 to +2	g
Wing joint strain	20	−2147 to +1743	μ in./in.
C.W.S. 53.2 strain	20	−1945 to +1945	μ in./in.
MLG bogie beam strain	20	0 to +3862	μ in./in.
F.S. 1108 stringer strain	20	0 to +1945	μ in./in.
NLG bulkhead strain	10	−307 to +3583	μ in./in.
Landing gear	1	Up or down	...
Landing gear strut	1	Extended or compressed	...
Spoilers	1	Up or down	...

1 in. = 0.0254 m.

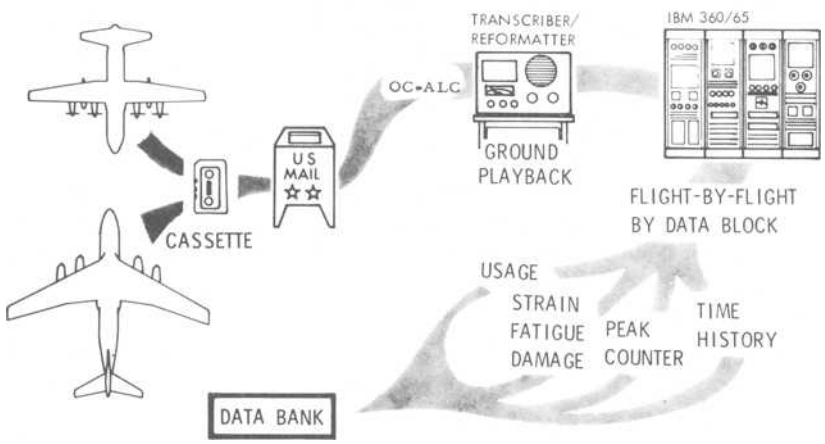

FIG. 3—*C-141/C-130 life history recording program data flow.*

for evaluating the accuracy of the crew data sheet based analyses. The LHRP data also provide a means for detecting any significant changes in the actual operational environment.

The multichannel recorder data include five channels of direct strain readings. These are processed by the data reduction program to output analytical fatigue damage data at five of the IASLMP structural monitoring

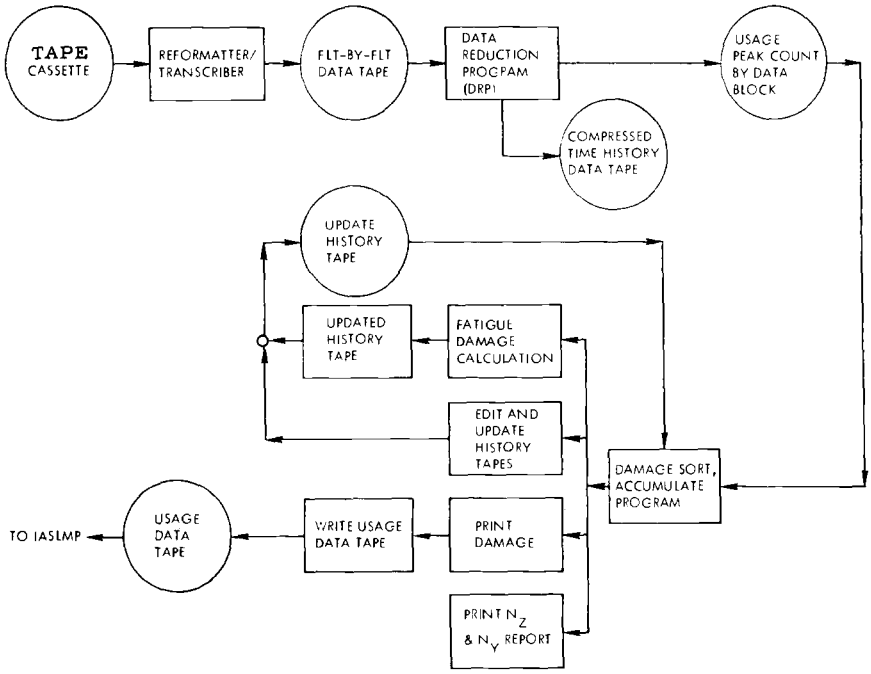

FIG. 4—*C-141A LHRP computer program data flow.*

locations. These data provide an independent evaluation of the IASLMP output.

The multichannel data are processed to provide quarterly and cumulative data for force management and IASLMP output evaluations. Use of the data in many other ways is also possible, such as confirming the flight environment, aircraft response to gusts, maneuvers, and runway roughness, and for data bank benefits of acquiring a statistically large sample of data from C-141A and other aircraft at one (ASIMIS) facility.

State-of-the-Art Changes: Durability and Damage Tolerance Assessment (DADTA)

In mid 1975, a major effort was begun to restudy the C-141A fixed primary structure using crack growth concepts for durability and damage tolerance evaluations. Figure 5 indicates the goals of this assessment. The study was supplemented by nondestructive inspections involving removal of over 4000 fasteners on the full-scale fatigue test airframes and service airplanes. Potential inspection or modification options were defined for the feasible operational goal of 45 000 flight hours which was indicated by the study. The results of this assessment are being used in present and future force management activities.

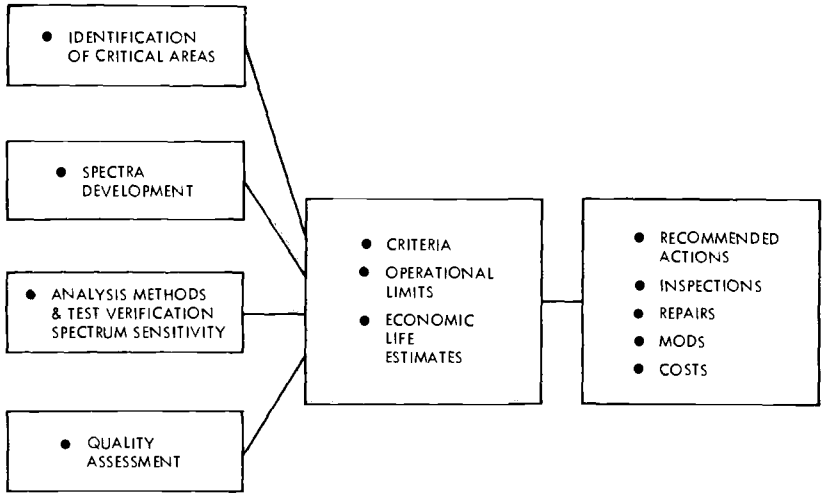

FIG. 5—*C-141A DADTA—assessment tasks.*

Anticipated Future Developments

A number of changes in the C-141 Structural Integrity Program are anticipated. These are summarized in Table 4. A structural modification program to increase the fuselage length by 7.11 m (280 in.) and add aerial refueling capability is expected to begin in 1978. The modification includes a new wing-to-fuselage fairing to improve the lift distribution and reduce drag. The effectiveness of this modification has been verified by flight tests of a prototype "stretched" C-141B. Productivity is increased by 30 to 50 percent for volume-limited missions, increasing the capacity of the C-141 fleet by the equivalent of 90 additional airplanes. Changes to the tracking program to reflect this configuration and the new mission descriptions are anticipated.

Full-scale durability testing of the C-141A continues to provide new information. Updating the IASLMP and LHRP computer programs to reflect

TABLE 4—*C-141 service life monitoring program anticipated developments.*

C-141A	→	C-141B (fuselage stretched)
Block spectrum fatigue test	→	Flight-by-flight durability test[a]
Fatigue analyses	→	Durability and damage tolerance assessment[a]
Fatigue-based individual aircraft tracking program	→	Fracture mechanics based individual aircraft tracking program
Isochronal structural inspection and maintenance	→	Maintenance based on individual aircraft usage?
		Updated inspection procedures (NDI)
		Updated inspection requirements (MSG-2)[a]

[a](Now implemented).

results of the test and of the Durability and Damage Tolerance Assessment and to incorporate crack growth methodology are in process. The inspection requirements are changing as nondestructive inspection methods are improved and as the "airlines type" MSG-2 zonal inspection program is implemented. Also, an operational goal of 45 000 flight hours is now projected rather than the original design goal of 30 000 flight hours. This increases the emphasis to be placed on IASLMP, LHRP, corrosion protection, additional durability testing, and inspection/modification programs.

In summary, the C-141A Service Life Monitoring Program is a dynamic, continual program to translate significant operational factors into cost-effective force management decisions pertaining to maintenance/inspection, timely replacement, and operational readinesss of this military airlifter.

N. E. Ashbaugh[1] *and A. F. Grandt, Jr.*[2]

Evaluation of a Crack-Growth Gage for Monitoring Possible Structural Fatigue-Crack Growth

REFERENCE: Ashbaugh, N. E. and Grandt, A. F., Jr., **"Evaluation of a Crack-Growth Gage for Monitoring Possible Structural Fatigue-Crack Growth,"** *Service Fatigue Loads Monitoring, Simulation, and Analysis, ASTM STP 671,* P. R. Abelkis and J. M. Potter, Eds., American Society for Testing and Materials, 1979, pp. 94-117.

ABSTRACT: The results of an experimental and analytical investigation on the use of a precracked coupon for monitoring the effect of service loads upon fatigue crack growth in a structure are discussed. The precracked coupon or "gage" is a simple device which provides a convenient means for determining the potential damage, that is, crack growth, in a structure since crack extension in the gage is a result of loads on the structure which cause the structural damage. Experimental results are reported for gages made from two aluminum alloys and having two types of crack geometries. These gages contained either a center crack or a single crack at the edge of a hole. The effect of load amplitude upon growth of the crack in the gage as a function of the crack growth in the structure was investigated. All tests were conducted under constant-amplitude cyclic load. The theoretical model is developed to predict the correlation between the growth of the cracks in the gage and in the structure. Two areas of major importance in the analysis are the load transfer from the structure through the ends of the crack gage and the crack-propagation law for the crack growth in the gage and in the structure. Comparison of the analyses and the experimental results is made.

KEY WORDS: crack gage, fatigue crack growth, fracture (materials), fatigue loads, structural damage, fatigue tests

It is well known that members of a group or a fleet of identical structures may be subjected to widely differing load histories during their service life. The service loading may differ from fleet member to fleet member and it may differ from the design spectrum for the structure. Thus, it is often extremely important to track the use of individual structures. The United States Air Force (USAF) has, for example, requirements for a tail-number tracking system of USAF aircraft [*1-3*].[3] The intent of this tracking system

[1] Senior physicist, Systems Research Laboratories, Inc., Dayton, Ohio 45440.

[2] Materials research engineer, Air Force Materials Laboratory, Wright Patterson Air Force Base, Ohio 45433.

[3] The italic numbers in brackets refer to the list of references appended to this paper.

is to measure and record load histories of service aircraft. Then the relative severity of the load histories on potential crack growth must be determined for the individual aircraft. Such requirements are, of course, not new and many techniques have been suggested for monitoring and recording loads—including pilot logs, velocity-acceleration-altitude (VGH) recorders, acoustic emission, and both electrical and mechanical devices for recording strains [*4–7*]. Common to most of these techniques is the need for reducing the information collected into a load history and then performing a crack-growth analysis with the use of conventional fracture-mechanics techniques. Such a procedure for reducing field-collected data to crack-growth response becomes very complicated and cumbersome and involves a considerable expense and introduces possibilities for errors. This paper describes an alternative approach for monitoring and determining the severity of service loads. The term severity connotes a qualitative evaluation of the effect of service loads on the growth of pre-existent cracks which are assumed to be in the structure.

The approach discussed here consists of mounting a pre-cracked coupon onto the structure. Loads induced in the structure will cause the crack in the coupon to grow. It is proposed that this measurable crack growth in the coupon can be related to extension of a structural flaw. The crack-gage concept for tracking fleet loads has been discussed by several authors, both in the context of crack initiation [*8*] and crack growth [*9–11*]. The results of experiments that were designed for the preliminary evaluation of this concept are discussed in the present paper.

Experimental

Many variables are involved in evaluating the potential of the crack gage for determining damage in a structure. In the present study, damage was considered to be the growth of a pre-existing flaw in the structure. This consideration was based upon USAF Document MIL-A-83444 which specifies design and size requirements for assumed pre-existing flaws in an aircraft structure. Some of the variables which apply to the structure and gage are: materials, crack geometry, environment, loading history, manner in which the gage is attached, and location of the gage. For this experimental investigation, the prime objectives were the determination of reproducibility of data obtained from a crack gage and the effects of cyclic-load amplitude upon the relationship between crack length in the structure and that in the gage.

Specimen Configuration and Test Matrix

The structural component was a 5.08-cm (2-in.) wide, 0.61-cm (0.24-in.) nominally thick strip, and the attached gage was 2.54 cm (1 in.) wide and

0.079 cm (0.031 in.) nominally thick having an effective 3.81-cm (1.5-in.) gage length. The test configuration of the gage and structural component and the nominal dimensions are shown in Fig. 1.

The test matrix for the experiments is given in Table 1. Two aluminum alloys were used for the gage—7075-T6 and 2024-T3. Two crack geometries in the gage were investigated—a center-cracked (CC) gage and a single-cracked hole (SCH) in the gage. For the structural component only one material—2219-T851—and an SCH crack geometry was used. Tests 2 and 3 essentially involved duplicate initial crack geometries run at approximately the same load amplitude. In Test 4 the same initial crack geometry was tested at a higher load. Test 1 was run to determine the effects of changing the initial crack lengths. In Tests 6 and 7 a different gage material was used and a different crack geometry investigated.

An adhesive was used to mount the gage onto the structural component. It was decided that bonding the gage onto the structure would be preferable to using rivets, which in a real structure would introduce additional holes and, in turn, could be potential sites for flaws. The choice of adhesive was based upon ease of application, availability, and reliability under laboratory conditions. Four available adhesives were used to attach uncracked gage coupons to the dogbone structure. These trial specimens were tested under conditions similar to those expected for the actual specimens. The ad-

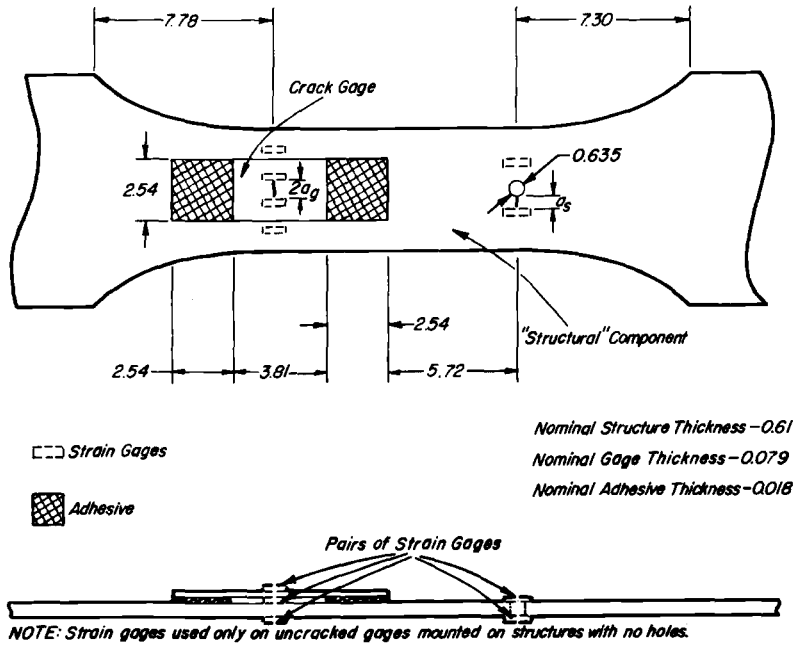

FIG. 1—*Specimen configuration (all dimensions in centimetres).*

TABLE 1—*Crack gage test matrix.*[a]

Test Number	Gage		Initial Crack Lengths		Maximum Nominal Structural Stress,[c] MPa
	Material	Crack Geometry[b]	Gage, mm	Structure, mm	
1	7075-T6	CC	8.92	6.35	103
2	7075-T6	CC	5.08	1.27	105
3	7075-T6	CC	5.03	1.40	103
4	7075-T6	CC	5.08	1.30	138
6	2024-T3	SCH (3.18)	0.18	0.36	183
7	2024-T3	CC	15.7	1.32	103

[a]All structural material was 2219-T851 with SCH (6.35) except Test 6 with SCH (7.94).
[b]Center crack indicated by CC. Single-cracked hole indicated by SCH with hole diameter (in millimetres) given in parentheses.
[c]$R = 0.1$

hesive which provided the most reliable bonding in laboratory usage and which was employed subsequently for all test specimens was Hysol Aerospace Adhesive EA 9628 Tape. It should be noted that it was beyond the scope of this investigation to evaluate adhesives for long-term usage in field applications. The metal surfaces to be bonded were cleaned and prepared using the same techniques as those used for the application of strain gages. The recommended conditions for the curing cycle were 0.17 MPa (24 psi) at 121°C (250°F) for 1 h. However, since the preliminary study of the adhesives had indicated that adequate bonding was obtained at 0.17 MPa at 121°C for 1/2 h, all test specimens underwent this 1/2-h curing cycle.

In order to maintain a uniform unbonded length on the crack gage, a 0.013-cm (0.005 mil) thick and 3.81-cm (1.5-in.) long TFE-fluorocarbon strip was placed between the gage and the structural component. Thus, the bonded areas on the gage had a straightedge under the gage and were ~2.54 cm (1 in.) long.

Crack-Growth Behavior

Since the primary intent of this investigation was the evaluation of the relationship between crack length in the structure and that in the gage, materials selection was based simply upon availability. It was beyond the scope of this study to optimize the response of the gage to the many variables that influence crack growth.

The material chosen for the structural component was 2219—T851 aluminum alloy which is also a representative airframe material. Two sheet materials of aluminum alloy were selected for the crack gage—2024-T3 and Alclad 7075-T6. To permit analysis of specimen results, baseline crack-growth data on these materials were obtained. Single-edge-notch (SEN) and center-cracked (CC) specimens of 2219-T851 (0.61 cm nominal thick-

ness and 5.08 cm wide) were tested under several constant-amplitude load levels. The orientation of the crack growth in these two types of specimens was *LT*, that is, the crack surface was normal to the rolling direction (*L*) and the crack propagated in the transverse direction (*T*). CC specimens of 2024-T3 and 7075-T6 (0.079 cm nominal thickness and 2.54 cm wide) were tested under several constant-amplitude load levels. The orientation of crack growth in 2024-T3 and 7075-T6 was *LT* and *TL*, respectively. In all baseline crack-growth tests, the ratio of minimum load to maximum load (*R*) was 0.1.

A least-squares-fit parabola to successive sets of five data points (crack length versus number of cycles) was used to obtain the slope for crack-growth rate and the crack length for the range of the stress-intensity factor, ΔK. Then a linear regression on log-log scale plot of the results for crack-growth rate as a function of ΔK was applied to obtain the constants (denoted by C and m) for the Paris' crack-growth law [*12*]. Values of these constants for the structure and gage materials are presented in Table 2 and labeled "Experimental." From the experimental data, the valid ranges of ΔK (in MPa · $m^{1/2}$) for the application of the constants are: $4.8 < \Delta K < 35$ for 2219-T851, $6.3 < \Delta K < 27$ for 7075-T6, and $5.6 < \Delta K < 30$ for 2024-T3. In order to obtain the largest range of ΔK in the test specimens and to allow application of the crack-growth law, the final precracking of the CC cracks in the gages and the SCH cracks in the structure was performed at $\Delta K = 6.6$ MPa · $m^{1/2}$.

A set of adjusted constants is also presented in Table 2. The adjusted values of C were obtained from a least-squares fit of the experimental data

TABLE 2—*Crack growth constants for Paris' law* (R = *0.1*).

$$\frac{da}{dN} = C(\Delta K)^m$$

$$\left(\frac{da}{dN} - m/\text{cycle};\ \Delta K - \text{MPa} \cdot \text{m}^{1/2} \right)$$

	Material		
	2219-T851[a]	7075-T6[b]	2024-T3[b]
		Experimental	
C	0.145×10^{-9}	0.4278×10^{-9}	0.4621×10^{-10}
m	2.855	2.816	3.13
		Adjusted	
C	0.1450×10^{-9}	0.3867×10^{-9}	0.8810×10^{-10}
m	2.855	2.855	2.855

[a] Nominal thickness—0.61 cm.
[b] Nominal thickness—0.084 cm.

for 7075-T6 and 2024-T3, with $m = 2.855$ (the exponent for 2219-T851). The application of these constants is discussed in a subsequent section on the predictive model.

Evaluation of Test Configuration

In order to develop a model for the specimens shown in Fig. 1, the characteristics of the load transfer into the gage and the possible effects of the gage upon the nominal stress field around the structural crack were evaluated. Strain gages were attached to a sample specimen which had an uncracked coupon mounted to simulate a crack gage, and which had no hole or crack in the structural component. Since the uncracked coupon was stiffer than a cracked gage, the limiting conditions for load transfer into a gage and the effects upon the nominal stress in the vicinity of the crack in the structural component were maximized. Pairs of strain gages were placed on top of the coupon, on top of the structural component beside the coupon, on the bottom of the structural component beneath the coupon, and on the top and bottom of the structural component at the location of the structural crack. These strain-gage locations are indicated in Fig. 1.

Three uncracked specimen configurations were tested. The first configuration was to simulate specimens where only the adhesive was used to attach the coupon to the structural component. The second configuration was identical to the first, except that two rivets in addition to the adhesive were placed along each edge of the unbonded section of the gage. The third configuration was similar to the first, except that the structural component was approximately twice as thick.

These three configurations were loaded to approximately the same nominal structural stress. At very low loads nonlinear behavior between strain and load was observed; this was attributed to the manner of load introduction into the specimen. When the structural load was increased, all strains exhibited essentially a linear dependence upon load. The slopes of the linear portions were determined, and an average value for each pair of strain gages was obtained for each location. These average values of the slopes were assumed to be characteristic for the full strain-load behavior of the specimens. The values of strain given in Table 3 for various locations on the test specimen were calculated at the same nominal stress level.

A comparison of the strain values in Table 3 indicated that bending was induced through the thickness of the structural component under the crack gage. Also, slight reverse bending occurred at the structural crack location. These bending effects are attributable to the asymmetrical specimen configuration. The strain values for the thicker structural component indicated that induced bending still occurred but that the magnitude was reduced due to the higher bending rigidity of the structure.

A comparison of the strain in the gage to that in the structure revealed

TABLE 3—*Strain values for uncracked gage mounted on structure with no hole.*

(Strains $- 10^{-3}$ cm/cm)

Strain-Gage Location	Adhesive Only[a]		Adhesive Plus Rivets	
	Crack-Gage Location	Proposed SCH Location in Component	Crack-Gage Location	Proposed SCH Location in Component
0.605-cm thick structure (σ_s = 130 MPa)				
Top of gage	1.36	...	1.38	...
Top of structure	1.45	1.75	1.44	1.77
Bottom of structure	1.66	1.69	1.70	1.72
1.33-cm thick structure (σ_s = 130 MPa)				
Top of gage	1.47	...		
Top of structure	1.59	1.72		
Bottom of structure	1.74	1.70		

[a] In all cases adhesive was Hysol EA 9628 tape.

another reduction of strain in addition to the reduction caused by bending. This decrement of strain was due to various factors such as deformation of the adhesive, some slight initial curvature in the gage, and the gage not conforming to the deformed curvature of the structure. Note that the strain decrement existed when rivets were placed along the edge of the bonded area. These strain results are employed later in the model in order to quantify some of the variables in the load-transfer relationship existing between the gage and the structural component.

Note that a small variation in strain occurred at the intended location of the SCH in the 0.605-cm thick structure having the adhesively bonded gage. Thus, the interaction between the crack gage and the nominal stress at the SCH location is assumed to be minimal.

Test Results

All specimens in the test matrix—Table 1, were tested under constant-amplitude, tension-tension, sinusoidal loading with R = 0.1. Measurements of gage and structure crack lengths and number of cycles were taken periodically during the loading history until the crack extended to the edge of the component in either the gage or the structure. An additional specimen planned for the test matrix yielded no data because an undetected debonding of the adhesive occurred early in the test. All specimens were tested in an MTS closed-loop hydraulic system and crack lengths were measured to the nearest 0.0254 mm (0.001 in.) with a Gaertner traveling microscope.

Typical sets of data for crack length as function of number of cycles are shown in Fig. 2 for Tests 3 and 4. In order to obtain the structural crack length as a function of gage crack length, the number of cycles was eliminated for each test. Figures 3 to 5 are plots of structural crack length, a_s, as function of gage half-crack length, a_g, for all test data. The nominal stress range, $\Delta\sigma$, for the structural component for each test, is noted in these figures. The subscript on $\Delta\sigma$ indicates the test number. In Test 4, laser-interferometric measurements of crack-surface displacements (IDG) were made for three crack lengths. This laser technique provides a method of evaluating the geometric factor in the expression for the stress-intensity factor. The use of the IDG data is discussed in the results section. A detailed description of this interferometric method is presented in Ref *13*.

The development of the model for predicting the theoretical curves in Figs. 3 to 5 is presented in the next section.

Predictive Model

A summary of basic concepts and assumptions which are discussed in detail in Ref *9* will now be presented. A crack-propagation law is needed to

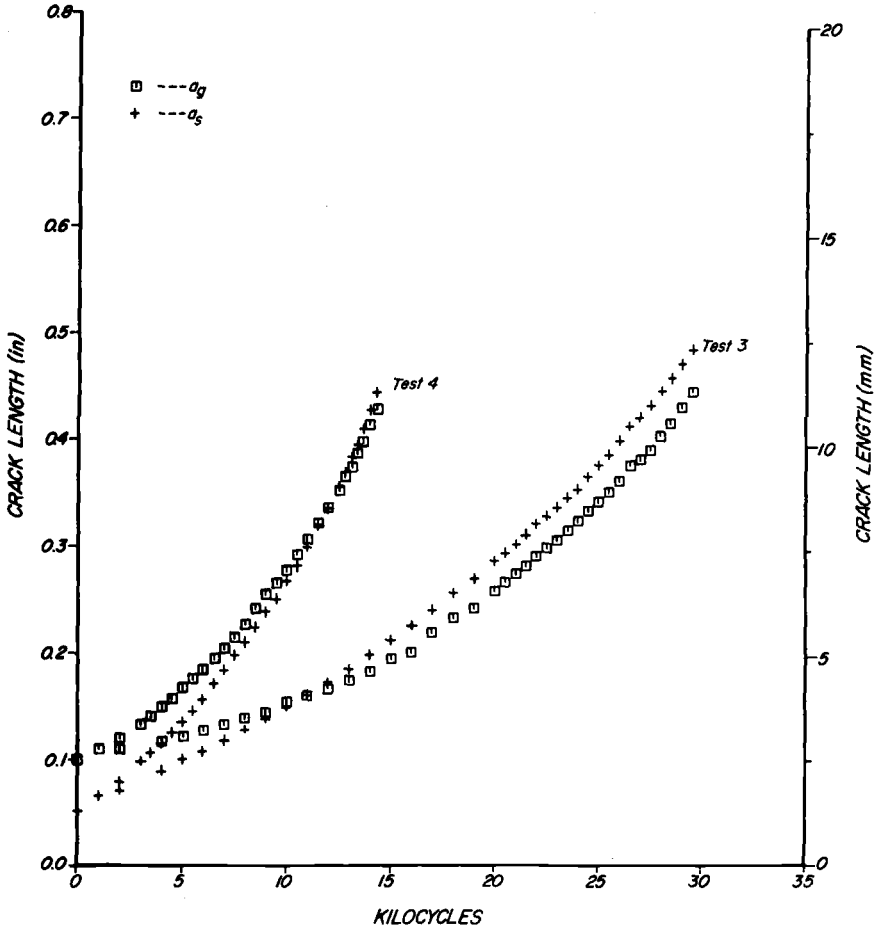

FIG. 2—*Comparison of crack-length results for two specimens having equivalent initial crack lengths and being tested under different load amplitudes.*

characterize the crack growth in both the gage and the structure. For this investigation the empirical relationship

$$\frac{da}{dN} = C(\Delta K)^m \tag{1}$$

is assumed to be valid over the range of loads experienced by both the gage and the structure. Other crack-growth laws which could be used are discussed in Ref *10*. The number of cycles to achieve a prescribed crack length, a, can be obtained by integration of Eq 1, which results in

$$N = \int_{a_i}^{a} \frac{d\alpha}{C[\Delta\sigma\beta\sqrt{\pi\alpha}]^m} \tag{2}$$

where α is a dummy integration variable for crack length, the range for the stress-intensity factor is given by $\Delta K = \Delta\sigma\beta\sqrt{\pi a}$, β denoting the geometric correction factor and a_i being the initial crack length.

For a crack gage attached to a structure, it is assumed that the following relationship exists between the nominal stresses in the gage and those in the structure

$$\sigma_g = \sigma_s f \tag{3}$$

where f is the load-transfer function. For Eq 3 and subsequent formulae, the subscripts g and s refer to the gage and structure, respectively. In general, the load-transfer function depends upon the geometry of both the structure and the gage, the combined geometry of the structure and the attached gage, the properties of the structural and gage materials, and the

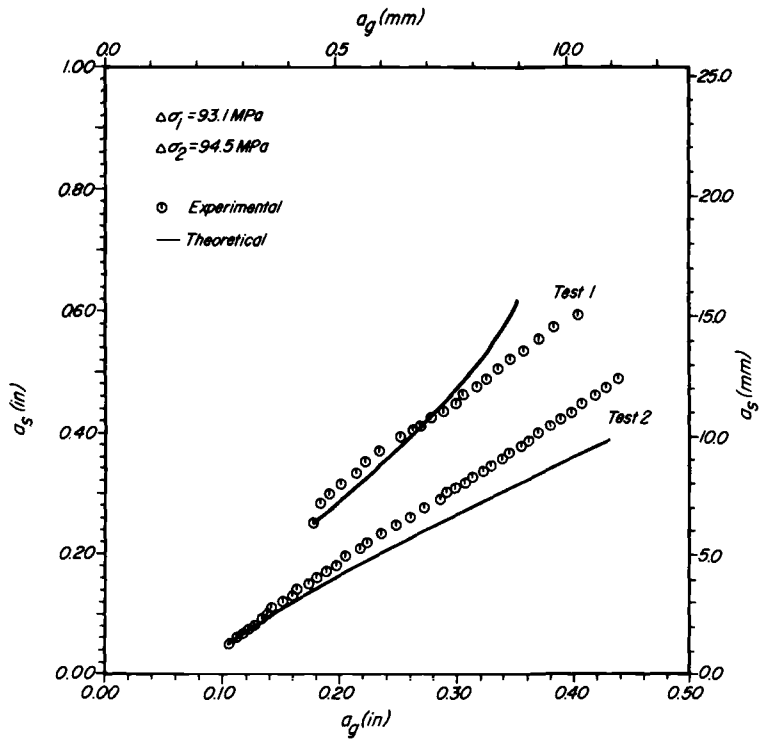

FIG. 3—*Experimental data and theoretical predictions for structural crack growth versus gage crack growth for two specimens having different initial crack lengths.*

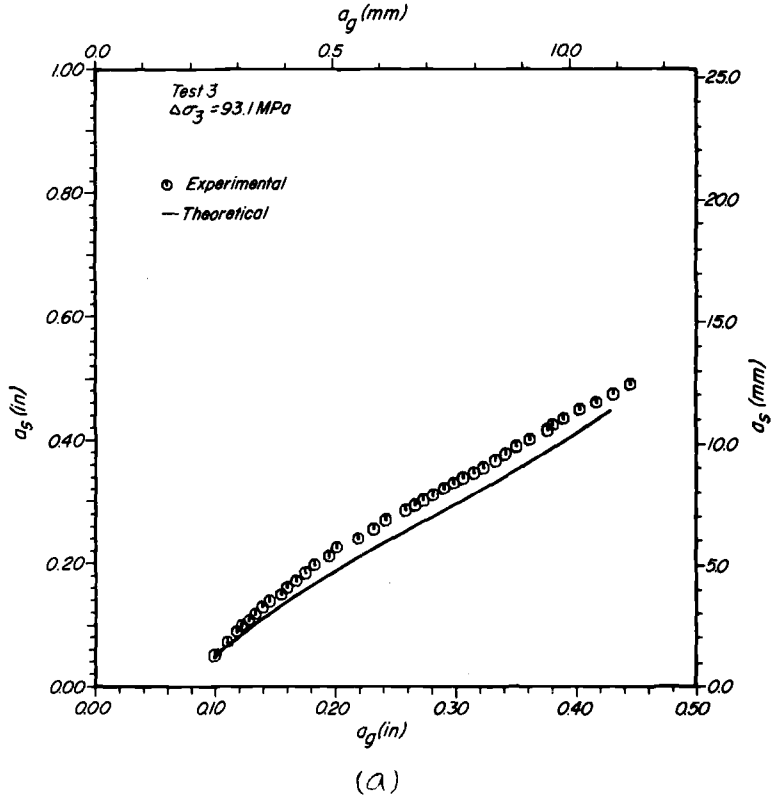

FIG. 4—*A replot of the test data in Fig. 2 after elimination of the dependence upon the number of cycles*: (a) *Test 3 with nominal stress range of 93.1 MPa and* (b) *Test 4 with nominal stress range of 124 MPa.*

material used for the attachment. A trivial implication from Eq 3 is that the gage and structural components undergo the same number of loading cycles. Thus, the number of cycles for crack growth is the same for the gage and structure.

Writing Eq 2 for the crack in the gage and the crack in the structure and equating the number of cycles, the following expression is obtained:

$$\int_{a_{si}}^{a_s} \frac{d\alpha}{C_s[\Delta\sigma_s\beta_s\sqrt{\pi\alpha}]^{m_s}} = \int_{a_{gi}}^{a_g} \frac{d\alpha}{C_g[\Delta\sigma_g\beta_g\sqrt{\pi\alpha}]^{m_g}} \tag{4}$$

which is a nonlinear expression relating crack lengths, material properties, and nominal stresses. Equation 4 can be simplified if the exponents are equal, that is, $m_s = m_g$. In general, the exponent for the gage material is not expected to be the same as the exponent for the structural material.

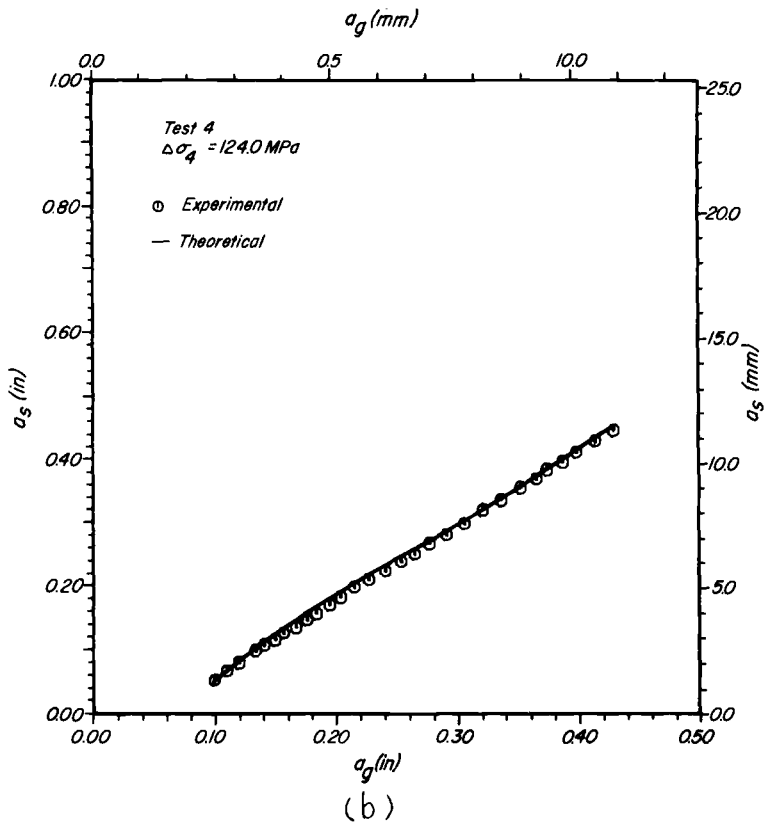

FIG. 4—(*Continued.*)

However, in the development of the model for the crack gage, equal values of the exponents are used. Hence, a correlation between prediction and experimental results would support the use of equal exponents in the crack-gage model. Letting $m_s \equiv m_g \equiv m$ and substituting Eq 3 (when written in terms of stress range) into Eq 4, the relation between gage and structural crack lengths becomes *independent of stresses*; thus

$$\frac{1}{C_s}\int_{a_{si}}^{a_s}\frac{d\alpha}{[\beta_s\sqrt{\pi\alpha}]^m} = \frac{1}{C_g}\int_{a_{gi}}^{a_g}\frac{d\alpha}{[f\beta_g\sqrt{\pi\alpha}]^m} \tag{5}$$

This expression is used to predict the relationship between the structural crack length and the gage crack length.

Determination of the material properties in Eq 5 which characterize baseline crack-growth behavior was discussed in the previous section. Since the exponents for crack-growth behavior are assumed to be equal for the

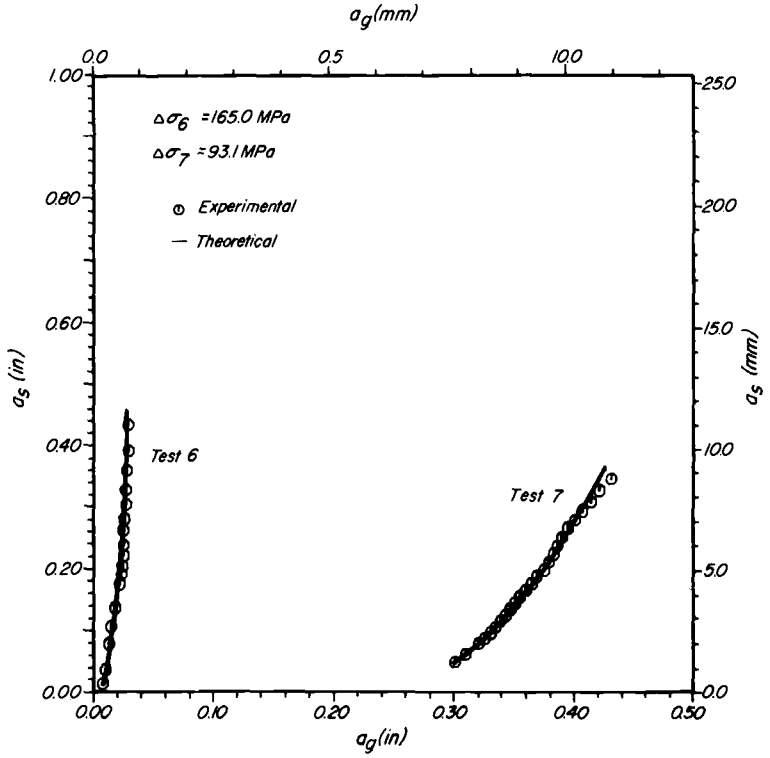

FIG. 5—*Plot of structural crack length versus gage crack length for specimens with gages made from 2024-T3 Al.*

theory, the exponent for the structural material, m_s, was chosen arbitrarily as the value for m. Then C_g for 7075-T6 and 2024-T3 was determined in order to achieve a least-squares fit to the experimental data. The adjusted values of C_g for the theory are given in Table 2.

For determination of the load-transfer function, the following analysis was made on a simplified model of the region of the structural component where the crack gage was located. The stress field, σ_s', in the structure was assumed to vary linearly through the thickness under the center of the gage

$$\sigma_s'(y) = T - \gamma My \tag{6}$$

where T, M, and γ are constants. The y-axis has its origin at the midplane of the structural component and is directed toward the gage. The constant γ is a factor which is intended to account for three-dimensional variations in the stress distribution, σ_s', in the structural component under the crack gage. Its value is determined experimentally.

If P_g is assumed to be the internal force in the gage and P_s is the externally applied force at the ends of the structure acting through the midplane, then the equilibrium of forces and of moments, respectively, produces the following expressions.

$$P_g + \int_{A_s} \sigma_s' d\mathfrak{A} = P_s \tag{7a}$$

$$P_g \left(\frac{B_s}{2} + B_a + \frac{B_g}{2}\right) + \int_{A_s} y\sigma_s' d\mathfrak{A} = 0 \tag{7b}$$

where A_s and B_s are the cross-sectional area and thickness, respectively, of the structural component and B_a and B_g represent the thickness of the adhesive and of the gage, respectively. Consideration of continuity of displacements between the gage and the top of the structure yields the expression

$$\mathcal{C}_g P_g + \mathcal{C}_a P_g = \frac{l_s}{E_s} \sigma_s' \quad \left(y = \frac{B_s}{2}\right) \tag{7c}$$

where $\mathcal{C}_g$ is the compliance of the crack gage, $\mathcal{C}_a$ is a compliance which includes the compliance of the adhesive and other factors causing additional displacements between the gage and the structure, l_s is a characteristic length of the structural component under the crack gage, and E_s is Young's modulus of the structure. The right-hand side of Eq 7*c* represents the change in length along the surface of the structural component under the crack gage. The value of compliance, $\mathcal{C}_a$, in Eq 7*c* is determined from the strain-gage results which were discussed in the previous section.

After substitution of Eq 6 into Eq 7 to eliminate σ_s', Eqs 7*a*, *b*, and *c* contain three unknowns—*T*, *M*, and P_g. In Eq 7*b*, *M* is expressed in terms of P_g, assuming one-dimensional beam bending, that is, $\gamma = 1$. Then this expression for *M* is substituted into Eq 7*c*. Upon using integration of the terms in Eq 7 and the definitions $\sigma_g \equiv P_g/A_g$ and $\sigma_s \equiv P_s/A_s$ for Eq 3, the load-transfer function can be written as

$$f = \frac{1}{E_s} \frac{l_g}{A_g} \left[\mathcal{C}_g + \mathcal{C}_s + \mathcal{C}_a + \gamma \mathcal{C}_b\right]^{-1} \tag{8}$$

where A_g is the cross-sectional area of the gage, $\mathcal{C}_s$ is the compliance of the structural component, and $\mathcal{C}_b$ is a bending compliance (the formula for $\mathcal{C}_b$ is given in the following discussion).

Evaluation of the compliances $\mathcal{C}_g$, $\mathcal{C}_s$, $\mathcal{C}_a$, and $\mathcal{C}_b$ and the factor γ will now be presented. For the crack gage the expression relating compliance

for a CC specimen, strain-energy release rate, and stress-intensity factor for plane-stress conditions is

$$\frac{1}{4}\frac{P^2}{B}\frac{\partial \mathcal{C}}{\partial a} = \mathcal{G} = \frac{K^2}{E}$$

After integration, the crack-gage compliance can be expressed as

$$\frac{1}{4}\frac{P_g^2}{B_g}(\mathcal{C}_g - \mathcal{C}_g') = \frac{1}{E}\int_0^{a_g} K_g^2 d\alpha$$

where $\mathcal{C}_g' = l_g/(E_g A_g)$ is the uncracked gage compliance. Substitution of the expression $K_g = \sigma_g \beta_g \sqrt{\pi \alpha_g} = P_g \beta_g \sqrt{\pi \alpha_g}/A_g$ yields

$$\mathcal{C}_g = \mathcal{C}_g' + \frac{4\pi\beta_g}{EA_g^2}\int_0^{a_g} a\beta_g^2 d\alpha$$

For the crack-gage geometry used in the tests, the geometric correction factor is obtained by interpolation with a polynomial curve-fit to the analytical results given in Ref *14*. In Eq 8 the structural compliance and the bending compliance denote the following quantities which are obtained from the solution of Eq 7

$$\mathcal{C}_s = \frac{l_s}{E_s A_s}$$

$$\mathcal{C}_b = \frac{l_s B_s}{2E_s I_s}\left(\frac{B_s}{2} + B_a + \frac{B_g}{2}\right)$$

where I_s is the moment of inertia of cross section, A_s, of the structural component.

The values of the two remaining terms, $\mathcal{C}_a$ and γ, are determined from the experimental strain-gage results, Table 3. If the deformation of the uncracked gage ideally followed the deformation of the structure, the strain in the midsection of the gage would be obtained by the linear continuation of the strain field in the structure. The value of $\mathcal{C}_a$ is calculated to account for the difference between the continuation of the strain field and the measured strain value. The value of γ is determined such that the assumed linear-strain distribution, $\epsilon_s' = \sigma_s'/E_s$, matches the measured strain values on the top and bottom of the structural component. As a result of these calculations, the following values are obtained for the terms in the load-transfer function for the test configuration in Fig. 1: $\mathcal{C}_g' = 2.51 \times 10^{-6}$

cm/N, $\mathcal{C}_s = 0.163 \times 10^{-6}$ cm/N, $\mathcal{C}_a = 0.171 \times 10^{-6}$ cm/N, $\mathcal{C}_b = 0.588 \times 10^{-6}$ cm/N, and $\gamma = 0.3$

The effect of the above quantities in the load-transfer function upon the predicted relation between a_s and a_g as given by Eq 5 is illustrated in Fig. 6. The ideal behavior of a crack gage [9] which undergoes the nominal deformation of the structure is given by Curve *a* in Fig. 6: For the ideal behavior the only term in brackets in the load-transfer function (Eq 8) is $\mathcal{C}_g$. Curves *b* through *d* are associated with successive inclusion of the compliances $\mathcal{C}_s$, $\mathcal{C}_a$, and 0.3 $\mathcal{C}_b$, respectively. Curve *e*, like *d*, is obtained through the use of all the terms in brackets in Eq 8 except $\gamma = 1$.

The theoretical curves in Figs. 3 to 5 are predicted from Eq 5, with

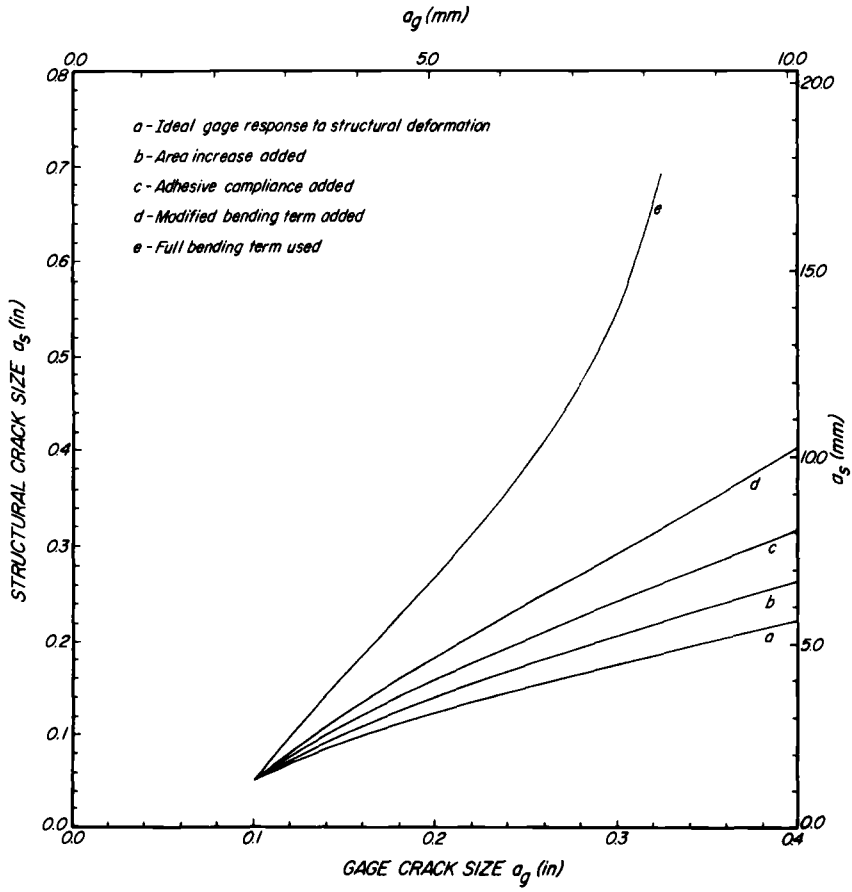

FIG. 6—*Cumulative effect of additional compliance terms in the load-transfer function upon the prediction of structural crack length versus gage crack length.*

$\gamma = 0.3$ in Eq 8. For the crack in the structural component, the geometric correction factor for the left-hand side of Eq 5 is calculated as

$$\beta_s = \beta_H \sqrt{\text{secant } [(a_s + D)/W_s]} \tag{9}$$

where β_H is the Bowie geometric factor for a single crack at a hole of diameter, D, in an infinite plate and W_s is the width of the structural component.

Discussion of Results

Prior to discussion of the measurements and the numerical predictions of the structural crack length and corresponding gage crack length, experimental measurements of the structural and the gage stress-intensity factors will be compared with values used in the numerical predictions. The stress-intensity factors are calculated from

$$K_s = \sigma_s \beta_s \sqrt{\pi a_s} \tag{10a}$$

$$K_g = \sigma_s f \beta_g \sqrt{\pi a_g} \tag{10b}$$

where β_s is given by Eq 9 and σ_g was eliminated by the use of Eq 3. Dimensionless forms of K are presented as a function of dimensionless crack length for the structural flaw in Fig. 7[4] and for the center crack-gage geometry in Fig. 8. These experimental results were obtained through the use of two procedures. First, the fatigue-crack-growth rates for the gage and structural cracks were converted to stress-intensity factors by means of Paris' crack-growth model previously established for the test material (see Table 2). The second experimental K calibration method employed laser-interferometric measurements crack surface displacement following the technique described in Ref *13*.

The constants C and m used to convert the gage-crack-growth rates to K by the first technique were the values originally established during the baseline testing for the two gage materials. In all cases, care was taken to ensure that the computed value of K from the measured gage and structural crack-growth rates fell within the linear range on a log-log scale of da/dN versus ΔK established in the baseline tests. Since the crack-growth models were not extrapolated, the only stress-intensity-factor data shown in Figs. 7 and 8 are those for crack-growth rates within the baseline da/dN ranges. Since practically all of the structural and gage crack-growth rates fell within the baseline da/dN range tested, very few points were omitted.

[4]Note that the maximum value of the nondimensional crack length in Fig. 7, that is, when the crack reaches the edge of the structural component, is 0.375.

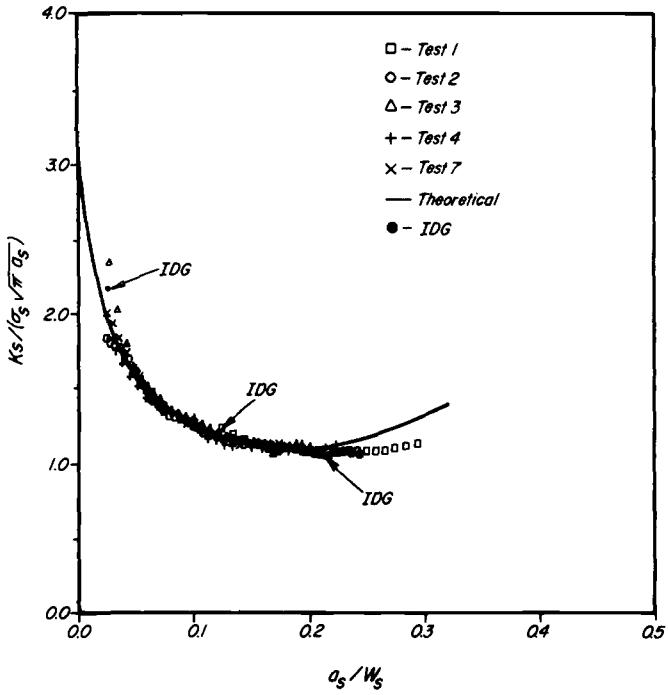

FIG. 7—*Comparison of the predicted dimensionless* K—*equivalent to the geometric correction factor—with the dimensionless* K *obtained from the experimental data on structural crack growth.*

Note in Fig. 7 that the dimensionless K values which are equivalent to values of β_s in Eq 10*a* for the structural crack geometry form a very narrow scatter band. For the majority of the structural crack lengths (that is, $a_s/W_s < 0.25$), the width-corrected Bowie geometric factor (Eq 9) agrees quite well with the experimental values, further verifying the assumption that placement of the gage on the structural member has no effect upon structural crack growth. The apparent divergence for a_s/W_s larger than 0.25 evidently indicates that the approximate width-corrected Bowie solution overcorrects for larger crack lengths.

Results of corresponding measurements of the dimensionless stress-intensity factor are given in Fig. 8 for all of the center-cracked gages including both the 7075-T6 (Tests 1 to 4) and the 2024-T3 (Test 7) material. From Eq 10*b* the dimensionless stress-intensity factor in Fig. 8 is equivalent to $\beta_g f\sqrt{a_g/W_g}$. Note that the dimensionless K for the 2024-T3 gages agrees well with the measured results for the 7075-T6 gages, as expected. There is considerably more scatter in the gage stress-intensity factors than in those in Fig. 7 for the structural cracks. This increased scatter might be expected due to the potential variability of loads in the gage. The load must be transferred to the crack gage through an adhesive, for example,

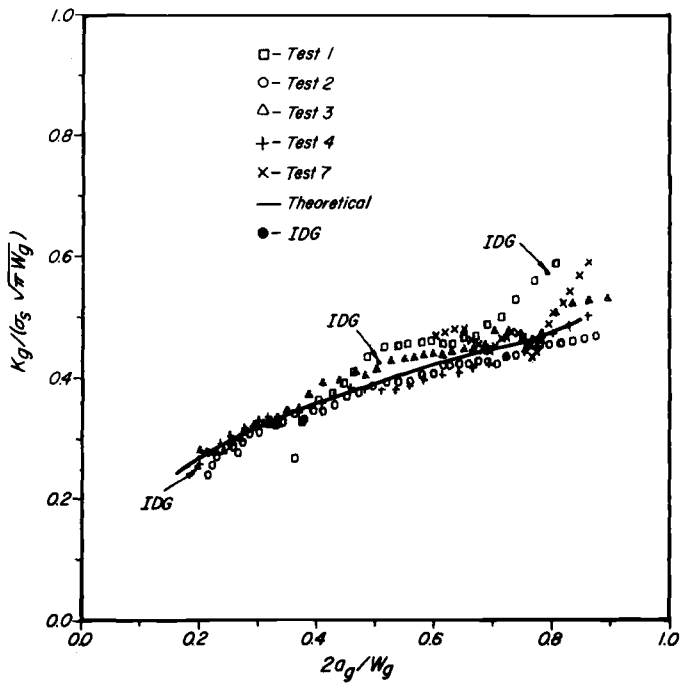

FIG. 8—*Comparison of the predicted dimensionless* K—*equivalent to the load-transfer function—with the dimensionless* K *obtained from the experimental data on gage crack growth.*

which introduces some variation in the geometry from test to test. Nevertheless, Eq 10*b* predicts gage stress-intensity factors which agree quite well with the experimental results, adding further confidence in the load-transfer model developed previously for the gage. The IDG results for the crack gage in Test 4 do not agree as well with the calculated dimensionless K results as do those obtained for the structural crack. At present the slightly different trend in the IDG results in comparison with the dimensionless K results is unexplainable.

Notice the agreement between experiment and theory in the gage-crack-versus-structural-crack results and the corresponding predictions for the six experiments presented in Figs. 3 to 5. It is significant that the predictions required no knowledge of the actual loads applied to the specimens. Although the agreement between predictions and test results for Tests 1 to 3 are not as good as those for Tests 4, 6, and 7, agreement between theory and experiment is still satisfactory for these cases. Possible sources of error will be discussed later.

Comparison of the result of Tests 2 and 3, which were initiated with approximately the same structural and gage initial crack lengths and approximately the same applied loads (see Table 1) shows that the two

tests have fairly reproducible results. A comparison of the results of Tests 2 and 3 with those of Test 4, again initiated with approximately the same initial crack lengths but at an appreciably higher stress level ($\Delta\sigma_4 = 124$ MPa rather than ~ 94 MPa) shows the structural-crack-length-versus-gage-crack-length data to be essentially independent of load level, with the data from all three tests falling within a relatively narrow band (see Fig. 9). Figure 2 which presents the original crack-length-versus-number-of-cycles data for Tests 3 and 4 demonstrates that load level does, of course, influence the cyclic life of otherwise identical specimens; however, as shown in Fig. 9, load level had no appreciable effect upon the a_s-versus-a_g curve.

This observation is in agreement with the mathematical model which led to the conclusion that these curves were independent of loading when crack-growth data could be expressed by a simple Paris-type model. Since as discussed in prior papers [9,10,15,16], crack-growth data due to variable-amplitude loading can often be described by such a model (that is, correlating crack growth per block of loading with an appropriate stress-intensity factor which characterizes the loading block), the results of these constant-

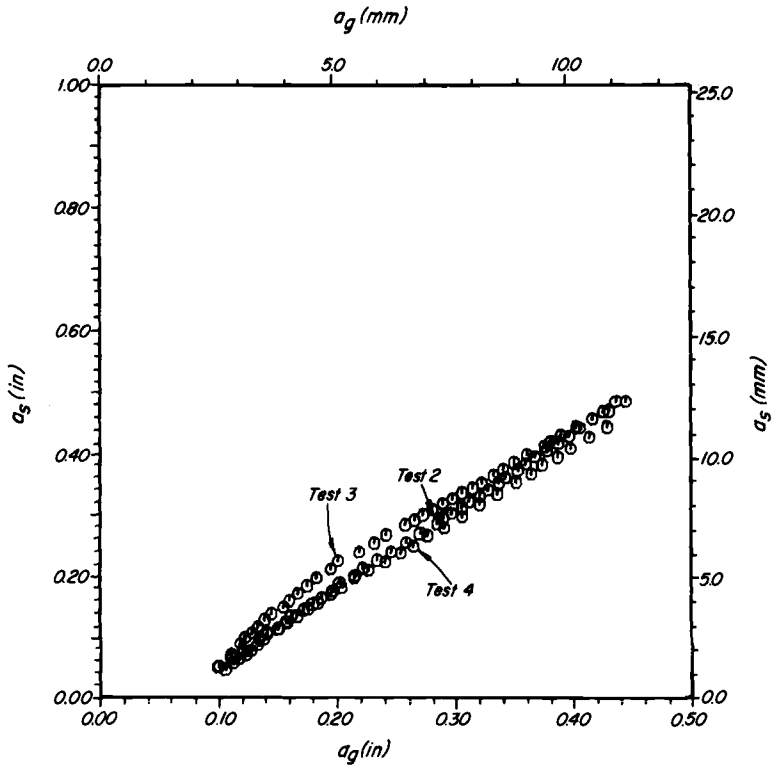

FIG. 9—*Experimental crack-growth data indicating both the reproducibility and the lack of dependence upon load amplitude of the gage response.*

amplitude tests suggest that—with limitations—crack gages may also be useful for variable-load histories characteristic of actual structures. In Refs 9 and 10 correlations were made between the growth of two flaws in the same specimen using the present computational technique. The gage in this case was considered to be an integral part of the structure. Those predictions that were again independent of load history, being a function of geometric and material variables only, agreed extremely well with results on experimental behavior when the test specimens were subjected to a complex variable-amplitude load profile chosen to simulate aircraft loading. Certainly, the application of crack gages to conditions of variable-amplitude and spectrum loading would require justification from laboratory tests.

One source of the discrepancy between prediction and experiment observed for Tests 1 to 3 may be the variability in gage fatigue-crack-growth rate caused by relative humidity changes. The crack gages for these three experiments were made from 7075-T6 aluminum, an alloy that is particularly susceptible to such environmental influences [*17*]. Since no attempts were made to control the test environment, perhaps some of the scatter for the 7075-T6 gages evident in the stress-intensity-factor measurements in Fig. 8 and in the predictions of the a_s-versus-a_g data for Tests 1 to 3 is due to changes in test humidity. These tests were conducted during the summer months when problems developed with the laboratory air-conditioning system and rather large, although unmeasured, changes in ambient temperature and humidity occurred. Consistent with this obsevation is the fact that the data for the 2024-T3 gages showed excellent agreement with theory. The 2024-T3 alloy, like the 2219-T85 alloy, is less sensitive to environmental changes than the 7075-T6 material.

Summary and Conclusions

The crack-growth gage has been discussed as a potential technique for monitoring the severity of structural loads by evaluating their influence upon the growth of possible structural cracks. Briefly stated, the concept consists of mounting a pre-cracked coupon (or gage) onto a load-bearing structural member. The coupon receives the load excursions which are related to the loads in the structure by the transfer function (Eq 3) and responds with a measurable crack extension. This crack growth in the gage may be correlated with extension of another defect located in the structural member by means of the techniques described here and in prior papers [*9,10*]. In essence, the cracked coupon acts as an analog computer which senses the load history, determines its effect upon crack growth, and responds with a measurable output-gage crack extension.

A mathematical technique for relating the gage crack length and the structural crack length has been described. The present model is an improvement over earlier versions [*9,10*) and takes into account such factors

as local reinforcement or bending caused by the crack gage and compliance of the adhesive bond. Predictions of crack-gage response were made by means of this model and subjected to experimental verification. Six crack-gage tests were conducted involving two different gage materials, two load levels, and two gage geometries. The mathematical predictions agreed well with the observed experimental behavior of the crack gages. Reproducibility in response of identical gages was obtained as well as preliminary verification for the correlation between gage crack growth and flaw growth in the structure being independent of load history. Although this conclusion is limited in the present tests to constant-amplitude loadings, there is evidence [*9,10*] to suggest that these findings may apply to more complex load histories which can be described by simple Paris- or Foreman-type [*18*] crack-growth models. Verification of the concept and identification of its limitations for variable amplitude loading requires further study.

No attempts were made to optimize the crack-gage design for structural applications. Efforts were directed instead toward experimentally evaluating the crack-gage *concept* for load tracking. Improved gage geometries, for example, almost certainly can be developed, along with selection of alternative adhesives for better long-term durability and structural application. Although the present results indicate that predictions can be made for crack gages made of materials which are different from those used for the structural member, it might be desirable to use identical materials in order to obtain similar retardation and acceleration effects caused by peak loads. Similar materials would also minimize differences in the environmental effects upon crack-growth rates encountered by the gage and structure in service. One final consideration which may be important in optimizing the gage design lies in the initial crack lengths and the precracking procedures used to introduce the gage flaw. For instance, perhaps the precracking loads should be less than service loads in order to minimize history effects in the gage. It may also be desirable to select an initial gage crack length leading to stress-intensity-factor excursions in the gage which are of similar magnitude to those seen by the structural defect.

In summary, the authors feel that the present results demonstrate the potential of crack-growth gages for monitoring service loads. The fact that an accurate relationship between gage and structural crack length can be predicted in advance (with no knowledge of subsequent load history and being dependent only upon geometric and material parameters) suggests that the crack gage is an extremely simple and useful device for recording and interpreting the effect of service usage upon possible structural crack growth. Although many steps remain in the development of a working device for a given service application, it would appear that potential problems are readily solvable by means of present engineering methods. We suggest that other investigators give the crack-gage concept serious consideration for their load-monitoring needs and encourage their research

and development efforts on this interesting technique for tracking damage due to crack growth in a structure.

Acknowledgment

In the testing portion of this investigation, considerable support was provided by J. G. Paine who bonded the many strain gages and the crack gages onto the specimens and G. F. Mornhinweg who precracked the gages and structural components and tested the specimens. Appreciation is also extended to D. E. Macha for his effort in making the laser-interferometric measurements.

References

[1] Coffin, M. D. and Tiffany, C. F., "New Air Force Requirements for Structural Safety, Durability, and Life Management," *Journal of Aircraft (AIAA)*, Vol. 13, No. 2, 1976, pp. 93-98.

[2] "Aircraft Structural Integrity Programs, Airplane Requirements," *Military Standard MIL-STD-1530A (11)* United States Air Force, 11 Dec. 1975.

[3] "Airplane Damage Tolerance Requirements," *Military Specification MIL-A-83444*, United States Air Force, 2 July 1974.

[4] King, T. T., "Some Developments in the Air Force Aircraft Structural Integrity Program (ASIP)," *AFFDL-TR-70-144; Proceedings*, Air Force Conference on Fatigue and Fracture of Aircraft Structures and Materials, H. A. Wood et al, eds., Air Force Flight Dynamics Laboratory, Wright-Patterson Air Force Base, Ohio, 1970, pp. 701-721.

[5] Whitford, D. H. and Dominic, R. J., "B-58 Fleet Life Monitoring and Usage Evaluation by Cumulative Fatigue Damage Method," *AFFDL-TR-70-144; Proceedings*, Air Force Conference on Fatigue and Fracture of Aircraft Structures and Materials, H. A. Wood et al, eds., Air Force Flight Dynamics Laboratory, Wright-Patterson Air Force Base, Ohio, 1970, pp. 847-864.

[6] Harting, D. R., "The S/N Fatigue-Life Gage: A Direct Means of Measuring Cumulative Fatigue Damage," *Experimental Mechanics*, Vol. 6, No. 2, Feb. 1966, pp. 19A-24A.

[7] Spanner, J. C. and McElroy, E., *Monitoring Structural Integrity by Acoustic Emission, ASTM STP 571*, American Society for Testing and Materials, 1975.

[8] Smith, H. W., "Fatigue Damage Indicator," U.S. Patent No. 3, 979, 949, assigned to The Boeing Company, Seattle, Wash. 14 Sept. 1976.

[9] Grandt, A. F., Jr., Crane, R. L., and Gallagher, J. P., "A Crack Growth Gage for Assessing Flaw Growth Potential in Structural Components," *Fracture; Proceedings*, 4th International Conference on Fracture, Vol. 3, Waterloo, Canada, 19-24 June 1977, pp. 39-45.

[10] Gallagher, J. P., Grandt, A. F., Jr., and Crane, R. L., "Tracking Crack Growth Damage in US Air Force Aircraft," *Journal of Aircraft*, Vol. 15, No. 7, 1978, pp. 435-442.

[11] Johnson, W. S. and Paquette, S. J., "Service Life Monitoring Coupons—Accounting for Potential Crack Growth in Fleet Aircraft," presented at the 18th Structures, Structural Dynamics, and Materials Conference AIAA/ASME, San Diego, Calif. 21-23 March 1977.

[12] Paris, P. C., Gomez, M. P., and Anderson, W. E., "A Rational Analytic Theory of Fatigue," *The Trend in Engineering*, Vol. 13, No. 1, University of Washington, Jan. 1961.

[13] Macha, D. E., Sharpe, W. N., Jr., and Grandt, A. F., Jr., "A Laser Interferometry Method for Experimental Stress Intensity Factor Calibration," *Cracks and Fracture, ASTM STP 601*, American Society for Testing and Materials, 1976, pp. 490-505.

[14] Isida, M., "Effects of Width and Length on Stress Intensity Factors of Internally Cracked Plates under Various Boundary Conditions," *International Journal of Fracture Mechanics*, Vol. 7, 1971, pp. 301-316.

[15] Gallagher, J. P. and Stalnaker, H. D., "Developing Methods for Tracking Crack Growth Damage in Aircraft," *Proceedings*, AIAA/ASME/SAE 17th Structures, Structural Dynamics, and Materials Conference, 5-7 May 1976, pp. 486-494.

[16] Rolfe, S. T. and Barsom, J. M., *Fracture and Fatigue Control in Structures*, Prentice Hall, Englewood Cliffs, N.J., 1977.

[17] Truckner, W. G., Staley, J. T., Bucci, R. J., and Thakker, A. B., "Effects of Microstructure on Fatigue Crack Growth of High Strength Aluminum Alloys," *AFML-TR-76-169*, Air Force Materials Laboratory, Wright-Patterson Air Force Base, Ohio, Oct. 1976.

[18] Forman, R. G., Kearney, V. E., and Engle, R. M., "Numerical Analysis of Crack Propagation in Cyclic Loaded Structures," *Journal of Basic Engineering; Transactions of the ASME*, Vol. 89, No. 3, 1967, p. 459.

Service Spectrum Generation and Simulation

J. T. Birmingham,[1] *N. V. Marchica,*[2] *F. F. Borriello,*[3] *and J. E. Beach*[4]

Development of a Fatigue Lifetime-Load Spectrum for a Large-Scale Aluminum Ship Model*

REFERENCE: Birmingham, J. T., Marchica, N. V., Borriello, F. F., and Beach, J. E., **"Development of a Fatigue Lifetime-Load Spectrum for a Large-Scale Aluminum Ship Model,"** *Service Fatigue Loads Monitoring, Simulation, and Analysis, ASTM STP 671,* P. R. Abelkis and J. M. Potter, Eds., American Society for Testing and Materials, 1979, pp. 121-143.

ABSTRACT: The fatigue load spectrum to be applied to the 30-m aluminum ship-evaluation model (ASEM) is presented. The ASEM will be tested in the David W. Taylor Naval Ship Research and Development Center, Carderock, Maryland. Spectra developed for design, analysis, and test purposes are given, based on a reference lifetime-load spectrum developed for a 90-m aluminum ship. Selected ship trial results that provide the basis for developing the lifetime-load spectrum for the 90-m ship are also presented. Results of sensitivity studies of fatigue crack growth indicate that a repeatable 1/100-year block spectrum, sequenced in a low-to-high-to-low order is a practicable compromise for fatigue testing ASEM.

KEY WORDS: ship lifetime-loads, fatigue testing, test spectra, crack growth, aluminum ships, ship model testing

The 30-m, 165-kN, aluminum ship-evaluation model (ASEM), which is shown in Fig. 1, is being prepared for testing at the David W. Taylor Naval Ship Research and Development Center (hereafter referred to as the Center). The tests will relate to what a conceptual 90-m ship is expected to sustain in its active service lifetime. Such testing will include cyclic loading of the primary longitudinal hull structure to represent the low-frequency (or wave-

[1]Project engineer, Science Engineering Analysis Co., Bethesda, Md. 20014.

[2]Structural engineer, David W. Taylor Naval Ship Research and Development Center, Bethesda, Md. 20084.

[3]Senior aerospace engineer, Naval Air Development Center, Warminster, Pa. 18974.

[4]Senior project engineer, David W. Taylor Naval Ship Research and Development Center, Bethesda, Md. 20084.

*The opinions or assertions made in this paper are those of the authors and are not to be construed as official or reflecting the views of the Department of the Navy or the naval services at large.

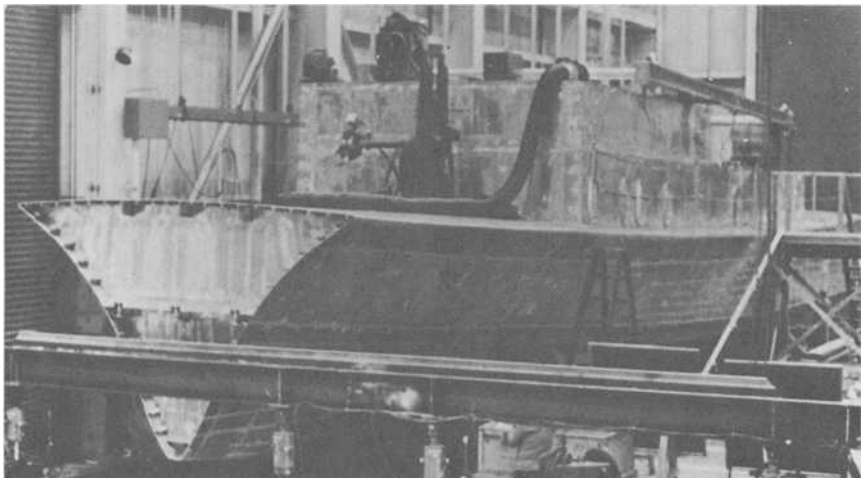

FIG. 1—*Aluminum Ship Evaluation Model (ASEM).*

induced) and the dynamic vibratory (or whipping) vertical and athwartship (or lateral or horizontal) bending moments.

Predicted midship bending-moment spectra have been prepared to represent the vertical and athwartship low frequency wave and whipping bending moments that a 90-m ship could experience during 7 at-sea years of a 20-year service life. These bending-moment spectra will provide the basis for developing lifetime-stress spectra for the 90-m ship and, with applicable scaling, ASEM. Sensitivity studies of fatigue crack growth were made to evaluate the significance of selected properties of the stress spectra. The results of these studies were used to develop practicable fatigue load-block spectra for testing ASEM.

The procedures used and the major assumptions included in developing the 90-m, ship-lifetime, bending-moment spectra and ASEM fatigue-load test spectra are given in the following sections. Results also are presented for full-scale ship experiments (or trials) by the Center that provide the basis for several of these assumptions. Selected results from these trials are provided [*1-6*].[5]

Lifetime Bending-Moment Prediction for a 90-m Aluminum Ship

Development of a lifetime-load spectrum for a ship requires consideration of several items that influence ship response in a seaway. Figure 2 gives the principal elements used in developing lifetime, midship bending-

[5]The italic numbers in brackets refer to the list of references appended to this paper.

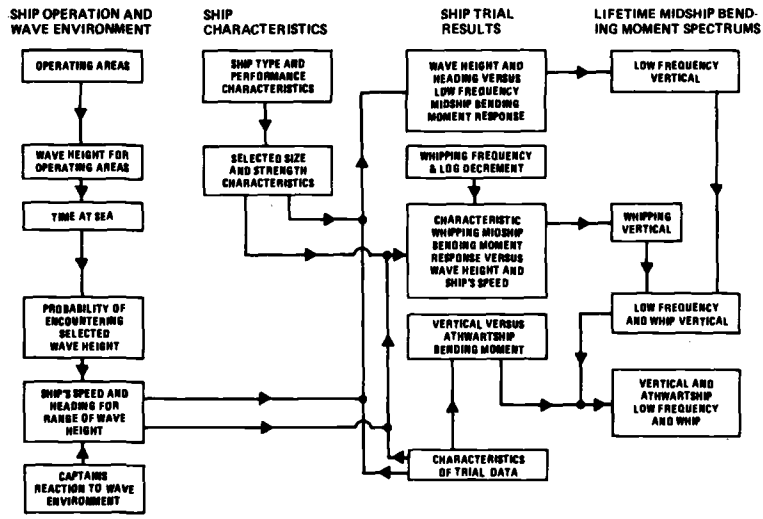

FIG. 2—*Interrelation of elements used in developing lifetime midship bending moment spectra for a 90-m aluminum ship.*

moment spectra for the 90-m aluminum ship. Elements shown in the first two columns of Fig. 2 are determined mainly by the ship mission. Elements in the first column are primarily ship-operation and wave environmental factors. Ship characteristics, noted in the second column, determine how the ship will perform or respond under the ship-operating and wave environmental conditions. Prediction of ship response is based mainly on the evaluation of results from the full-scale trials shown in the third column. The flow indexes show the interrelationship of the various elements in developing the load spectra shown in the fourth column.

Figure 3 shows the predicted lifetime spectrum of low-frequency, wave-induced, midship longitudinal bending moments, due to vertical bending, for the conceptual 90-m aluminum ship. These low-frequency bending moments generally occur at approximately the frequency of encounter with waves that produce significant bending-moment response, that is, waves with lengths ranging from approximately 0.7 to 1.5 times the ship length. Figure 4 shows a similar lifetime-load spectrum for the dynamic vibratory or whipping bending moments. Significant longitudinal whipping bending moments generally contain the frequency of the fundamental mode of vertical and athwartship hull vibration. Figure 5 shows a lifetime spectrum that includes both ordinary wave and whipping bending moments. Figure 6 shows lifetime-load spectra of equivalent vertical bending moments that produce the same average deck stress as the maximum main and 01 level deck-edge stresses, resulting from combined vertical and athwartship bending.

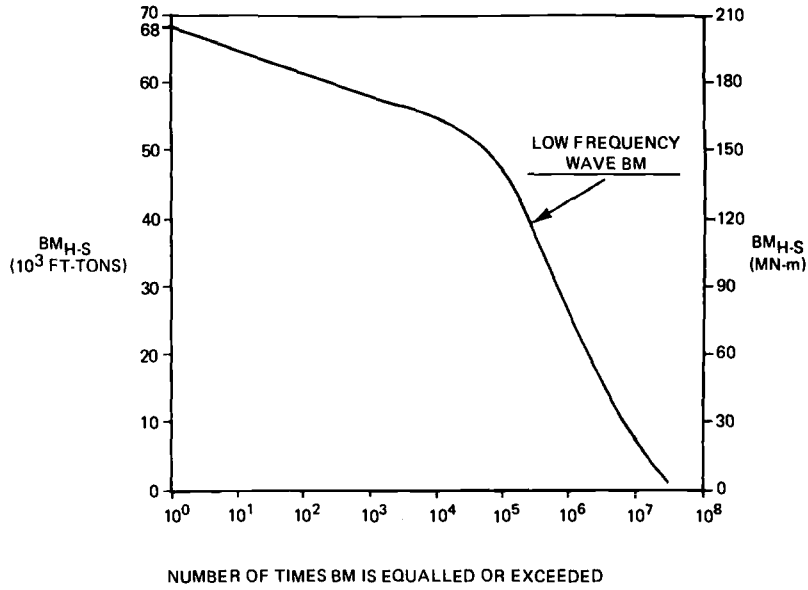

FIG. 3—*Lifetime midship vertical wave bending moment for a 90-m aluminum ship.*

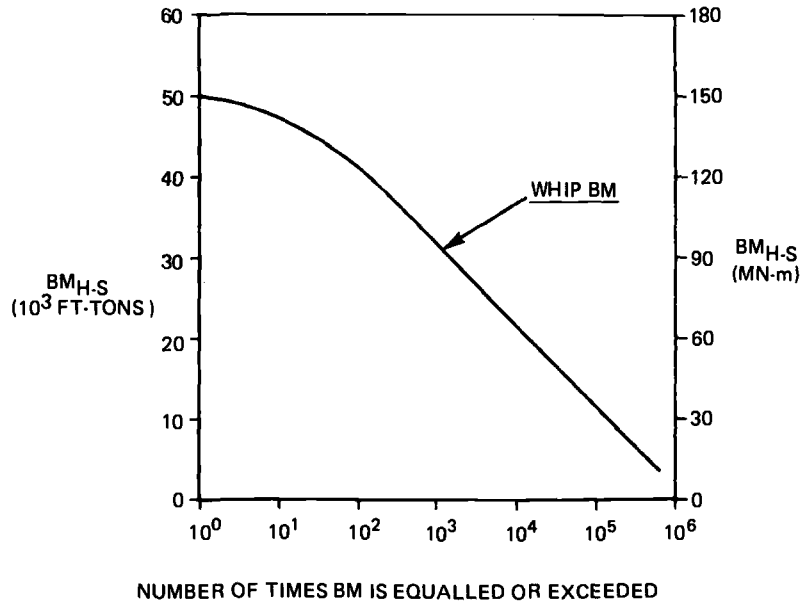

FIG. 4—*Lifetime midship vertical whipping bending moment for a 90-m aluminum ship.*

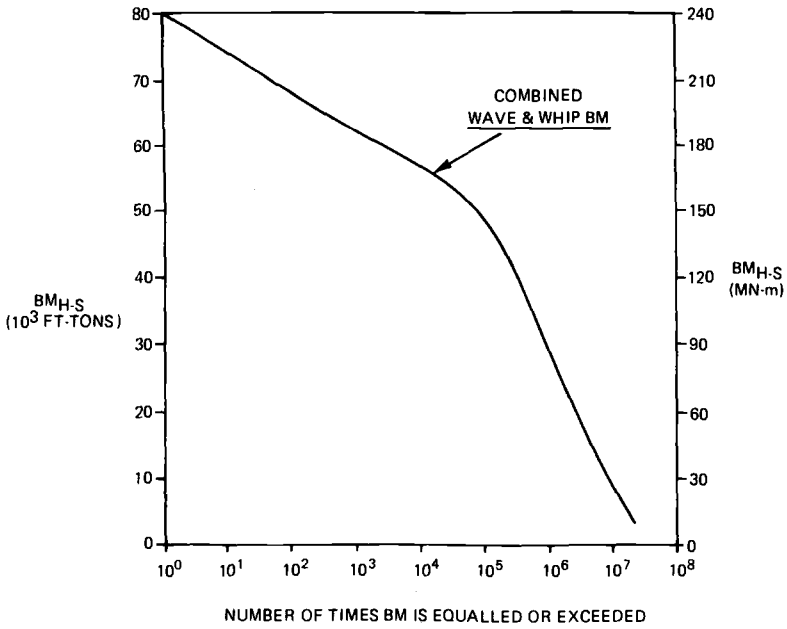

FIG. 5—*Lifetime midship vertical wave and whipping bending moment for a 90-m aluminum ship.*

A brief description of the procedure used to predict lifetime bending moments for the 90-m ship is given in the Appendix.

Fatigue Load Test Spectrum for the Aluminum Ship-Evaluation Model

Analyses of fatigue crack-growth sensitivity were performed for the lifetime bending-moment (BM) spectra developed for the 90-m ship to determine the fatigue test spectrum to be applied to ASEM.

Predicted Lifetime-Load Spectra

Figure 5 is reshown in Fig. 7 in terms of percentage of maximum bending where 240 MN-m (80 × 10^3 ft-tons) is the 100-percent maximum BM. (The use of this type of normalization allows changes in maximum bending moment to occur without changing distribution of the basic design spectrum, for application of this spectrum to any similar type of ship.) A basic spectrum of one 20-year block in 10-percent increments may be developed from Fig. 7. The 20-year block may be divided into 1, 1/10, and 1/100-year blocks or 20, 200, and 2000-blocks, corresponding to the 20-year service life of the ship; see Table 1. The high cycles for the basic 20-year block have been adjusted, and the number of cycles have been rounded off so

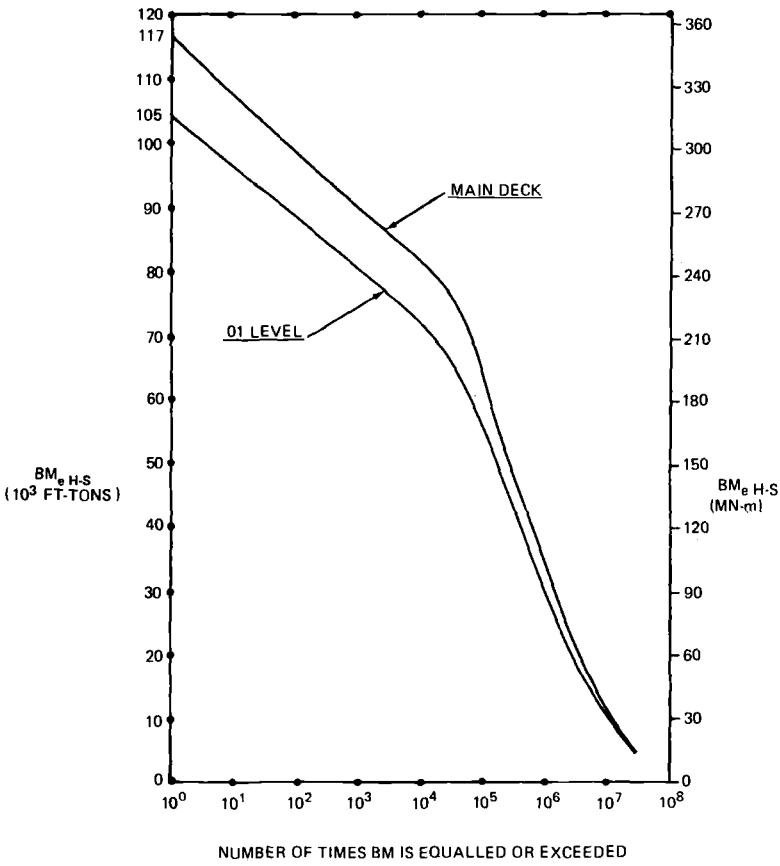

FIG. 6—*Lifetime midship effective vertical wave and whipping bending moment for a 90-m aluminum ship.*

as to have an even number of cycles in the shorter blocks. The effect of these changes is insignificant because most of the damage occurred at the 30- to 50-percent levels of the spectrum. Analyses of crack-growth sensitivity then were made to determine the effect of block size and stress elimination on the life of the ship at the keel.

No significant effect on life for the 1/10- and 1/100-year blocks was noticed when sensitivity investigations were made. The 1-year block gave a slightly longer life; see Table 2. It is desirable when performing analyses and tests to use small block sizes; then, whenever an unscheduled event occurs, the number of blocks can be translated readily into weeks of service life. The 1/100-year block is also a reasonable representation of the period in which the ship will experience the range of sea loadings that may result from passage of a storm. Reference 7 notes that small block size is similarly representative for fatigue testing of aluminum aircraft structure.

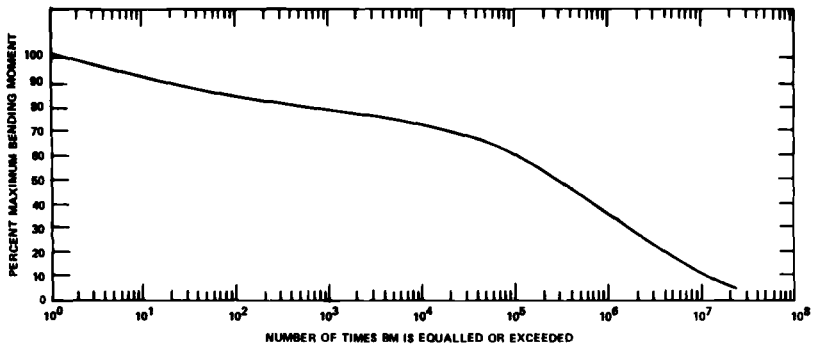

FIG. 7—*Cumulative frequency for a 20-year life vertical and athwartship bending moment for a 90-m aluminum ship.*

TABLE 1—*Block spectra for 10 percent increments of loads.*

Percent Max BM H-S	Number of Cycles, n			
	20-Year Block	1-Year Block	1/10-Year Block	1/100-Year Block
100	6	1/3	1/33	1/333
90	100	5	1/2	1/20
80	4000	200	20	2
70	52 000	2600	260	26
60	124 000	6200	620	62
50	280 000	14 000	1400	140
40	660 000	33 000	3300	330
30	1 480 000	74 000	7400	740
20	4 200 000	210 000	21 000	2100
10	18 000 000	900 000	90 000	9000
Total	24 800 106	1 240 005 + 1/3	124 000 + 1/2 + 1/33	12 400 + 1/20 + 1/333

A stress-elimination investigation was conducted with the 1/100-year spectrum. The results, Table 3, showed that stresses less than 6.9 MPa (1 ksi) did not contribute appreciably to crack growth.

Associated with each vertical moment cycle there is an athwartship cycle. The athwartship bending-moment spectrum is the same as the vertical, except that the value of athwartship bending moment is one half of the vertical bending moment. Half of the athwartship cycles lag the vertical by 60 deg, and the other half lag by 240 deg. This results because half of the time one side of the ship is assumed to be the weather side; half, the leeward.

The bending-moment variations represented in the load spectra, vertical and athwartship, are not completely symmetrical. For most load levels the

TABLE 2—*Effect of block size on basic spectrum.*

Stress, MPa	Number of cycles, n		
	1/10-Year Block	1/100-Year Block	1-Year Block
48.3	1/25	1/250	1/2
43.5	4	1	40
38.6	281	28	2810
33.8	465	46	4650
29.0	850	85	8500
24.2	1650	165	16 500
19.3	3250	325	32 500
14.5	8000	800	80 000
9.7	23 500	2350	235 000
4.8	82 000	8200	820 000
	120 000	12 000	1 200 000
a_f(mm)	227	227	257
N(year)	16.3	16.25	17

NOTE—1 ksi = 6.9 MPa
1 in. = 25.4 mm
a_f = final crack length
N = life

TABLE 3—*1/100-year basic spectrum load elimination.*

Load Level	Stress, MPa	Number of Cycles, n		
		1/100-Year Block	Eliminate Load Level 10	Eliminate Load Levels 9 and 10
1	48.3	1/250	1/250	1/250
2	43.5	1	1	1
3	38.6	28	28	28
4	33.8	46	46	46
5	29.0	85	85	85
6	24.2	165	165	165
7	19.3	325	325	325
8	14.5	800	800	800
9	9.7	2350	2350	
10	4.8	8200		
		12 000	3800	1450
a_f(mm)		227	226	226
N(years)		16.25	16.48	18.41

NOTE—1 ksi = 6.9 MPa
1 in. = 25.4 mm
a_f = final crack length
N = life

effect of this mean level is insignificant to structural life. The 100- and 90-percent levels are exceptions when the maximum whipping bending moment combines with the ordinary wave bending moment so that the bending-moment variation is 60-percent sag and 40-percent hog. Sagging bending moment produces tensile stress in the ship keel and compressive stress in the main or upper strength deck.

Test Load Spectra

Owing to the large number of cycles (24.8×10^6) in the lifetime load spectrum and the long time needed to apply them to ASEM, the decision was made to develop a test spectrum having fewer cycles (approximately 4×10^6) to be applied in a reasonable time (Fig. 8). The criteria for developing the test spectra were:

(*a*) They should be equivalent in damage to the design spectrum with the keel stresses used for the sensitivity studies.

(*b*) Load levels in the low-cycle fatigue regime (60- to 100-percent maximum BM) should remain as in the design load spectrum, while load levels in the high-cycle fatigue regime were to be changed to achieve the equivalent damage. Since failure modes vary along the S-N curve, equivalent damage should be within similar failure mode ranges.

An approximate spectrum was obtained by comparing the damage from the lifetime-load spectrum with the test spectrum. Midship keel stresses were used in the fatigue analysis, which was based on Miner's linear cumulative damage theory $\Sigma(n/N) = 1.0$ [*8*]. Since sufficient basic fatigue

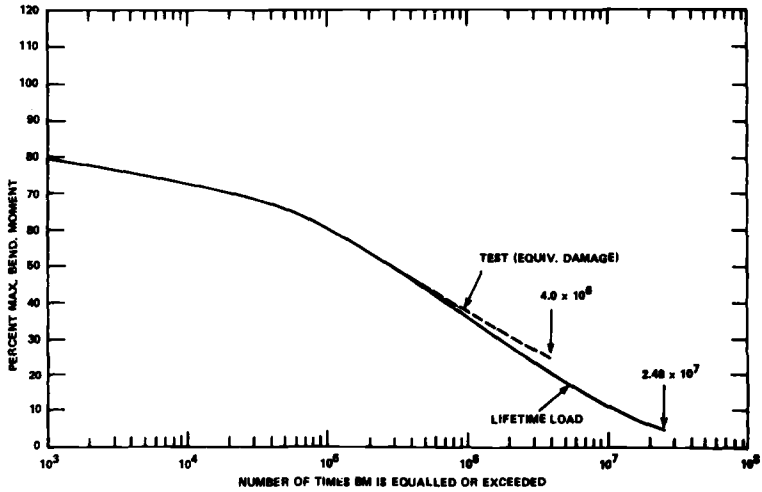

FIG. 8—*Cumulative frequency for 20-year life vertical and athwartship bending moment for a 90-m aluminum ship—test and design.*

data were not available for ASEM's 5456 series aluminum alloy, S-N data for 7075 and 2024 aluminum were used [*9-11*]. These data were revised and presented as percent ultimate for different stress-concentration factors. The test spectrum cycles were adjusted until the crack propagation life was equivalent to the life predicted for the design (lifetime-load) spectrum.

Test Stress Spectra

Stress spectra were developed from the test-load spectra for the conceptual 90-m ship, based on section properties determined from PVC (poly vinyl chloride) model experiments and calculated values for ASEM. A bending moment scale factor of 17.34 was used to obtain equivalent stresses on ASEM and the 90-m ship.

The maximum allowable primary stress for the design of the hull structure of the 90-m ship was chosen to be 54.7 MPa (3.5 tons/in.^{2}). The predicted maximum, lifetime, low-frequency, single amplitude bending moment for the 90-m ship was 120 MN-m (40 200 ft-tons). This corresponded to a keel stress of 55.6 MPa (3.6 tons/in.^{2}), comparing favorably with the design allowable. The stress range at the keel resulted from vertical wave and whip-bending moment only (M_v). The 100-percent maximum hog-to-sag stress range was 112 MPa (16.0 ksi).

Analysis Stress Spectra

The three primary areas of interest on both the 90-m ship and ASEM were at midship for the keel and the deck edges at the main and 01 levels. Longitudinal hull-girder stresses at the keel were obtained readily as previously indicated and resulted from vertical bending only. Stresses at the main and 01 deck edges resulted from both vertical and athwartship bending. On the leeward side of the ship, the vertical and athwartship bending combined to produce a tensile stress greater than vertical bending alone. During the same period, the weather side experienced a tensile stress less than vertical alone.

For purposes of analysis, the spectra for the deck edges have been presented in terms of equivalent vertical bending moments (M_e). The equivalent vertical bending moment produces the same average stress as the maximum deck-edge stress resulting from combined vertical and athwartship bending. At the main deck of the 90-m ship, the following relationships may be obtained: $M_e = 1.464\, M_v$ (leeward), and $M_e = 0.884\, M_v$ (weather). The corresponding formulas for the 01 level are: $M_e = 1.31\, M_v$ (leeward) and $M_e = 0.866\, M_v$ (weather). For one half the life of the ship at sea, waves are assumed to approach on the starboard side, thus, starboard is the weather side, and port is leeward. For the other half life at sea, port is assumed the weather side and starboard is leeward. Therefore, using the

previously described formulas for M_e, a lifetime spectrum of loads corresponding to deck-edge stresses for either port or starboard is obtained. The predicted lifetime spectra for the deck edges at the main and 01 levels are shown on Fig. 9. These spectra are also generally applicable for analysis of ships similar to the 90-m aluminum ship.

Test Procedure

In the test procedure for ASEM, the athwartship loading will be applied so that maximum deck-edge stresses will alternate port and starboard every other block. This was accomplished by modifying the test spectra of Table 4 by increasing the number of cycles at 90-percent maximum from 100 to 105 cycles. The additional 5 cycles will not have a significant effect on life since the fatigue analyses showed that the major damage occurred in the middle range of loading. This modification caused the block numbers for the 90- and 100-percent levels to alternate odd and even, automatically alternating maximum tensile stress at the deck edge from port to starboard when initial block-cycle direction was keyed to the block number.

The test spectrum shown in Table 5 will be applied to ASEM in a low-high-low stress level sequence. The ASEM test will take approximately 108 weeks with a load rate of 1 cps. This also provides for downtime, inspection, and repairs.

Conclusions

1. Full-scale, ship trial results, limited though they are, provide a reasonable empirical basis for developing a lifetime-load spectrum for fatigue designing and testing a large-scale aluminum ship model.

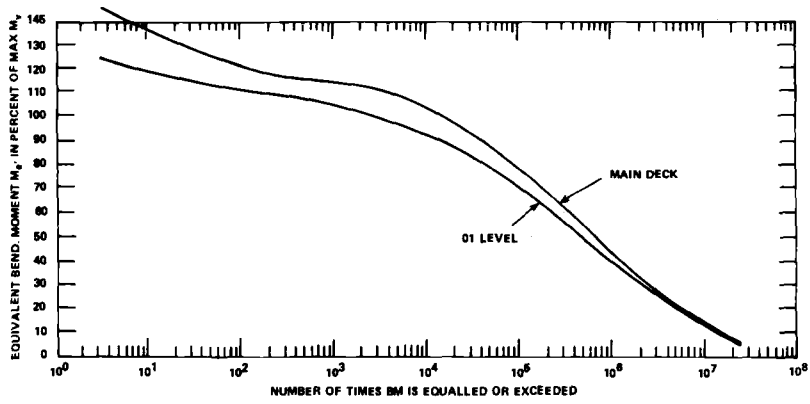

FIG. 9—*Cumulative frequency for 20-year life deck edge bending moment for a 90-m aluminum ship.*

TABLE 4—*Test spectra for 90-m aluminum ship.*

Percent Max Bending Moment	Number of Cycles, n			
	Vertical Bending Moment		Lateral Bending Moment 1/100-Year Block	
	20-Year Block	1/100-Year Block	Starboard	Port
100	6	1/333	1/666	1/666
90	100	1/20	1/40	1/40
80	4000	2	1	1
70	52 000	26	13	13
60	124 000	62	31	31
50	320 000	160	80	80
40	800 000	400	200	200
30	2 700 000	1350	675	675
20	0	0	0	0
10	0	0	0	0
0				
Total	4 000 106			

TABLE 5—*Test spectrum for the Aluminum Ship Evaluation Model.*

Vertical Loads		Athwartship Loads	
Percent M_v	1/100 Year	Percent M_v	1/100 Year
30	675	15	675
40	200	20	200
50	80	25	80
60	31	30	31
70	13	35	13
80	1	40	1
90	1/19	45	1/19
100	1/323	50	1/323
80	1	40	1
70	13	35	13
60	31	30	31
50	80	25	80
40	200	20	200
30	675	15	675

2. Fatigue crack-growth sensitivity studies indicate that a 1/100-year block spectrum, which represents a 3- to 4-day at sea period for the conceptual 90-m ship, is a practicable compromise for conducting the fatigue test on ASEM.

3. The ASEM test results will be used to develop design, fabrication, and repair guidelines for future aluminum ship structures.

Acknowledgments

The support of this work by the Materials and Mechanics Division of the Naval Sea System Command and the Center is gratefully acknowledged.

APPENDIX

Prediction Procedure for Lifetime Bending Moment

A brief description of the items considered in the lifetime bending-moment prediction procedure of a midship longitudinal hull girder and an illustration of application for the 90-m ship follows.[6]

Predict Ship-Operating Areas

During the 7 years of the 20-year active life that the 90-m ship is expected to be at sea, it is assumed that it will operate in the following areas:

Operating Area:	*Percent of Time*
North Atlantic between 30 and 50 deg North	50
North Atlantic above 50 deg North	10
Mediterranean	25
Caribbean	15

Predict Wave Heights and Periods

The probability of encountering selected ranges of significant wave height in these operating areas as well as the wave periods and the number of variations that pertain for the wave heights for the 7-year underway period are given in Table 6. (In the figures and tables used in this discussion, the fractions following the designation of bending moment and wave height such as BM 1/3 and WH 1/3 or WH 1/10, represent average values of the highest 1/3 hog-to-sag (H-S) bending moments and highest 1/3 or 1/10 crest-to-trough (C-T) wave height variations. The average of the highest one third is also called the significant value.)

Predict Relations Between Bending Moment and Wave Height

Figure 10 shows the predicted relation between low-frequency, midship bending moment and wave height for the 90-m ship. This relationship was obtained by a

[6]Unpublished information used in the development of Figs. 3 through 6 was prepared for the Structures Department at DTNSRDC by Science Engineering Analysis Co., Bethesda, Md., under Contract N00167-76-M8193 (October 1976).

TABLE 6—*Wave conditions.*

Significant Crest-To Trough Wave Height (WH 1/3)				
Range, ft	Midrange, ft	Occurrence, percent	Average Period of WH Variations, s	Number of WH Variations (N),[a] million
0 to 2	1.0	2.1	2.0	2.32
2 to 5	3.5	31.9	3.7	18.83
5 to 7	6.0	23.0	4.9	10.36
7 to 10	8.5	22.0	5.8	8.33
10 to 15	12.5	14.8	7.7	4.25
15 to 20	17.5	4.2	8.4	1.11
20 to 25	22.5	1.5	9.5	0.349
25 to 30	27.5	0.37	10.5	0.078
30 to 35	32.5	0.10	11.4	0.019
35 to 40	37.5	0.02	12.3	0.0036
		99.99		45.65

[a]Seven years at sea.
NOTE: 1 m = 3.3 ft

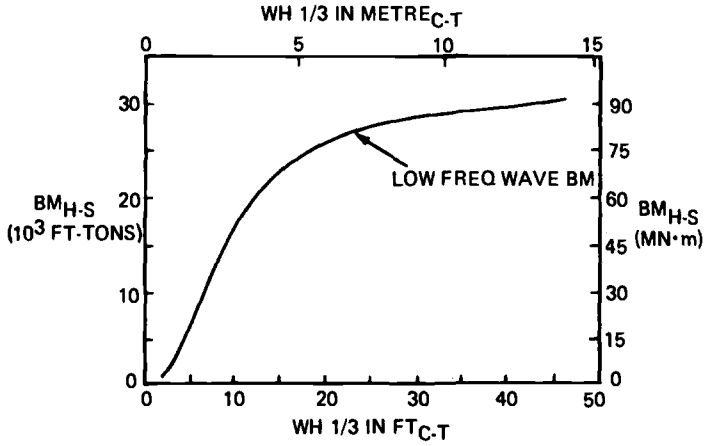

FIG. 10—*Predicted midship vertical wave bending moment versus wave height for 90-m aluminum ship.*

method described in Ref *2*. It is assumed that ship course and speed changes will not alter significantly the relations depicted in Fig. 10.

Predict Lifetime Wave-Bending Moment Occurrences

Ten significant values of midship bending moment, corresponding to the ten significant values of wave height listed in Table 6, are determined from the relation between bending moment and wave height depicted in Fig. 10 for the 90-m ship. A prediction is then made of the frequency of occurrence for a range of selected values of bending moment for each of the ten levels characterized by the significant

values. This prediction is made on the basis of ship trial results that show the Rayleigh probability distribution applies to values of hog-to-sag variations of low-frequency bending moment.

Use the previously described results to prepare Fig. 3.

Predict Conditions for Whipping Occurrences

The product of the fractions of time that the ship will operate at speeds, wave heights, and heading to the waves conducive to the generation of whipping responses and the lifetime hours at sea are used to predict the number of hours (Table 7) that conditions for dynamic whipping occurrence will exist for the 90-m ship.

Predict Representative Value of Whipping Bending Moment

Figure 11 depicts representative midrange-average values of maximum whipping bending moments, measured during five ship trials at which significant whipping responses were recorded. (The TALBOT and MCDONNELL are structurally similar ships.) These data were used to estimate a similar average, considered representative of the midrange between mild and severe whipping, for the 90-m ship as indicated by the dotted line on Fig. 11. The meaning of average of maximum whipping bending moment as used herein is illustrated in the sketch accompanying Fig. 12.

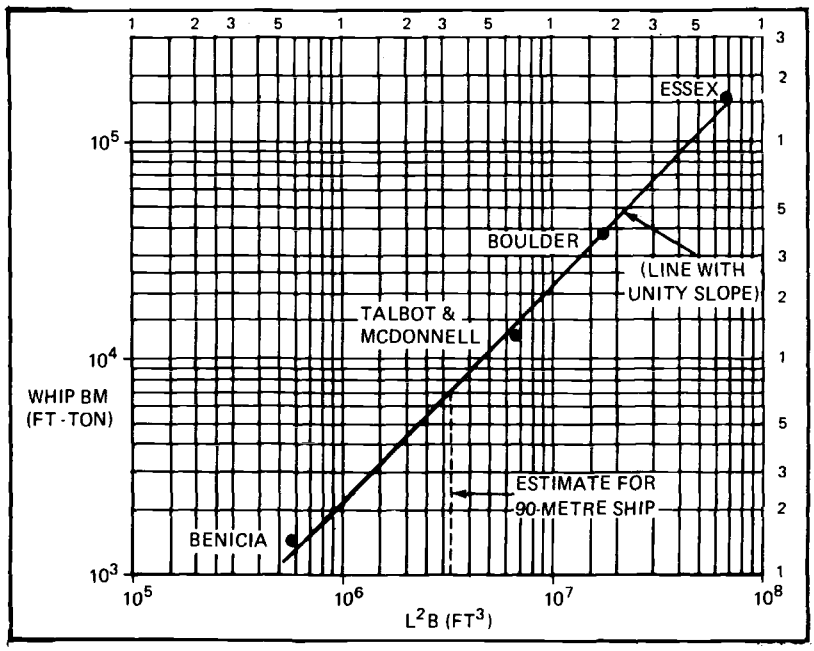

Note: L^2B in cubic feet ≈ 35 times L^2B in cubic metres
BM in foot-ton ≈ 0.33 times BM in kilonewton-metres.

FIG. 11—*Representative midrange average midship vertical whipping bending moment versus* L^2B.

TABLE 7—*Dynamic whipping response for 90-m ship.*

Relative Ship Speed,[a] knots	WH 1/10, m	Average of Maximum Hog-to-Sag Whipping Bending Moment, MN·m	Number of Hours for Whipping Condition	Whipping Occurrance or Slam Rate, Slams/h	Total Number of Slams
24.7	3.1	20.	11	113	1240
24.7	5.8	32.	11	185	2035
25.4	3.1	21.	59	115	6770
25.4	5.8	32.	59	188	11 000
20.8	3.1	15	301	88	26 500
20.8	5.8	26.	301	150	45 150
16.2	3.1	9.	1019	68	69 300
16.2	5.8	21.	1019	115	117 000
25.4	2.3	18.	103	100	13 030
25.4	3.1	21.	103	115	11 800
32.3	2.3	26.	12	150	1800
32.3	3.1	29.	12	173	2080
11.5	5.8	14.	1084	88	95 390
12.4	5.8	16.	219	91	19 920
15.9	5.8	20.	82	114	9390
19.4	5.8	25.	2.6	143	370

[a]Relative ship speed equals ship speed relative to wave celerity or speed. It is assumed that whipping occurs only when the ship is heading directly into the waves or is taking them somewhat less directly on the port or starboard bow.

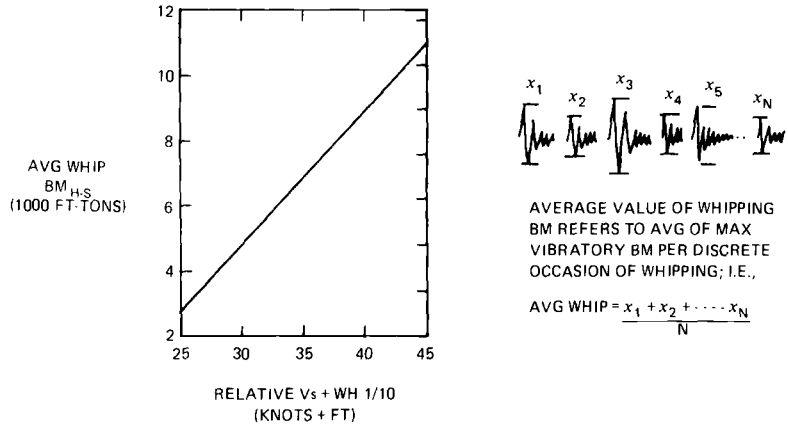

Note: *WH* 1/10 in feet ≈ 3.3 times WH 1/10 in metres

FIG. 12—*Average midship vertical whipping bending moment versus relative ship speed and wave height for 90-m ship.*

Predict Relation Between Wave Height and Ship Speed and Whipping Bending Moment

Values for the average of maximum whips for discrete occasions of whipping versus relative ship speed and wave height for the 90-m ship are shown in Fig. 12. Figure 13 shows the relation between related values of these quantities for measurements obtained on USS ESSEX (CVA-9).

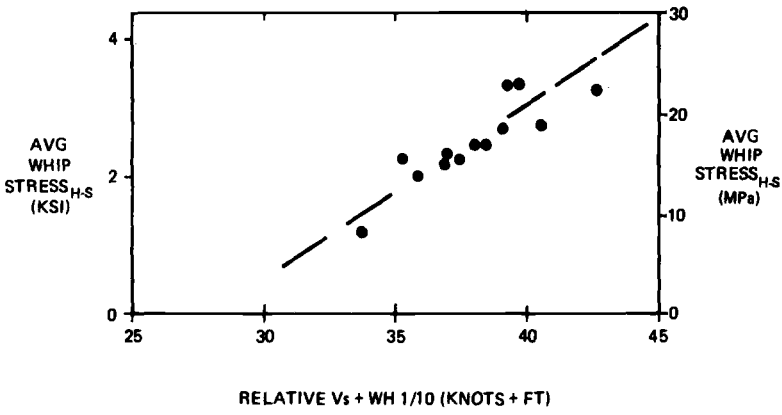

Note: 1 ksi stress ≈ 69 000 ft-tons of midship vertical bending moment
WH 1/10 in feet ≈ 3.3 times WH 1/10 in metres.

FIG. 13—*Average of maximum midship whipping main deck stress versus relative ship speed and wave height for thirteen 1-h test runs on USS ESSEX (CVA9).*

Predict Whipping Rate

The slam (or whipping occurrence) rate versus relative ship speed and wave height is shown in Fig. 14. Figure 15 shows the relation between related values of these quantities for measurements obtained on USS BOULDER (LST-1190).

Predict Frequency and Decay Rate of Whipping Vibration

The frequency of the fundamental mode of vertical, flexural hull vibration and the logarithmic decrement of this vibration versus ship length for hull girder-whipping responses measured on several ships is shown in Fig. 16. Figure 16 indicates that values of 2.1 and 0.21 are applicable for whipping frequency and logarithmic decrement, respectively, for the 90-m ship. Springing vibration levels that are not excited by ship-to-wave impacts are not expected to be significant for the 90-m ship.

Predict a Typical Time History for an Occasion of Whipping

Figure 17 shows a predicted typical time history for an occasion of whipping for the 90-m ship. This time history is the time-domain sum of low-frequency wave and whipping bending moment. The time history represents assumptions as to where whipping initiates in the low-frequency wave cycle of hull flexural bending and the effect of dynamic sag addition to the low-frequency bending moment. The relatively rapid decay rate of the vibratory bending moment shown in Fig. 17 eliminates concern that significant whipping vibrations will persist and overlap the following whipping occurrence. Figure 18 shows a typical time history that includes whipping responses measured during full-scale experiments on a U.S. Navy ship.

Predict Number and Severity of Whipping Occurrences

A prediction is made of the frequency of occurrence of a range of selected values of whipping variations, characterized by each of the average values of maximum

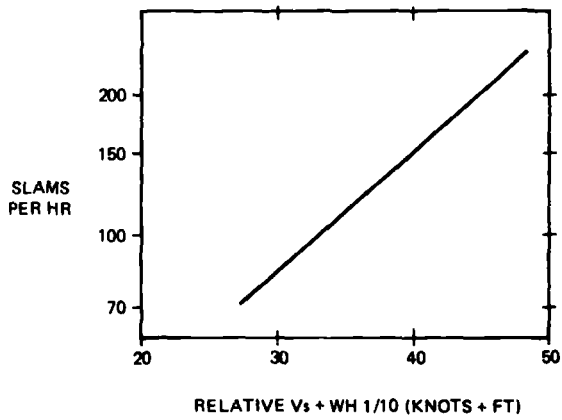

Note: WH 1/10 in feet ≈ 3.3 times WH 1/10 in metres.

FIG. 14—*Slam rate versus relative ship speed and WH 1/10 for 90-m aluminum ship.*

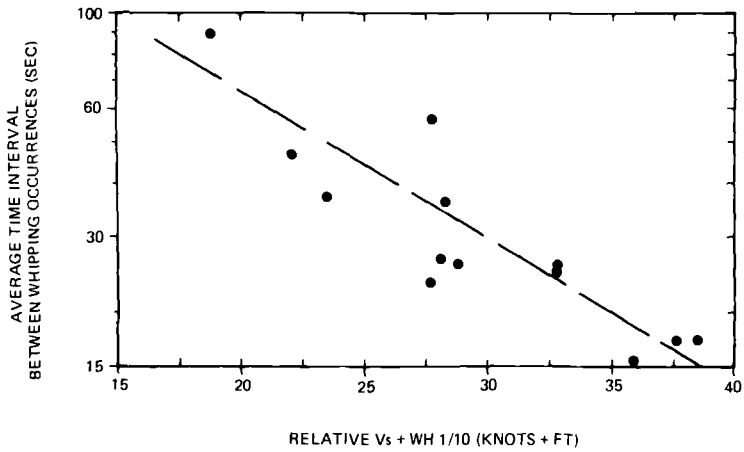

Note: WH 1/10 in feet ≈ 3.3 times WH 1/10 in metres.

FIG. 15—*Average time interval between vertical whipping occurrences versus relative ship speed and wave height for thirteen 30-min test runs on USS Boulder (LST 1190).*

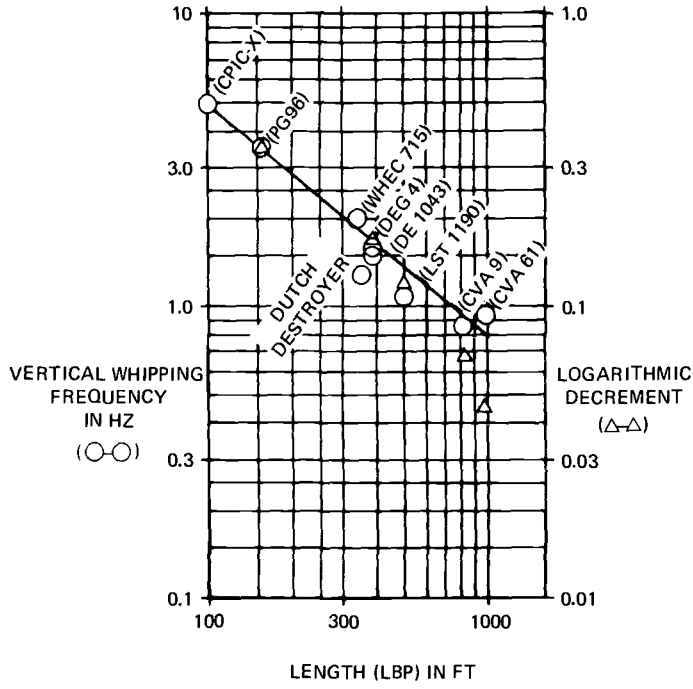

Note: LBP in feet ≈ 3.3 LBP in metres.

FIG. 16—*Frequency and logarithmic decrement of whipping versus ship length.*

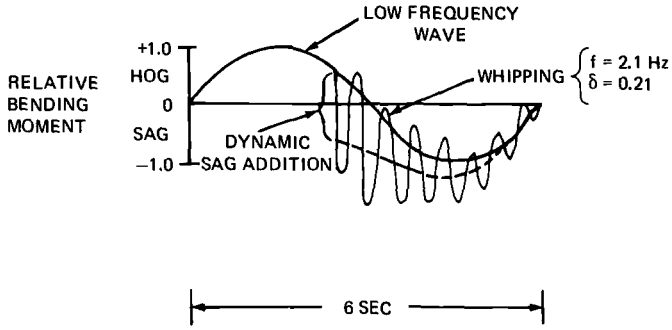

FIG. 17—*Predicted typical time history of midship vertical bending moment for an occasion of whipping for 90-m ship.*

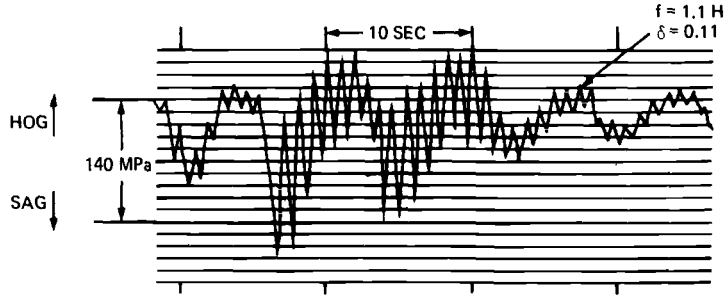

FIG. 18—*Sample oscillogram of midship keel vertical bending stress for USS BOULDER (LST 1190).*

vibratory bending moment given in Table 7. This prediction is made on the basis of ship trial results, showing that the exponential probability distribution applies to the distribution of maximum vibratory bending moment for discrete occasions of whipping.

Predict Lifetime Maximum Whipping Bending Moment

Figure 19 shows the probability that the extreme value will exceed a selected whipping bending moment during a 15-min period when the 90-m ship is operating in the limiting environment. The predicted lifetime-extreme value of midship, vertical whipping bending moment for the 90-m ship is taken as about 150 MN-m hog-to-sag. This value reflects modifications to ship operations, such as reducing speed, when the ship captain is likely to intercede to ease the severity of whipping.

Predict Lifetime, Vibratory Bending-Moment Occurrences

Vibratory bending moments include ringing vibrations that follow the initial whip variation for each occasion of whipping. The number of ringing variations for each whipping occurrence is determined by the value of the initial variation and

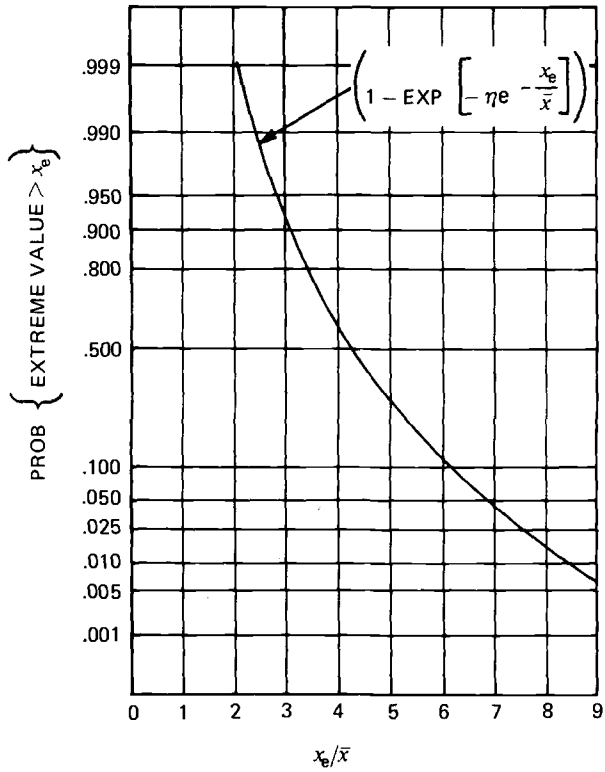

FIG. 19—*Probability that extreme value exceeds a selected midship vertical whipping bending moment.*

the number of cycles required for the subsequent ringing variations to decay to the selected lower truncation value.

Use the previously described results to prepare Fig. 4.

Predict Lifetime Combined-Wave and Vibratory Bending Moment Occurrences

A preliminary investigation of fatigue crack growth sensitivity was made to determine the detail required for combining the low-frequency wave and vibratory bending moments.

Use the previously described results to prepare Fig. 5.

Predict Relation Between Vertical and Athwartship Bending Moment

Athwartship bending-moment variations of the longitudinal hull girder are assumed to be 50 percent of the corresponding vertical bending-moment variations for all wave heights and ship headings and speeds. The athwartship bending moments also are assumed to have a constant value of phase difference with the corresponding vertical bending moments. Ship trial data show there is not a constant amplitude and phase relation between time histories of the vertical and athwartship bending strains. However, the constant amplitude and phase assumptions are considered rational simplifications for predicting deck-edge stress.

Predict Lifetime Equivalent Vertical Bending-Moment Occurrences

Estimates of the magnitude and number of occurrences of equivalent midship bending moment that produce the same average deck stress as the maximum main and 01 level deck-edge stress resulting from combined vertical and athwartship bending of the hull girder, were obtained by application of the Law of Cosines.

Use the previously described results to prepare Fig. 6.

Predict Reference Mean-Bending Moment

The reference mean value comprises the effects of stillwater bending moment, ships-own-wave smoothwater bending moment, shift in mean value when the ship travels in waves, and thermal effects. A resultant reference mean of 15 MN-m in hogging is assumed for midship vertical bending moment for the 90-m ship. A zero-reference mean value is assumed for athwartship bending moment.

References

[1] Jasper, N. H. and Birmingham, J. T., "Strains and Motions of USS ESSEX (CVA-9) During Storms Near Cape Horn," *TMB Report No. 1216*, David W. Taylor Naval Ship Research and Development Center, Carderock, Md., Aug. 1958.

[2] Birmingham, J. T., "Longitudinal Bending Moment Predictions Derived from Results of Seven Ship Trials," *NSRDC Report No. 3718*, David W. Taylor Naval Ship Research and Development Center, Carderock, Md., Sept. 1971.

[3] Birmingham, J. T., Brooks, R. L., and Jasper, N. H., "Statistical Presentation of Motions and Hull Bending Moments of Destroyers," *TMB Report No. 1198*, David W. Taylor Naval Ship Research and Development Center, Carderock, Md., Sept. 1960.

[4] Birmingham, J. T. and Palmer, F. W., Jr., "Stresses and Motions of a Destroyer Escort in Random Seas," *NSRDC Report No. 2610*, David W. Taylor Naval Ship Research and Development Center, Carderock, Md., March 1968.

[5] Birmingham, J. T. and Dinsenbacher, A. L., "Stresses and Motions of a Liberty Ship in Random Seas," *TMB Report No. 2081*, David W. Taylor Naval Ship Research and Development Center, Carderock, Md., Nov. 1965.

[6] Andrews, J. N., "Structural Responses and Motions of USS WILLIS A LEE (DL-4)," *NSRDC Report No. 2997*, David W. Taylor Naval Ship Research and Development Center, Carderock, Md., March 1969.

[7] Breyan, W., "Effects of Block Size, Stress Level and Loading Sequence on Fatigue Characteristics of Aluminum-Alloy Box Beams," *Effects of Environment and Complex Load History on Fatigue Life, ASTM STP 462*, American Society for Testing and Materials, Philadelphia, Pa., 1970.

[8] Miner, M. A., *Journal of Applied Mechanics*, Vol. 12, 1945, p. A-159.

[9] "Metallic Materials and Elements for Aerospace Vehicle Structures," *Military Handbook MIL-HDBK-5B*, Department of Defense, Washington, D.C., Sept. 1971.

[10] "Aerospace Structural Metals Handbook," *AFML-Technical Report-68-115*, Mechanical Properties Data Center, Belfour Stulen, Inc., Watertown, Mass., 1976.

[*11*] Naumann, E. C., Hardrath, H. F., and Guthrie, D. W., "Axial-Load Fatigue Tests of 2024-T3 and 7075-T6 Aluminum-Alloy Sheet Specimens Under Constant-And Variable-Amplitude Loads," *NASA Technical Note D-212*, National Aeronautics and Space Administration, Washington, D.C., Dec. 1959.

N. H. Sandlin,[1] *R. R. Lauridia,*[1] *and D. J. White*[1]

Flight Spectra Development for Fighter Aircraft

REFERENCE: Sandlin, N. H., Lauridia, R. R., and White, D. J., **"Flight Spectra Development for Fighter Aircraft,"** *Service Fatigue Loads Monitoring, Simulation, and Analysis, ASTM STP 671,* P. R. Abelkis and J. M. Potter, Eds., American Society for Testing and Materials, 1979, pp. 144-157.

ABSTRACT: A method is presented for deriving realistic flight-by-flight stress spectra which are valid for any point in the structure of fighter or attack type aircraft. This method uses regression equations to define the relationships among stresses and flight parameters. The statistical distributions of aircraft motion parameters are derived and defined in multi-parameter response tables. These tables are combined with assigned mission profile data to establish all of the required flight parameters which are used in the regression equations to develop stress spectra. These spectra then are sequenced into a flight-by-flight order which can be used as input to a damage determination model or as a load program for laboratory testing.

KEY WORDS: stress spectra, regression analysis, multiparameter response, mission profiles, flight-by-flight, flight loads, environment model, distribution, operational usage, spectra ordering, fatigue tests

In support of MIL-STD-1530A, "Aircraft Structural Integrity Program," the contractor is required to develop flight-by-flight stress spectra for the initial design of the airframe [*1*].[2] These spectra are called design service loads spectra and are based on the Air Force supplied mission requirements. These spectra are used in the preliminary analyses and development tests needed to design and size the airframe to meet the damage tolerance and durability requirements. See Ref *1* for definition of terms.

As information concerning the actual aircraft usage becomes available during the loads and environment spectra survey (L/ESS) as well as during the individual aircraft tracking program (IAT) the previously developed design service loads spectra is revised to form the baseline operational spectra. This "updated" spectra is used in the final analyses to determine the inspection and modification requirements of each individual aircraft.

[1]Engineering specialists and technical project engineer, respectively, Structural Life Management, Vought Corp., Dallas, Tex. 75265.

[2]The italic numbers in brackets refer to the list of references appended to this paper.

A method, called FLISPEC, has been developed that satisfies these requirements for producing flight spectra. FLISPEC has undergone many changes during its development. Today it is fully tested and proven. FLISPEC was used extensively during the A-7D ASIP program to develop the design service loads spectra and then the baseline operational spectra [*2*].

This paper describes the significant steps in FLISPEC and gives sample results for the A-7D airframe.

Methodology Overview

FLISPEC has been developed for fighter/attack type aircraft and includes only the maneuver loads of the aircraft since it was proven to be reasonable in the case of small, rigid airframes such as the A-7D to exclude the gust, landing, and taxiing portions of the total environment. However, this is not the case with aircraft that experience high sink landings such as carrier based aircraft or gust encounters by large flexible aircraft. These loading conditions are being added to FLISPEC.

The FLISPEC overview is shown in Fig. 1 where the three main elements (regression analysis, environment model, and spectra ordering) represent separate computer routines. The necessary elements specified by the durability design requirements [*3*] are represented by the mission profiles, normal maneuver load factor spectra, and the resulting flight-by-flight stress sequences at any point in the airframe.

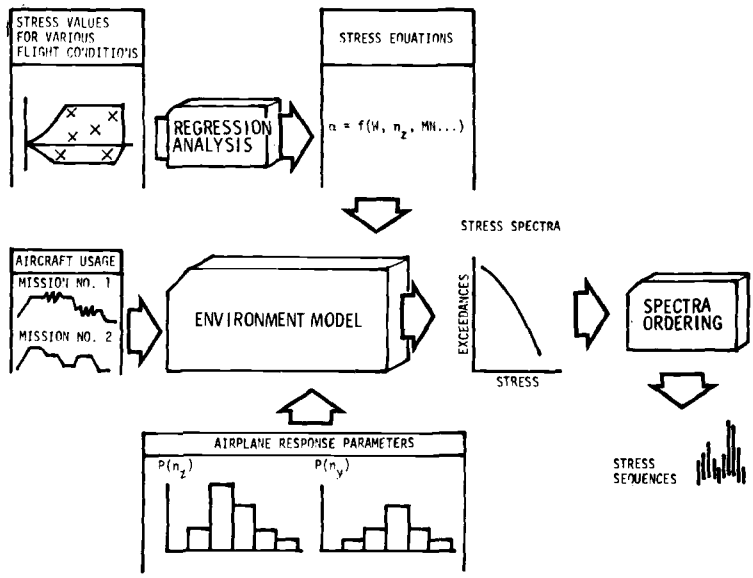

FIG. 1—*Flight spectra development methodology.*

The outstanding feature of FLISPEC is the ability to relate the airframe stresses as a function of flight parameters, such as gross weight, Mach number, altitude, wing sweep angle, store configuration, normal load factor, pitch velocity, yaw acceleration, etc. These relationships are determined by using a stepwise multiple regression analysis of the stress and flight parameter data obtained from either analytical means or from measured flight test data.

During the aircraft design phase, aircraft usage is supplied by the flying organization in mission profiles, which consist of flying times spent at combinations of weight, altitude, speed, store configuration, etc. Following deployment of the aircraft, these usage data are supplied by the L/ESS program measurements during actual operations.

The statistical information describing the aircraft response parameters is derived from existing multiparameter flight data and specification requirements. As the aircraft becomes operational, these data are obtained from the L/ESS program.

The stress regression equations, aircraft usage, and airplane response parameters are used in the environment model to produce the unordered stress spectra. The spectra ordering routine sequences these stresses into a flight-by-flight order for use in damage determination.

Regression Analysis

A typical fighter aircraft may require over 50 000 different load conditions to completely define the flight-by-flight stress values. These load conditions are comprised of various combinations of weight, altitude, airspeed, configuration, airplane response, etc. Because of the large number of load conditions, the regression equation approach is needed to make the problem manageable; it is far more economical than table interpolation methods or direct calculations. Regression analysis is an accepted procedure for computing control surface deflections, loads, and stresses and has been used on various aircraft including the A-7D [*4*].

The stepwise multiple regression procedure used in FLISPEC is a statistical technique for analyzing the relationship between a dependent variable and a set of independent variables, whereby the independent variables are selected in the order of their importance. Importance is determined by the reduction of sums of squares, and the independent variable most important in this reduction is entered in the regression. As shown in Fig. 2, the first step in this analysis (and perhaps the most important) is to select flight conditions that cover the full operational range of speed, altitude, weight, and configuration. For the development of the design service loads spectra, this selection would come necessarily from the predicted operational envelope of the aircraft. Selection of conditions from the measured flight loads survey and even from the loads/environ-

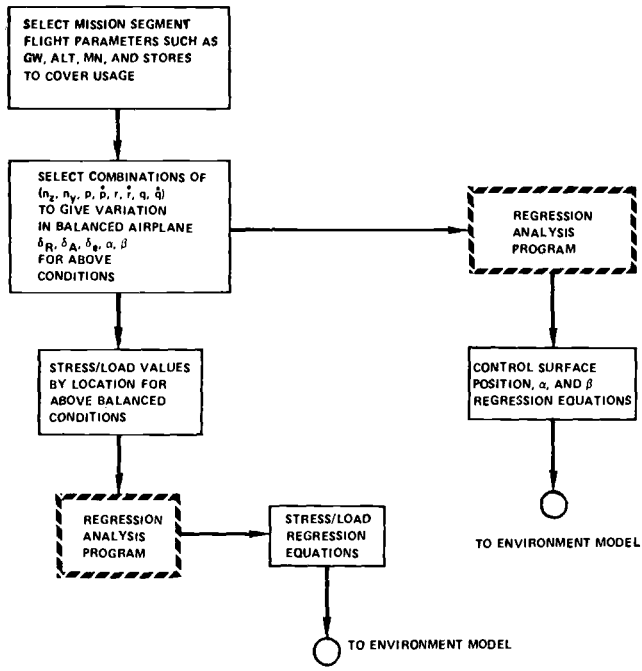

FIG. 2—*Regression analysis.*

ment spectra survey would be used for the revised baseline operational spectra.

Next, for the aforementioned selected flight conditions, choose combinations of response parameters to give a variation in balanced airplane control surface deflections, angle of attack, or sideslip. To be valid for all structural components of the airplane, it is necessary to have good variation in translational and angular accelerations that cover symmetric, asymmetric, abrupt, and smooth maneuvers. Once the independent variables have been determined, they are selected and combined in different ways to form parameters to be used by the routine in deriving the stress regression equations for each structural location. These selected parameters generally are similar for all types of aircraft. A typical parameter consists of the product of two variables, such as a control surface position multiplied by dynamic pressure. The significant parameters vary for different structural components. For example, the normal load factor multiplied by airplane weight is the important parameter for stress in the wing, while either lateral load factor or sideslip angle multiplied by dynamic pressure is the important parameter for the vertical stabilizer.

For development of the design service loads spectra during aircraft design, the dependent stresses are determined analytically. In the case of the A-7D, analytical unit stresses were determined using panel unit air-

loads and panel unit inertia in a NASTRAN analysis for each of the selected flight conditions. For the baseline operational spectra, measured stress information from the flight loads survey and from the L/ESS program is used to define the stress to flight condition set of data for regression analysis.

The data sets consisting of a dependent variable (stress or load) and several flight parameters are entered into regression which results in an equation for stress or load at a structural point as a function of only the necessary flight parameters.

An example presented to illustrate this methodology is the regression equation developed for the A-7D left wing aft attachment lug at F.S. 480. Since no measured flight stress data were available at this critical point, an analytical approach identical to an initial design effort was conducted. A regression equation relating lug axial stress to analytical flight parameters was determined. For this problem, there were 110 observations (or points-in-the-sky) with 21 variables associated with each observation, one of which was the calculated lug stress. Each of these 110 calculations of lug stress used the analytical unit stress derived from panel unit airloads and inertia as input to the finite element structural model. These 110 observations were made up of symmetric and asymmetric maneuvers as well as symmetric maneuvers with pitching acceleration. The 20 "independent" variables were combined in varied fashion to form 26 additional parameters for a total of 46 parameters which could be related to lug stress. These parameters are listed in Table 1.

TABLE 1—*Parameters for lug stress regression.*

		Combinations	
Q	Dynamic pressure, psi	MN^2	*IXY*AX*
ALPHAT	Horizontal stabilizer angle-of-attack, deg	ALT^2	*IYY*AY*
NZ	Normal load factor, g	GW^2	*IZZ*AZ*
GW	Gross weight, lb	*STWT1*NZ*	*MN*NY*
IYY	Moment-of-inertia (y-axis), lb-in-s^2	*STWT2*NZ*	*ALT*NY*
AY	Pitching acceleration, rad/s^2	*STWT3*NZ*	*GW*NY*
σ_{Lug}	Lug stress, psi	*WFW*NZ*	MN^2**NY*
MN	Mach number	*MN*NZ*	ALT^2**NY*
ALT	Altitude, ft	*ALT*NZ*	GW^2**NY*
ALPHAF	Fuselage angle-of-attack, deg	*GW*NZ*	*DELR*Q*
BETA	Fuselage side-slip angle, deg	MN^2**NZ*	*BETA*Q*
DELR	Rudder position, deg	ALT^2**NZ*	*ALPHAF*Q*
AX	Rolling acceleration, rad/s^2	GW^2**NZ*	*ALPHAT*Q*
AZ	Yawing acceleration, rad/s^2		
NY	Lateral load factor, g		
IXX	Moment-of-inertia, (x-axis), lb-in-s^2	1 psi = 6894.757 Pa	
IZZ	Moment-of-inertia (z-axis), lb-in-s^2	1 deg = 0.0174533 rad	
WFW	Wing fuel weight, lb	1 lb weight = 0.4535924 kg	
STWT1	Store weight at inboard station, lb	1 lb force = 4.448 N	
STWT2	Store weight at center station, lb	1 lb-in-s^2 = 0.1129792 kg·m^2	
STWT3	Store weight at outboard station, lb	1 in. = 0.0254 m	

In the first step of the regression process *MN*NZ* was chosen as the most important of the 46 parameters by the least stress sum of squares and was allowed to enter in regression. At each succeeding step, the parameter entered in the regression is that which explains the greatest amount of variance between it and the dependent variable (stress) that is, the variable with the highest partial correlation with stress. After investigating the standard error of estimate, checking the correlation coefficient and performing the F-test and t-test at each step, step 17 was chosen to stop the regression, which means 17 parameters were allowed to define the regression equation. As shown in Fig. 3, going even several steps past 17 adds very little to the regression equation. The final form of the lug stress regression equation follows, with the 17 parameters appearing in the order of their importance.

$$\begin{aligned}\sigma_{LUG} = &- 2281.1\,(MN*NZ) + 116.09\,(BETA*Q) - 0.20979\,(STWT2*NZ)\\ &+ 0.11279\,(GW*NZ) - 0.32592\,(STWT1*NZ) + 45061\,(MN^2)\\ &- 62143\,(MN) - 112.25\,(ALPHAT*Q) - 26.377\,(DELR*Q)\\ &- 0.2308\,(STWT3*NZ) - 0.00066613\,(IYY*AY)\\ &- 0.18472\,(WFW*NZ) + 1709.7\,(MN^2*NZ)\\ &+ 0.032631\,(GW*NY) - 52.586\,(ALPHAF*Q)\\ &- 0.92647*10^{-6}\,(ALT^2) - 0.22418*10^{-6}\,(GW^2) + 20884.67\end{aligned}$$

The validity of this lug stress equation is shown in Fig. 4 where the predicted versus actual points fall close to the perfect fit 45 deg slope line.

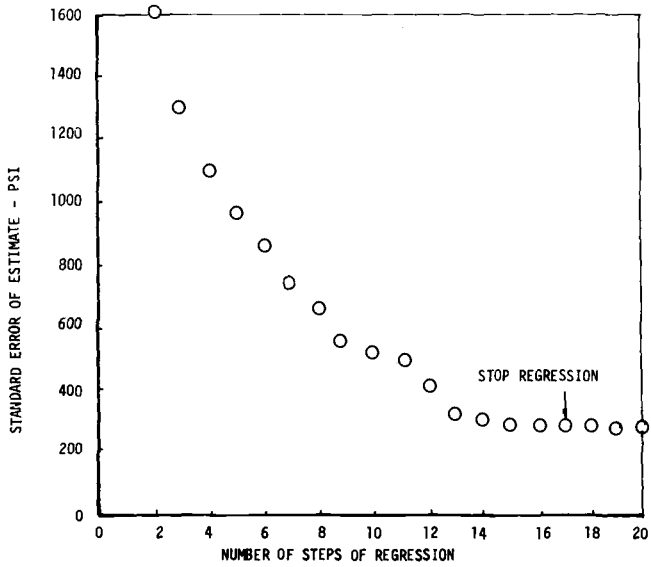

FIG. 3—*Error versus steps of regression.*

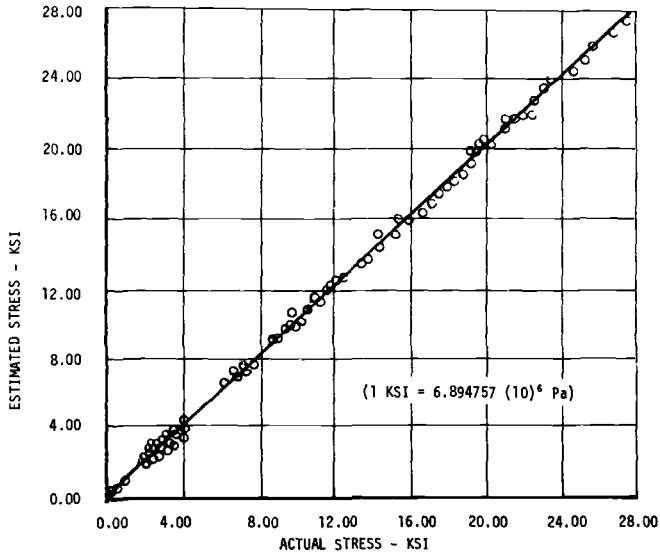

FIG. 4—*Actual versus estimated lug stress.*

In like manner, regression analysis was used to establish a relationship between measured flight parameters and measured A-7D wing stress (σ_W) on the lower skin at wing station 32 [5]. This type of data is analogous to using flight loads survey or L/ESS data needed for generating the baseline operational spectra. The regression was performed on 54 595 data observations representing 1256 h of recorded A-7D flight data. Each observation consisted of nine variables (σ_W, *NZ, GW, ALT, MN, WFW, STWT1, STWT2, STWT3*). From regression analysis it was determined that wing stress at W.S. 32 (σ_W) could be predicted as a function of the flight parameters as follows

$$\sigma_W = 644 - 0.05325\,(ALT) + 1266\,(MN^2) - 2974\,(NZ{*}MN) + 0.22775\,(NZ{*}GW) + 2617\,(NZ{*}MN^2) - 0.00000275\,(NZ{*}GW^2)$$

The validity of this wing stress equation is shown in Fig. 5. Instead of plotting predicted versus measured stress for all 54 595 points as was done in Fig. 4, Fig. 5 shows the spectrum (exceedances of stress level) for raw measured stresses as well as for the predicted stresses using the regression equation. Both curves were normalized to a 1000-h basis.

Environment Model

The environment model program is a specialized bookkeeping routine that combines a large amount of data from two sources (response param-

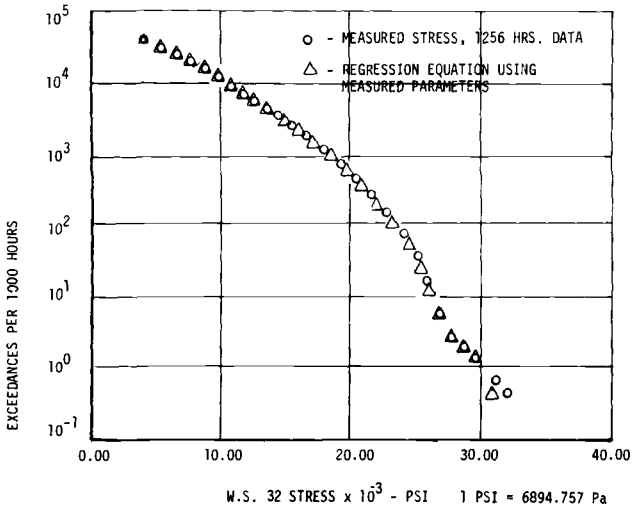

FIG. 5—*Actual versus estimated wing stress.*

eters and flight parameters) to calculate stress spectra (see Fig. 6). The purpose of the Block 1 task is to generate a table of multiparameter sets of aircraft flight response parameters for each type of mission segment and put each table on file to be recalled later. The flight response parameters are only those that are required from the stress regression equations. In the case of the A-7D analytical service loads spectra determination, the response parameters consisted of eight variables; vertical and lateral load factor with roll, pitch, and yaw velocities and accelerations.

Data input consists, for each response parameter, of the marginal and conditional distributions, which are the independent and dependent relative frequency of occurrence data. These parameter data come from various sources according to whether the aircraft is in the design phase or if measured L/ESS data is available from operational usage. For the A-7D analytic design service loads spectra determination, the normal load factor distribution for each mission segment came from the durability specification [*3*] as modified by existing counting accelerometer data. The other multiparameter distributions were obtained from the F-105D multichannel data flight loads program [*6*]. When measured multiparameter data become available during the L/ESS these newly formed parameter distributions are used in FLISPEC to determine the baseline operational spectrum.

A sample of a small portion of the air-to-air mission segment multiparameter set table that was generated for the A-7D is shown in Table 2. Even though hundreds of millions of possible combinations of these eight response parameters were possible in forming the air-to-air multiparameter sets, the use of a minimum probability of occurrence combines most sets

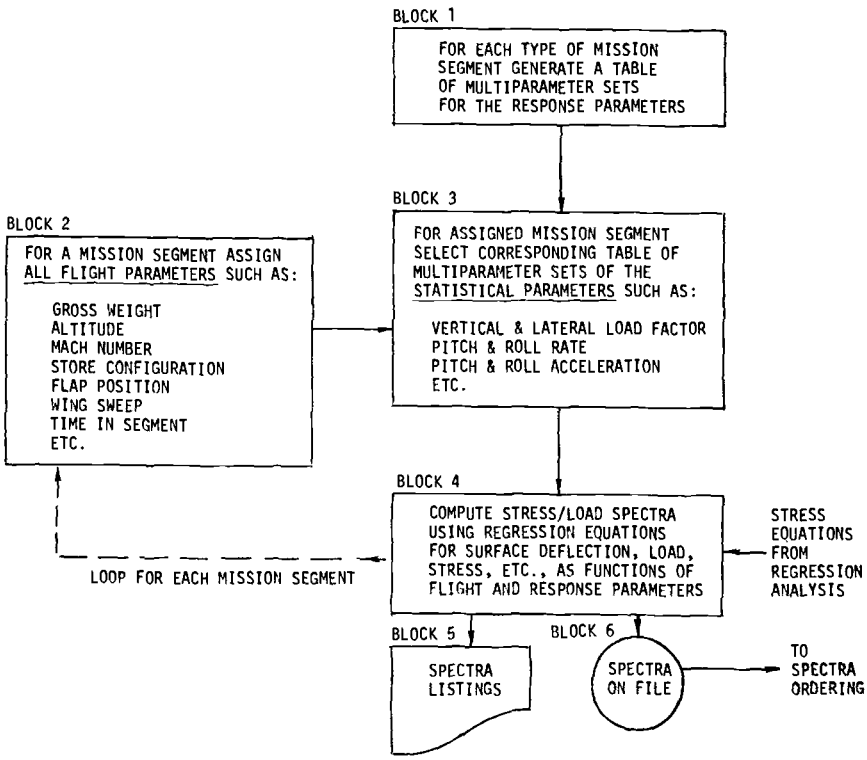

FIG. 6—*Multiparameter environment model.*

with others such that just over 2000 sets remain for investigation. No occurrences are lost in this process. In like manner, each mission segment is assigned its own table of multiparameter sets.

The flight parameters are entered into the problem by way of the Block 2 effort (see again Fig. 6). The lifetime usage of the aircraft is defined by user supplied mission profiles where frequencies of each mission type (or hours spent in each mission) are given. Each mission consists of a series of mission segments each with its own defined group of flight parameters such as weight, speed, altitude, as well as length of time spent in this mission segment. Table 3 illustrates these mission data for the A-7D navigation training mission. As L/ESS measured data from operational usage become available, these mission segment flight parameters will be revised for determination of the baseline operational spectrum.

The Block 3 effort consists of combining the mission assigned flight parameters with the multiparameter response data. For each defined mission segment of Block 2 the assigned values of the flight parameters such as weight, altitude, speed, hours, etc. are combined with each multiparameter set of the appropriate mission segment multiparameter table. These

TABLE 2—*Response parameter multiparameter table (portion of, air-to-air mission segment).*

N_Z	N_Y	p, deg/s	$\dot{p}$, deg/s^2	q, deg/s	$\dot{q}$, deg/s^2	r, deg/s	$\dot{r}$, deg/s^2	Peaks per 1,000 h
−2.5	0	0	0	−7.5	22.5	0	0	0.65
7.0	−0.2	0	0	12.5	−22.5	0	0	0.82
7.0	−0.2	0	0	7.5	0	0	0	1.23
7.0	−0.2	0	0	0	0	0	0	0.68
7.0	−0.1	45	−60	7.5	−22.5	0	0	1.76
7.0	−0.1	0	0	12.5	−37.5	0	0	1.20
7.0	−0.1	0	0	7.5	0	0	0	13.18
7.0	−0.1	0	0	7.5	−22.5	0	0	12.86
7.0	0	0	0	12.5	−52.5	0	0	1.07
7.0	0	0	0	7.5	0	0	0	64.58
7.0	0	0	0	7.5	−22.5	0	0	72.18
7.0	0	0	0	12.5	−37.5	0	0	5.69
7.0	0.1	45	60	7.5	−22.5	0	0	11.17
7.0	0.1	0	0	7.5	−37.5	0	0	1.89
7.0	0.1	0	0	12.5	0	0	0	20.28
7.0	0.1	0	0	7.5	−22.5	0	0	20.19
7.0	0.2	0	0	7.5	−22.5	0	0	1.38
7.0	0.2	0	0	12.5	0	0	0	1.72
7.0	0.2	0	0	0	0	0	0	0.73
11.0	0	0	0	7.5	−22.5	0	0	0.73

NOTE—1 deg = 0.0174533 rad

TABLE 3—*Mission data, flight parameters, navigation training (8 percent of peacetime usage).*

Condition I.D.	*GW*, lb	*ALT*, ft	*MN*	*V*, *KTAS*	*V*, *KEAS*	*t*, min	Occurrence Data MIL-A-8866A	Wing Fuel Weight (per side), lb	Store Weight (No. 1 and 8), lb	Store Weight (No. 2 and 7), lb	Store Weight (No. 3 and 6), lb
Initial	35 608							2305			2191
Takeoff	34 961	0						2305			1868
3.01	34 427	15 000	0.72	450	360	15	ascent	2305	0	0	1601
3.02	30 342	30 000	0.80	471	288	140	cruise	1634	0	0	229
3.03	26 705	25 000	0.70	421	282	10	descent	0	0	0	229
3.04	26 419	12 500	0.40	250	206	5	descent	0	0	0	229
3.05	25 905	0	0.27	180	180	10	loiter	0	0	0	229
Landing	25 591	0									
Post Flight	25 501		*FLT t* = 180								

NOTE—1 lb weight = 0.4535924 kg
1 ft = 0.0348 m
1 KAS = 0.514444 m/s

parameters joined together make one complete set of all needed independent parameters of the regression equations for stress. Accompanying this set of parameters the corresponding number of occurrences. Each of these sets of parameters is applied to all of the stress regression equations previously supplied from the regression analysis (see Block 4). The calculated stress values and their corresponding number of occurrences on a segment-by-segment basis are saved for spectra presentation on a segment-by-segment basis, a mission basis, and a total life basis.

Calculated stress spectra for the A-7D wing station 32 for a total life (exceedances per 1000 h) is presented in Fig. 7. A spectrum is presented for the analytical design service loads as well as one for the baseline operational spectrum resulting from the L/ESS updated usage information. In addition, the A-7D horizontal tail spectra (tail station 31.6) is shown in Fig. 8 for the analytical and baseline loads.

Spectra Ordering

This program for ordering the spectra serves as a link between the environment model and the damage prediction program or test load program. Peak stresses are ordered randomly in each mission segment and with each segment occurring in the order that the mission is flown. Then the missions

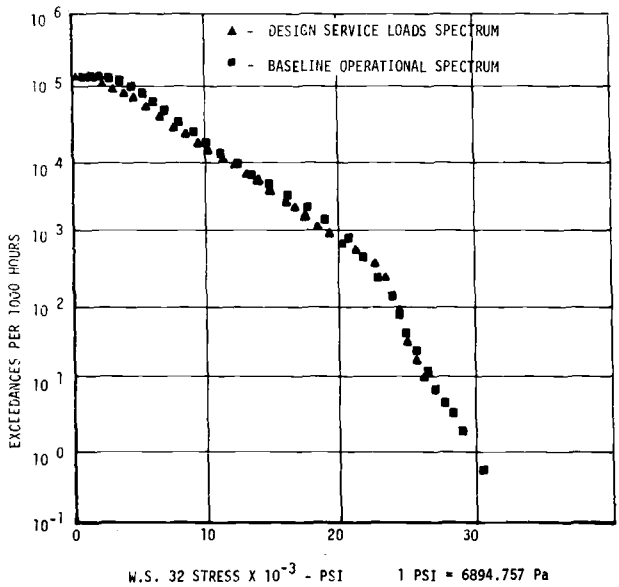

FIG. 7—*Design spectra to baseline spectra comparison, wing.*

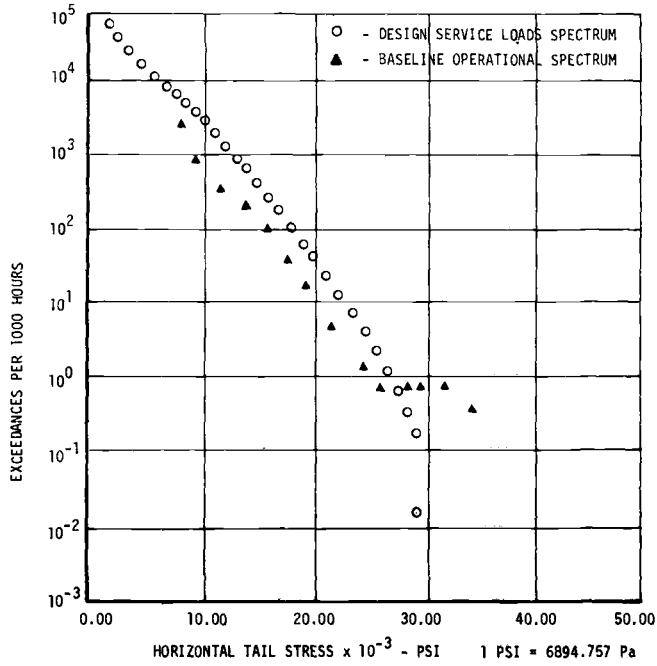

FIG. 8—*Design spectra to baseline spectra comparison, horizontal tail.*

themselves are ordered in a random fashion. The random flight-by-flight spectra may be modified and broken into repeating equal blocks of missions. When this is done, stress cycles occurring less frequently than once per block are added back into randomly selected blocks and placed in the proper mission and mission segment. The resulting sequenced spectra is then essentially repeatable at block intervals. An option allows stress cycles in each flight to be reordered into a low-high-low sequence on a flight-by-flight basis.

FLISPEC also is capable of simplifying the analysis through stress truncation and stress clipping. Stress truncation reduces the number of occurrences, and clipping limits the maximum and minimum stress values. The spectra are stored on disk or magnetic tape and represent the input to a damage determination model or may be used directly as a spectrum load program for laboratory tests.

Conclusions

FLISPEC is an active and validated technique now being used for producing flight-by-flight stress spectra for fighter/attack type aircraft and is compliant with current specifications regarding multiparameter flight response data. FLISPEC produces a valid sequence of loadings for any

point in the aircraft structure for use during the initial design stage or for the spectra update following the load/environment spectra survey. Expansion of this method to produce spectra also for gust loading, landing, and taxiing is planned.

References

[1] "Aircraft Structural Integrity Program, Airplane Requirements," *Military Standard MIL-STD-1530A(11)*, 11 Dec. 1975.

[2] Dumesnil, C. E. et al, "A-7D ASIP Part 1, Damage Tolerance and Fatigue Assessment Program," *Vought Report 2-53440/7R-5928*, 31 Jan. 1977.

[3] "Airplane Strength and Rigidity Reliability Requirements, Repeated Loads and Fatigue," *Military Standard MIL-A-008866B (USAF)*, 22 Aug. 1975.

[4] Yost, J. D. and Johnson, G. S., *Journal of Aircraft*, Vol. 9, No. 3, March 1972, pp. 199-204.

[5] Lauridia, R. R., "A-7D ASIP Part 2, Flight Recorder Program," *Vought Report 2-53470/7R-5929*, 31 Jan. 1977.

[6] Lopatoff, M. et al., "F-105 Statistical Flight Loads Program," *SEG-TR-66-16, Vol. 2*, USAF Research and Technology Division, Wright-Patterson Air Force Base, June 1966.

A. G. Denyer[1]

Flight-by-Flight Spectrum Development

REFERENCE: Denyer, A. G., **"Flight-by-Flight Spectrum Development,"** *Service Fatigue Loads Monitoring, Simulation, and Analysis, ASTM STP 671*, P. R. Abelkis and J. M. Potter, Eds., American Society for Testing and Materials, 1979, pp. 158-175.

ABSTRACT: A method of developing the design flight-by-flight sequenced stress spectrum at any location within the primary airframe structure is presented.

The procedure commences with the applicable procurement specifications for the aircraft and concludes with the detail's local stress spectrum suitable for fatigue and fracture mechanics analyses or testing. The stress spectrum is created within a computer program that utilizes input data comprising mission profiles, structural location data, libraries of load factor exceedance data, balanced external load conditions, and corresponding internal loads solutions. The output consists of the spectrum in tabular form and the time trace graphs of the stress amplitude.

Included is a typical spectrum developed for a variable geometry bomber with terrain-following capability, and discussion as to load sequence effects and the structural internal loads solutions necessary to describe the stress trace on a mission-by-mission basis.

Finally, the system-generated spectrum is discussed in terms of its effect on fatigue and fracture mechanics analysis.

KEY WORDS: load spectrum, randomization, fatigue (materials), crack growth, structural tests, fatigue tests

Recent developments in fatigue and fracture mechanics analysis reflect the significance of load sequence, particularly with reference to residual stresses and retardation of cracks caused by high loads. Consequently, flight-by-flight sequenced spectra need to be produced from the airplane usage specifications.

The spectrum generation method outlined herein was developed for a bomber aircraft using the United States Air Force requirements for durable and damage-tolerant design and proof of conformance testing. A computer program was written to provide the following:

1. Stress spectra at any location within the primary airframe structure for fatigue and fracture mechanics analysis

[1] Member of the Technical Staff, Rockwell International, El Sequndo, Calif. 90245.

2. Test spectra of balanced load conditions, compatible with the design spectra and suitable for testing large and small components as well as a complete vehicle.

The system first develops baseline spectra applicable to as many airplane components (wing, fuselage, empennage, etc.) as possible from the airplane usage requirements. Secondly, it links the generated spectra with an off-line data bank of internal load solutions for each of the airplane components in order to create the local load or stress spectrum. The baseline spectrum is the airplane response in terms of load factor at the center of gravity of the airplane. The choice of airplane load factor allows spectrum compatibility between one location in the airplane and another, while keeping the number of internal load solutions to a minimum; it also allows a balanced spectrum suitable for any size specimen.

Mission Profiles

Any load spectrum is based on the expected usage. This is supplied to the designers by the aircraft user or procuring agency in the form of mission profiles describing the type of flights to be flown, such as training or combat missions. Table 1 gives a sample of the combination of such missions expected in the life of a bomber. The missions are presented in terms of performance parameters; typically, airplane gross weight, Mach number, and altitude with the appropriate time scale. Mission profiles represent the normal rational utilization of the airplane and usually will not contain values of the performance parameters at the extremes of the design envelope. A bomber training mission is shown (Fig. 1) in terms of the history of the performance factors for one flight from pretakeoff taxi to postlanding taxi.

Outline of Spectrum Generation Method

The fatigue damage or crack growth accumulated on a part during the mission is a function of the local stress variation. For conversion to the

TABLE 1—*Design missions for a bomber lifetime usage.*

Mission Title	No. of Missions per Life	No. of Hours per Mission	No. of Landings per Mission
1. Training mission (with payload)	800	8	3
2. Training mission (without payload)	300	6.25	1
3. Design mission	100	10	1
4. Combat crew training sortie	25	8	5
5. Airborne alert	150	24	1

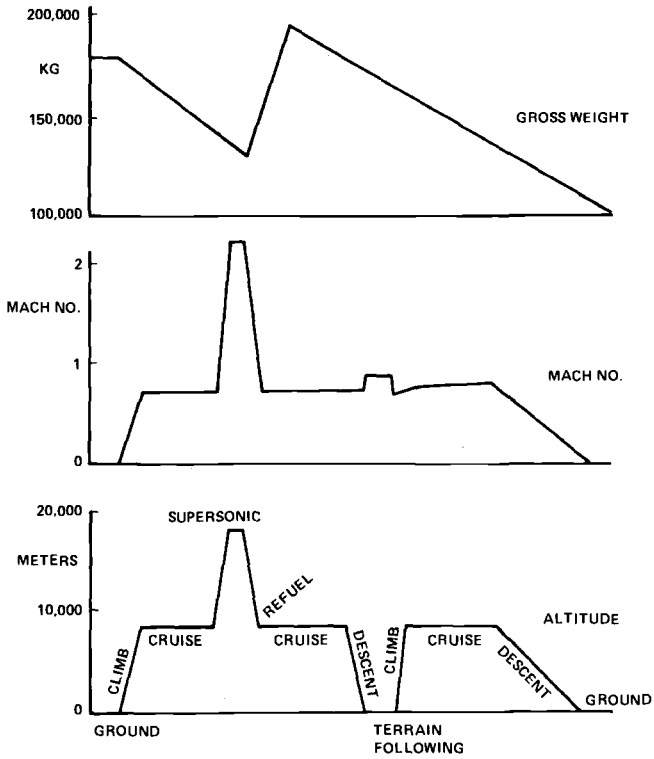

FIG. 1—*Mission performance parameters for bomber training mission.*

load or stress trace, the mission profile breakdown must account for all events that create significant external or internal load changes.

The spectrum is developed separately for each mission type as follows:

1. The mission is segmented to define the conditions used to describe the steady-state (1 g) load trace. The segmentation will include all events whose sequence is dictated by mission profile and which normally will reflect variation in weight, Mach number, altitude, and airplane geometry during the flight.

2. A load factor spectrum for each mission segment is produced from the airplane response to gusts, maneuvers, and ground handling. The sequence of these events is related only indirectly to airplane usage and tends to be random.

3. The load factor spectrum is converted to internal load or local stress at any selected structural location.

Fatigue and fracture mechanics analysis then is performed, using the developed stress spectra for each mission in a predetermined sequence of mission types.

Mission Segmentation

The degree of mission segmentation necessary is a function of the airplane usage and design, and requires a knowledge of the response of the structure to various flight and ground conditions.

Ground and flight conditions produce such a load variation that they obviously must be differentiated by proper segmentation. Ground conditions produce downbending on the wings and aft fuselage and, usually, upbending on the forward fuselage; flight conditions produce wing upbending and fuselage downbending.

Typical for all aircraft is the effect of weight and corresponding center-of-gravity variation during the flight due to the use of fuel. The wing-loads, in particular, vary with fuel usage, while the effect on other components is dependent on the location of fuel tanks. Furthermore, deployment of the flaps and slats will create load changes on the wing, horizontal tail, and aft fuselage.

The design of the B-1 bomber, which has a variable geometry wing, necessitates that the profile identify each major wing sweep. The various wing positions result in significant stress distribution changes in the wing center section structure, wing pivot, outboard wing panel close to the pivot, and fuselage side longerons. The swing wing is controlled by actuators at the front spar. These important structural members are loaded primarily by wing drag loads while the wing is stationary and by operational forces (including pivot friction) during the sweeping operations. The blended wing/fuselage concept of the B-1 causes a considerable proportion of the airplane lift to be generated over the fuselage midsection, leading to the midfuselage loads being more affected by airplane gross weight variation than they would be on conventional airplanes.

The performance and geometric parameters that control the 1 g stress levels are averaged for each mission segment.

The final mission segmentation for the example bomber training mission is shown in Table 2, and the significance of such a mission breakdown is shown in the 1-g stress plots for various airplane components in Fig. 2. The stresses were obtained with internal loads solutions for the conditions outlined in Table 2, using the appropriate aerodynamic and structural stiffness data.

Generation of Load Factor Spectrum

Figure 3 shows the load factor variations for the bomber training mission. Variations arise from gusts and maneuvers in flight segments, and from taxi and ground handling in ground segments. The source of load factor data is Military Specifications MIL-A-008866B [*1*][2] and MIL-A-008861A

[2]The italic numbers in brackets refer to the list of references appended to this paper.

TABLE 2—*Mission profile segmentation.*

Mission Segment	Time, min	Weight, kg	Mach No.	Altitude, m	Wing Angle, deg	Flap/Slat Setting	Speed Brakes Setting
Ground	1 taxi period	180 000	0	0	15	0/0	0
Posttakeoff	5	180 000	0.34	0	15	25°/20°	0
Subsonic climb	15	170 000	0.65	5 000	25	0/0	0
Subsonic cruise	60	150 000	0.70	8 000	25	0/0	0
Supersonic climb	10	140 000	1.60	15 000	67.5	0/0	0
Supersonic cruise	15	135 000	2.20	18 000	67.5	0/0	0
Supersonic descent	5	130 000	1.60	15 000	67.5	0/0	70°
Refuel	30	160 000	0.70	8 000	25	0/0	0
Subsonic cruise	60	187 000	0.70	8 000	25	0/0	0
Subsonic descent	5	180 000	0.70	5 000	25	0/0	0
Terrain following	15	155 000	0.85	0	67.5	0/0	0
Subsonic climb	15	140 000	0.65	5 000	25	0/0	0
Subsonic cruise	60	130 000	0.70	8 000	25	0/0	0
Subsonic descent	20	125 000	0.65	5 000	25	0/0	70°
Prelanding	60	120 000	0.35	0	15	25°/20°	0
Ground	1 taxi period	100 000	0	0	15	0/0	0

NOTE—Total flight time = 6.25 h.

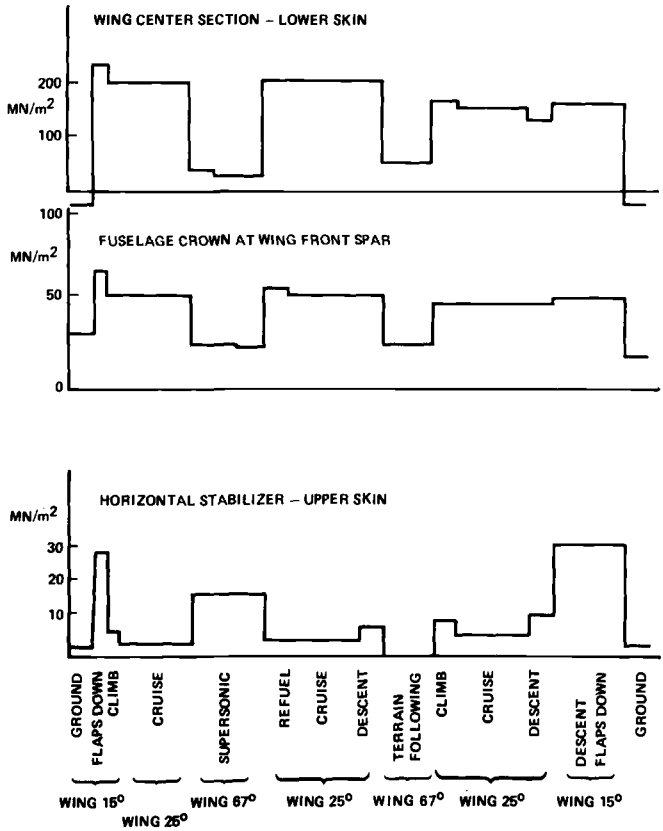

FIG. 2—*1 g stress level variation during mission.*

[*2*]. The wing and fuselage are designed to symmetric conditions only; the empennage and landing gear spectra include both symmetric and asymmetric conditions.

Symmetric Maneuvers

The symmetric maneuver spectrum for each mission segment except terrain following is specified in Tables I through IV of Ref *1* for various classes of aircraft. An example of these data is shown in Fig. 4 as a cumulative occurrence curve representing 1000 h of cruise flying for a bomber and is presented in terms of both positive and negative load factors.

First, the exceedance data are converted to discrete loads by a procedure described in Fig. 4. The appropriate exceedance curve is drawn for the one mission segment time (1 h), and the curve then is converted to average loads for discrete numbers of occurrences.

The starting point for the load steps is the load level that will be equaled

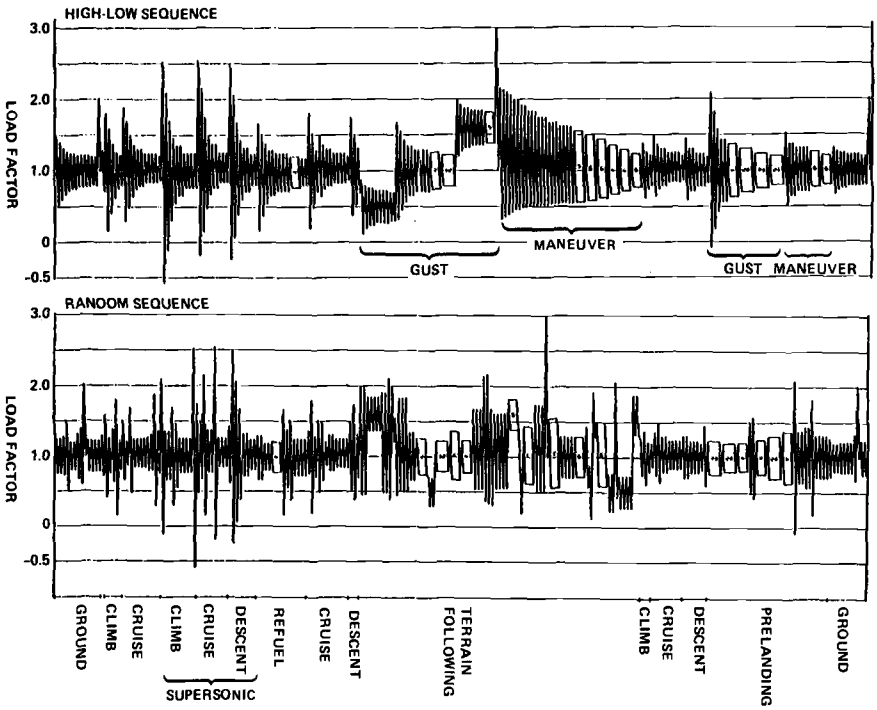

FIG. 3—*Load factor spectrum for a bomber training mission.*

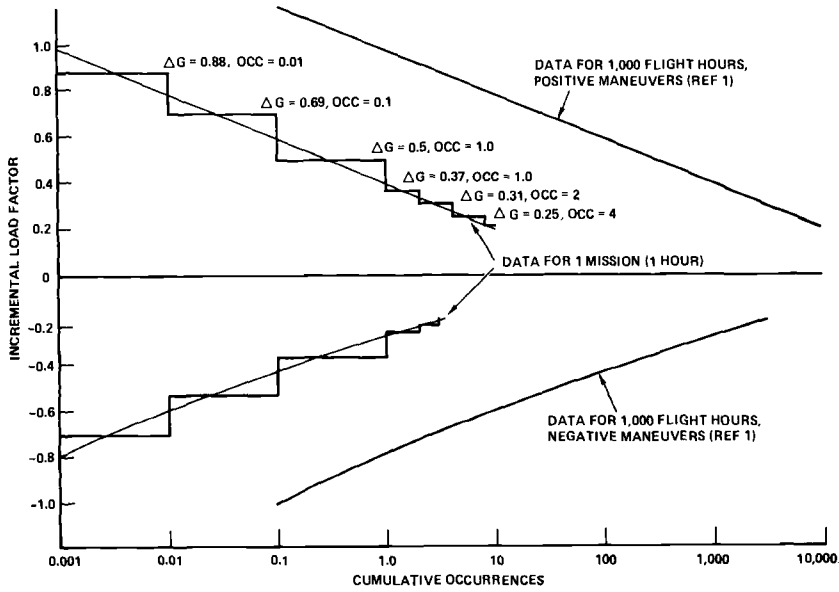

FIG. 4—*Cumulative occurrences of maneuver load factors during cruise.*

or exceeded every mission. Higher load levels will be included as those loads that are equaled or exceeded once in every 10 flights or once every 100 flights. Load levels that occur more than once per mission are stepped with a convenient degree of refinement to any desired truncation level. A delta load factor of 0.2 g is the minimum incremental load factor included in the Military Specification tables [*1*].[2]

Once data from flight records have been converted to exceedance data with no other information recorded [*1*], the true sequence of loads is lost. Consequently, some assumptions are inevitable when describing the maneuver load trace. The selection of a load sequence requires definition of both the maneuver cycle and the sequence of the discrete loads from the exceedance curve. This program defines each maneuver load cycle as either a positive maneuver from 1 g to a peak of 1 g + Δ g and back to 1 g, or as a negative maneuver from 1 g to a valley of 1 g − Δ g and back to 1 g. Sequence options in this program include the arrangement of loads from high to low, from low to high, or randomly. The effect of such sequencing is illustrated in Fig. 3, and its impact on fatique damage and crack growth is discussed later.

The procedure is repeated for all mission segments, using the appropriate load factor exceedance curve from the data in Ref *1*.

Vertical Gusts

The vertical gust exceedance data are generated using continuous turbulence analysis (power spectral density) in accordance with Military Specification MIL-A-008861A [*2*] for the conditions outlined in the mission profile. The equivalent load factor at the airplane center of gravity is computed with the exceedance equation from paragraph 3.22.2.1.1 of Ref *2*.

The gust exceedance data then are converted to discrete load factor cycles in the method employed for maneuvers, assuming the mean load for all gusts is 1 g, with the gusts described as plus and minus increments from 1 g.

Combination of Gusts and Maneuvers

With the exception of terrain-following conditions discussed in the following paragraphs, the cycles due to gust and maneuver are assumed to be independent. However, the gust cycles will be distributed randomly among the maneuver load cycles.

Terrain Following

The long period of time spent at low altitude results in high gust frequency coupled with frequent high load factor maneuvers.

The terrain-following maneuver loads are based on recordings made on

the flight simulator over specific routes, and from this load trace, the maneuver exceedance curve is derived. The gust exceedance data are developed separately using the power spectral density (PSD) analysis. The gust and maneuver spectra are combined in a rational manner, retaining the maneuver spectrum and superimposing the dynamic gust spectrum on different load factor levels of the maneuver spectrum. Based on the maneuver loads trace, an estimate is made of the time spent at each of a series of discrete load factor levels, which thus become the mean loads for the gust cycles. The gust cycles are distributed to each mean load in proportion to the maneuver time assigned to the load factor level. The maneuver exceedance curve and the series of gust curves are converted to discrete load steps and sequenced by the method previously described.

Ground Conditions

The taxi conditions are treated as maneuver conditions, using the exceedance data in Table VIII of Military Specification MIL-A-008866B [*1*]. The spectrum for ground handling conditions (that is, braking, towing, and turning) is specified in Ref *1* in terms of a series of discrete static loads.

Relationship Between Load Factor and Local Stress

In order to obtain the stress spectrum at any location, it is necessary to perform detailed internal loads solutions for the required fatigue conditions described in the mission segmentation. It is assumed that the external load distributions and corresponding internal loads are linear with respect to airplane load factor at the center of gravity, thus keeping the number of internal load solutions to a minimum. Conditions representing 1 g, delta 1 g due to maneuver, and delta 1 g due to gust normally are required for each segment in the mission profile breakdown. For example, the loads for a 3-g maneuver then can be computed by adding the 1-g load to twice the incremental load due to maneuver.

Dynamic incremental gust loads for both vertical and lateral gusts are determined by developing distributed airplane loads to match key items of shear, moment, and torque from the PSD analysis. The incremental gust loads then are combined with the 1-g trim loads.

A sample of the stress spectrum for one flight of the bomber training mission is shown in Figs. 5 and 6. The stresses were computed for the wing center section lower cover, showing the impact of the variable wing geometry of the B-1 throughout the sequence of flight segments. Under these conditions, the gust and maneuver cycles are of less importance than the excursion of the 1-g mean stresses. The little difference between high/low and random sequencing of loads within each mission segment is apparent by comparison of Figs. 5 and 6.

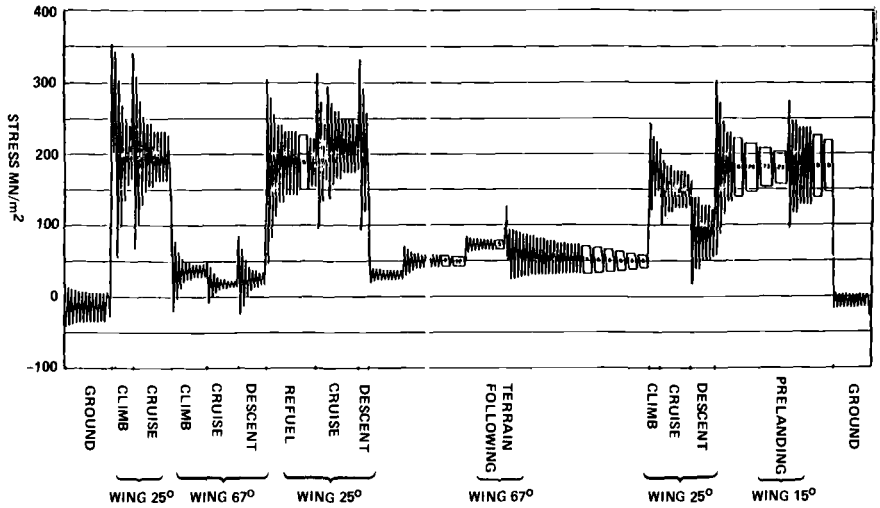

FIG. 5—*Stress spectrum for wing center section lower surface with high/low sequence.*

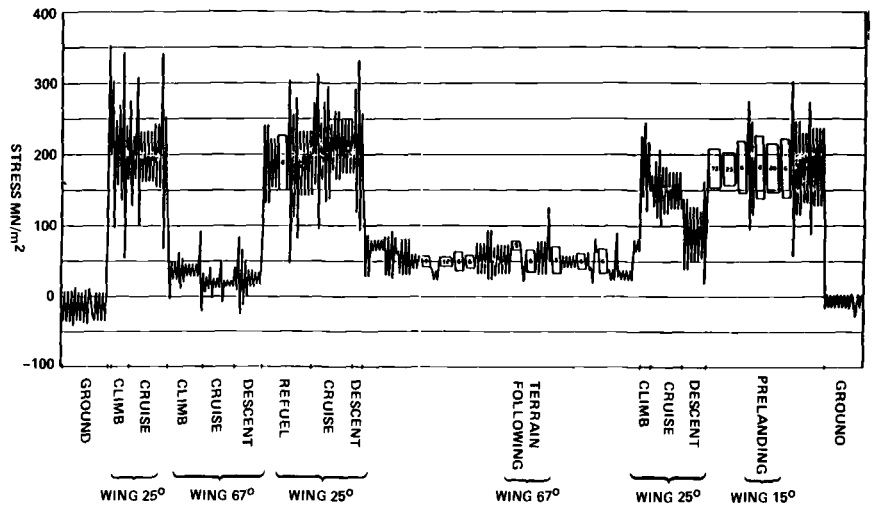

FIG. 6—*Stress spectrum for wing center section lower surface with random sequence.*

Computer Program

The methodology for spectra generation has been automated in a computer program described in Fig. 7. The program was written to facilitate spectrum development with minimum user input. It makes extensive use of off-line disk storage, and outputs the spectra in written tables (Table 3), on cathode-ray tube (CRT) plots (Figs. 5 and 6), and on tapes or disks for direct mounting on computers linked to fatigue test machines.

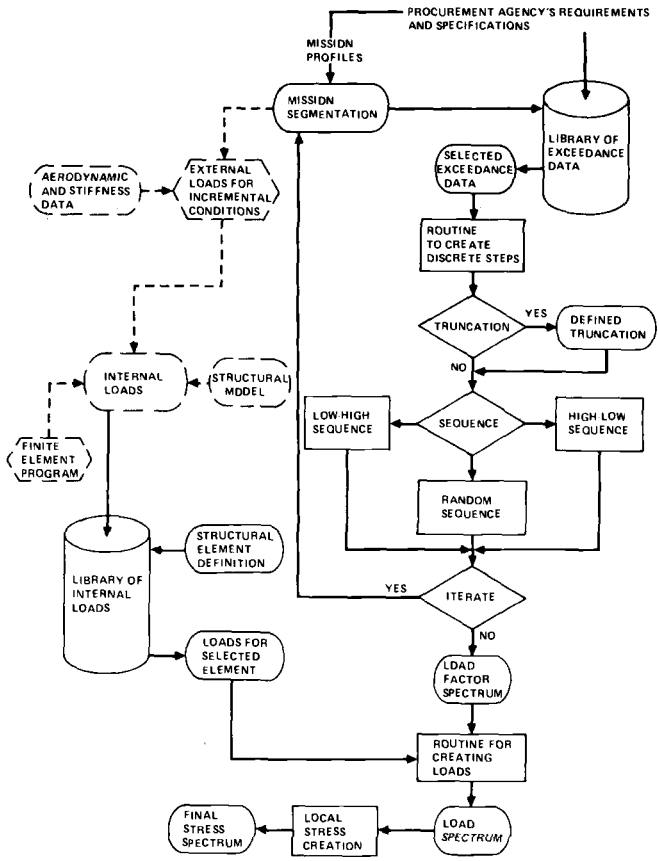

FIG. 7—*Computer program flow chart.*

TABLE 3—*Wing center section lower skin, bomber training mission stress spectrum.*

Step	Mission Segment	Wing Angle	Load Type	Gross Stress max	Gross Stress min	Cycles/ Mission
1	Ground	15	taxi	−35.23	7.00	2.00
2				−35.98	7.75	1.00
3				−41.61	13.38	0.01
4				−34.00	5.77	2.00
5				−37.43	9.20	1.00
6				−39.54	11.31	0.10
7			braking	−0.40	−28.23	1.00
8			taxi	−34.49	6.26	4.00
9	Post takeoff	15	maneuver	353.31	201.71	1.00

TABLE 3—*Continued.*

Step	Mission Segment	Wing Angle	Load Type	Gross Stress max	Gross Stress min	Cycles/ Mission
10	Subsonic climb	25	maneuver	304.14	97.66	0.10
11				248.16	156.90	1.00
12				269.39	134.69	1.00
13				342.93	54.55	0.01
14				240.72	164.61	1.00
15	Subsonic cruise	25	maneuver	275.19	128.57	1.00
16				226.41	166.75	1.00
17				308.67	99.74	0.10
18				232.48	162.12	4.00
19				242.85	154.21	2.00
20				341.58	68.05	0.01
21				253.16	146.30	1.00
22	Supersonic climb	67.5	maneuver	76.76	−3.28	0.10
23				50.10	24.70	2.00
24				62.60	11.74	1.00
25				53.91	20.78	1.00
26				46.37	28.53	4.00
27				92.48	−20.58	0.01
28	Supersonic cruise	67.5	maneuver	33.66	5.98	1.00
29				28.06	10.26	1.00
30				42.20	−0.94	0.10
31				25.43	12.16	2.00
32				50.59	−8.48	0.01
33				23.05	13.86	3.00
34	Supersonic descent	67.5	maneuver	42.21	9.08	1.00
35				84.06	−24.51	0.01
36				67.43	−12.63	0.10
37				51.90	0.23	1.00
38				37.88	13.45	2.00
39				34.50	16.99	2.00
40	Refuel	25	maneuver	240.83	131.53	2.00
41				221.89	154.21	2.00
42				226.41	150.12	8.00
43				304.04	47.05	0.01
44				256.29	111.90	1.00
45				278.84	82.39	0.10
46				232.48	141.86	4.00
47	Subsonic cruise	25	maneuver	271.57	156.64	1.00
48			gust	312.54	94.68	0.01
49				243.30	163.93	1.00
50				273.39	133.84	0.10
51			maneuver	295.26	137.56	1.00
52				242.80	178.63	1.00
53				260.48	165.15	2.00
54				249.33	173.65	4.00

TABLE 3—*Continued.*

Step	Mission Segment	Wing Angle	Load Type	Gross Stress max	Gross Stress min	Cycles/ Mission
55	Subsonic descent	25	maneuver	292.29	119.30	0.10
56				332.15	93.16	0.01
57				258.15	147.65	1.00
58	Terrain following 85	67.5	maneuver	86.82	28.96	2.00
59			gust	79.41	64.91	4.00
60			maneuver	84.01	30.07	2.00
61				91.58	26.49	1.00
62			gust	83.89	60.43	1.00
63				65.94	33.11	0.10
64			maneuver	81.17	30.93	3.00
65			gust	59.70	39.35	2.00
66				56.99	42.06	7.00
67				36.72	24.61	2.00
68				55.94	43.11	12.00
69			maneuver	63.00	37.04	6.00
70				58.32	40.88	6.00
71				75.18	32.22	3.00
72				92.59	25.38	0.10
73				93.60	24.35	0.01
74			gust	69.64	29.41	0.01
75			maneuver	72.83	32.72	4.00
76			gust	78.46	65.85	5.00
77				39.66	21.67	1.00
78			maneuver	65.56	35.22	6.00
79				77.91	31.67	3.00
80			fly up	124.97	49.53	1.00
81			maneuver	70.51	33.24	5.00
82			gust	58.21	40.84	4.00
83			maneuver	60.59	38.95	6.00
84			gust	62.32	36.73	1.00
85				41.95	19.38	1.00
86				81.60	62.72	1.00
87			maneuver	68.14	33.92	6.00
88			gust	38.56	22.77	2.00
89			maneuver	89.78	27.69	1.00
90			gust	37.45	23.88	4.00
91				80.52	63.80	2.00
92	Subsonic climb	25	maneuver	224.20	140.80	1.00
93				243.60	120.51	1.00
94				217.40	147.85	1.00
95	Subsonic cruise	25	maneuver	171.02	127.09	1.00
96				190.72	112.03	1.00
97				206.94	98.97	1.00
98				183.13	117.86	2.00
99				175.49	123.68	4.00

TABLE 3—*Continued.*

Step	Mission Segment	Wing Angle	Load Type	Gross Stress max	Gross Stress min	Cycles/ Mission
100	Subsonic descent	25	maneuver	137.97	38.62	2.00
101				126.94	49.85	3.00
102				121.31	55.21	1.00
103				161.79	18.42	1.00
104	Pre-landing	15	gust	207.67	153.52	73.00
105				203.67	157.52	23.00
106			maneuver	218.53	146.03	6.00
107				274.14	95.05	1.00
108			gust	246.00	115.19	1.00
109			maneuver	226.23	138.68	8.00
110			gust	214.58	146.62	20.00
111				221.83	139.36	6.00
112				302.94	58.26	0.01
113			maneuver	247.02	115.54	2.00
114			gust	229.75	131.44	2.00
115				273.35	87.84	0.10
116			maneuver	236.62	128.00	4.00
117	Ground	15	taxi	−16.21	3.49	1.00
118				−15.32	2.60	2.00
119				−15.54	2.82	4.00
120				−16.87	4.14	1.00
121			braking	−0.40	−28.23	1.00
122			taxi	−15.88	3.16	2.00

The initial input of the program is the mission profile segmentation. For each segment, the program selects the appropriate exceedance data from the disk-stored library of data from Refs *1* and *2*, and also selects the conditions for which external and internal loads are needed. The development of airplane external loads from aerodynamic and structural stiffness data and corresponding internal structural loads is performed outside the spectrum development program. The internal loads solutions are performed on existing finite-element computer programs such as Automated System of Kinematic Analysis Program (ASKA) [*3*] and NASA Structural Analysis Program (NASTRAN) [*4*], thus obtaining the loads in each element of the structure as defined by the structural model. The output tapes from the various internal loads programs are used to load the disk files for accessibility by the spectrum program.

Each of the selected exceedance curves is converted first to discrete load steps as outlined previously. At this point, two user input decisions are made in order to define the truncation level of both the high- and low-load

levels and the sequence of the discrete load steps in each segment. Figure 3 shows the plot form of a one-flight load factor spectrum, with segments sequenced as per the mission profile.

The computer program has data management routines that automatically extract the appropriate internal loads for the selected structural elements and combine these incremental conditions to produce loads corresponding to each load factor. The resultant stress spectrum can be modified with a FORTRAN program to relate the load or stress compiled by the internal loads program to the local stress at the fatigue critical location. The final stress spectrum then is used for fatigue or fracture mechanics analysis.

Test Spectra Development

Military Specification MIL-A-008867B (United States Air Force) [5] requires both design development tests and design verification tests to support the durability and damage-tolerance analysis.

Design development specimens normally take the form of elements and small components. The spectra for such tests are acquired easily from the spectrum computer program by selection of the internal loads model element appropriate to the specimen. The complete spectrum is produced automatically in the same manner as the design spectrum. Test spectra so produced retain the design stress levels and frequently contain more cycles than can be applied in a reasonable test program schedule. The test calendar time can be reduced by removal of the high-frequency/low-load cycles, which would produce insignificant fatigue damage or crack growth. This truncation procedure is supported by fatigue and crack growth analysis and can be undertaken within the program.

Design verification specimens take the form of large components or a complete vehicle. Large component specimens, such as the horizontal and vertical stabilizer support fitting, are loaded usually by hydraulic jacks representing the boundary loads to that component. The boundary loads are available within the computer program in terms of the loads in one or more elements of the structural model.

A complete vehicle spectrum requires a set of test laboratory jack loads that are compatible with the analytically derived external load distributions for the mission profile parameters. The balanced jack loads (representing 1 g, Δg maneuver, and Δg gust conditions) are stored in a computer disk library and then converted to a complete spectrum within the program as outlined in Fig. 7.

Fatigue and Fracture Mechanics Analysis

Both conventional fatigue analysis methods (which compute cumulative damage based on combining the effect of individual cycles ($\Sigma n/N$)) and

fracture mechanics analysis methods (which predict crack growth based on successive individual stress cycles ($\Sigma da/dN$)) require a definition of cycles from the stress trace. Typical of the cycle counting procedures is range pair counting, which selects peak-to-valley range for the primary, secondary, and tertiary waves, and so on until the complete trace is accounted for.

Fatigue and fracture mechanics analysis was performed on the wing lower surface spectrum shown in Figs. 5 and 6, using titanium material properties. Comparison of the high-/low-sequenced spectrum with the random-sequenced spectrum revealed no difference in either cumulative damage or crack growth. The lack of difference is due to a combination of the complex mission profile of the B-1 and the design concept of a variable geometry wing. Large percentages of the damage are caused by the major waves in the spectrum. Such a spectrum has infrequent high loads distributed throughout the mission, owing to the segmentation; consequently, retardation effects are relatively consistent, immaterial of the sequence of loads within one segment.

Table 4 indicates the response of other airplane components to various spectrum effects. The distribution of damage caused by various types of load cycles is primarily a function of mission profile, the response of the structure to various load conditions, the flight length and, to a lesser extent, the design stress levels and the material properties.

For the wing and fuselage structure, the ground-air-ground damage varies from a maximum of 67 percent on the forward fuselage crown to only 10 percent on the side longerons of the aft fuselage. The variable geometry accounts for as much as 25 percent of the damage over most of the structure. Damage from gust and maneuvers is between 25 and 60 percent of the total, thus indicating where randomization within a segment may be important.

The notable exception to the preceding is the empennage. Here the vertical stabilizer is affected only by lateral loads, and the horizontal stabilizer is affected predominantly by roll and lateral gust loads (because of the B-1 rolling tail).

Conclusion

The B-1 procurement requirements include high-altitude supersonic flight and low-altitude terrain following at high subsonic speeds. The resultant mission profile, coupled with the variable geometry design concept, necessitated a fatigue spectrum described by 50 external load distributions. Due to the large number of conditions, an automated system was very desirable for the analyst. The program provided bulk data storage in readily accessible form, allowing analysis to be performed on many parts simultaneously with little preparation and low computer cost.

TABLE 4—*Relative damage for various airplane components, bomber training mission.*

Component	Percentage of Total Damage					
	Profile-Controlled Load Cycles		Environment-Controlled Load Cycles			
	Ground-Air-Ground	Airplane Geometry[a]	Vertical Gusts	Vertical Maneuvers	Roll[b]	Lateral Gusts
Wing carry-through lower surface	46	27	2	25	...	...
Wing outer panel lower surface	40	25	2	33	...	...
Forward fuselage crown (pilot station)	67	6	26	1	...	...
Forward fuselage crown (wing front spar)	30	20	18	32	...	...
Aft fuselage crown	20	10	10	60	...	...
Aft fuselage side longeron	10	24	42	24	...	...
Horizontal stabilizer upper skin	...	14	...	...	36	50
Vertical stabilizer skin	...	...	...	...	30	70

[a] Wing sweep movements and flap, slat, and speed brake operations.
[b] The horizontal tail for the B-1 bomber is a rolling tail.

Adequate fatigue and fracture mechanics analysis can be performed only with the best estimate of the local stresses. Modern trends have gravitated toward the use of finite-element methods for calculating local stresses within a complex structure. However, finite-element programs are very expensive in terms of computer time. The spectrum development system outlined herein used existing finite-element programs, but any stress analysis method could be substituted.

Although the program was developed for the B-1 bomber, the author believes that this basic approach can be applied to any airplane designed to the current United States Air Force requirements. However, for aircraft with less complex mission profiles and without variable geometry, the derivation of the load factor spectrum will be relatively more important than the mission profile breakdown. For such airplanes, it may be necessary to refine the procedure for reduction of exceedance data to sequenced discrete loads.

Acknowledgments

The author wishes to thank K. K. Karlsten, who produced the very efficient computer software, and G. E. Fitch and M. A. McGahey for guidance and assistance.

References

[1] "Airplane Strength and Rigidity Reliability Requirements, Repeated Loads, and Fatigue," *Report No. MIL-A-008866B*, Department of the Air Force, 22 Aug. 1975.

[2] "Airplane Strength and Rigidity Flight Loads," *Report No. MIL-A-008861A*, Department of the Air Force, 31 March 1971.

[3] Argyris, J. H., "Linear Static Analysis," Automated System of Kinematic Analysis (ASKA) Program, Institute für Statik und Dynamik der Luft und Raumfahrkonstruktionen, University of Stuttgart, 1971.

[4] "NASA Structural Analysis Theory Manual," NASA Structural Analysis (NASTRAN) Program, *NASA Report No. SP-221/03*, National Aeronautics and Space Administration, Washington, D.C., March 1976.

[5] "Airplane Strength and Rigidity Ground Tests," *Report No. MIL-A-008867B*, Department of the Air Force, 22 Aug. 1975.

W. W. Wilson[1] *and J. E. Garrett*[1]

Methods of Gust Spectra Prediction for Fatigue Damage*

REFERENCE: Wilson, W. W. and Garrett, J. E., **"Methods of Gust Spectra Prediction for Fatigue Damage,"** *Service Fatigue Loads Monitoring, Simulation and Analysis, ASTM STP 671,* P. R. Abelkis and J. M. Potter, Eds., American Society for Testing and Materials, 1979, pp. 176-192.

ABSTRACT: The prediction of aircraft responses to atmospheric turbulence using a general exponential gust exceedance equation is based on the assumption that altitude dependent spectra curve fit parameters contained in the exceedance equation are representative of the atmosphere and thus equally applicable to accelerations, loads, stresses, etc. Using vertical acceleration gust data recorded during fleet operations of the USAF C-5A transport aircraft, altitude dependent curve fit parameters were developed; these parameters were then shown to accurately predict the recorded wing stress gust experience at three wing locations, thus supporting the assumption of their uniformity between response parameters. This gust analysis then was substantiated with a second, independent analysis in which the recorded vertical acceleration gust data were converted directly to stress spectra by means of analytical stress to acceleration ratios.

KEY WORDS: damage, fatigue (materials), mathematical-predictions, gust-loads, spectrum-analysis, fatigue tests

The ability to describe accurately the operational environment in which aircraft operate is of primary importance to the design of new aircraft as well as to the prediction and tracking of damage on existing aircraft. One such operational environment is atmospheric turbulence.

Most of the work that has been accomplished in the past 20 years toward the description of the atmospheric turbulence load source has been based on data recording programs in which the vertical acceleration at the aircraft center of gravity was recorded during day-to-day flight operations of various types of aircraft. Using cumulative peak spectra formed from these vertical acceleration recordings, the typical approach has been to develop a mathematical description of the atmospheric turbulence load source using some type of exceedance equation containing altitude de-

[1] Structures engineers, senior, Lockheed-Georgia Co., Marietta, Ga., 30063.

* This work was sponsored by the Air Force Systems Command under Contract No. AF33657-76-D-0873.

pendent curve fit parameters. These curve fit parameters are assumed to be representative of the atmosphere and thus equally applicable to not only all types of aircraft but also to all response parameters, that is, they may be used to predict loads spectra, stress spectra, etc., with equal accuracy.

At the Lockheed-Georgia Company an operational loads recording program on the USAF C-5A transport aircraft has been going on since 1973. This recording program, unlike similar programs on other aircraft, is not limited to recordings of the vertical acceleration. Wing stresses, lateral accelerations, control surface motions, and landing gear loads, in addition to the usual vertical accelerations and flight condition parameters (fuel weight, cargo weight, Mach number, and altitude), have been recorded during fleet operations. These additional recordings, particularly the wing stress recordings, have made possible a more complete analysis of the atmospheric turbulence load source and an opportunity to evaluate the assumption of uniformity of the altitude dependent curve fit parameters between response parameters.

After a brief description of the data recording, processing, and reduction methods, this paper will discuss the techniques used to describe the atmospheric turbulence load source and show results of the application of this model to response parameters other than those on which the model is based.

Recording System Description

The basic signal acquisition system is a digital recording system. Figure 1 presents the parameters that are recorded and shows the sensor locations. The analog signals output by the various sensors are detected, amplified, filtered, and conditioned as required. The conditioned signals then are sampled to an order or sequence controlled by the onboard digital computer. The number of times per second that a particular data signal is sampled is called the sample rate. Each sampled value is digitized and compared with the last recorded value of the same parameter. If the new value differs from the last recorded value by more than a prescribed amount, then the new digitized value is recorded, otherwise not. This recording concept, sometimes called a "moving window" technique, results in data compression, that is, large quantities of data of relatively constant magnitude result in only small quantities of recorded data. The data that meet recording requirements pass into a buffer and then eventually onto the magnetic tape of the data recorder. A more detailed description of the recording system is presented in a Lockheed-Georgia Company technical report [*1*].[2]

[2] The italic numbers in brackets refer to the list of references appended to this paper.

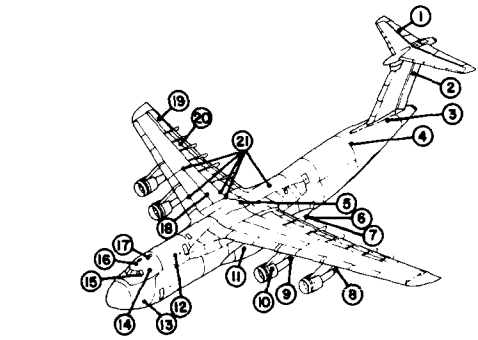

MOTION PARAMETERS:
- (5)- VERTICAL ACCELERATION, FS 1383
- (5)- LATERAL ACCELERATION, FS 1383
- (3)- LATERAL ACCELERATION, FS 2494
- (12)- PITCH ACCELERATION

CONTROL SURFACE PARAMETERS:
- (1)- RIGHT OUTBOARD ELEVATOR
- (2)- UPPER RUDDER
- (19)- RIGHT AILERON
- (20)- FLAPS

DISCRETE EVENT PARAMETERS:
- (4)- AIR DROP
- (6)- TAKEOFF/LANDING
- (8)- OUTBOARD THRUST REVERSER
- (9)- INBOARD THRUST REVERSER
- (14)- TERRAIN FOLLOWING
- (15)- PITCH AUTOPILOT ENGAGEMENT
- (16)- AERIAL REFUELING
- (17)- KNEELINGS
- (18)- GROUND SPOILER ACTUATION

DOCUMENTARY PARAMETERS:
- (7)- GROUND SPEED
- (12)- MACH NUMBER
- (12)- ALTITUDE
- (12)- RADAR ALTITUDE
- (16)- FUEL WEIGHT

STRESS PARAMETERS:
- (21)- RIGHT WING, 6 LOCATIONS
- (21)- AFT FUSELAGE

LANDING GEAR VERTICAL LOADS:
- (6)&(11)- 4 MAIN GEAR
- (13)- NOSE GEAR

LANDING GEAR TURN ANGLES:
- (6)- LEFT AFT MAIN GEAR
- (13)- NOSE GEAR

PROPULSION PARAMETERS:
- (10)- 4 ENGINE PRESSURE RATIOS
- (10)- 4 ENGINE COMPRESSOR SPEEDS
- (10)- 4 ENGINE FUEL FLOW RATES

FIG. 1—*Aircraft instrumentation.*

Data Processing and Reduction

As the data recorder magnetic tapes become full they are replaced and the recorded data are transmitted to a central data bank to await extraction. It is at this stage that the recorded data begin undergoing tests and checks to determine their suitability for data analyses. The recorded data must pass successfully through three phases of data handling before being accepted into the analysis phase. To pass the first phase, which is data extraction, several data validity checks must be passed. These checks are of a broad nature and designed primarily to ensure that the data recorder was operating properly. Data next enter the data edit phase. The primary function of data edit is to detect and eliminate spurious recordings on the extracted data tapes. Data edit is performed initially by computer and finally by manual inspection. Also included in the data edit phase is the generation of a flight profile for each recorded flight. The recorded time histories of all data parameters are interpreted by an ordered set of logical statements to separate each flight into recognizable chronological load

source oriented segments, for example, taxi, takeoff, traffic flight, ordinary flight, etc. This information, in the form of segment codes and times of occurrence, serves as a "road map" to the flight recorded data for use in the reduction phase. It is within the data reduction phase that the recorded time histories of the response parameters are peak counted and the atmospheric turbulence load source takes its identity. Figure 2 shows a portion of a typical vertical acceleration recorded time history with recorded points represented by the circles. Threshold limits are placed about the mean (1.0 g) and peaks are defined to be the largest excursion of the recorded data between successive crossings of either of the threshold limits. In Fig. 2, those recorded points determined to be peaks are shown as solid circles. Recorded time histories of other parameters are peak counted using this same "mean crossing" peak counting technique, however, threshold limits and the mean about which the peak counting is performed vary by parameter, for example, for recorded stress time histories it is necessary to first compute a time varying mean stress before the peak

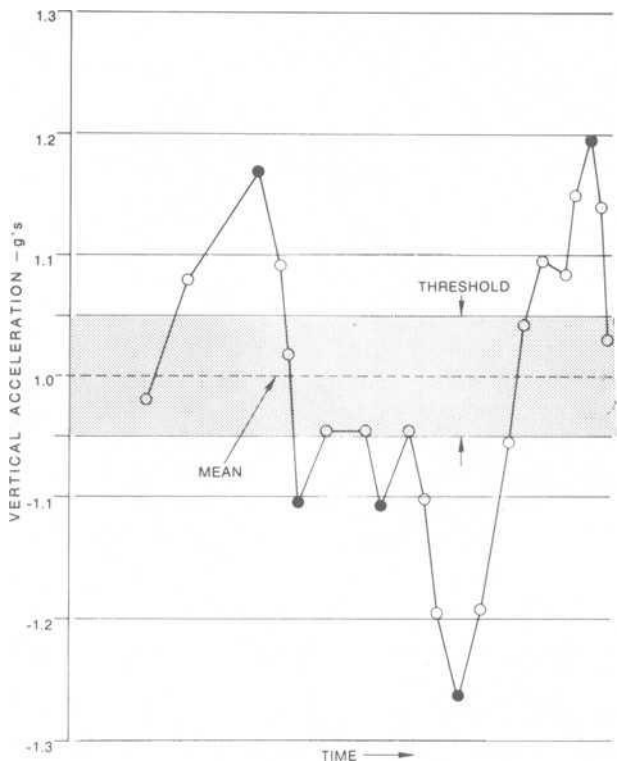

FIG. 2—*Peak counting technique.*

counting operation begins. This mean crossing peak counting technique is discussed in greater detail in Refs *2* and *3*.

Upon completion of peak counting, each peak recorded during flight is determined to be either gust induced or maneuver induced. This load source separation is performed first on the vertical acceleration data with all peaks having time durations of more than 2.3 s defined as maneuver induced. These vertical acceleration maneuver peaks then are paired with time corresponding stress peaks to complete the separation process. The peak counted data determined to be gust induced are summed and converted into frequency distributions. These distributions are related to the flight condition parameters, namely, fuel weight, cargo weight, Mach number, and altitude, that is, the frequency distributions are computed and stored separately by "data block" where each data block number represents a unique combination of the flight condition parameter ranges. Finally, the frequency distributions are summed over all flights and over all aircraft by data block. These distributions along with the total amount of flight time spent in each data block provide the basic data input to the data analysis phase. Figure 3 illustrates this flow of the recorded data from the onboard recorder to the analysis phase.

Analysis of Gust Data

The mathematical model for response to atmospheric turbulence was developed using the general gust exceedance equation

$$Np(\Delta X) = \left[P_1 \text{EXP}\left(\frac{-\Delta X}{b_1\sigma}\right) + P_2 \text{exp}\left(\frac{-\Delta X}{b_2\sigma}\right) \right] N_0 T \qquad (1)$$

where

$Np(\Delta X)$ = cumulative number of cycles of ΔX,
ΔX = incremental values of a given response parameter,
P_1, P_2, b_1, b_2 = altitude dependent curve fit parameters,
N_0 = characteristic frequency of response to a unit root mean square (rms) gust velocity input,
σ = rms amplitude of the response to a unit rms gust velocity input,
T = time.

Detailed discussions of this exceedance equation may be found in Refs *4*, *5*, and *6*.

A computer program was developed to compute frequency distributions using this gust exceedance equation. Since the values of σ and N_0 in Eq 1 are functions of fuel weight, cargo weight, Mach number, and altitude, analytical four dimensional grids of σ and N_0 for each response parameter

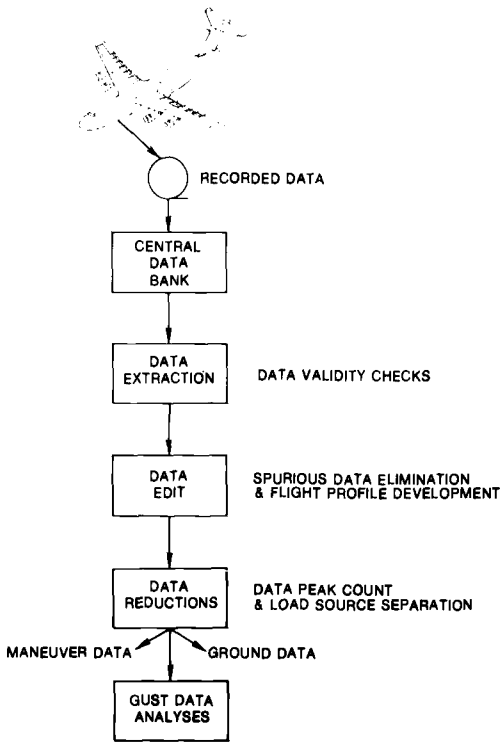

FIG. 3—*Data flow diagram.*

to be studied are an integral part of this computer program. Analytical response spectra can thus be computed for direct comparison with the recorded spectra by inputting to the computer program the recorded utilization of the desired response parameter, that is, the recorded amounts of time spent in each data block.

In practice, a data block number and corresponding time are input, the values of σ and N_0 are interpolated to the flight conditions represented by the data block number. The desired curve fit parameter values are then input and the cumulative number of cycles are computed and output at any desired levels of ΔX. The output spectra then can be directly compared with the corresponding recorded gust spectra. This procedure is illustrated in Fig. 4.

To test the assumption of uniformity of the curve fit parameter values between different response parameters, the values of the curve fit parameters were established using the recorded aircraft center of gravity vertical acceleration spectra and then used to compute other response spectra for which corresponding recorded spectra were available.

Since the curve fit parameters are assumed to be altitude dependent, the

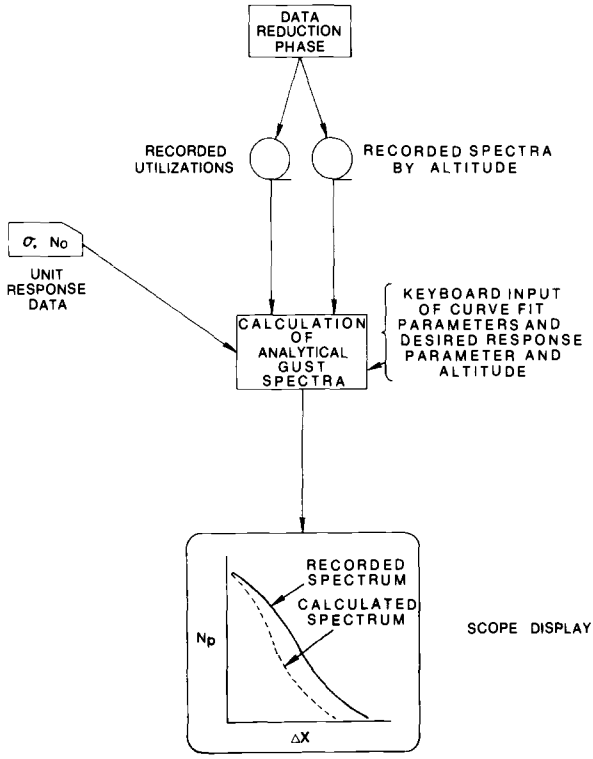

FIG. 4—*First analysis method.*

computer program was designed to compute and sum automatically the analytical gust spectra for all data blocks having common altitude ranges. The process of establishing the curve fit parameter values then becomes one of iteration. Parameter values are input until the resulting calculated vertical acceleration spectra are judged to be in the best possible agreement with the corresponding altitude summed recorded spectra. This process is made rather simple by utilizing a remote graphics cathode ray tube (CRT) connected to the computer. Parameter values for the desired altitude range are merely input by keyboard at the CRT and the resulting analytical and recorded gust spectra are displayed graphically. Once the curve fit parameter values have been established, the assumption of their uniformity between response parameters can be tested by utilizing the same technique. The recorded utilizations for different response parameters are input along with the vertical acceleration derived curve fit values and the resulting analytical and recorded spectra, for the desired altitude range, are displayed on the CRT for visual inspection.

The preceding methods were followed using available recorded vertical

acceleration and wing stress data.[3] The analytical incremental wing stress gust spectra resulting from the vertical acceleration derived curve fit parameters were lower than the corresponding recorded incremental wing stress gust spectra at all altitudes and at all three wing stations. These results, of course, do not support the uniformity assumption of the curve fit parameters.

As these works were being conducted, a second gust analysis was being performed. This independent analysis had the same objective but utilized a different technique. While it did utilize the same recorded aircraft center of gravity vertical acceleration data, this analysis did not involve the calculation of curve fit parameters. The recorded incremental acceleration spectra were converted to incremental stress spectra by converting the lower limit band values of incremental acceleration to lower limit band values of incremental stress and by converting the cumulative number of recorded incremental acceleration cycles to the cumulative number of incremental stress cycles corresponding to each incremental stress band. The first conversion was performed using the equation

$$\Delta S = \Delta g \times \frac{\Delta S}{\Delta g} \tag{2}$$

where

ΔS = lower limit incremental stress band value,
Δg = lower limit incremental vertical acceleration band value, and
$\frac{\Delta S}{\Delta g}$ = analytical value of incremental stress per incremental acceleration.

The second conversion utilized the equation

$$Np(\Delta S) = Np(\Delta g) \times \frac{No_s}{No_g} \tag{3}$$

where

$Np(\Delta S)$ = cumulative number of incremental stress cycles at a given value of incremental stress,
$Np(\Delta g)$ = cumulative number of recorded incremental acceleration cycles at a given value of incremental acceleration,
No_s = characteristic stress frequency, and
No_g = characteristic acceleration frequency.

These conversions were accomplished separately for each data block since

[3]Three wing locations were investigated. Exact physical locations of the wing strain gages are shown in Ref *1*, pp. 42, 43, and 45.

the values of $\Delta S/\Delta g$ in Eq 2 and the values of No_s and No_g in Eq 3 vary with fuel weight, cargo weight, Mach number, and altitude. As can be seen from inspection of Eq 2, the fact that the values of $\Delta S/\Delta g$ vary by data block results in a similar variation of the values of ΔS. This non-uniformity of ΔS values made direct addition of the cumulative number of incremental stress cycles (as computed in Eq 3) across data blocks impossible, yet the altitude dependent nature of the vertical gust damage source dictated addition across data blocks having a common altitude in order to make meaningful comparisons with the incremental stress spectra computed from Eq 1 of the first analysis.

Method of Summation

In explaining the devised summation method, it is first necessary to make the following definitions:

measured/analytical stress spectra—the incremental stress spectra which result from Eqs 2 and 3. There are two such types of incremental stress spectra:

Type I—The incremental stress spectra that result from data blocks in which incremental vertical acceleration gust peaks were recorded in but one acceleration magnitude band.

Type II—The incremental stress spectra that result from data blocks in which incremental acceleration gust peaks were recorded in two or more acceleration magnitude bands.

fixed stress values—the preselected values of incremental stress at which the total spectra are summed.

In addition to these definitions it is assumed that all incremental stress spectra will be exponentially decaying in nature. This assumption is in agreement with the usual gust prediction method which utilizes an exponentially decaying exceedance equation. Interpolation and extrapolation of the measured/analytical stress spectra to the fixed stress values can then be accomplished using Eqs 4, 5, and 6:

$$Np\,(\Delta Sf) = A \times \exp\,[B \times \Delta S] \tag{4}$$

where

$$B = \frac{\ln\,(Np_{\Delta S2}) - \ln\,(Np_{\Delta S1}),}{\Delta S2 - \Delta S1} \text{ with } \Delta S2 > \Delta S1 \tag{5}$$

and

$$A = \exp\,[1n\,(Np_{\Delta S2}) - B \times \Delta S2] \tag{6}$$

where

$Np(\Delta Sf)$ = cumulative number of incremental stress cycles at a given fixed stress value,
$\Delta S2$ and $\Delta S1$ = incremental stress values as obtained from Eq 2,
$Np_{\Delta S2}$, $Np_{\Delta S1}$ = cumulative number of incremental stress cycles at $\Delta S2$ and $\Delta S1$,
B = slope of the line between points $\Delta S2$ and $\Delta S1$, and
A = intercept on the Np axis corresponding to slope B.

All Type II measured/analytical stress spectra are operated on first. For a given Type II curve each two existing adjacent incremental stress values are compared to the fixed stress values. The cumulative number of incremental stress cycles at fixed stress values falling between two adjacent incremental stress values are computed by interpolation using Eqs 5, 6, and 4, respectively. Next, the two lowest existing adjacent incremental stress values are used to extrapolate the cumulative number of incremental stress cycles to the next lower fixed stress value. After operation on all Type II measured/analytical stress spectra is complete, summation of the spectra over data blocks by altitude is performed at each fixed stress value.

Next, all Type I measured/analytical stress spectra are operated on. The cumulative number of incremental stress cycles at the one existing incremental stress value is extrapolated to the next higher and the next lower fixed stress values. This is accomplished by assuming a slope through the existing incremental stress value that is equal to the slope, as computed using Eq 5, between the two fixed stress values for the summed spectra, for the proper altitude, resulting from the Type II measured/analytical stress spectra. After operation on all Type I spectra the resulting spectra are summed over data blocks by altitude at each fixed stress value and then summed with the corresponding altitude spectra formed from the Type II spectra. The resulting incremental stress spectra by altitude may now be compared directly with the corresponding analytical stress spectra obtained by the general gust exceedance equation of the first analysis. Figure 5 outlines the procedure followed for the second analysis.

As in the case of the first analysis, this analysis was performed using all available recorded vertical acceleration and wing stress gust data. Again the analytical wing stress gust spectra were lower than the corresponding recorded spectra at all altitudes and at all three wing locations and thus the assumption of uniformity of the gust analysis between response parameters remained unsupported. The analytical incremental wing stress gust spectra resulting from the two independent analyses are compared with the corresponding recorded incremental wing stress spectra in Figs. 6, 7, and 8.[4] As can be seen, the spectra resulting from the two analyses are in

[4]Spectra shown in these figures have been summed over all altitudes.

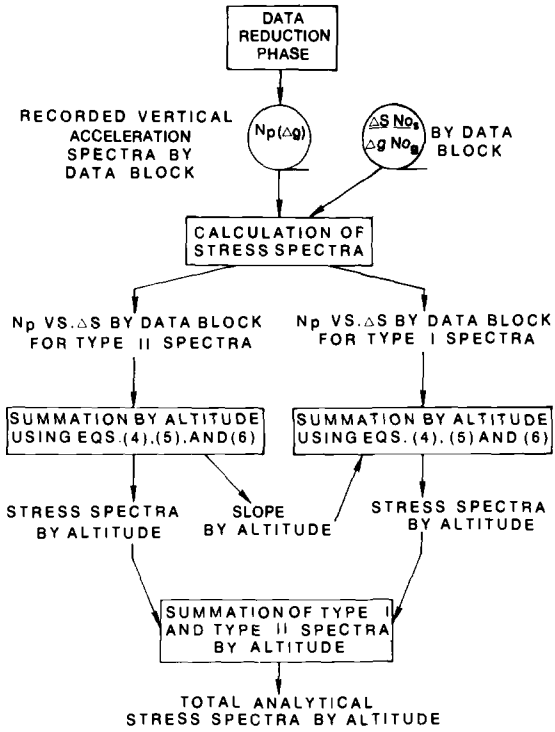

FIG. 5—*Second analysis method.*

good agreement with each other but not in good agreement with the recorded spectra.

The search for an explanation for the differences observed between the analytical and recorded stress spectra was centered around determining if any inaccuracies existed in the two analyses. The fact that the results of the two analyses were in good agreement indicated an inaccuracy common to the two analyses and since the recorded data were not suspect, this left the unit response data, that is, the analytical four-dimensional σ and N_o grids. These analytical data are common to the analyses since the analytical values of $\Delta S/\Delta g$ used in Eq 2 of the second analysis are computed by ratioing analytical stress and acceleration σ's.

The capability to evaluate the accuracy of the analytical unit responses existed since these types of data had been recorded during dynamic response tests of the C-5A aircraft and published in Ref 7. The gust loads observed during these tests were recorded under controlled conditions in which the aircraft was flown "hands off" through turbulence. Comparison of analytical and recorded wing bending moment loads showed that the analytical σ's at wing stations 197, 329, and 577 should be increased by

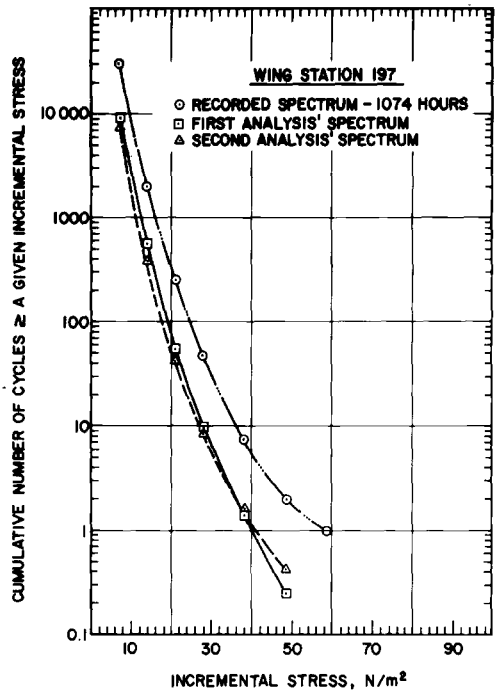

FIG. 6—*Comparison of wing stress gust spectra at wing station 197.*

factors of approximately 1.63, 1.73, and 1.67, respectively in order to correlate with the recorded data. These differences between analytical and measured unit responses are attributed to the fact that the analytical values are based on a one-dimensional vertical gust analysis while the recorded unit response values inherently include longitudinal and lateral gust effects. Similar inspection of vertical acceleration σ's indicated that a factor of 1.19 should be applied to the analytical vertical acceleration σ values. Since the curve fit parameters had previously been established, the latter factor was not applied but was accounted for by reducing the bending moment factors by 16 percent ($1 - 1/1.19$). Since the stresses at the wing locations under investigation were almost entirely wing bending moment induced, similar correlation factors for the other load components were not derived and the corrected stress four-dimensional grids were computed by directly applying the bending moment factors. New values of $\Delta S/\Delta g$ for use in Eq 2 of the second analysis then were computed and both analyses were repeated.

The resulting analytical incremental stress gust spectra are again compared to the corresponding recorded spectra in Figs. 9, 10, and 11.[4] Excellent correlation is now displayed at all three wing locations.

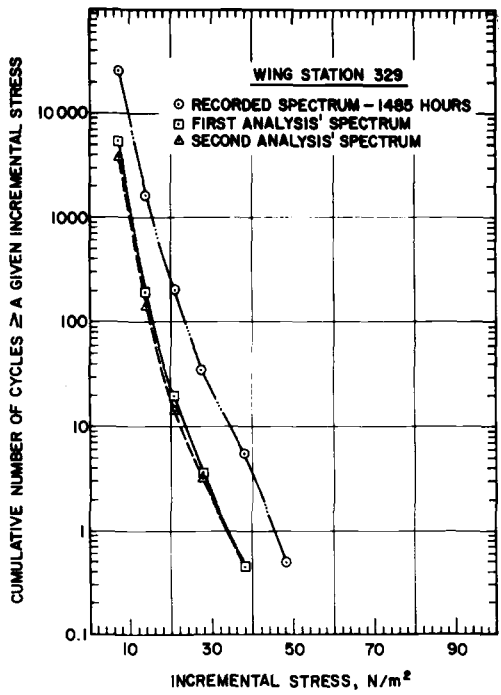

FIG. 7—*Comparison of wing stress gust spectra at wing station 329.*

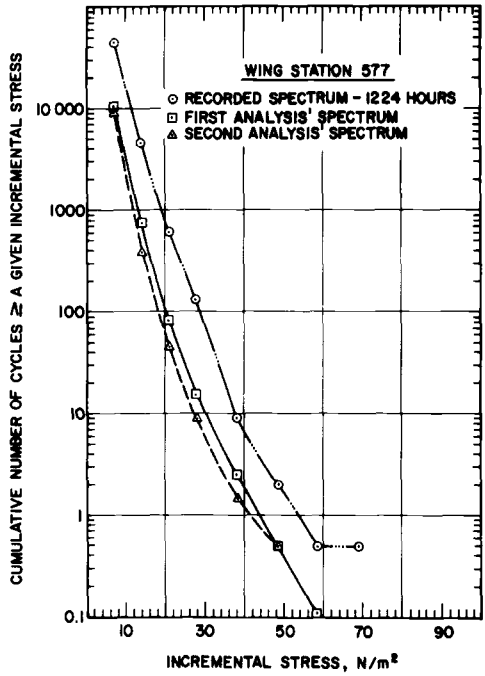

FIG. 8—*Comparison of wing stress gust spectra at wing station 577.*

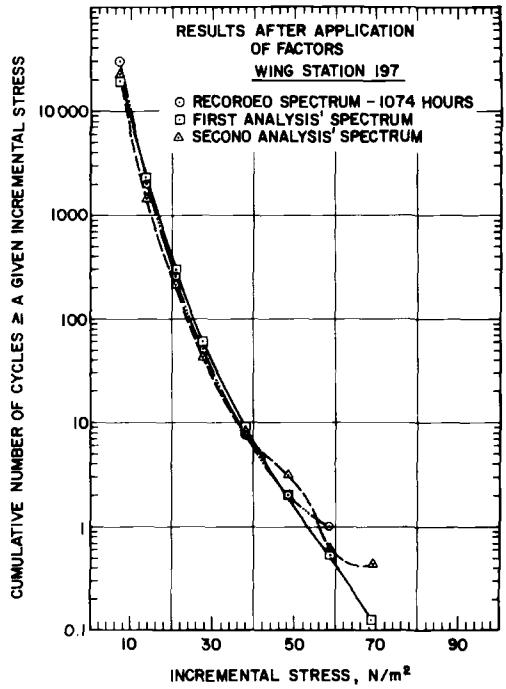

FIG. 9—*Comparison of wing stress gust spectra at wing station 197 after application of factors.*

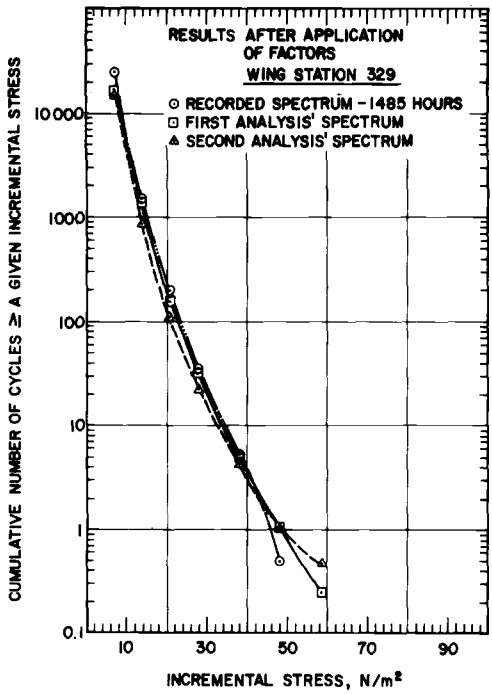

FIG. 10—*Comparison of wing stress gust spectra at wing station 329 after application of factors.*

Conclusions and Application

The results of both analyses, when corrected analytical unit response data were incorporated, were in good agreement with each other and with the recorded data. The assumption of uniformity of the analyses between different response parameters was substantiated for vertical acceleration and wing stresses at three locations on the wing. Based on these results, the dynamic response test recorded data were used to develop spanwise wing bending, torsion, and shear correction factors. Similar procedures were followed by Lockheed-Georgia engineering personnel to develop factored loads for the other aircraft surfaces and these corrected loads and altitude dependent curve fit parameters have been incorporated into the C-5A damage tracking system.

Acknowledgments

The authors wish to express their appreciation to S. F. Burrin for development of the required computer programs and to J. S. Wilson for technical discussions during the course of the data analyses.

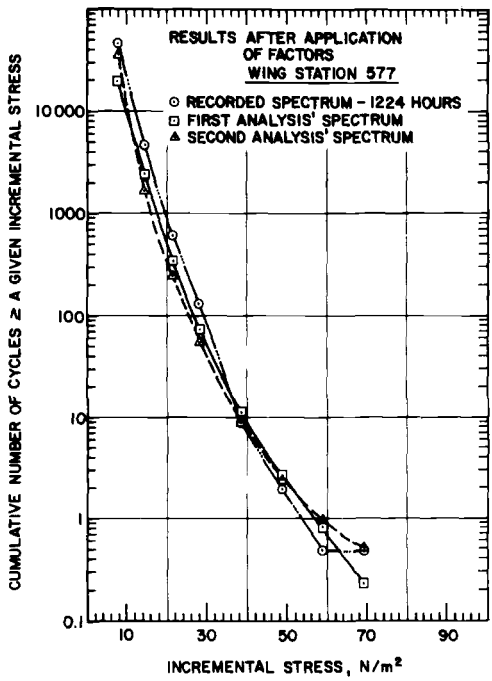

FIG. 11—*Comparison of wing stress gust spectra at wing station 577 after application of factors.*

References

[1] "C-5A Service Loads Recording Program Instrumentation Systems Report," *Technical Report LG1D1-S-3570-2*, Engineering Staff, Lockheed-Georgia Company, Marietta, Ga., 15 April 1974.

[2] Schijve, J. in *Fatigue of Aircraft Structures*, W. Barrois and E. L. Ripley, eds., Macmillan Co., New York, 1963, pp. 115-149.

[3] van Dijk, G. M., "Statistical Load Data Processing," NASA SP-309 paper presented at 6th ICAF Symposium, Miami, Fla., May 1971.

[4] Press, H. and Steiner, R., "An Approach to the Problem of Estimating Severe and Repeated Gust Loads for Missle Operations," *Technical Note 4332*, National Advisory Committee for Aeronautics, Washington, D. C., Sept. 1958.

[5] Neuls, G. S., Maier, H. G., Lerwick, T. R., Robb, E. A., and Webster, I. J., "Optimum Fatigue Spectra," *Technical Report No. ASD-TR-61-235*, Flight Dynamics Laboratory, Aeronautical Systems Division, Air Force System Command, Wright-Patterson Air Force Base, Ohio, April 1962.

[6] Houbolt, J. C., Steiner, R., and Pratt, K. G., "Dynamic Response of Airplanes to Atmospheric Turbulence Including Flight Data on Input and Response," *NASA Report TR R-199*, National Aeronautics and Space Administration, Washington, D. C., June 1964.

[7] "C-5A Dynamic Response Test Analysis and Evaluation Report-Flight," *Technical Report LG1UT63-2-3*, Engineering Staff, Lockheed-Georgia Company, Marietta, Ga., 26 July 1974.

M. P. Kaplan,[1] *J. A. Reiman,*[1] *and M. A. Landy*[1]

Derivation of Flight-by-Flight Spectra for Fighter Aircraft

REFERENCE: Kaplan, M. P., Reiman, J. A., and Landy, M. A., **"Derivation of Flight-by-Flight Spectra for Fighter Aircraft,"** *Service Fatigue Loads Monitoring, Simulation, and Analysis, ASTM STP 671,* P. R. Abelkis and J. M. Potter, Eds., American Society for Testing and Materials, 1979, pp. 193-207.

ABSTRACT: The importance of predicting the durability and damage tolerance capability of aircraft structures has underscored the need to derive a realistic flight-by-flight stress spectrum. This stress spectrum is generated from an analysis of the projected usage (mission profiles), combined with load factor exceedance curves that are obtained either from MIL-A-8866B or recorded data. The mission profiles are defined by the using command (the organization which flies the aircraft) and contain such information as mission length, number of times flown per aircraft lifetime, fuel load, weapons configuration, and a breakdown of the mission by segment, for example, takeoff, climb, cruise, descent, etc.

This paper describes two different approaches for obtaining load factor exceedance curves: (1) MIL-A-8866B and (2) data recorded from a different aircraft flying a similar mission. In the first example, the spectrum is derived for a ground-attack fighter that is in the design phase (that is, has never flown) and in the second case, the spectrum is derived for an aircraft that has already been built but is being used in a new mission (flight demonstration squadron). In this second case, a large amount of recorded load factor exceedance data exists from a different aircraft flying the same mission. Using either exceedance curve approach, these data are combined with the mission profile data to develop a stress-exceedance curve for each mission. The stress-exceedance information then is input to a computer program, along with some additional data such as the number of times a given mission is flown. The computer program first generates a random mission ordering and then randomly orders the stresses within each mission. The final result is a random flight-by-flight stress spectra suitable for use in performing damage tolerance and durability analyses and tests.

KEY WORDS: durability, damage tolerance, flight-by-flight, stress spectrum, load factor exceedance curve, mission profiles, usage, fatigue tests

Accurately predicting the life of structural components is a necessary but complex task. This complexity is due, in part, to the variability of loading conditions, materials, external environments, and usage. Thus, many disciplines are required to work together for completion of this task. In the case of aircraft, these disciplines include external and internal loads,

[1]Aerospace engineers, Fracture and Durability Branch, Structures Division, Wright-Patterson Air Force Base, Ohio, 45433.

spectrum development, stress, fatigue, fracture, and test. Among these, spectrum development plays a key role. This unit has two main functions. It must first determine a set of load factor exceedance curves for each mission (cross country, ground attack, air combat maneuver, etc.) and mission segment (takeoff, cruise, loiter, etc.). Each load factor then must be combined with a particular point in the sky (velocity, altitude) and airplane condition (weight, store configuration, yaw rate, etc.). When the load factor-point in the sky-airplane condition matching is complete, this group performs its second task, that of developing the spectrum.

Spectrum development consists of taking these discrete load conditions and sequencing them into a flight-by-flight spectrum that can be used for both testing and analysis. The importance of a correct sequence cannot be overstated. Experimental evidence indicates that spectra developed in different ways from a single exceedance curve significantly affects the life of structural components.

The purpose of this paper is to discuss two methods of obtaining the usage data and developing a flight-by-flight spectrum. In one case, the spectrum is derived for a ground attack fighter that is in the design phase and in the second case, the spectrum is developed for an existing aircraft that has undergone a significant change in usage.

Loading Spectrum Determination

The structural life of an aircraft is dependent upon how the aircraft is utilized, that is, what types of missions it flies. For design, the aircraft is assumed to fly in a particular way. The materials chosen, the stress level at design limit load, and in some cases the detail design are predicated on this assumption. Implicit in this hypothesis is the individual mission usage—both type and mix (percentage and time). A typical example is shown in Table 1. Each of these missions, for example, ground attack, utilizes a certain aircraft configuration and set of established maneuvers. It is through these parameters and the fuel burn-off rate that the important variables for each mission segment are established. Some of these are shown in Fig. 1.

A technique that has been useful in illustrating the severity of a particular usage is the load-exceedance curve, illustrated in Fig. 2. These exceedance curves can be determined from recorded data or from the tables in MIL-A-008866B (Table 2). As the mission profile states the time for each mission segment, the total number of load factor exceedances per segment can be determined.

After the load factor occurrences per segment are determined, it becomes necessary to associate each of them with a particular velocity, altitude, weight, roll rate, yaw rate, etc. The method used to accomplish this is entirely dependent upon the information that is available. For example, if MXU-553 recorder (a type of multichannel recorder) data are available,

TABLE 1—*Typical fatigue design mission profile combat employment—close air support.*

	1	2	3	4	5	6	7	8	9
Condition (Segment)	Initial Gross Weight, lb	Altitude, ft	Fuel Used, lb	Distance in Nautical miles	Speed Keas	Power Setting	Time, min	Total Time, percent	Total Time, min
Taxi	45007						7.0	3.1	7.0
Takeoff	45007	0 to 1000	94	0	0 to 198	max	0.9	0.4	7.9
Ascent	44913	1000 to 20 000	980	53	198 to 179	int	14.0	6.1	21.9
Cruise	43933	20 000	1656	169	211	part	34.0	14.9	55.9
Descent	42277	20 000 to 5000	62	28	178	idl	7.5	3.3	63.4
Loiter	42215	5000	1735	...	162	part	42.1	18.5	105.5
Combat (payload) (11025 lb)	40484	1000 to 6000	4046	...	275 to 330	idl-max	50.0	21.9	155.5
Ascent	25409	5000 to 25 000	350	23	197 to 170	int	5.0	2.2	160.5
Cruise	25059	25 000	1055	1.74	168	part	41.3	18.1	201.8
Descent	23993	25 000 to 1000	158	50	136	idl	17.5	7.7	291.3
Approach and landing	23835	1000 to 0	503	...	134 to 0	part to idl	1.7	0.7	221.0
Taxi	23332	0	...				7.0	3.1	228.0
Total			10 650					100.0	

NOTE—
1 lb = 454 g
1 ft = 304.8 mm

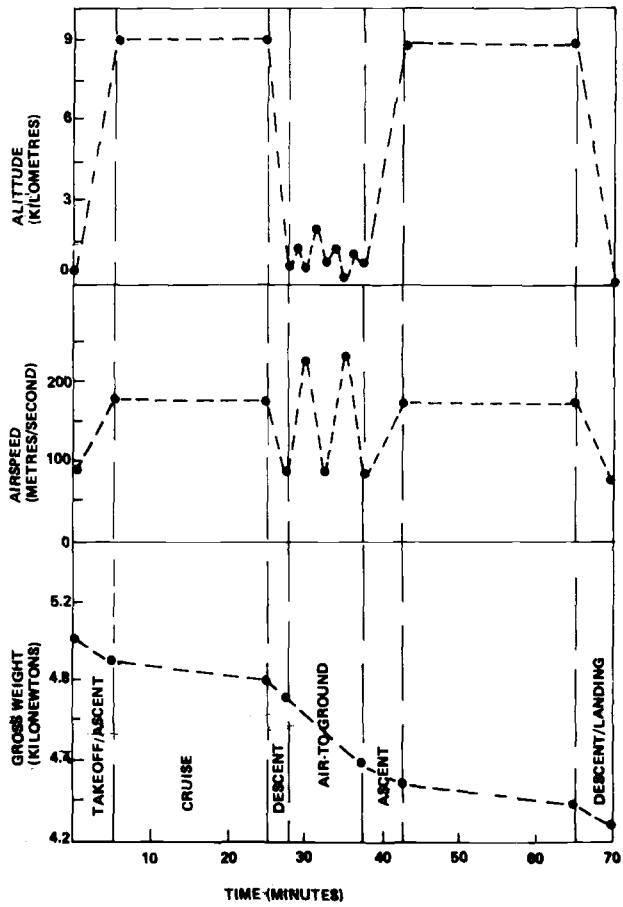

FIG. 1—*Important mission parameter variations.*

many of these parameters are already coupled per mission or mission segment and few assumptions have to be made. If just VGH (airspeed, vertical load factor, altitude) data are available per mission or mission segment, more assumptions are necessary. If only counting accelerometer data (g counters) are available, the mission profile becomes extremely important because it is only through this information that the important parameters can be coupled.

For the attack aircraft considered here, the mission profiles were defined by the Air Force and were based upon projected usage. The data in Tables 1 and 2 were combined to obtain Table 3, the number of occurrences per load factor per mission segment; Table 1 is used with Table 3 to ensure proper selection of velocities, altitudes, and weights across each segment. At all times, data compiled like that shown in Table 4, the actual point

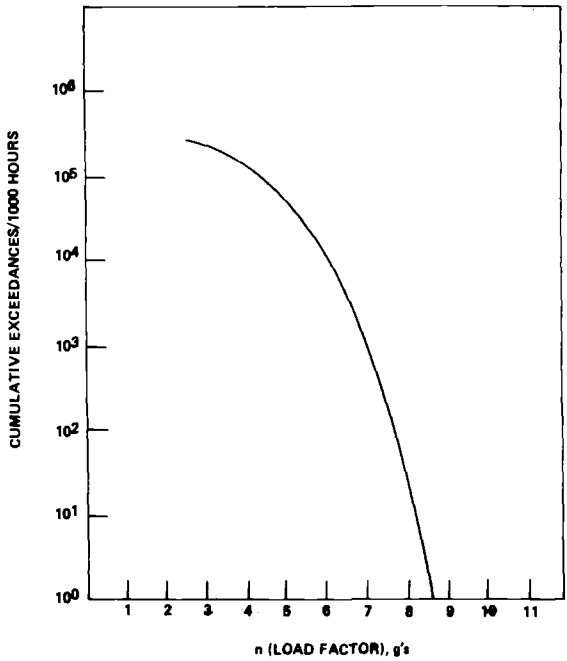

FIG. 2—*Maneuver load factor exceedance curve.*

in the sky analysis, must be checked with the *V-n* diagram (Fig. 3) to make sure no occurrences are associated with a combination of velocity, altitude, and weight that is impossible for the aircraft to achieve.

The analysis for the T-38 Thunderbird aircraft was more complicated as there were no mission profiles or exceedance curves defined. However, by using the Thunderbird show syllabus and information obtained from the aircrews and ground personnel, it was possible to construct a set of mission profiles. The repeatability of the Thunderbird mission makes it possible to represent the usage with just three missions, each comprised of four mission segments. The exceedance data used were developed from data recorded on F-4 aircraft used for the Thunderbird mission.

The rationale for using F-4 Thunderbird exceedance data to develop a T-38 Thunderbird spectrum is best summarized by Fig. 4, an exceedance diagram with curves representing the usage of previous Thunderbird and Navy Blue Angel aircraft.[2] These curves show that all previous air demonstration squadrons fly approximately the same usage. The rationale was justified further by noting that the Thunderbird show syllabus calls out maneuvers by load factor and speed. This is the reason for the similarity

[2]Clay, L., Nash, J., Rockafellow, R., and Shope, C., "Structural Flight Loads Data from F/RF-4 and Thunderbird F-4E Aircraft, January 1972 through June 1973, *ASD-TR-74-2*, Jan. 1974.

TABLE 2—*Maneuver load factor spectra, cumulative occurrences per 1000 flight hours by mission segment.*

N_Z	Ascent	Cruise	Descent	Loiter	Air-Ground	Special Weapon	Air-Air
			Positive				
2.0	5000	10 000	20 000	15 000	175 000	70 000	300 000
3.0	90	2 500	5 500	2 200	100 000	25 000	150 000
4.0	1	400	500	250	40 000	7 500	50 000
5.0		1	1	25	10 000	2 000	13 000
6.0				1	1 500	250	2 500
7.0					200	15	900
8.0					15	1	180
9.0					1		60
10.0							15
			Negative				
0.5					10 000		44 000
0					350		4 000
−0.5					30		1 200
−1.0					7		350
−1.5					3		60
−2.0					1		8
−2.5							1

TABLE 3—*Mission 1—combat employment.*

Phase / *Nz*	Takeoff/ Ascent	Cruise	Descent	Loiter	Combat	Ascent	Cruise	Descent/ Landing
2	314	1430	630	2660	36 800	105	1740	1623
3	5.6	358	174	372	21 000	2	435	446
4	0.06	57	16	45	8400	0.02	69	41
5		0.14	0.3	5	2100		0.17	0.08
6				0.18	316			
7					42			
8					3.2			
9					0.21			
10								
.5					2100			
0					73.5			
−.5					6.3			
−1.0					1.5			
−1.5					0.63			
−2.0					0.21			
−2.5								

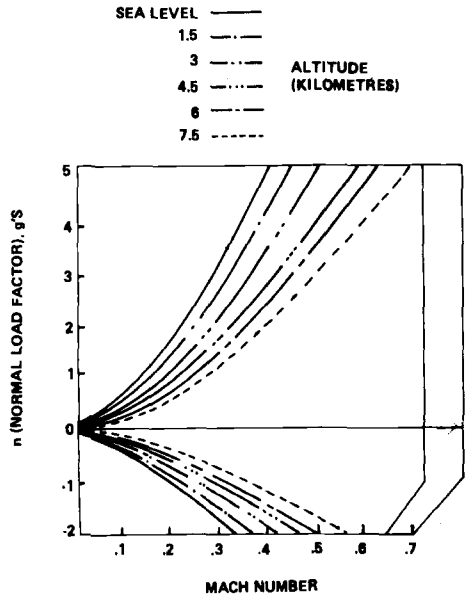

FIG. 3—*Velocity-vertical load factor* (V-n) *diagram.*

TABLE 4—*Mission description for close air support aircraft.*

Mission	Weight		Velocity	Altitude,
	Takeoff	Landing	Knots, max	ft
Close-air support	45 000	23 300	250	25 000
Escort	39 300	23 300	240	5 000
Armed-reconnaisance	41 800	23 300	260	25 000
Navigation	45 500	25 000	280	25 000
Transition	30 000	20 000	260	25 000
Instrument training	29 000	25 000	260	25 000
Weapons delivery training	30 600	24 300	260	25 000
Ground attack training	30 600	24 300	260	25 000
Combat maneuver training	30 100	26 500	260	25 000
Refueling training	29 100	24 900	370	20 000
Navigational check	29 100	26 900	270	25 000

in the exceedance curves. To use the F-4 n_z exceedance data to develop the T-38 spectrum, it was necessary to ensure that the T-38 could fly the same combinations of airspeed, altitude, and load factor as the F-4. This was accomplished by comparing the *V-n* diagrams of the F-4E and T-38. This comparison showed that there were no F-4 Thunderbird maneuvers which were outside the T-38 envelope.

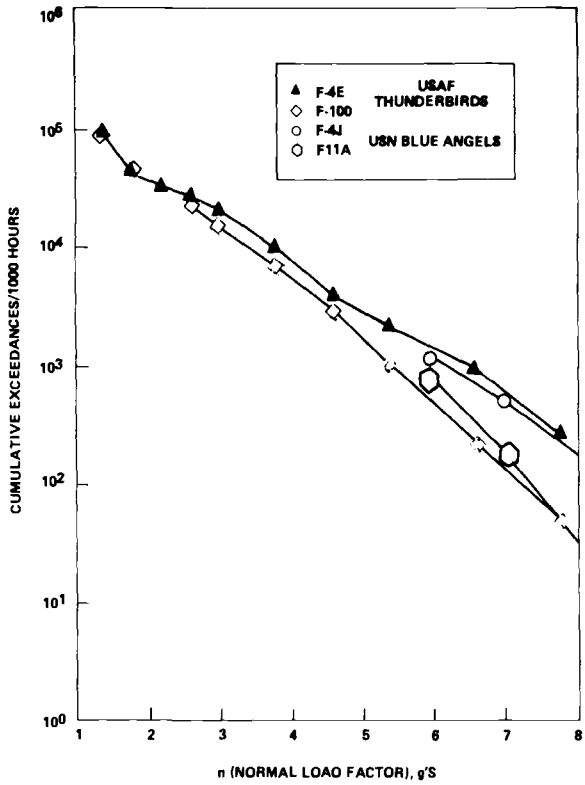

FIG. 4—*Typical demonstration squadron maneuver load factor exceedance curves.*

The F-4 Thunderbird exceedance data[2] were broken out by mission segment and replotted in order to be able to determine more precisely the exceedance at any given load factor. Both positive and negative exceedance curves were replotted (Figs. 5 and 6, respectively).

Once the n_z occurrences were associated with a velocity, altitude, and weight, the bending moments were calculated from the following

$$M_{x\,\text{air}}\,(V,\ W) = a\,V^2 + bW$$

$$M_{x\,\text{inertia}}\,(W) = nf(W)$$

$$M_{x\,\text{total}} = M_{x\,\text{air}} + M_{x\,\text{inertia}}$$

where

V = velocity,
W = gross weight,
f = function dependent upon the gross weight,
n_z = vertical load factor,

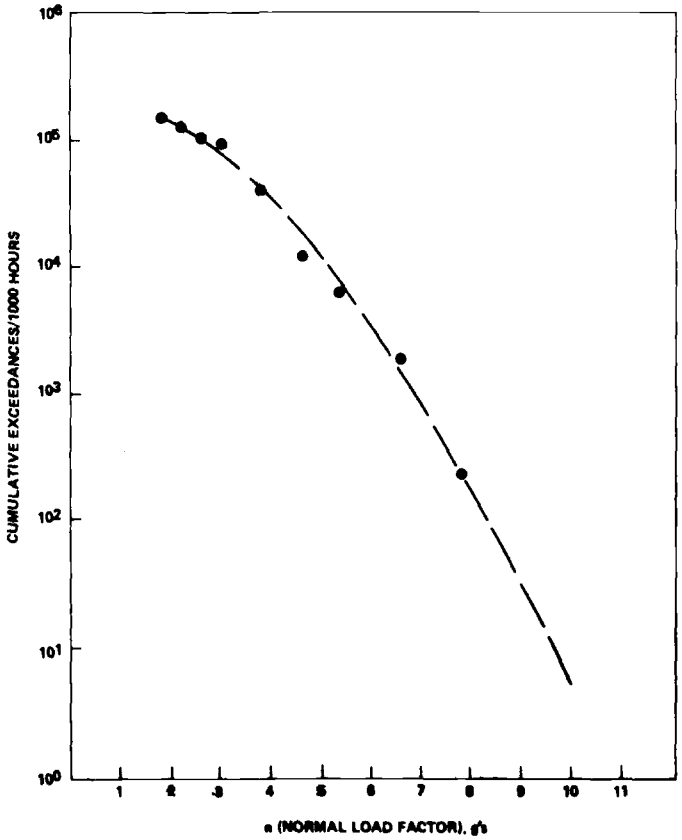

FIG. 5—*F-4/T-38 Thunderbird positive exceedance curve—demonstration mission.*

$M_{x\,\text{air}}$ = moment due to aerodynamic forces,
$M_{x\,\text{inertia}}$ = moment due to inertial forces,
$M_{x\,\text{total}}$ = total moment, and
a and b = constants.

These calculations were performed using a computer program developed by Lincoln.[3]

Since there is a unique stress for each combination of load factor, weight, altitude, and velocity, there can be hundreds of different stress levels for a mission. Therefore, it is desirable to consolidate the different stress levels into a more manageable number. This was accomplished with the computer program already mentioned. A frequency distribution histogram of the stresses is constructed. The total area under the histogram is normalized to

[3]Lincoln, J. W., "Development of an Aircraft Maneuver Load Spectrum Based on VGH Data," ASD-TR-7X-XX, to be published.

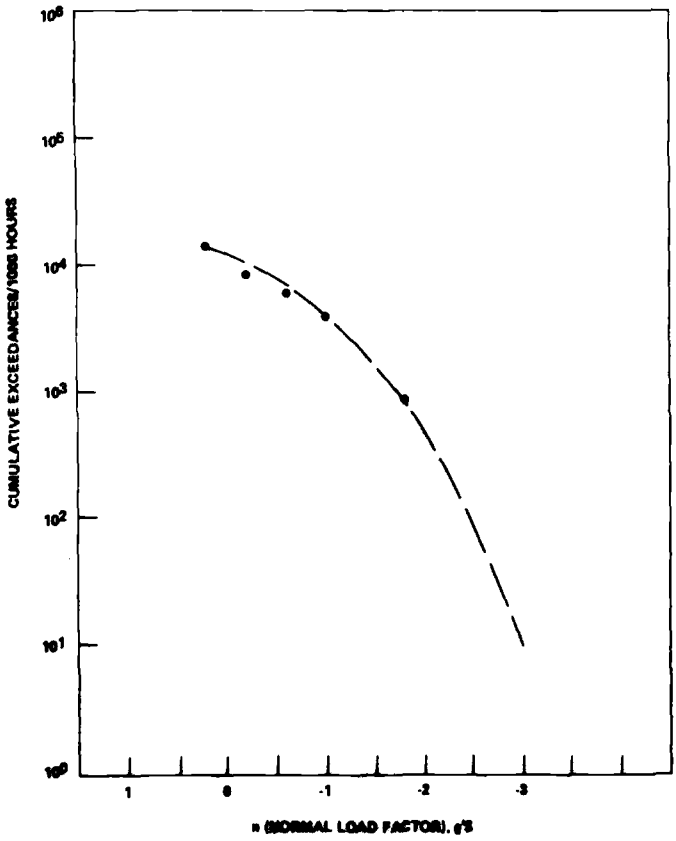

FIG. 6—*F-4/T-38 Thunderbird negative exceedance curve—demonstration mission.*

unity, giving a probability density function. Twenty discrete intervals of stress then are chosen, and the fraction of the total number of occurrences within each interval is calculated. The number of intervals (20) and the width of the interval is arbitrary; engineering judgment should guide the exact choice. The interval width need not be constant, and in the two examples discussed here, the intervals were finer at high absolute values of load factor in order to obtain a more precise distribution of the cycles that critically affect fatigue life. Once the histogram is divided into the defined intervals, a weighted average value of stress over the interval is calculated.

To review, 20 stress levels, representative of the range of peak stress occurrences in the mission (or mission segment), have been calculated along with the corresponding fraction of the total number of occurrences. The number of occurrences of each level is calculated by simply multiplying the fraction by the total number of occurrences. This process is repeated for

positive and negative maneuvers and the 1*g* conditions resulting in a total of 60 stress levels and the number of occurrences of each level.

Derivation of Random Flight-by-Flight Spectra

After the occurrences for positive, negative, and 1*g* conditions have been determined, the resulting stresses were combined to form a discrete point-by-point stress-time history, or stress spectrum. To accomplish this, a decision must be made about the order of occurrence of the missions and the order of the stresses within each mission. It was not possible to predict either the order of the mission or the order of the stresses within the mission, therefore, a random order was selected.

To accomplish this end, the authors have developed a computer program that generates such a random spectrum. The spectrum can be generated in two ways; either on a mission-by-mission basis or on a mission segment-by-mission segment basis.

Mission Segment-By-Mission Segment

Development of the spectrum for the T-38 Thunderbird aircraft was done on a mission segment-by-mission segment basis. It is the more complex of the two methods. A flow diagram detailing this spectrum generation scheme is shown in Fig. 7.

Within each segment, the ordering of the maximum (positive) stresses is done randomly. The stresses are chosen from the list of stress occurrences for the particular mission segment. The list of every-flight occurrences, representing the occurrences that occur at least once per flight, are generated by dividing the total lifetime occurrences (per stress level per mission segment) by the number of flights containing that mission segment and disregarding the fractional part of the quotient, which will be accounted for momentarily. To this list are added occurrences that happen less than once per flight. These occurrences will be referred to as remainders. These remainders are nothing more than the sum of all the fractional parts resulting from the division process used to obtain the every-flight occurrences. The remainders are not added to the every-flight occurrences during every flight mission that the segment appears in but rather are added selectively throughout all flights according to a placement key. The entries in the placement key represent flights of a particular mission in which the segment appears to which a remainder will be added. In other words, an entry, N, in the placement key means that a remainder will be added to the occurrences of the segment in question in every Nth time that a mission containing that segment is flown. Of course, they will be added only until they are used up. Each time a remainder is used up, it is subtracted from the remainders left and the table is checked before the next remainder is added.

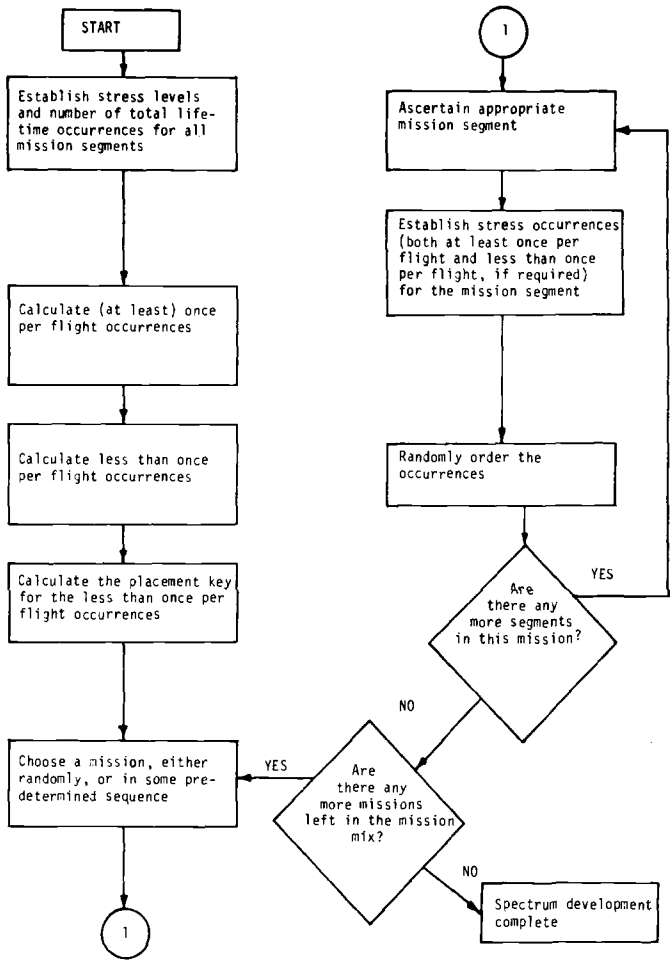

FIG. 7—*Flow diagram for random spectrum generation procedure.*

The placement key array entries are generated as a function of the number of remainders at that stress level and the number of total flights containing that segment.

The minimum (1*g* and negative) stress occurrences are randomized in a similar manner, that is, the minimum stresses are paired randomly with the maximum stresses. The number of minimum stress occurrences in any segment is forced to be the same as the number of maximum stress occurrences. This is done, as necessary, by adding occurrences to the minimums to make the total minimum occurrences equal the total maximum occurrences. These additional minimum stress occurrences are taken from randomly chosen stress levels of the minimum remainders and are, of course, placed in the same level from which they are taken. The minimum re-

mainders are not added to the every-flight occurrences according to a placement key. A minimum remainder is added every time a maximum remainder is added. This is done to keep the total number of minimum occurrences equal to the total maximum occurrences. However, the stress level to which the minimum occurrence is added is chosen randomly.

After establishing the random sequencing of stresses within each segment, the appropriate segments are linked together to form flights. The flights then are ordered in a random fashion to complete the generation of the spectrum. It is important to note that the segments maintain their order of occurrence during each flight. Due to this ordering, a stress associated with a landing load, for instance, will not occur before a stress associated with a cruise load. A representation of a typical mission segment-by-mission segment stress spectrum is shown in Fig. 8.

Mission-By-Mission

The spectrum for the attack aircraft was generated on a mission-by-mission basis. The stress occurrences for this spectrum are generated similarly to those of the mission segment-by-mission segment spectrum. The major difference between the two methods is that the load and stress exceedance data are not broken down into mission segments. The stress occurrences are generated for, and ordered randomly within, each mission. The missions then are ordered randomly as with the mission segment-by-mission segment spectrum.

With this type of random sequencing, the general ordering of stresses

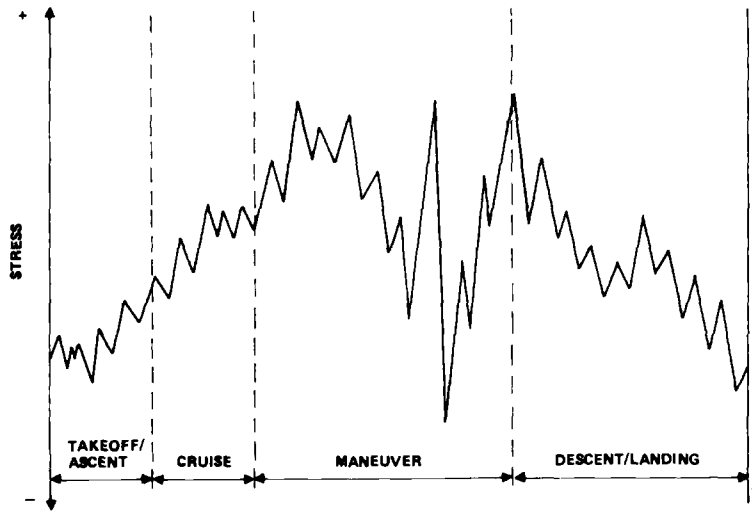

FIG. 8—*Typical random flight generated by mission segment.*

within each flight is lost. That is, a stress associated with a landing load, for instance, may occur before a stress associated with a cruise load.

Another difference between the two spectra is the addition of stress occurrences resulting from ground loads. At the time the mission-by-mission spectrum was being generated, the authors felt that it was important to add these ground loads to complete the ground-air-ground (GAG) cycle in each flight. The GAG cycle normally provides one of the largest (if not the largest) stress ranges in the spectrum and may account for a significant portion of the damage. The GAG cycle was included in the mission-by-mission spectrum by adding representative ground loads (stresses) to the spectrum. A maximum and minimum stress occurrence was added at the beginning (takeoff) of each mission and another was added at the end (landing) of each mission. The same ground loads were added to all the missions. Further studies by the authors[4] showed that inclusion of ground loads had little effect on analytical crack growth life for fighter/strike aircraft. This is most likely due to the fact that the maneuver loads of a fighter produce larger and more frequent stress ranges than the GAG cycle. Thus, stresses resulting from ground loads were not included in the mission segment-by-mission segment spectrum development.

Conclusions

1. Feasibility of generating a random flight-by-flight spectrum has been demonstrated for:

(*a*) Mission segment by mission segment
(b) Mission by mission

2. The assumptions made in developing a spectrum depend on the type of basic data available; for example, recorded exceedance data versus MIL-A-8866.

3. The procedures for generating a realistic stress spectrum can be defined adequately.

[4]Landy, M., Kaplan, M., and Reiman, J., "Derivation and Analysis of Loading Spectra for USAF Aircraft," *ASD-TR-76-1*, Jan. 1976.

M. P. Weiss[1]

Simulation and Monitoring of Loads in Crane Beams

REFERENCE: Weiss, M. P., **"Simulation and Monitoring of Loads in Crane Beams,"** *Service Fatigue Loads Monitoring, Simulation, and Analysis, ASTM STP 671,* P. R. Abelkis and J. M. Potter, Eds., American Society for Testing and Materials, 1979, pp. 208-221.

ABSTRACT: The fracture mechanics approach to design of steel structures uses the stress range distribution function as the main parameter that governs crack propagation and possible failures. It is an accepted fact that all welded structures contain existing small cracks that propagate as a function of varying stress ranges and stress intensity factors. The main problem is to predict correctly the nature of the varying stresses and to analyze them for fatigue evaluation.

Crane structures are exposed constantly to different static and dynamic loads and their stress distribution is quite complex. In this study, stress distributions in an overhead travelling bridge crane beam are evaluated by computer simulation and by monitoring real structures with a specially developed test setup.

The simulation starts with generating beta distributed random loads, and random loading and unloading places in the service area. These points are generated by means of a new general distribution model. Stress peaks and ranges are calculated and counted per each loading cycle.

The test setup uses regular load cells, with specially designed fixtures and A/D converters, to record data on perforated tapes.

The simulations were used to plot general distributions of stress peaks and ranges. The test results are special cases of the general distributions.

The results of this study are being used currently to evaluate fatigue lives and safe stresses in crane structures, and to update design codes.

KEY WORDS: peak stresses, crack propagation, fatigue damage, crane beams, service loads, stress history, fatigue tests

Overhead travelling bridge cranes are typical examples of dynamic structures, in which varying stresses, fatigue, and crack propagation are the dominant design factors. The varying stresses are influenced mainly by the loads and their displacements. Crane structures often are built of welded mild steel elements and small cracks are inherent in the vicinity of welds. These small cracks tend to propagate; to be able to predict the

[1]Adjunct professor of Mechanical Engineering, Technion, Israel Institute of Technology, Haifa, Israel, 33485.

crack propagation rate, one needs the peak stress distribution for the first stage, and the distribution of stress ranges for the later stage of crack propagation. The stress distributions can be measured experimentally, studied analytically, or estimated by computer simulations. An analytical study was detailed by Weiss [*1, 2*].[2] Experimental and simulation studies will be introduced in this paper.

Crane Model

A bridge crane with a trolley on top of it can be modeled by a simple beam with two connected moving loads. The beam and corresponding moments are described in Fig. 1. We are interested in the most severely stressed point on the beam X_s, and it is shown [*1*] to be

$$X_s = \frac{L}{2} - \frac{e}{4} \tag{1}$$

where

L = Beam's span, and
e = trolley's span.

The general expression for the moment M_s in that point due to live load is

$$M_s = C_{i1} \cdot P + C_{i2} \cdot P \cdot X; \tag{2}$$

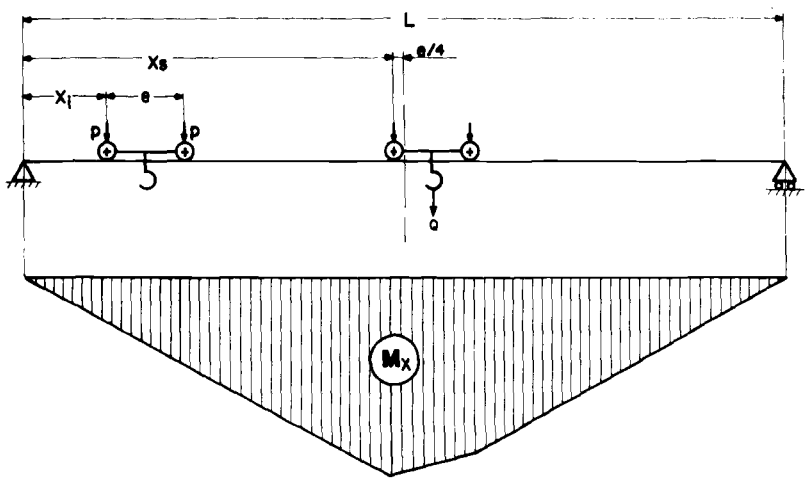

FIG. 1—*A crane beam model.*

[2]The italic numbers in brackets refer to the list of references appended to this paper.

where

P = load on each trolley's wheel (kg),
X = load's location on the beam (m), and
C_{ij} = constants.

The constants C_{ij} vary according to the exact location of X as follows

when

$$\begin{aligned} X < X_s - e \quad & \text{then } i = 1 \\ X_s - e \le X < X_s \quad & \text{then } i = 2 \\ X_s \le X < L - e \quad & \text{then } i = 3 \end{aligned}$$

$$C_{ij} = \left| \begin{array}{c} \dfrac{e(2L+e)}{4L}; \dfrac{2L+e}{2L} \\ \dfrac{(2L-e)(L-e)}{4L}; \dfrac{e}{2L} \\ \dfrac{(2L-e)^2}{4L}; \dfrac{e-2L}{2L} \end{array} \right| \tag{3}$$

Equation 2 describes the vertical moments in a crane beam due to moving live loads. We have to consider also dead loads due to weight, dynamic, horizontal, and vertical loads due to sudden loading, braking and vibrations, wind loading, and secondary effects. These factors are taken care of in the current design codes.[3] A full derivation of the stresses in a crane beam had been made by Weiss [2], and results in a simple expression for the instantaneous tensile stress—S_s, in the most vulnerable point of the beam—X_s as follows

$$S_s = C_2 M_s + C_3 \tag{4}$$

where

M_s is taken from Eq 2, and
C_2 and C_3 = dimensional constants which are function of the crane type, dimensions, class, state of loading and geometry.

We can describe the dependence of the stress on the load P and the load displacement X as follows

$$S_s = F(P; X; C_{ij}; C_2; C_3) \tag{5}$$

The only varying parameters in Eq 5 are P and X.

[3]The FEM rules for the design of hoisting appliances; DIN 15018; AISE Standard No. 6 and others.

Stress Cycles

Several counting methods have been proposed [3,4] to evaluate stress histories for fatigue calculations. Most of them use different variations or combinations of stress peaks and stress ranges. We will try to find the stress peak distribution function, and stress range distribution function. In the crack initiation stage the peak stresses have the dominant role; in the crack propagation stage the stress ranges are more important.

The hoisting cycle of our crane is as follows: in every cycle a load Q, is picked up at point X_1 of the crane's span, and dropped at X_2. One can describe the hoisting cycles in a graph form of displacement—X, load on trolley's wheel—P and stress—S, all as changing in time t. One can see in Fig. 2, that in every cycle there are one or two positive peak stresses.

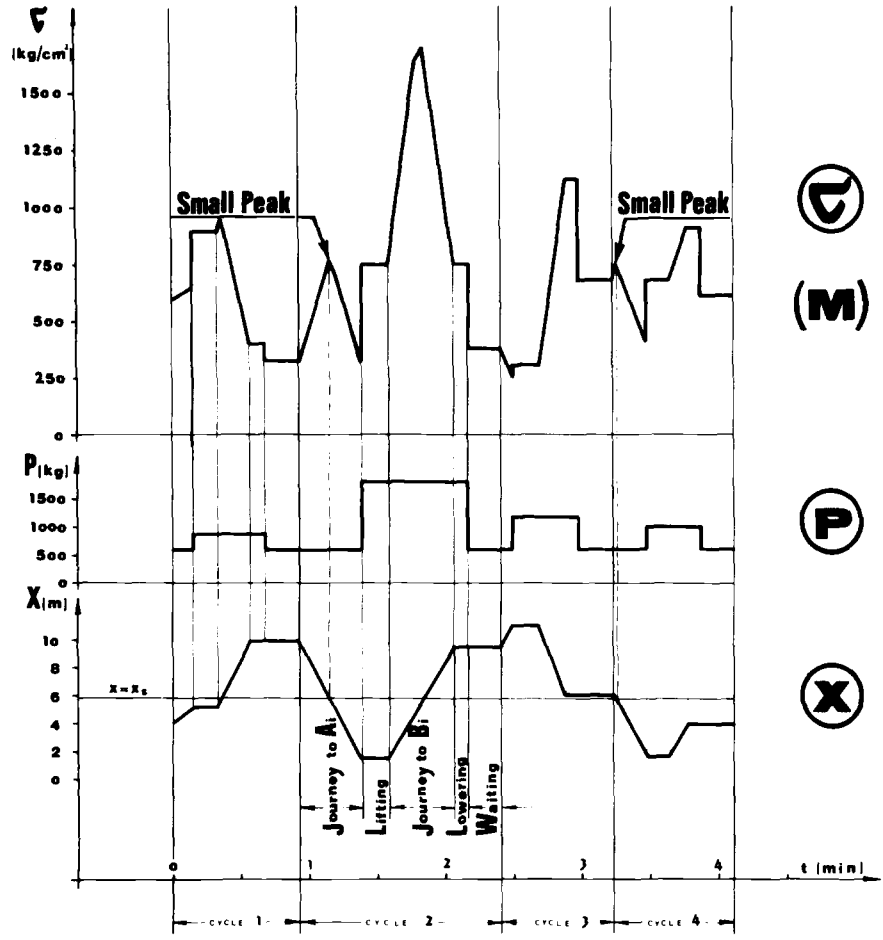

FIG. 2—*Stress cycles in a crane beam.*

One is the peak that is caused by load Q in the proper position, and the other is due to crossing of the empty trolley through point X_s. The other peak always has the same stress value, and will be called the "small peak." Figure 2 is a combination of measured and calculated values. The displacement can be measured directly, as can the value of the load P on each wheel of the trolley. The value of S_s is a calculated one by Eq 4. It is possible to measure the stress S_s directly by means of a strain gage at point X_s, but we are interested in simulating the most unfavorable combination of loads, wind, and dynamic factors, and those conditions do not exist in each cycle. Therefore, we must calculate the simulated stress, and include a certain safety factor in the process.

Once we have the stress function as shown in Fig. 2, we can count the positive and negative stress peaks and ranges, and use different fatigue damage or crack propagation rules, as will be shown later.

Fatigue of Structures

Currently there are two different approaches to evaluate fatigue behavior in metals under varying stresses. The now classic way is the use of the linear cumulative damage rule and some kind of counting method to analyze the varying stress function. The more modern method uses linear elastic fracture mechanics, crack propagation, and stress intensity factors as the important criteria in the study of fatigue behavior. Both ways are considered frequently in the fatigue of structures; therefore, we will use them and a possible common interface between them.

The linear cumulative fatigue damage rule is known as the Palmgren-Miner law [5,6]. It is the damage rule most frequently employed, and has been incorporated into numerous design procedures for fatigue and design codes for different structures. To be on the safe side, we will apply Miner's rule on the peak stresses in our stress history. We will count all the positive stress peaks and all the negative ones, then pair them into couples of the same magnitude but different signs. We get pairs of peaks stresses that can be considered as the equivalent history. Since the linear rule does not distinguish between different orders of loading, one can use the peak counting method. The end of fatigue life is considered when the damage sum equals unity.

The crack propagation rate power law was proposed originally by Paris and Erdogan [7]. The law relates the crack propagation rate per n cycles—da/dn to the stress intensity factor range ΔK by material parameters C and m as follows

$$da/dn = C \cdot \Delta K^m \tag{6}$$

The law has been shown to fit many test data and is now used widely. It

has been demonstrated that the Paris-Erdogan power law is very useful in Stage II of the crack propagation rate diagram shown in Fig. 3. Propagation can be predicted fairly well when parameters C and m have been established by previous tests.

At the left part of Fig. 3 one can see a stress intensity range threshold—ΔK_{th} under which crack propagation cannot be measured. The meaning

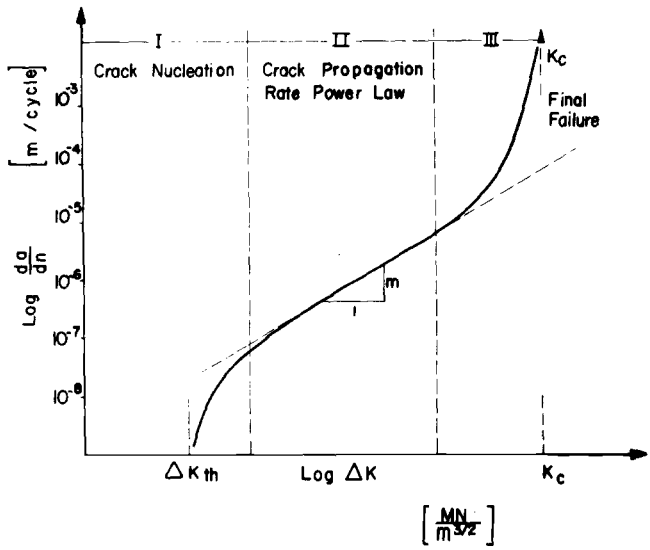

FIG. 3—*Fatigue crack propagation rate* da/dn *as a function of different values of stress intensity range,* ΔK.

of the threshold is that with very small initial microcracks, even in high stresses, when ΔK is smaller than ΔK_{th}, no crack propagation can be measured, and the power law (Eq 6) has no meaning. This law can be and is used extensively when there are initial cracks in a structure, as is often the case in welded steel structures.

It is a known fact that even under the stress intensity range threshold, when stress ranges are higher than fatigue limit, accumulation of fatigue damage exists. The specimen eventually develops a crack or suffers total failure. This case has to be analyzed by the linear cumulative damage law in the first part of the process, and by fracture mechanics laws in the successive part, after an initial crack has been observed.

A qualitative explanation of a combined fatigue crack initiation and propagation process in metals has been proposed by Weiss [*8*], and is shown in Fig. 4. A general expression for the stress intensity factor range is

$$\Delta K = \Delta S \cdot \sqrt{A \cdot \pi} \cdot F(A) \tag{7}$$

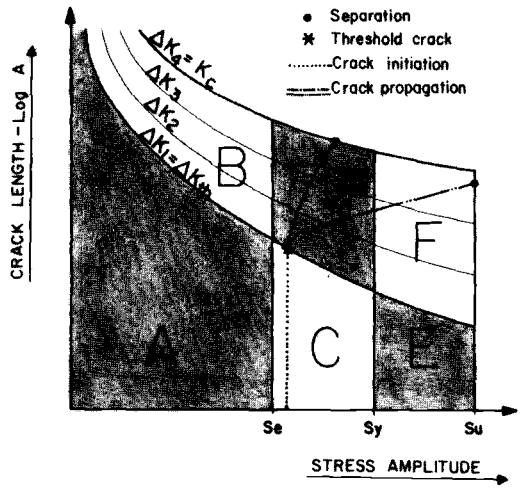

FIG. 4—*The fatigue phase diagram.*

where

ΔS = varying stress range,
A = crack length, and
$F(A)$ = nondimensional number which depends on crack length and specimen geometry.

Figure 4 shows a plot of Eq 7 for different parametric values of ΔK, between the threshold, ΔK_{th}, and fracture toughness, K_c. The plot is for simple sinusoidal loading with zero mean stress. The different lines in Fig. 4 divide the area into six zones A to F which are distinguished by different fatigue behavior as follows:

Zone A is below the fatigue limit S_e, as well as ΔK_{th}; therefore no fatigue cracks are initiated, nor will propagation be possible.

Zone B is below S_e, but above ΔK_{th}; therefore only crack propagation can be detected.

Zone C is below ΔK_{th} but above S_e; therefore "fatigue damage" will be accumulated. The definition of what constitutes damage will be explained.

Zone D is both above S_e and ΔK_{th} and therefore damage as well as crack propagation will be accumulative.

Zones E and F are similar to C and D, but are in the plastic region, and therefore in a low cycle fatigue regime. The transition across the S_y line is smooth rather than abrupt and elastoplastic behavior must be considered. The dotted line in Fig. 4 depicts fatigue damage accumulation in a smooth specimen with initial stress amplitude higher than fatigue limit. While being in Zone C, a crack is initiated. When crossing the ΔK_{th} line, a threshold crack has been reached and crack propagation started. In Zone D a

combined model for crack propagation and fatigue damage accumulation must be used. In most cases of fatigue in structures, the stresses are relatively low, and the initial cracks considerable; therefore, Zone B is the more typical for practical purposes.

Stress Distribution—Analytical Approach

The loads and their displacements vary randomly, and are different for each cycle. One can assume that the loads vary between zero and some Q_{max} and are beta distributed, with the distribution parameters $\alpha \geq 1$ and $\beta \geq 1$ as follows

$$Q = \delta \cdot Q_{max}; \qquad 0 \leq \delta \leq 1$$

$$f(\delta) = \frac{\Gamma(\alpha + \beta)}{\Gamma(\alpha) + \Gamma(\beta)} \cdot \delta^{\alpha-1} \cdot (1 - \delta)^{\beta-1} \tag{8}$$

where

α, β = distribution parameters,
δ = variant of beta distribution, and
$\Gamma(a)$ = incomplete gamma function of (a).

Let us assume that every point in the area serviced by the crane has the same probability to be chosen as loading or unloading point, which means that the displacement X is distributed uniformly.

The crane model, and the distributions for Q and X can be analyzed, and with some limiting details, peak stress distributions can be derived. The analysis had been done by Weiss [*1*,*2*] and very complicated expressions were found. These expressions can be solved numerically for some special cases only, and therefore are not general and not convenient to use.

Stress Distribution—Computer Simulation

For simulations on a computer one can use more realistic, although more complicated models. Our assumption for the load distribution is a good one to use. The uniform distribution for the service area is a special case only. For loading and unloading points there are usually preferred places in the service area, which have a greater probability of being chosen than other ones. For example in some factories the bridge crane serves mainly one big machine in a production line, and the rest of the area only occasionally. In this case the uniform distribution will not be adequate any more. In a general case, one would be interested in a model that allows the assignment of arbitrary probabilities to several special points, and the rest of the area to be uniform. Another option is to attach to each loading

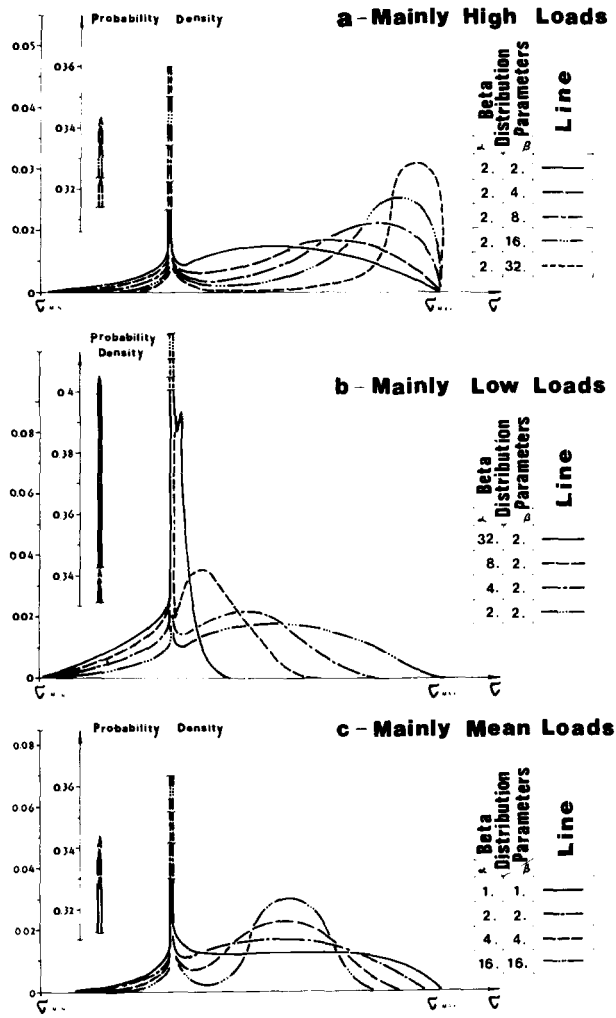

FIG. 5—*Probability density of stress peaks in a crane beam.*

point a special unloading point, to be more realistic and practical. Such a model has been done, and it has the option to choose up to 49 special loading points.

The simulation is done as follows: for every loading cycle three random numbers are generated: a load Q which is beta distributed, a loading point X_1, and an unloading point X_2 by the previously explained model. The beta distributed load is generated by a special random generator which uses the rejection procedure and an IBM subroutine [*9*]. The generator is called GENBETA and is detailed in Ref *2*.

For every cycle all important details of the stress history are calculated

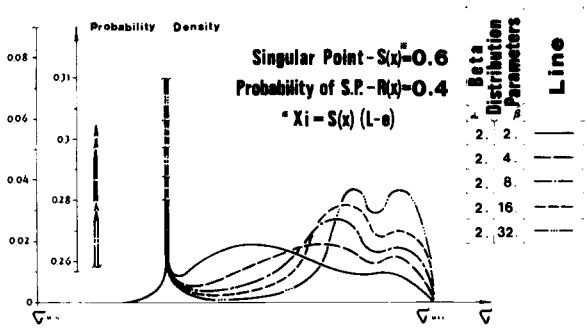

d- Singular Point Close to Center of Beam

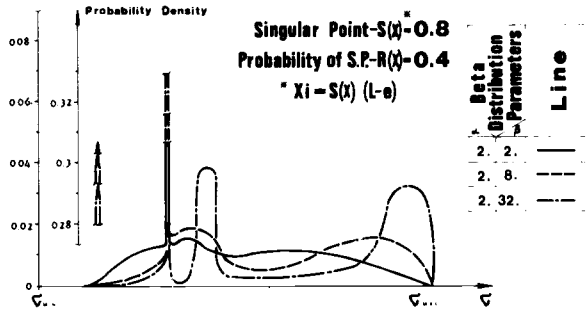

e- Singular Point Close to Side of Beam

FIG. 5—(*Continued.*)

and stored in arrays. These values include the stress peaks, ranges, and means. The simulation is performed several hundred times using the Monte Carlo method, and then the arrays are plotted.

The next stage is to evaluate the Miners summation of the stress peaks and fatigue crack propagation by the stress ranges.

The densities of stress peaks in a crane main beam are shown in Fig. 5. Only few examples are shown, out of many that were performed. The high probability of the small peak can be seen, as predicted, in all cases. It is roughly one third of the total number of peaks. The high probability of large peaks in *a* can be seen, when mainly high loads are being lifted.

When low loads are more probable, the stress peaks are also smaller. In *d* and *e* we see the case when a singular point is defined as close or remote to the center of the beam. A two peaked distribution can be seen in these cases. With several singular points multiple peaked distribution is found.

The peak stress distributions in Fig. 5 are typical to many crane structures and can be found for any special case. They should be used as basis for life estimation.

The Test Program

In previous studies [*10*], stress histories for crane beams have been measured by means of strain gages and indicators. Those histories were analyzed by peak counting methods, and evaluated by the normal distribution. No distinction between loads and displacements has been possible. In our case we were interested in such a distinction and therefore different transducers and recorders had to be used. The loads were being measured by a direct reading load cell which was mounted on the axis of the equalizing roller on the trolley, by means of a special beam. The movement of the trolley was measured by a rotating transducer which was activated by a cable, tensioned to both sides of the bridge. The transducer consisted of a load cell, loaded by a spring and mounted on the trolley. The whole test setup was mounted on a bridge crane which served a production line of rolling machines in a steel mill, and a general purpose machine shop. Parts of the setup are shown in Fig. 6, and the mounting on the crane in Fig. 7. Results were recorded on a perforated tape and were used as input to a digital computer. Results were recorded digitally every 2 s, for a long period. The recordings were analyzed and the load distribution was found to be a special case of the beta distribution, according to the initial assumption. The displacement random generator was found to be very close to the real displacement distribution found. Therefore Fig. 5 describes stress distributions that also fit the test measurements. Full numerical details can be found in Ref *2*.

Fatigue Life Estimations

The varying stress results have been used with the Miners model and safe life was estimated. The results showed that the permissible stresses in certain design codes are rather conservative and could be elevated. But such an act would cause more sensitivity to crack propagation which should be analyzed. The estimates of safe life, using the combined crack initiation and propagation model which was explained before, are in the stage of progress.

The peak stress distributions shown in Fig. 5 explain very nicely some

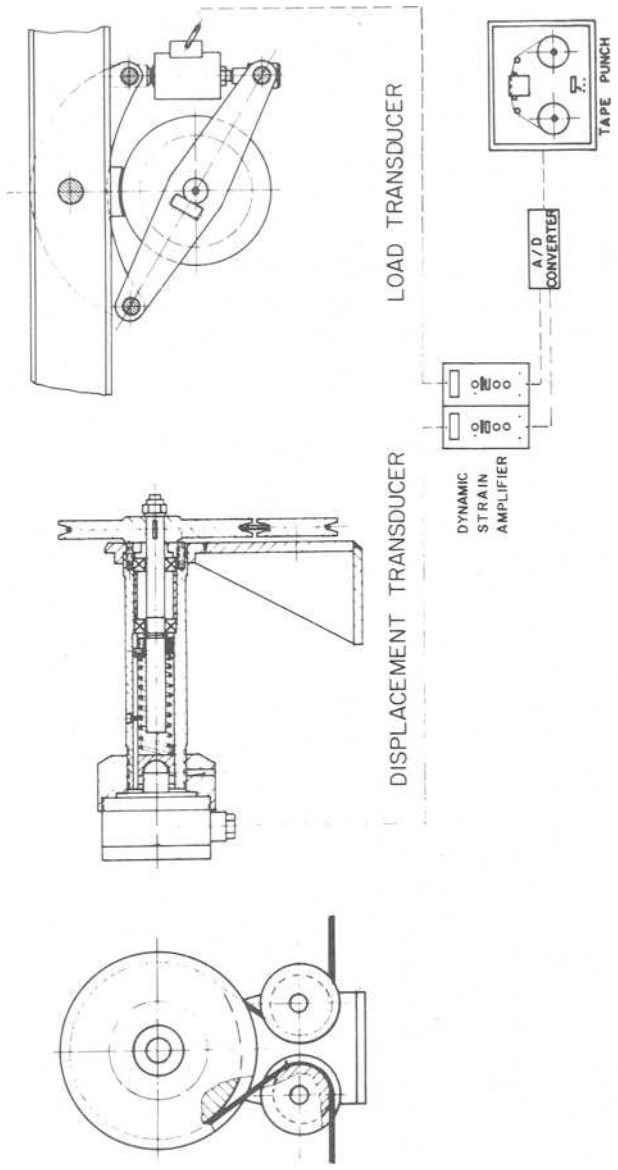

FIG. 6—*Load and displacement transducers.*

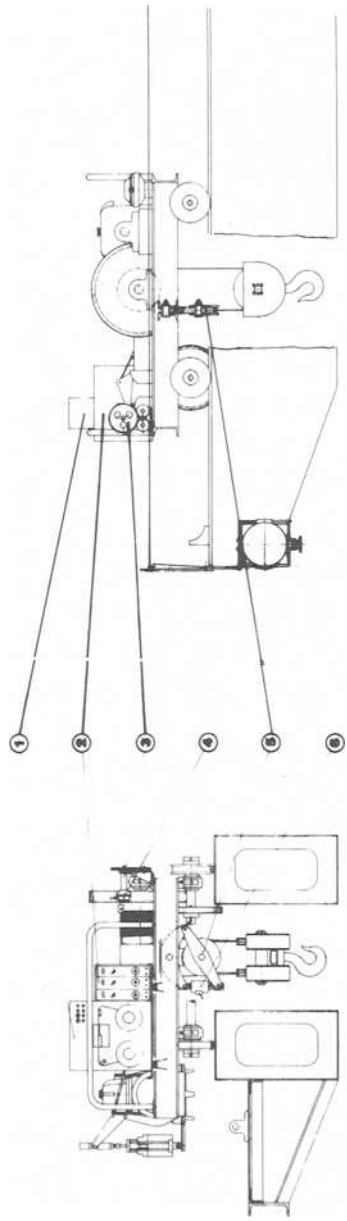

FIG. 7—*The test setup on a crane. 1 is the tape punch; 2, the strain indicator; 3, the trolley displacement transducer; 5, the equalizing beam; 4, 6 are load cells.*

irregularities in measurements that were obtained by Schweer [*10*] and not fully cleared at that time.

Summary

A simulation method to calculate stress histories and distributions in bridge crane beams has been developed. Stress distribution families have been found and detailed. A test setup was built and the tests which were performed confirmed the simulation results. Previous tests by others fit better to the proposed model than to normal distribution.

Life estimations using Miner's linear rule have been done, and show that current design codes are rather conservative. Additional life estimations, using a combined fatigue crack initiation and propagation model and the fatigue phase diagram, are currently in simulation stage.

References

[*1*] Weiss, P. M., Publication 75-DE-48, American Society of Mechanical Engineers, 1975.
[*2*] Weiss, P. M., D.Sc. thesis, The Technion, Haifa, Israel, 1973.
[*3*] Haas, T., *Engineers' Digest*, Vols. 3, 4, and 5, 1962.
[*4*] Ravishankar, T. J., *UTIAS Review*, No. 29, N70-33724, 1970.
[*5*] Palmgren, A., *Zeitschrift Vereinigte Deutsche Ingenieure*, Vol. 68, 1924, pp. 339-341.
[*6*] Miner, M. A., *Transactions*, American Society of Mechanical Engineers; *Journal of Applied Mechanics*, Vol. 12, 1945, pp. A159-A164.
[*7*] Paris, P. C. and Erdogan, F., *Transactions*, ASME Series D, American Society of Mechanical Engineers, Vol. 85, 1963, p. 528.
[*8*] Weiss, P. M., *Transactions*, American Society of Mechanical Engineers; *Journal of Engineering Materials and Technology*, Jan. 1977, pp. 23-25.
[*9*] IBM System 360 Scientific Subroutine Package (360-CM-03X), Version 3.
[*10*] Schweer, W., D.Sc. thesis, Technical University of Hanover, 1964.

Ernst Gassner[1] *and Wilhelm Lipp*[2]

Long Life Random Fatigue Behavior of Notched Specimens in Service, in Service Duplication Tests, and in Program Tests

REFERENCE: Gassner, Ernst and Lipp, Wilhelm, **"Long Life Random Fatigue Behavior of Notched Specimens in Service, in Service Duplication Tests, and in Program Tests,"** *Service Fatigue Loads Monitoring, Simulation, and Analysis, ASTM STP 671,* P. R. Abelkis and J. M. Potter, Eds., American Society for Testing and Materials, 1979, pp. 222-239.

ABSTRACT: The actual service fatigue life of notched steel and aluminum specimens was determined using a special testing device installed in a passenger car and operated by the vertical displacements of a car rear wheel; the specimens are subjected to reversed bending. The tests were carried out over a distance of more than 2×10^5 km. The testing device was equipped with counting instrumentation to ensure direct correlation between the individual test result and the relevant frequency distribution of level-crossings.

The results of the service test series are statistically evaluated and presented as stress/life curves for SAE 5140 and for 2024 T 3 specimens. The corresponding stress/life curves, obtained in service duplication tests were not significantly different.

However, the conventional eight-step program tests overestimate the fatigue life observed in service and service duplication tests by a factor which may be as high as five.

The results of the test series were also compared to fatigue calculations. It was found that the application of a modified linear fatigue damage rule, which does not account for the sequence effect of load changes, yielded fatigue life data which are very much on the nonconservative side. This confirmed the now generally accepted fact that valid fatigue life prediction models must account for the sequence of individual peaks and troughs.

KEY WORDS: random fatigue, automobile engineering, notched specimens, reversed bending, aluminum, steel, random load sequence, statistical load analysis, service tests, service duplication tests, program tests, random fatigue life curves, cumulative damage, fatigue life prediction, fatigue tests

[1]Professor, former director of the Laboratorium für Betriebsfestigkeit, Forschungsinstitut der Fraunhofer-Gesellschaft (LBF), Darmstadt, Germany.

[2]Research engineer, head of the Department for Fatigue Analysis of Structures and Components, Laboratorium für Betriebsfestigkeit, Forschungsinstitut der Fraunhofer-Gesellschaft (LBF), Darmstadt, Germany.

Nomenclature

H	Cumulative frequency
H_0	Frequency of mean crossings with positive slope for a defined block size (sequence length)
H_p	Number of all incremental stress peaks above and below the mean stress S_m
I	H_0/H_p, irregularity factor
k, $\bar{k}$	Exponent of the S_a/N curve or $\overline{S}_z/N_0$ curve respectively
n	Number of tests
N	Number of cycles to failure, constant amplitude loading
N_0	Number of mean crossings with positive slope to failure, random loading and program loading
R	Stress ratio for constant amplitude tests, S_{min}/S_{max}
$\overline{R}$	Stress ratio for random and program tests, $\overline{S}_{min}/\overline{S}_{max}$
$\overline{S}/N_0$ curve	Random fatigue life curve for random loading, and program-loading respectively
S_a (N/mm^2)	Nominal stress amplitude, constant amplitude loading
S_e (N/mm^2)	Endurance limit of the S/N curve
S_m (N/mm^2)	Mean stress
S_z (N/mm^2)	Maximum nominal incremental stress of the cumulative frequency distribution, occuring once within the return period, random-and program-loading, respectively
W (mm)	Displacement of the rear car wheel

The specific aim of the present study which is to provide a correlation between service tests and service duplication tests, justifies adherence to the usual nominal stress concept. Service tests are road tests in which the road induced loading is applied directly to the specimens; service duplication tests are laboratory tests for which the loading is obtained from prior recording of field loading. However, the results appear to be applicable also for checking life predictions based on the local strain concept [*1-3*][3] the use of which has become more general in the past few years.

The study began quite some time ago when the Palmgren-Miner rule was still held in high esteem, and load spectrum testing had to be carried out without the aid of modern servohydraulic equipment. At this time it was considered of great importance to prove the validity of cumulative damage hypotheses. Thereby, all methods had to be excluded which, by more or less arbitrary simplifications, modified the sequence of actual service loads. A different approach based on results of actual field loading was considered here to be more useful for achieving generalizable statements.

In studies extending well over 10 years concerning mainly a steel, 41 Cr

[3]The italic numbers in brackets refer to the list of references appended to this paper.

4 (SAE 5140), and an aluminum alloy, AlCuMg 2 (2024 T 3), statistically defined lives were obtained for specimens with notches representative of components ($K_t = 2.14$) subjected to actual field load spectra. These notched specimens were fitted to a special multispecimen testing device which, after placement in the trunk of a car is actuated by the vertical displacements of a rear wheel. Thus, the specimens receive true field loading (Fig. 1). Some road tests of this type, also known as service tests, are described in Refs *4-6*. These tests offer a reliable basis for comparisons with laboratory tests that simulate field loading in various ways, for example the service duplication test and the program test *7-11*. For the validity of such a comparison, one of the most important requirements is that, in simulating field loading, the more important statistical characteristics in these two types of test do not differ from those measured in the field; these statistical characteristics mainly refer to frequencies of exceedances of certain load levels and to the probability of occurrence of the maximum load [*12*]. In the service duplication tests the sequence of individual peaks and troughs is of course the same as in the road test.

The determination of the characteristics of the field loading required for comparing the three types of test (service test, service duplication, program fatigue test) are described and the test results obtained are discussed as follows.

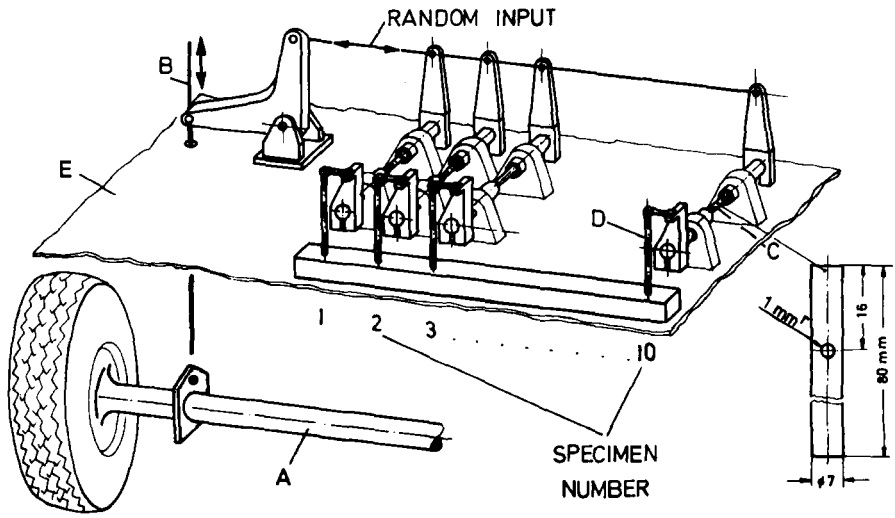

A—Rear car axle.
B—Connecting rod to statistical counter.
C—Torque rod.
D—Test specimen.
E—Car body.

FIG. 1—*Mode of operation of multiple testing device, installed in a Volkswagen.*

Determination of Field Loading in Road Tests

Counting Level Crossing Frequencies

By means of a statistical counter operating simultaneously with a multi-testing specimen device installed in the vehicle, it was possible to ascertain the number of level-crossings to fracture for each of the specimens tested. The final result of counting covering about 93 000 km for the notched specimens of 41 Cr 4, and about 71 000 km for those of AlCuMg 2 are shown in Fig. 2. The two results are in very good agreement both as to the straightline character of the frequency distribution (log-linear) and as to the distance traveled when converted to the same number of mean-crossings H_0.

These "long-time measurements," considered to be most realistic, confirm that it was correct to expect log-linear frequency distribution of level crossings from "short-time-measurements" [*13*]; although this type of distribution has been found to be valid also in other areas of engi-

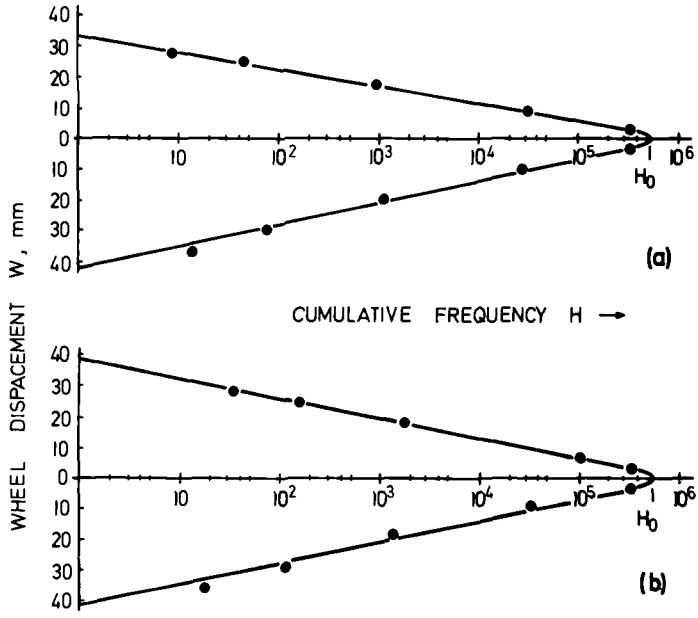

(*a*) Road test of 93 400 km duration, material of specimen 41 Cr 4, —converted to $H_0 = 6 \times 10^5$ mean crossings, equivalent to 2 800 km.
(*b*) Road test of 70 700 km duration, material of specimen AlCuMg 2, —converted to $H_0 = 6 \times 10^5$ mean crossings, equivalent to 2 900 km.

FIG. 2—*Cumulative frequency distributions of wheel displacements, determined by level-crossing counting.*

neering, for example, aircraft design and shipbuilding, results of random tests such as the ones presented here are of more general significance.

Continuous Recording of Displacement/Time History

For carrying out service duplication tests by means of servohydraulic equipment using the same multiple testing device that is used for the road tests, a command signal (magnetic tape) is necessary which duplicates faithfully all service loads in magnitude and sequence. The first recordings were made over 1000 km of secondary roads only. Comparing the distributions of ten arbitrarily chosen test runs with the resulting distribution of 93 000 km (Fig. 3), we see in both cases straight line distributions that, with reference to the ratio of minimum and maximum displacement, for $H = 1$, differ so little that the result obtained from 1000 km must be considered a valid indication of the overall result. Sample of traces from the road recordings are shown in Fig. 4.

In fact, tape recording was extended to cover 1550 km and its evalua-

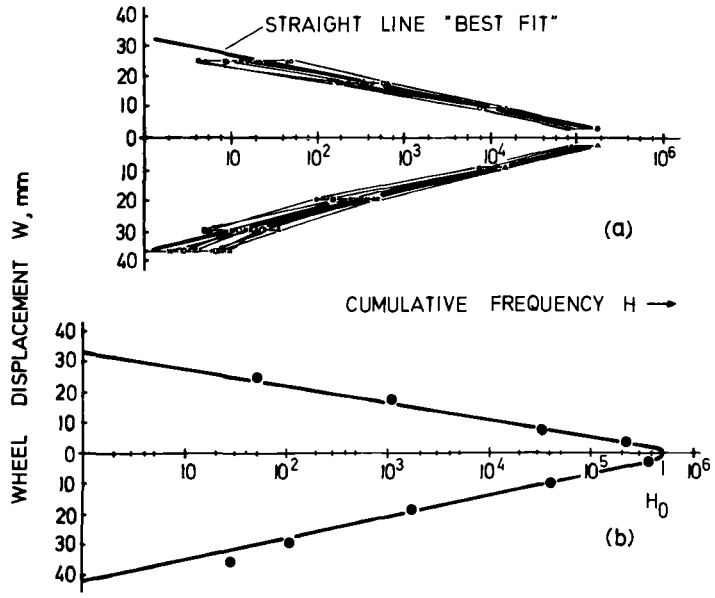

(*a*) Scatter of exceedances H from ten road tests, each of 1000 km run.
(*b*) Frequency distribution from magnetic tape recording of 1550 km run, with $H_0 = 2.41 \times 10^5$ mean crossings used for converting mean crossings N_0 to kilometres in Figs. 6 and 7.
—converted to $H_0 = 5 \times 10^5$ mean crossings, equivalent to 3 880 km.

FIG. 3—*Cumulative frequency distributions of displacements from shorter road runs, determined by level-crossing-counting.*

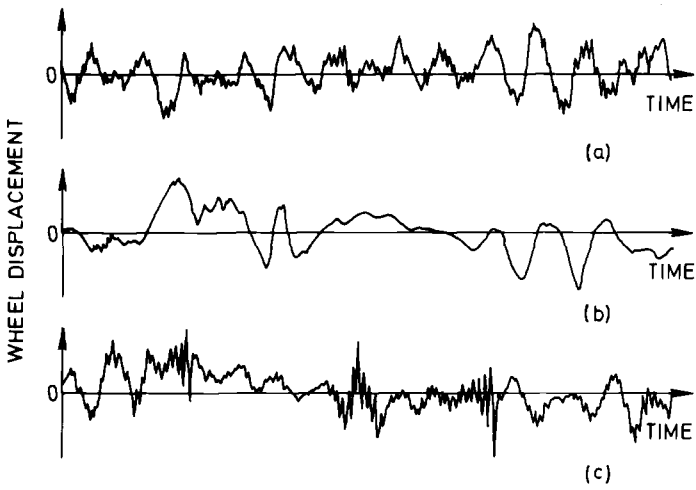

(*a*) Road roughness. (*c*) Maneuvers and road roughness.
(*b*) Maneuvering.

FIG. 4—*Sample traces of random displacements from road recording.*

tion is shown in Fig. 3*b*; for comparison, the number of level-crossings counted during the test runs are plotted in the figure.

With reference to the frequency distributions shown in Fig. 2 which have the same number of mean-crossings, $H_0 = 6 \cdot 10^5$, it should be noted that by extrapolating the straight line to $H = 1$, the resulting value of displacement accounts for the extreme value $\overline{S}$ contained in the tape recordings. A detailed analysis of the records is given by Buxbaum [*14*].

The small difference between the maximum displacement for $H = 1$ in Fig. 2*b* and that of Fig. 2*a* is taken into account in evaluating the result from the service test (road test).

For a complete assessment of the load/time history, to be used as a command value input for service duplication tests, the Appendix contains the result of counts according to the level crossing, range-pair and peak between mean methods (see Fig. 5). The small differences between the results of the three counting methods may be explained by the fact that vertical loads dominate over maneuver loads.

Thus, for the first time in the history of random loading simulation, the requirements for unrestricted comparability of fatigue lives are given as they are obtained under field conditions in service duplication tests and others.

Test Results

For more information regarding the material and properties, the shape

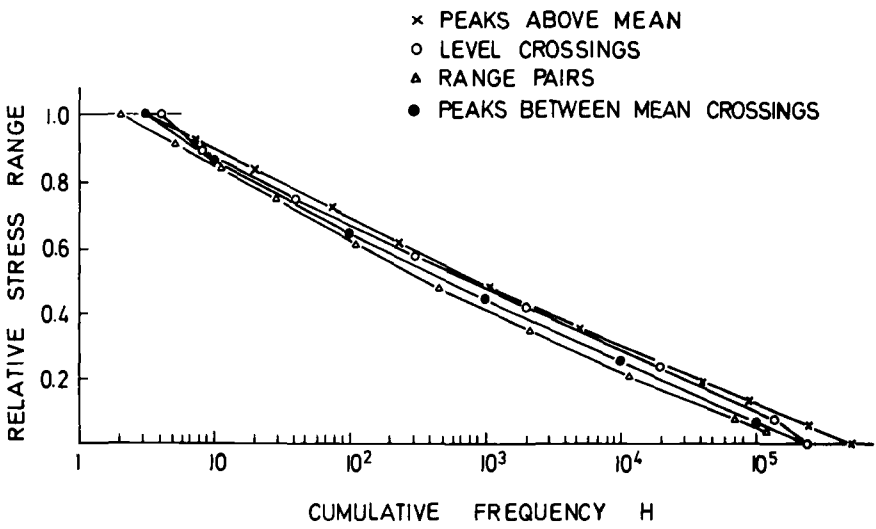

FIG. 5—*Analysis of the random load time history, using four counting methods.*

and dimensions of the test specimens, the details of the test series and the test equipment, the reader is referred to the Appendix.

Constant Amplitude Tests, Series A

Tests were carried out for the two materials under constant nominal stress amplitudes (S_a/N tests) at $R = -1$. These tests were made for comparative purposes and to serve as a basis for cumulative damage calculations. Log/mean S_a/N - curves[4] were determined by testing at least ten specimens at several stress levels (see Table 1). The exponent k for the finite life range was found to be 5.8 for 41 Cr 4, and 6.2 for AlCuMg 2.

Service Tests, Series E_1

After having calibrated displacements in terms of the maximum nominal incremental stress $\overline{S_z}$, random fatigue life curves $\overline{S_z}$ (N_0)[5] were determined by road tests. These serve as a basis for the assessment of the results of other test series, particularly of the directly comparable service duplication tests. N_0 refers to the failure number of mean-crossings with positive slope.

The most extensive documentation was obtained by the random fatigue tests under reversed bending ($\overline{R} = -1$) for the material 41 Cr 4. A statistical evaluation of results at five stress levels between $N_0 = 10^6$ and $N_0 = 10^7$ mean crossings yielded for the log-mean values a straight line with a slope

[4] $N = 5 \cdot 10^4 \, (S_a/S_{a,\,5 \cdot 10^4})^k$

[5] $N_0 = 10^6 (\overline{S}_z/\overline{S}_{z,10^6})^k$ [9].

TABLE 1—*Series A, original* S_a/N *data for fatigue test with notched specimens,* $K_t = 2.15$ *and* $R = -1$.

Material 41 Cr 4	Material AlCuMg 2		
Stress Amplitude, S_a (N/mm^2)	Stress Amplitude, S_a (N/mm^2)	Number tested	Number of cycles, N, P_s = 50 percent
480	208	10	10^4
300	124	10	10^5
215	86	10	5×10^5
S_e 190	S_e 86	10	$\approx 2 \times 10^6$

of $\bar{k} = 4.5$ (Fig. 6) and Ref *9*. The same applies to the specimen AlCuMg 2, again with $\bar{k} = 4.5$ (Fig. 7).

Service Duplication Tests, Series E_2

For the materials 41 Cr 4 and AlCuMg 2 individual test results of service duplication tests also are plotted in Figs. 6 and 7. These results lie together with those of the service tests in the shaded range. With the exception of only one stress level, there is no difference between the results of the service tests and the service duplication tests.

Whether there is any significance in the distinct tendency of both materials toward a lesser slope in Series E_2 cannot as yet be stated, especially as there are no comparable test results in the literature. The following reasons for the change in slope are conceivable:

1. The frequent recurring loading pattern of the service duplication test (stored on magnetic tape having a block size of $H_0 = 2.41 \cdot 10^5$) while the service test is free of repetitions.

2. Corrosion effect as a result of the considerably longer time required for service tests under environmental conditions.

Considering that service duplication tests lead to practically the same results as service tests (although the latter require a much greater effort), the service duplication tests only were supplemented by tests for $\bar{R} = 0$. The results for both materials confirm the fact known from program tests (see section on eight-step program tests, Series B) that, for the same number of mean-crossings to failure N_0, the corresponding incremental stresses to failure $\bar{S}_{zn}$ are considerably lower than for $\bar{R} = -1$, and that the exponents $\bar{k}$ of the random fatigue life curves are reduced noticeably.

With regard to service duplication tests, it is worth mentioning that results of a recently completed test series throw some light on the much discussed problem of the admissibility of simplifications for complex load-time histories. In one case, the problem is clarified by means of a computer based model of life prediction [*15*], in another by a method first used by Naumann [*16*].

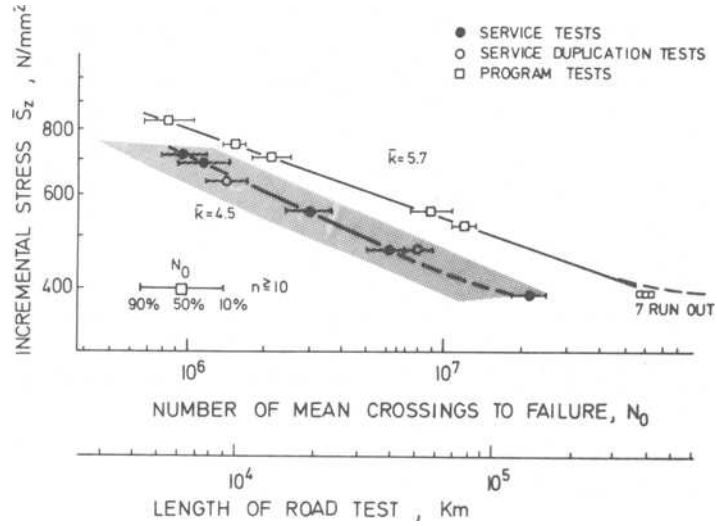

FIG. 6—*Fatigue life curves for material 41 Cr 4,* $K_t = 2.15$, $\bar{R} = -1$, *plane bending.*

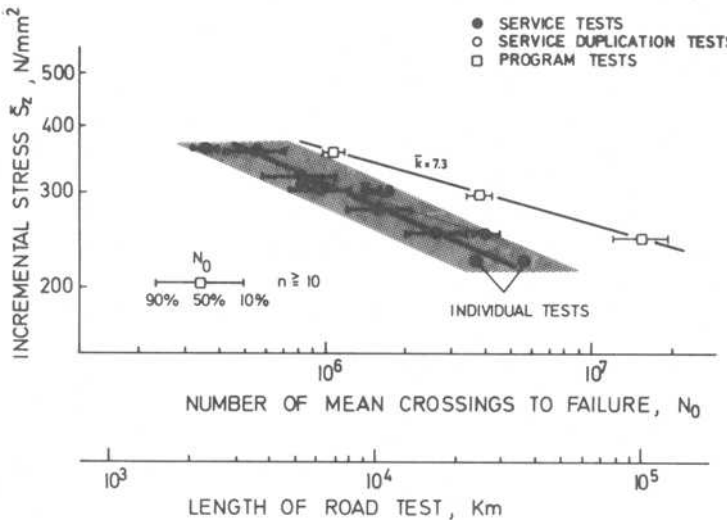

FIG. 7—*Fatigue life curves for material AlCuMg 2,* $K_t = 2.15$, $\bar{R} = -1$, *plane bending.*

The latter refers to the strict maintenance of the sequence, while retaining only those peaks that lie between consecutive mean-crossings only; in other words, the load/time history is devoid of superimposed vibrations.

In these tests, there was an insignificant increase in the number of mean-crossings to failure by 5 percent with reference to mean values. Moreover, with the same tape length as in Series E_1, testing time was reduced to one fifth because of the superior frequency response of the servohydraulic

testing machine. Thus, for verifying a life of 80 000 km, only about 2.5 weeks were necessary.

In looking for a relationship between life under constant amplitude loading and that under random loading in terms of a fatigue life ratio V, experience shows [*17*] that it is convenient to choose a stress level S_a which will result in $N = 5 \times 10^4$ ($P_s = 50$ percent) cycles to failure. The fatigue life ratios

$$V = \frac{N_0}{N}(S_{a,\,5 \times 10^4} = \overline{S}_z)$$

are 320 for 41 Cr 4 and 810 for AlCuMg 2, respectively.

Comparing these fatigue life ratios with those for 15 other materials obtained under comparable conditions, it will be found that they lie in a scatter range between 320 and 1700. Contrary to Bussa, Sheth, and Swanson [*18*], there does not seem to be any possibility of an unambiguous correlation between groups of materials, stress concentration factors, stress ratios and loading conditions so that, at present, constant amplitude tests do not provide a reliable means for predicting fatigue behavior under random loading.

Programmed Random Tests, Series E_3

From relevant literature [*19*] it is known that the occurrence of a log-linear frequency distribution of level-crossings can be explained as a synthesis of individual Gaussian distributions of different sizes and intensities. Therefore, it should also be possible to subdivide the frequency distribution used in the present study into five Gaussian distributions and store them on magnetic tape in increasing/decreasing groupings as control for programmed random load tests. This was to be used for controlling the special random tests of Series E_3, (see Fig. 8*c*, and Table 2. The ten check tests, carried out on notched specimen of material 41 Cr 4, yielded lives significantly longer than those from service tests and service duplication tests. This is probably due to the interference with the sequence of field loading by the inherent order in the five loading groups.

Therefore, when synthesizing load/time histories having log-linear frequency distributions of level-crossings, it is apparently better to proceed in the way described by Swanson and Jaeckel [*20*], who randomized root mean square (rms) sequences.

Eight-Step Program Tests, Series B

Results from conventional eight-step program tests (Gassner, programmed constant amplitude tests, see Fig. 8 and Table 3) [*8,9*] are plotted for both materials in Fig. 6 and 7 for direct comparison with fatigue life curves obtained from service duplication tests.

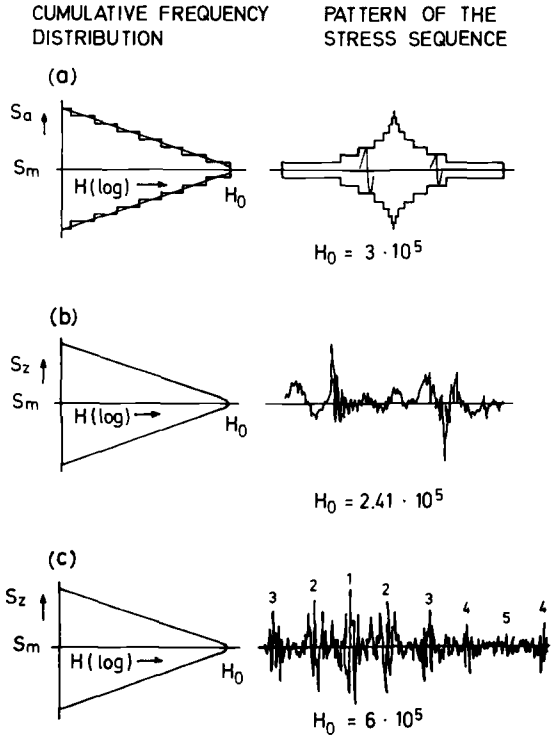

(*a*) Eight-step program test with $H_0 = 3 \times 10^5$.
(*b*) Service test, service duplication test with $H_0 = 2.41 \times 10^5$.
(*c*) Random test having five repeatedly occurring load groupings of different intensities and sizes with $H_0 = 6 \times 10^5$.

FIG. 8—*Data pertaining to test series.*

For both materials, the simulation of field loading through program tests leads to a higher number of mean-crossings to failure N_0 than is the case with either the service tests or the service duplication tests. This applies to the log-linear frequency distribution to which the present tests refer. The difference in lives N_0 increases considerably with decreasing incremental stresses $\overline{S_z}$. However, there is no change in the linearity of the fatigue life curve in its upper region which, for material 41 Cr 4, has here an exponent of $\overline{k} = 5.7$, and for material AlCuMg 2 an exponent of $\overline{k} = 7.3$.

The preceding statement concerning different $\overline{k}$ - values for program testing the two materials at $\overline{R} = -1$ applies also to the stress ratio $\overline{R} = 0$. The tendency towards decrease of the exponent $\overline{k}$ in the transition from $\overline{R} = -1$ to $\overline{R} = 0$ is observed in both the service duplication test and the program test; this tendency is marked particularly with the material AlCuMg 2.

TABLE 2—*Series* E_3, *parameters* $\bar{S}_{zi}/\bar{S}_{zl}$ *and* $H_{0,i}$ *of the five intervals of a programmed random signal with* $H_0 = 6 \times 10^5$.

Step i	$\bar{S}_{zi}/\bar{S}_{zl}$	$H_{0,i}$	Remarks
3	0.645	50 000	
2	0.845	9 000	
1	1.000	1 000	
2	0.845	9 000	block size
3	0.645	50 000	$H_0 = 6 \times 10^5$
4	0.410	150 000	
5	0.260	181 000	
4	0.410	150 000	

TABLE 3—*Series B, parameters* $S_{zi}/\bar{S}_z$ *and* h_i *of the eight-step program test with* $H_0 = 3 \times 10^5$.

Step i	$S_{zi}/\bar{S}_z$	h_i	Remarks
4	0.625	87	
3	0.750	15	
2	0.875	3	
1	1.000	1	
2	0.875	3	
3	0.750	15	
4	0.625	87	block size
5	0.500	487	$H_0 = 3 \times 10^5$
6	0.375	2 732	
7	0.250	15 425	
8	0.125	262 500	
7	0.250	15 425	
6	0.375	2 732	
5	0.500	487	

In comparing the results of the program test with those of service duplication test for equal incremental stress $\bar{S}_z$ we see that the life under service duplication is shorter, as was the case in Series E_3. This must be due to the very considerable modifications in the sequence of the field loads (Fig. 8). Therefore, a suggestion made by Lipp [*21*] for better mixing of test loads may be worth following.

Regarding recent investigations, the fact that both sets of laboratory tests (service duplication and program tests, see Fig. 6 and 7) tend to about the same slope ($\bar{k}$) cannot be generalized.

Fatigue Life Prediction

An assessment of the fatigue life to be expected from service tests can be calculated by using Haibachs' modified linear cumulative damage hypothesis [*22*].

Because the endurance limit and the residual static strength continuously

decrease as random fatigue increases Haibach applies a modified $\overline{S_a}/N$ curve. His exponent will change at the "knee" of the $\overline{S_a}/N$ curve from k to $2k-1$.

For notched specimens of 41 Cr 4 in the range between $N_0 = 10^6$ and 10^7, this life is the sixfold and twelvefold value of the test results respectively; for the alloy AlCuMg 2 the calculated life is the four-fold to six-fold of the test results. By no means do these values represent isolated results; with other random loading tests they lie within the limits 2 to 100 that is, always on the nonconservative side, and thus they are even more unreliable than program test results (see Fig. 9). According to Gassner, Lowak, and Schütz [*23*], these calculated results, which are based as usual on the frequency distribution of level-crossings, cannot be much improved by using the frequency distribution of range-pair counts (see Fig. 5), as both methods take no account of sequence effects. The program test, like any other test that neglects sequence effects, is thus unsuitable for checking the validity of cumulative damage hypotheses.

For reasons of completeness, a most remarkable result of a supplementary investigation shall be mentioned. In Fig. 10 the fatigue life obtained

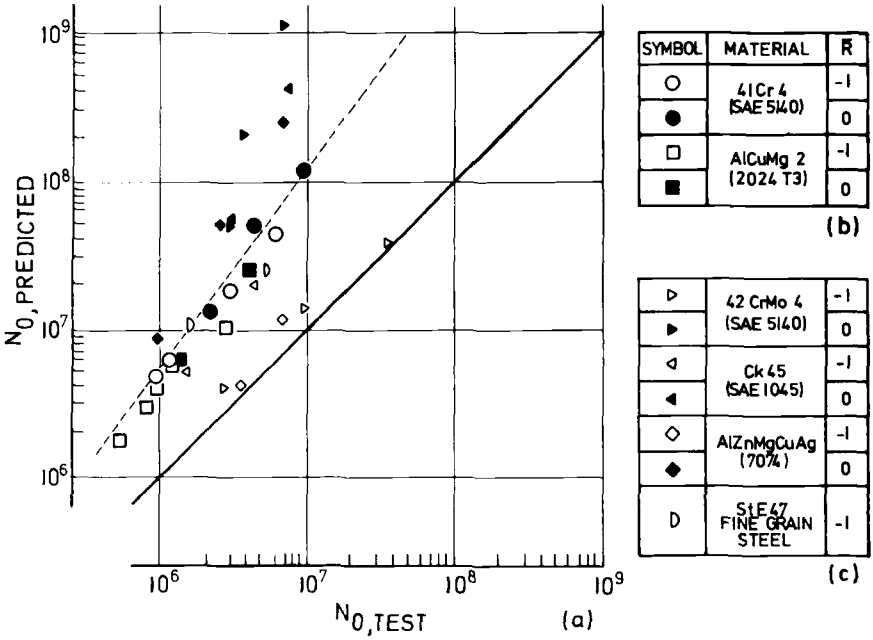

(*a*) Life predictions.
(*b*) Results from present study.
(*c*) Results from applicable LBF data.

FIG. 9—*Results of life prediction by using the modified linear cumulative damage hypothesis* [22].

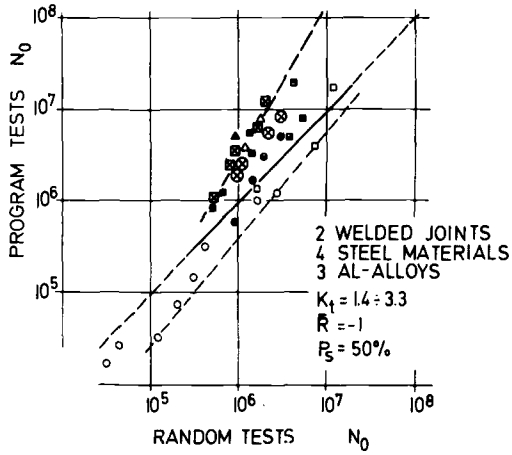

FIG. 10—*Effect of load sequence on fatigue life.*

in program test versus the random fatigue life is shown for various other materials and stress ratios $\bar{R} = -1$.

The results of the present study are marked especially (⊠, ⊗). With these tests it could be proved that the sequence effect is the most severe one because in the relevant test series no other statistical parameters have been varied. With both testing procedures the irregularity factor ($I = 1$) and the level crossing distributions are the same (Gaussian).

Summary

The more important results of this study can be summarized as follows:

1. Random fatigue life curves obtained by service tests (road tests), expressing the relation between maximum incremental stress $\bar{S}_z$ and the number of mean-crossings to failure N_0, do not differ significantly from those obtained by service duplication tests (laboratory tests) when paying due regard to scatter in fatigue. This statement applies to notched specimens of 41 Cr 4 and of AlCuMg 2 for a stress ratio of $\bar{R} = -1$ if subjected to random loading with a log linear frequency distribution of level crossings.

2. There appears to be a tendency toward shorter fatigue lives from service tests as opposed to service duplication tests, which may be explained by corrosion being effective in the service tests for higher values of N_0. While road testing took several years to complete under changing environmental conditions, laboratory testing could be carried out without interruption and under constant test conditions.

3. The program test, although being the most frequently used type of simulation of field loading histories, leads to an extraordinarily high overestimate of fatigue life, particularly so when the number of mean

crossings N_0 is greater than 10^7, as should be expected for automotive components.

4. Most probably, a more thorough mixing of loads in the program test could achieve better approximation to the results of the road test. Recommendations regarding a modified version of the program test will only be possible if investigations show that the effect observed occurs also in the region of mean-crossings $N_0 > 10^7$ and that it is material-independent.

5. With the availability of service test results, it is possible for the first time to make comparisons with estimated lives using cumulative damage hypotheses, especially in the region of lives encountered in the field ($N_0 > 10^7$). The estimates obtained by using the modified cumulative damage hypothesis [*22*] are so far on the nonconservative side that their application to predicting the lives of components subject to random loading of the type considered here is no longer justified. It is recommended that new prediction methods be checked based on the local strain concept by using the results of this study and also to attempt to prove or disprove their sensitivity to sequence effects if such effects are present in program tests.

Acknowledgment

We wish to express our gratitude to V. Dietz for his most helpful technical assistance, especially in performing service duplication tests, program tests, and S_a/N tests.

APPENDIX

Frequency Distributions

The stress/time history, recorded on magnetic tape and used for controlling the service duplication tests, leads to frequency distributions shown in Fig. 5 when using level crossings, range pairs, peaks, and peaks between mean crossings as counting methods.

Inspite of the low value of the irregularity factor $H_0/H_p = 0.3$ the distributions resulting from the use of the preceding counting methods differ only slightly from each other. Thus, the existing differences between the results of service duplication tests and of program tests are primarily due to sequence effects.

Specimen

The requirement that a multiple testing device be place into and operated by a passenger car necessitates relatively small specimen dimensions. The round specimen has a circular notch. Its stress concentration factor $K_t = 2.15$ (according to Peterson) is representative for an automobile component; specimen diameter $D = 7$ mm, notch diameter $d = 1$ mm.

Materials

To assess the effect of random loading on different materials by service tests and service duplication tests, two materials have been chosen; the heat-treated steel 41 Cr 4 and the aluminum alloy AlCuMg 2.

Steel 41 Cr 4 (Material No. 1.7035, Similar to SAE 5140)

(*a*) Tensile strength $S_u = 901$ N/mm^2, 0.2 percent proof stress $S_y = 795$ N/mm^2.

(*b*) Chemical composition: carbon-0.42, silicon-0.28, manganese-0.66, phosphorus-0.27, sulfur-0.016, and chromium-0.99.

(*c*) The wire, rolled to 13 mm in diameter was oil-hardened at 840° C, and annealed at 580° C for 4 h.

(*d*) After having been drawn to 12 mm in diameter, it was stretched, and stress-relieved at 500° C for 4 h.

Aluminium Alloy AlCuMg 2 (Similar to 2024 T 3)

(*a*) Tensile strength $S_u = 450$ to 475 N/mm^2, 0.2 percent proof stress $S_y = 415$ to 435 N/mm^2.

(*b*) Semifinished material: round stock 8.5 mm in diameter.

Testing Device

In order to obtain statistically based results, a test fixture was employed capable of the simultaneous loading of ten specimen. This fixture was used in the car for service tests as well as in the laboratory for service duplication tests and programmed fatigue tests.

Characterization of Test Series

Series E and B have the same log-linear frequency distribution (based on level-crossing exceedances). The individual test series are distinguished by the type of simulation involved.

Series A

Tests with constant nominal stress amplitudes (S_a/N tests), frequency of cycles $N/\text{s} = 20$.

Series B

Conventional eight-step program tests having a block size of $H_0 = 3 \times 10^5$ mean crossings as given in Fig. 8 (*a*) and Table 2. The simplification of the program test consists of bringing order into random loading with respect to the frequency distribution of incremental stresses. Frequency of mean crossings $N_0/\text{s} = 20$: testing time for 5×10^5 mean crossings = 7.5 h.

Series E_1

Represents a service test with no periodic repetitions. A typical wave trace is shown in Fig. 8 *b*. Mean crossings $N_0/\text{s} = 2.7$.

Series E_2

Represents a service duplication test with periodicity. The block size corresponds to the length of the magnetic tape ($H_0 = 2.41 \times 10^5$ mean crossings, see Fig. 8 *b*). Mean crossings $N_{0S} = 2.7$. Testing time for 5×10^5 mean crossings = 52 h.

Series E_3

Represents the simulation of a straight-line distribution by a rising/falling sequence of five individual random load groups. The groups have different intensity and typify Gaussian processes. A wave trace is shown in Fig. 8 *c*. The five load groupings are characterized by S_{zi} and H_i, given in Table 2. The block size corresponds to the length of the magnetic tape ($H_0 = 6 \times 10^5$ mean crossings). Mean crossings $N_{0S} = 12.6$. Testing time for 5×10^5 mean crossings = 11 h.

References

[1] Wetzel, R. M., "A Method of Fatigue Damage Analysis," Ph.D. Thesis, University of Waterloo, Ontario, Canada, 1971.

[2] Landgraf, R. W., Richards, F. D., and LaPointe, N. R., "Fatigue Life Predictions for a Notched Member Under Complex Load Histories," *Paper No. 750040*, Society of Automotive Engineers, 1975.

[3] Dowling, N. E., *Journal of Materials*, Vol. 7, No. 1, March 1972, pp. 71-87.

[4] Gassner, E. and Lipp, W., "Wirklichkeitsgetreue Lebensdauerfunktion für Fahrzeugbauteile," in *Beispiele Angewandter Forschung*, Jahrbuch der Fraunhofer-Gesellschaft, München, 1963, pp. 63-69.

[5] Gassner, E., "Zur experimentellen Lebensdauerermittlung von Konstruktionselementen mit zufallsartigen Beanspruchungen," *Materialprüfung* 15, Nr. 6, 1973, pp. 197-205.

[6] Gassner, E., Lipp, W., and Dietz, V., "Schwingfestigkeitsverhalten von Bauteilen im Betrieb und im Betriebslasten-Nachfahrversuch," Technische Mitteilung des Laboratoriums für Betriebsfestigkeit, Darmstadt, TM 76/76.

[7] Gassner, E., "Festigkeitsversuche mit wiederholter Beanspruchung im Flugzeugbau," *Luftwissen*, Bd. 6, Nr. 2, 1939, pp. 61-64; English Translation: "Strength Investigations in Aircraft Construction Under Repeated Application of the Load," *Technical Memo 1087*, National Advisory Committee for Aeronautics, 1946.

[8] Gassner, E. in *Fatigue in Aircraft Structures*, A. M. Freudenthal, ed., Academic Press, New York, 1956, pp. 178-206.

[9] Gassner, E. in *Proceedings*, International Conference on Fatigue of Metals, Institution of Mechanical Engineers, ed., London, 1956, pp. 304-309.

[10] Gassner, E. and Schütz, W. in *Proceedings*, 9th International Automobile Technical Congress, G. Eley, ed., The Institution of Mechanical Engineers, London, 1962, pp. 195-205.

[11] Gassner, E. and Schütz, W. in *Full Scale Fatigue Testing of Aircraft Structures; Proceedings*, ICAF-Symposium, Amsterdam, F. J. Plantema and J. Schijve, eds., Pergamon Press, Oxford, London, New York, Paris, 1961, pp. 14-40.

[12] Buxbaum, O. and Svenson, O., "Zur Beschreibung von Betriebsbeanspruchungen mit Hilfe statistischer Kenngrössen," *ATZ 75*, No. 6, 1973, pp. 208-215.

[13] Svenson, O., "Beanspruchungskollektiv und Betriebsfestigkeit als Bemessungsgrundlage für schwingbruchsichere Konstruktionen," *Rheinstahl-Technik 10*, No. 1, 1972, pp. 7-12.

[14] Buxbaum, O., "Beschreibung einer im Fahrbetrieb gemessenen Beanspruchungs-Zeit-Funktion mit Hilfe der spektralen Leistungsdichte," *Bericht des Laboratoriums für Betriebsfestigkeit*, Darmstadt, No. TB-102, 1972.

[15] Haibach, E. and Lehrke, H. P., "Das Verfahren der Amplituden-Transformation zur Lebensdauerberechnung bei Schwingbeanspruchungen," *Archiv Eisenhüttenwesen 47*, No. 10, 1976.

[16] Naumann, E. C., "Fatigue Under Random and Programmed Loads," *Technical Note D-2629,* National Aeronautics and Space Administration.

[17] Gassner, E., "Betriebsfestigkeit," in *Lueger Lexikon der Technik, Band Fahrzeugtechnik,* Deutsche Verlagsanstalt, Stuttgart.

[18] Bussa, St. L., Sheth, N. J., and Swanson, S. R., *Materials Research and Standards,* Vol. 12, No. 3, 1972, pp. 31-42.

[19] Press, H., Meadows, M., and Hadlock, K., "A Reevaluation of Data on Atmospheric Turbulence and Airplane Gust Loads for Application in Spectral Calculations," *Report No. 1272,* National Advisory Committee for Aeronautics, 1965.

[20] Jaeckel, H. R. and Swanson, S. R., *SAE Journal,* Society of Automotive Engineers, Vol. 77, No. 11, Nov. 1969, pp. 42-47.

[21] Lipp, W., "Zuverlässigere Lebensdauerangaben durch bessere Vermischung der Lasten im 8-Stufen-Programmversuch," *Materialprüfung 12,* No. 11, 1970, pp. 381-382.

[22] Haibach, E., "Modifizierte lineare Schadensakkumulations-Hypothese zur Berücksichtigung des Dauerfestigkeitsabfalls mit fortschreitender Schädigung," *Technische Mitteilung des Laboratoriums für Betriebsfestigkeit,* Darmstadt, TM 50/70.

[23] Gassner, E., Lowak, H., and Schütz, D., "Bedeutung der Unregelmässigkeit Gauss'scher Zufallsfolgen für die Betriebsfestigkeit," *Bericht des Laboratoriums für Betriebsfestigkeit,* Darmstadt, No. FB-124, 1976.

L. L. Jeans[1] *and W. L. Tribble*[1]

Test Simulation of Fighter Aircraft Maneuver Load Spectra

REFERENCE: Jeans, L. L. and Tribble, W. L., **"Test Simulation of Fighter Aircraft Maneuver Load Spectra,"** *Service Fatigue Loads Monitoring, Simulation, and Analysis, ASTM STP 671*, P. R. Abelkis and J. M. Potter, Eds., American Society for Testing and Materials, 1979, pp. 240-254.

ABSTRACT: This paper studies the use of power spectral density (PSD) and related random data analysis techniques in the test laboratory to characterize low frequency loading spectra output response, measured from a specimen, for the purpose of comparing test machine responses. In recent years digital techniques have been developed that simulate aircraft maneuver spectrum loading in the time domain. In this study one of these techniques is used to generate the input load spectrum signal to an electrohydraulic closed-loop test machine for fatigue testing of graphite/epoxy to titanium step lap bonded joints at various frequencies and PSD shapes. The output signal was measured directly from the specimen by recording on tape the dynamic strain gage signal. This signal then was processed to determine the PSD response and root mean square (RMS) time history. These data were compared with the recorded strain amplitude time history and the input load amplitude, frequency, and PSD information. A qualitative correlation was found between variations in specimen fatigue life, output signal waveform and amplitude, and variations in PSD. PSD is a measure of loading energy in the time domain and can be influenced both by load amplitude and waveform variations. Thus, the way a fatigue test machine processes an input load and frequency signal can affect the measured fatigue life of certain materials.

KEY WORDS: fatigue tests, composite materials, power spectral density, random data analysis, load spectrum

Random data analysis techniques have become fairly standard tools in aircraft analysis and testing. Many events that characterize an airplane's operational environment are nondeterministic, random phenomena best described by probabilistic statistical models. Aircraft gust and taxi loads are examples of such events which are time-variant and random in nature and are characterized routinely by such statistical functions as probability density or power spectral density. These loading types are generally high frequency (>1 Hz) and as such are important in structural dynamic response studies.

[1]Manager, Structural Life Assurance Research, and senior test engineer, respectively, Northrop Corp., Hawthorne, Calif. 90250.

Structural fatigue analysts have not been concerned greatly in the past with loading spectrum cyclic frequency content, and test frequencies usually were selected for convenience. However, the increased use of materials suspected of being cyclic frequency sensitive, such as advanced composite materials or adhesively bonded metallic material, has placed a greater importance on defining the cyclic frequency even for such low frequency loading as that associated with fighter aircraft maneuvers. In recent years digital techniques have been developed and employed in the test laboratory that simulate aircraft fatigue spectrum loading in the time domain [*1-3*].[2] These techniques approximate spectrum frequency content by nonlinear transformations involving representative spectral densities and cyclic loading spectra. Resulting load amplitude and cyclic frequency data then can be formulated on magnetic tape to produce the proper load amplitude and frequency content input signal to the fatigue test machine.

The accuracy with which an electrohydraulic closed-loop test machine processes an input load and frequency signal is important in measuring the effect various input spectrum loading parameters have on specimen fatigue life. Variations in calibration and the effectiveness of the test hardware and software supporting systems can produce small variations in output load frequency, waveform, and stress amplitude, making comparisons of fatigue data from one test machine to another difficult if the specimens are sensitive to these variations. However, identifying subtle differences in these sensitive parameters is not straightforward in the case of complex loading and frequency testing. The most commonly used technique is to examine visually digital or analog data recorded on paper tape to assess the output load signal accuracy. This is both laborious and limited in the amount of data that can be collected and examined in a reasonable time. Also, the increasing trend toward multispecimen fatigue testing in parallel banks of test machines has accelerated the need for more rapid and efficient means of evaluating and comparing test machine output response.

One approach, of course, is to utilize the random data statistical analysis procedures commonly used in acoustic loading, dynamic response, and gust loading studies. The study described here uses these spectral density and related random data signal analysis techniques in the test laboratory to characterize low frequency loading spectra output response, measured from a specimen, for the purpose of comparison with digital input spectra and with different test machine responses. Where fatigue tests corresponding to the measured output response have been completed, test data comparisons are made with trends suggested by the output signal analysis. This study is part of a larger program at Northrop to investigate fatigue spectrum sensitivity of advanced composite materials under an Air Force contract [*4*].

[2]The italic numbers in brackets refer to the list of references appended to this paper.

Random Spectrum Methodology

The digital load factor spectrum used in this investigation was generated by a computer program that simulates real-time loading spectrum cyclic frequency by one-dimensional narrowband frequency distributions (bandwidth limited white noise) and mission segment load exceedence data and mission profile data [*1*]. The "real-time" load factor spectral output from this program served as input to another program that converts the load factor amplitudes to stress or specimen load amplitudes based on transfer functions similar to the one shown in Fig. 1 for air-to-air combat [*2*]. The resulting cumulative stress spectrum is shown in Fig. 2. A segment of a typical flight-by-flight time history is shown in Fig. 3.

The spectrum severity was established by setting the maximum spectrum load at 70 percent of the specimen "B basis" static strength. In this case, the specimen stresses (or strains) at the peak spectrum load are approximately 5 percent greater than the so called "design limit" stress.

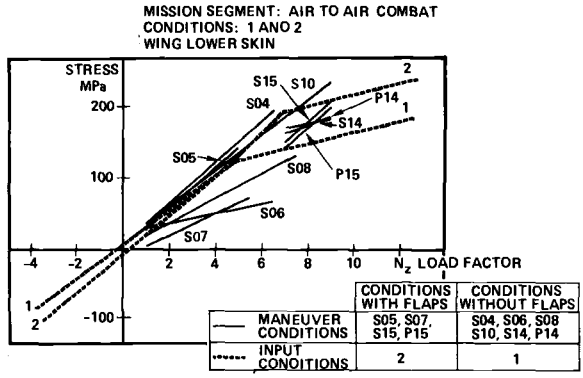

FIG. 1—*Load factor to stress transfer function relationship.*

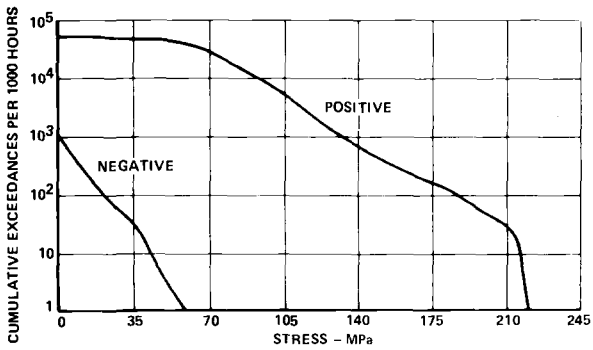

FIG. 2—*Cumulative stress spectrum for fighter aircraft maneuver and ground loading.*

Measuring Fatigue Spectra Output Response

A typical system for complex random spectra fatigue testing will consist as a minimum of one or more minicomputers and magnetic tape transports (digital-to-analog converter), in addition to the electrohydraulic test machines. Additional supporting test hardware is available for signal conditioning and data acquisition. Most of this equipment is "off the shelf" with known accuracy and reliability, although unexpected variations in performance do occur, usually to a small degree. However, the manner in which they are integrated in the test system can cause vast variations. Additional variations may occur in laboratory related factors such as in the electrical or hydraulic power supply, the experience of the test engineer, and the software systems used for linking all the various hardware elements through minicomputers. To identify the effect of some of these variations comparisons must be made of recorded strain responses under different test conditions.

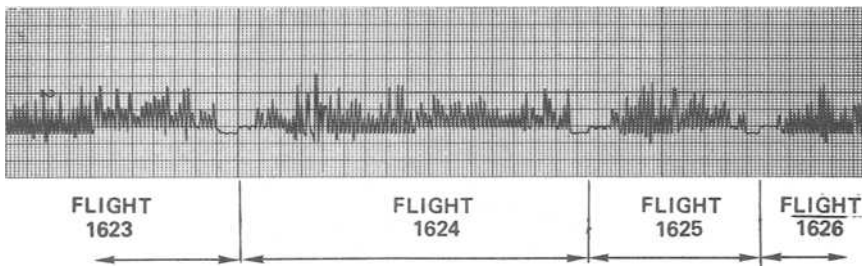

FIG. 3—*Typical fighter aircraft flight-by-flight time history (constant frequency) generated by digital technique used in this study.*

It's important that the proper spectrum parameters be used in making these comparisons. We are conditioned from normal fatigue experience to think of amplitude probability density or peak probability density as being the only important parameters in characterizing fatigue spectra from low frequency aircraft maneuvers. However, where frequency and waveform as well as loading intensity are significant spectrum characteristics contributing to fatigue strength degradation, knowledge of the spectrum power spectral density (PSD) and root mean square (RMS) may also be useful in comparing spectra severity. Just how useful is demonstrated in the following sections.

Power Spectral Density (PSD)

Power spectral density ($G(f)$) is a measure of loading intensity or energy

in the frequency range and is a function of load amplitude, load symmetry, and waveform. PSD is generally expressed as

$$G(f) = 2/\pi \int_0^\infty R(\tau) \cos \omega\tau d\tau \tag{1}$$

where $R(\tau)$ is the autocorrelation function

$$R(\tau) = \lim_{T\to\infty} \frac{1}{T} \int_0^T X(t)X(t + \tau)\, dt \tag{2}$$

The information contained in $G(f)$ and $R(\tau)$ is technically the same since they are Fourier transform pairs; however, the frequency format of $G(f)$ is more useful in this case.

Root Mean Square (RMS)

RMS is a quantitative measure of loading intensity and is equal to the square root of the area under the PSD diagram.

$$\text{RMS} = \left[\int_0^\infty G(f)\, df \right]^{1/2} \tag{3}$$

Experimental Procedures

Fatigue test equipment used in this study for system control included minicomputers in a disk operating system, multi-channel DA (digital-analog) and AD (analog-digital) converters, interactive cathode ray terminal, teletype, printers, etc. The control signal was made up of triangular pulses applied at a rate of from 0.5 to 5 pulses per second (pps) depending on the test.

Data Acquisition and Processing

Three signals were recorded from each test condition measured, the control signal, test machine load cell signal, and specimen strain responses. The data were recorded on a 14-channel FM analog recording system. The computer control signal was fed directly to the FM recorder tape system as a $\pm$10-V signal. The load cell output was taken from the MTS control system and fed directly to the tape system as a $\pm$10-V signal. In the case of both the load cell and control signal a zero and $\pm$10-V calibration signal was recorded prior to each test.

Strains were measured by electric resistance wire 350-Ω gages bonded to the Gr/E laminate portion of the specimen. One active gage and three 349-Ω resistors were used per specimen side to form one complete bridge

network, necessary for correct signal measurement. Balance and calibration were obtained by use of a commercial type bridge balance box. A shunt calibration resistor of 40 Ω was switched through each bridge circuit prior to each test. That provided an equivalent strain output of 4130 μm/m. Each bridge circuit was fed to a data amplifier (gain = 200) and then to the FM tape system for recording. The functional diagram of the data acquisition system is shown in Fig. 4.

Control, load cell, and specimen strain signals were reproduced from FM recorder magnetic tapes as time histories on an 8-channel pen recorder. These history records were scaled using the calibration signals recorded prior to each test. The data then were passed through normalizing amplifiers to provide outputs of 1 V = 1 V (load cell or control) and 1 V = 1000 μm/m (strain gage signal).

The normalized amplifier signals were processed with a Fast Fourier Transform analyzer, the number of resolution elements equaled 400 per spectrum, the nominal bandwidth was 1/400 frequency range, and the noise bandwidth 1.5 times the nominal (that is, at 50 Hz frequency range the resolution = 0.187 Hz). The 0 to 50-Hz bandwidth was chosen to display the total harmonic content of the response.

Each PSD plot consists of the mean of the square of 32 statistically independent sample spectra taken over a period of 132 s. Most of the data samples were taken starting at simulated flight number 1625 and ending at number 1632 out of a total test tape of 3244 flights.

Some of the tests were conducted at a rate of 0.5 Hz, and for these tests the data were analyzed in real time (approximately an 11-min data sample). In addition to plotting the PSD versus frequency, the RMS level for each data sample was computed by the particular spectral analyzer used. The functional diagram for the complete data processing system is shown in Fig. 5.

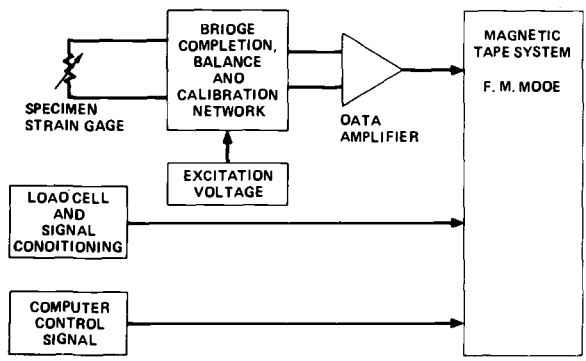

FIG. 4—*Functional diagram of data acquisition system.*

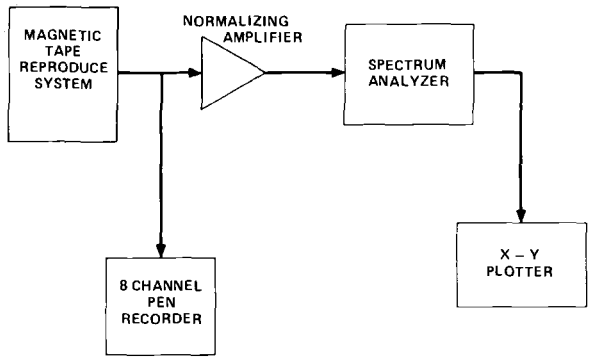

FIG. 5—*Functional diagram of data processing system.*

Data Analysis and Discussion

Figure 6 shows specimen strain responses during four different cyclic fatigue tests on identical specimens and identical digital input spectra. Some of these test conditions were contrived and others may occur within the limits of what is considered generally as acceptable test machine accuracy. The specimens were step-lap bonded Gr/E to titanium joints similar to Fig. 7. The strain responses shown in Tests 1 and 2 are essentially identical in amplitude but different in waveform. Test 3 spectrum amplitudes are consistently about 10 percent less than that of Tests 1 and 2 and slightly different in waveform. Test 4 represents still another variation with most strain amplitudes 5 to 15 percent greater than shown in previous figures. In each case the strain responses were considered possible under certain normal operational conditions that can occur in the laboratory. With this procedure spectral density plots and RMS values were determined for each of the output strain responses shown in Fig. 6. Similar data also were determined for control and load cell signals; however, the interpretation of these data is not discussed here.

PSD plots and RMS values for Tests 1, 2, and 3 of Fig. 6 are shown in Fig. 8. The frequency bandwidth of interest is principally in the 1 to 10-Hz range since the desired test machine frequency was 5 Hz. Below 1 Hz the value of $G(f)$ approaches a finite value at zero frequency that is representative of the steady state component in the cyclic strain signal. Above 10 Hz the spectral response is characterized by higher harmonics at frequencies of about 15, 25, 35, and 45 Hz. The consistent presence of these harmonics suggests that they are due to magnetic tape "noise" and are considered of no consequence to this study.

It is evident from Fig. 8 that in Test 1 the desired 5-Hz fundamental frequency was not attained. The value was actually slightly less than 4 Hz. Apart from the possible implications on frequency sensitive materials, these tests would have taken at least 20 percent longer to run than ex-

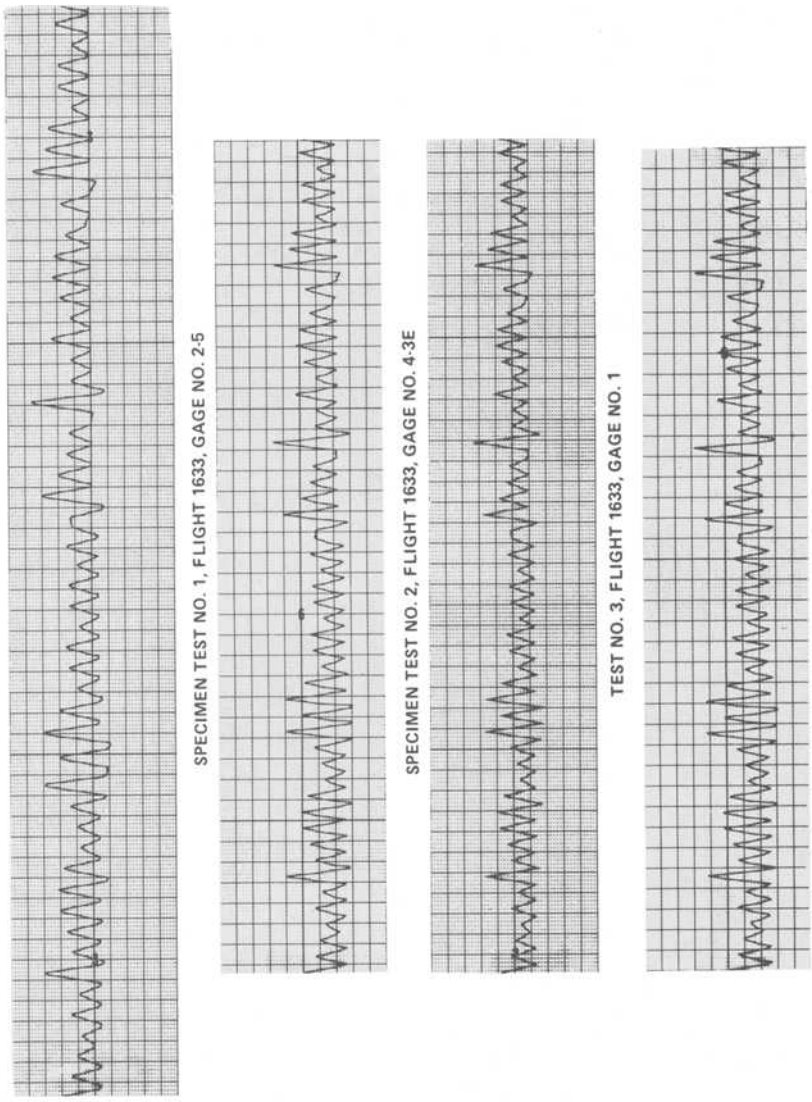

FIG. 6—*Sample output responses for identical input spectrum.*

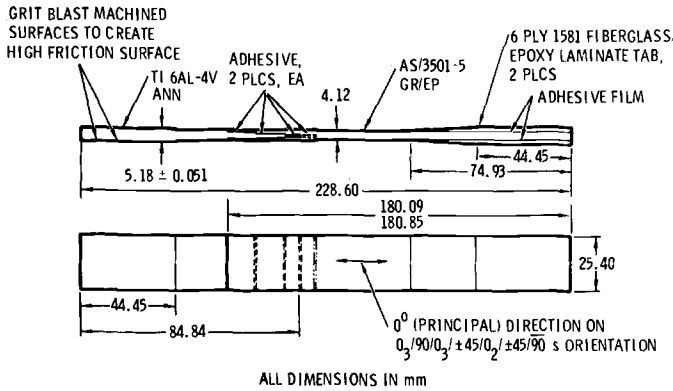

FIG. 7—*Step-lap bonded joint specimen.*

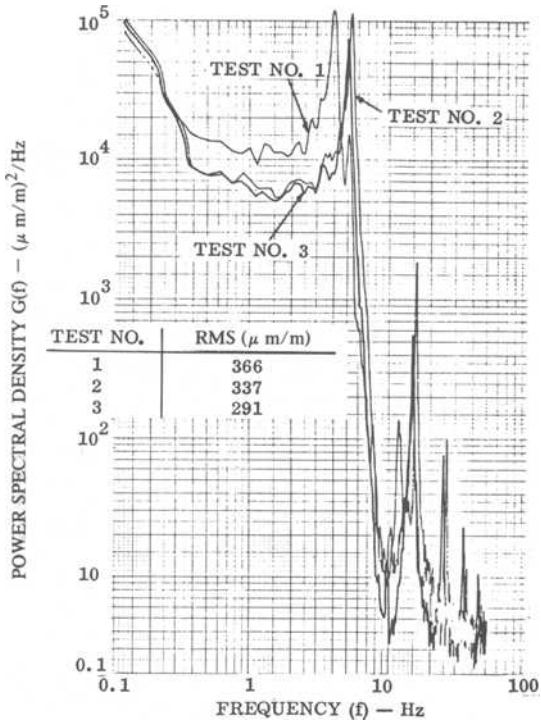

FIG. 8—*Spectral density and RMS characterization of strain response for Test Nos. 1, 2, 3 of Fig. 6.*

pected. In addition, Test 1 spectral density appears more severe (greater loading intensity) in the 0.5 to 10-Hz frequency range than the other two tests. This is verified by the RMS values which progressively decrease from Tests 1 through 3. Tests 2 and 4 are compared in Fig. 9. Whereas the RMS difference between Tests 1 and 2 is attributed to cyclic waveform differences, a similar difference between Tests 2 and 4 is due to variations in load amplitude. Alternatively to Eq 3, RMS can be expressed as [5]

$$\text{RMS} = \left[\frac{1}{T}\int_0^T x^2(t)\,dt\right]^{1/2} \tag{4}$$

where T is the sampling time and $x(t)$ is the voltage signal time history. Determining RMS by analog techniques amounts to taking the square root of the square of the instantaneous signal value. Thus RMS can be influenced both by cyclic waveform and wave amplitude.

To further explore spectral density and RMS characterization of strain

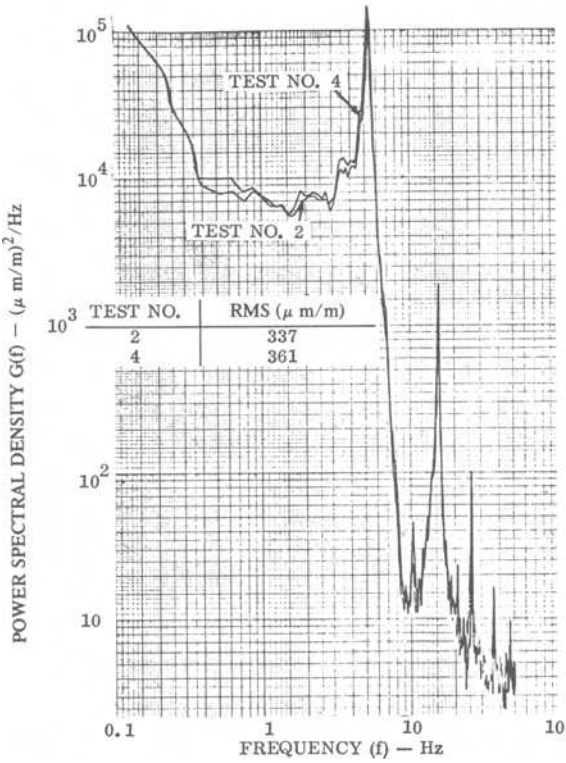

FIG. 9—*Spectral density and RMS characterization of strain response for Test Nos. 2 and 4 of Fig. 6.*

signal response in fatigue testing, identical input spectra were run at two different frequencies on the same test machine and control system. These two fundamental frequencies were 5 and 0.5 Hz and the output strain signal analysis is shown in Figs. 10 and 11, respectively. The PSD plots have similar shapes in both figures while the 0.5 Hz spectral density has greater amplitude and is shifted an order of magnitude lower on the frequency scale. However, the RMS values are essentially the same. This is consistent with the theory of time compression in random analog data analysis to compensate for filter bandwidth limitations. Thus everything else being equal, a frequency shift in a given spectrum load application should produce no difference in RMS value.

To investigate another form of load application frequently used in spectrum fatigue testing, a test was run in which the rate of load application was maintained constant at about 83 MPa/s. The output strain PSD plot for this type of test, together with a sample of the output response, is shown in Fig. 12 and is characterized by large spectral amplitude responses

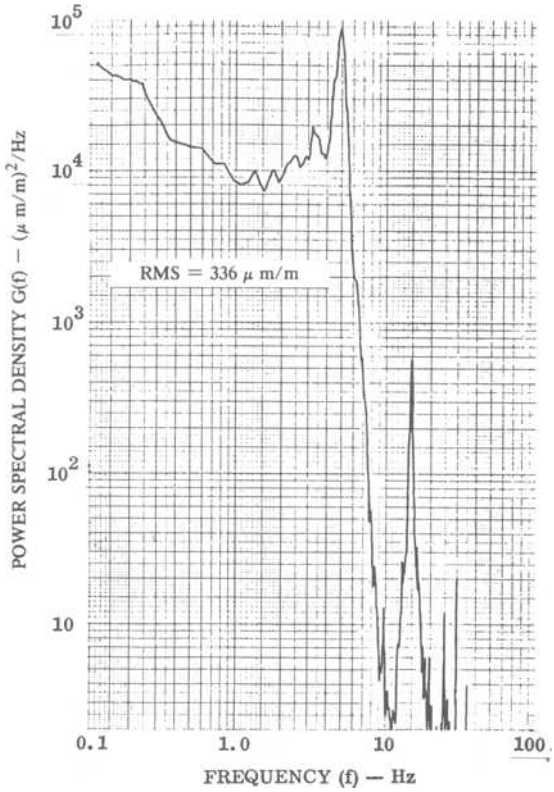

FIG. 10—*Analysis of 5-Hz strain response signal.*

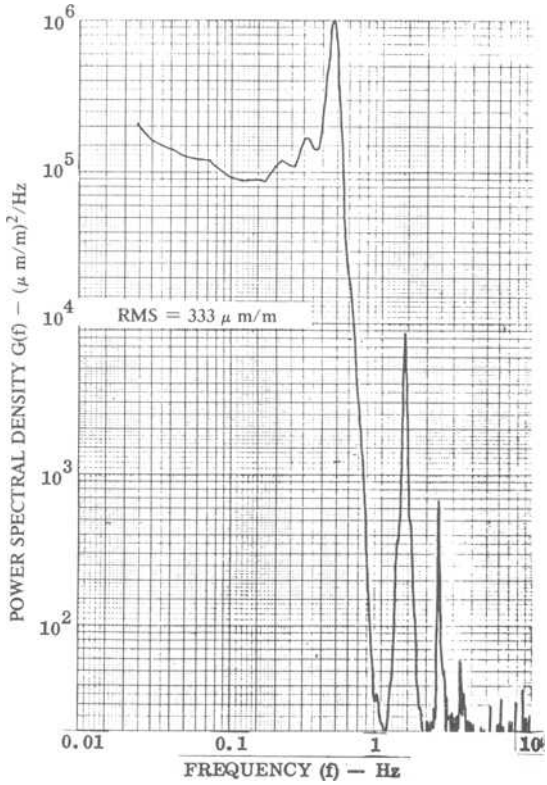

FIG. 11—*Analysis of 0.5-Hz strain response signal.*

at frequencies of about 1.5 and 2.7 Hz. Also note that the RMS value is 386 μm/m, suggesting this type of waveform may be more severe than the constant frequency data discussed previously. This may be due to the fact that in this type of loading, more time is spent proportionally at higher loads than at lower loads. This occurs since the load ramp time is in direct proportion to the load magnitude.

Statistical data analysis of the strain response signal was not particularly sensitive to differences in flight number samples, as seen in Fig. 13. A particular analysis of flight numbers 1627 through 1633 is compared with a similar analysis of flight numbers 1630 through 1636. The RMS values are within about 3 percent and the spectral amplitudes differ only in the lower frequency ranges. In each case the number of flights in the sample are the same; however, the total number of load cycles will differ due to the random nature of the flight load composition. Analyzing longer data samples has a tendency to smooth out the PSD plots without significantly changing them.

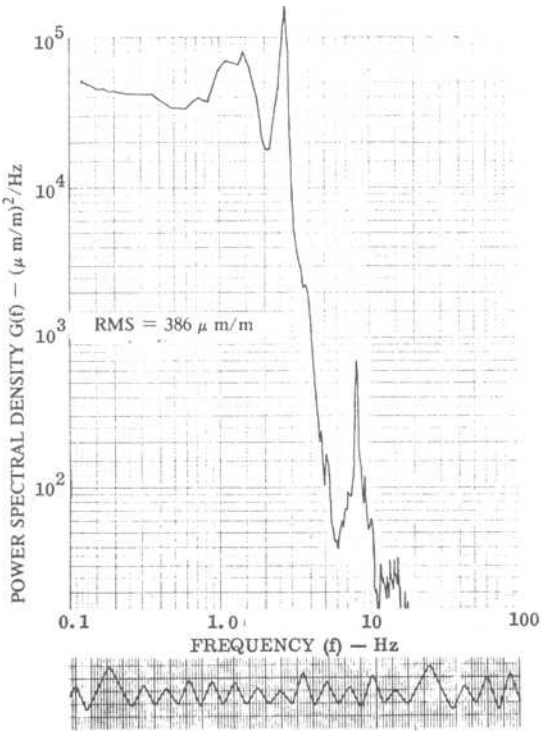

FIG. 12—*Analysis of strain signal for constant rate of load application.*

Fatigue Test Results

A limited amount of testing was performed corresponding to some of the strain response variations analyzed previously. Multiple specimen tests were completed for the strain response conditions of Fig. 6. Testing was conducted on 20 and 200 KIP MTS servohydraulic test machines. The 200 KIP test frame was rigged to test 20 specimens at a time in 4 trains of 5 specimens each. The results are shown in Fig. 14. Weibull shape parameter ($\hat{\alpha}_f$) and 95 percent confidence scale parameter ($\hat{\beta}$) are given for each series of data. What is clearly evident in Fig. 14 is that the fatigue results follow the trends indicated by the RMS values in Fig. 8. The 51 percent increase in fatigue life of Test 2 over Test 1 was indicated by the difference in RMS values shown in Fig. 8. This is not too surprising considering the known frequency sensitivity of matrix dominated composite laminates. The variations in load amplitude are likely the significant factor in Test 3 results compared to Tests 1 and 2.

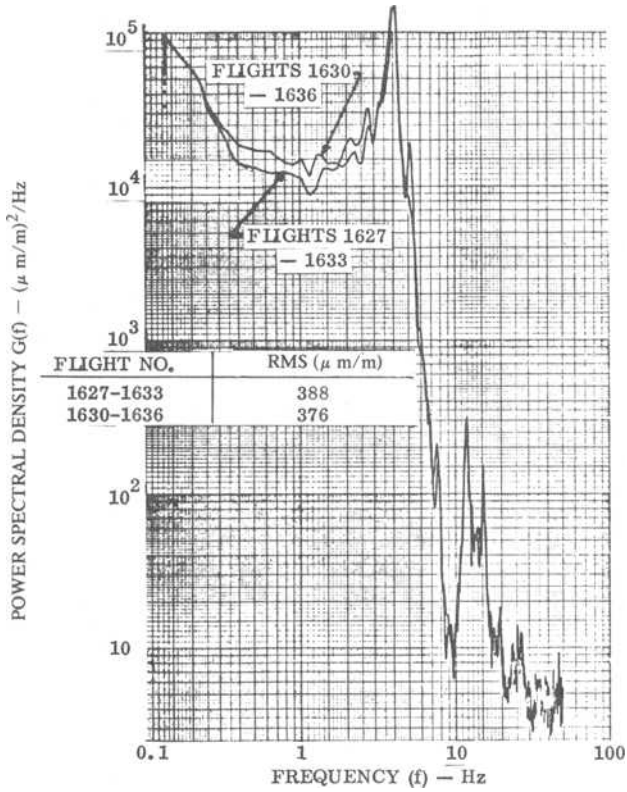

FIG. 13—*Analysis comparison for different flight ranges.*

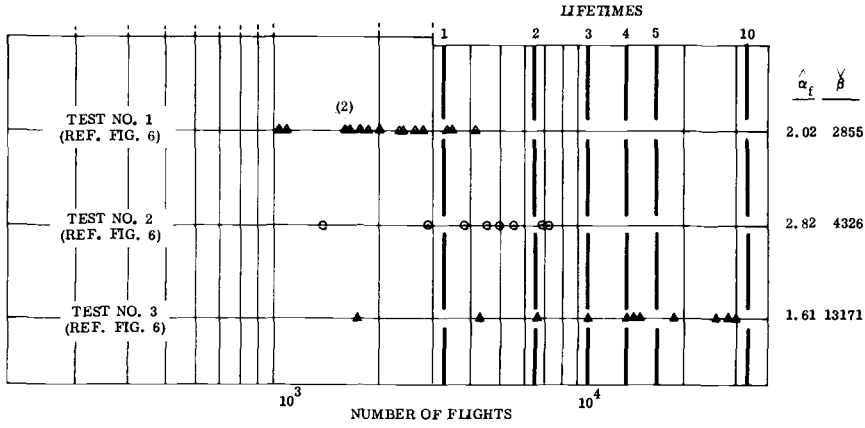

FIG. 14—*Fatigue tests conducted for spectra of Fig. 6.*

Summary

Random data analysis techniques have been shown to be a useful tool in characterizing specimen strain response due to a low frequency digital loading spectrum. Such strain data can be collected readily and processed by analog techniques to determine power spectral density and RMS data. Subtle differences in test equipment response can be identified using this type of statistical data. Small, or not so small, variations in stress amplitude, cyclic frequency, or waveform of the strain signal under an identical input spectrum will show up as variations in the PSD plot or RMS value. In certain material systems such variations will affect the fatigue data and possibly mask other parameters being studied.

Acknowledgment

The authors wish to acknowledge J. Mays and D. Dittmer for their extensive efforts in generating the test data, and Dr. C. Hwang for his advice in interpreting the statistical data. This work was done under Air Force Flight Dynamics Laboratory Contract F33615-75-C-5236, "Fatigue Spectrum Sensitivity Study for Advanced Composite Materials." Dr. E. Demuts is the Air Force monitor.

References

[*1*] Waddoups, M. E. et al, "Reliability of Complex Large Scale Composite Structure—Proof of Concept," *AFML-TR-73-160,* Air Force Materials Laboratory, Dayton, Ohio, July 1973.

[*2*] Jeans, L. L. and Van Siclen, R. C., "Fatigue Spectrum Sensitivity Study for Advanced Composite Materials," *Interim Technical Reports Nos. 1–4,* Air Force Flight Dynamics Laboratory, Dayton, Ohio, June 1975 through June 1976.

[*3*] Dill, H. D. and Young, H. T., "Stress History Simulation: Volume I-A User's Manual for a Computer Program to Generate Stress History Simulations," *AFFDL-TR-76-113,* Air Force Flight Dynamics Laboratory, Dayton, Ohio, Vol. I, March 1977.

[*4*] Jeans, L. L. and Grimes, G. L., "Fatigue Spectrum Sensitivity Study for Advanced Composite Materials," *Interim Technical Report No. 9,* Air Force Flight Dynamics Laboratory, Dayton, Ohio, Oct. 1977.

[*5*] Bendat, J. J. and Piersol, A. C., in *Random Data: Analysis and Measurement Procedures,* Wiley, New York, 1971.

Pedro Albrecht[1] *and Kentaro Yamada*[2]

Simulation of Service Fatigue Loads for Short-Span Highway Bridges

REFERENCE: Albrecht, Pedro and Yamada, Kentaro, **"Simulation of Service Fatigue Loads for Short-Span Highway Bridges,"** *Service Fatigue Loads Monitoring, Simulation, and Analysis, ASTM STP 671,* P. R. Abelkis and J. M. Potter, Eds., American Society for Testing and Materials, 1979, pp. 255-277.

ABSTRACT: A mean stress range histogram and corresponding frequency distribution function for single truck crossings over short-span highway bridges, derived from 106 published histograms, is proposed. A major portion of this load history was applied to a welded transverse stiffener detail in blocks varying from 100 cycles to 100 000 cycles. When the number of cycles in the block was 1000 cycles or less, the block size had no significant effect on the total number of cycles to failure. Block loading simulated then random loading, and the root-mean-cube stress range provided a reasonable transfer function between block loading and constant amplitude cycling.

KEY WORDS: fatigue tests, bridges, steel, load simulation

This study addresses the large majority of highway bridges which typically have multiple girders and short spans of, for instance, less than 35 m between supports. Such bridges have two important features. First, the live load induced stress range constitutes a significant portion of the maximum stress which results from the combination of bridge weight and live load. As a result, the design of a specific detail on a steel girder may be governed by fatigue, that is, stress range, rather than maximum stress. Second, the passage of a single truck is the principal event that produces a significant stress range cycle. Trucks closely following each other on the same lane could conceivably cause a larger stress range at the detail under consideration. But since high stress excursions during multiple truck passages are rare events, the induced fatigue damage is insignificant [*1*].[3]

The purposes of this study were: (1) to develop a useful load history for short-span highway bridges, and (2) to study the block size limits for experimental modeling of a random loading often encountered in bridge

[1] Structural mechanics analyst, Metallurgy and Materials Research Branch, U.S. Nuclear Regulatory Commission, Washington, D.C. 20555.

[2] Lecturer, Nagoya University, Nagoya, Japan.

[3] The italic numbers in brackets refer to the list of references appended to this paper.

structures. The representative load history was derived from 106 histograms reported in the literature. The block size limit was determined with a series of experiments in which the size of the same basic block was varied from 100 000 cycles down to 100 cycles. The lower value corresponds, for all practical purposes, to random loading. Influences of reordering are discussed in terms of known facts pertaining to overloads.

Mean Stress Range Histogram

The mean histogram used in this study was developed from 106 individual stress range histograms for truck traffic across 29 bridges located in eight states. The data were reported in Refs *2* through *11*. The bridges were located on heavily traveled arteries of which 19 were interstate highways, six were U.S. routes, and four were state roads. Detailed information about these bridges, the characteristic features of the stress range histograms, and a plot of each of the 106 histograms can be found in Ref *12*.

Not included were ten Ohio bridges located in rural and suburban areas, because many of the 78 histograms [*13*] exhibited very high proportions of low-to-high stress range counts, a condition that is not typical of arteries heavily traveled by trucks and bridges prone to fatigue damage.

Type of Bridge

A breakdown by type of bridge shows that the records utilized in this study were obtained from 16 single-span bridges, 8 three-span continuous bridges, 2 end-anchored bridges, 2 suspended span bridges, and 1 semi-suspended span bridge.

Most bridges had short spans with lengths between supports varying from 11.6 to 24.4 m. This range is typical for steel girder bridges. Only five bridges had longer spans: Two I-96 bridges over the Grand River in Michigan with spans of 29 and 39.3 m [*2*], the Yellow Mill Pond twin bridges on I-95 in Bridgeport, Conn., with a span of 34.6 m [*10*], and the Lehigh Canal Bridge on U.S. 22 near Bethlehem, Pa., with a span of 43.9 m [*11*].

Rolled sections were used as girders in 20 bridges, of which 19 bridges were with welded cover plates. Two bridges with longer spans had welded plate girders [*2*], and one had riveted plate girders [*11*]. The remaining six bridges were of concrete construction, either reinforced [*8*] or prestressed [*2,5*]. The slabs were attached to the girders with shear connectors in all but 4 [*4,6,8*] of the 23 steel girder bridges. The thickness of the concrete deck varied from 15 to 20 cm.

Stress Range Histograms

The events considered in this evaluation of recorded load histories are

stress ranges produced by single truck passages. The actual values measured were strain ranges which were then converted into stress ranges by multiplying with Young's modulus. The number of stress ranges (bar height) that fell in preselected stress range intervals (bar width) then were counted, and the results presented in the form of a stress range histogram (bar chart).

The number of stress range events that went into each of the 106 histograms varied, in 92 of 106 cases, between 500 and 10 000. Seven histograms contained less than 500 events and seven histograms had more than 10 000 events.

Most strain range measurements, 77 out of 106, were taken with strain gages attached to the bottom flange either at midspan or near the end of the cover plates. Records from strain gages attached to slabs [*4*], reinforcing bars in the slab [*4*], and tie plates [*11*] were not included because they were affected by wheel loads rather than truck loads.

Important differences between the 106 histograms were observed with regard to (*a*) bar width, (*b*) maximum stress range, and (*c*) lower cutoff point. These differences, as illustrated with the histograms plotted in Figs. 1 through 3, are discussed as follows.

For steel girder bridges, the bar width, preselected by the investigators for purposes of data presentation, varied from a minimum of 1.4 MPa [*4*] to a maximum of 8.3 MPa [*11*]. Most of the bar widths, in 69 out of 87 histograms, varied from 2.8 to 4.1 MPa. For concrete girders, a bar width of about 0.3 MPa was used [*2,5*]. Two typical histograms of about equal maximum stress range and lower cutoff point, but with significantly different bar widths of 1.4 and 4.1 MPa are shown in Fig. 1. Both were recorded at the midspan of simple beams, with strain gages attached to the extreme fiber of the bottom flange. The number of recorded stress ranges were 673 for the solid-line histogram and 2982 for the dashed-line histogram. The frequency scale gives the number of events within a stress range interval relative to the total number of events for the histogram. Consequently, the sum of all bar heights in one histogram must equal 100 percent.

The maximum stress range recorded in each histogram varied from 1.2 MPa for a prestressed concrete girder [*5*] to 72.3 MPa measured at the bottom flange of a three-span continuous riveted plate girder [*11*], as shown in Fig. 2. The number of recorded stress ranges in these two histograms were 138 and 158, respectively. Thirty-five of the 87 steel girder histograms had a maximum stress range larger than 35 MPa.

Sixty-six stress range histograms were presented with a cutoff point below which no stress ranges had been recorded [*5,8–11*], whereas the remaining 40 were presented with the lowest stress range bar starting at the origin. This is illustrated in Fig. 3 which shows one histogram with a cutoff point of 4.1 MPa obtained from a strain gage attached to the bottom flange at midspan of a simple beam [*10*], and one without a cutoff point

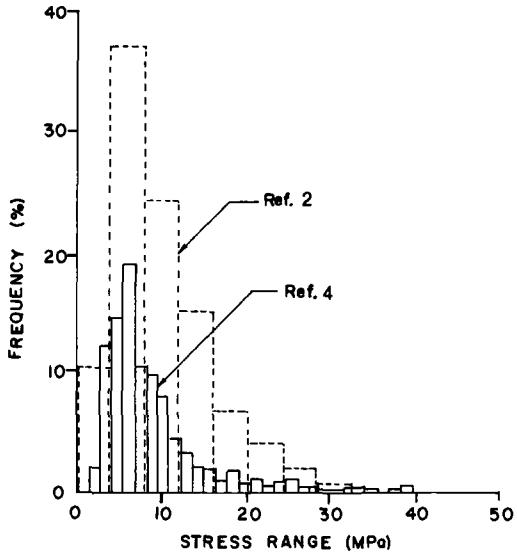

FIG. 1—*Histograms with extreme differences in bar width.*

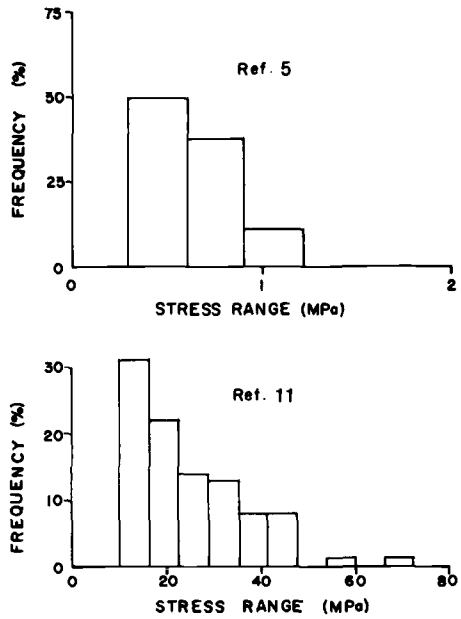

FIG. 2—*Histograms with extreme differences in maximum stress range.*

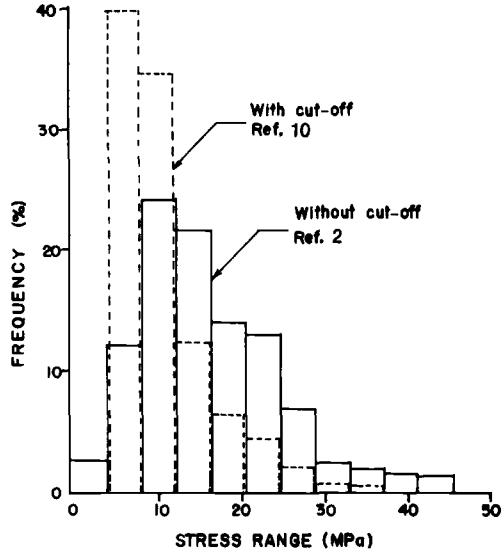

FIG. 3—*Histograms with and without lower stress range cutoff.*

recorded at the quarter point of a simple span welded plate girder [*2*]. The number of stress ranges recorded in these two histograms were 12 603 and 2547, respectively. Although both histograms have the same bar width, and nearly equal maximum stress ranges, the one with cutoff point exhibits a descending frequency distribution, whereas the one without cutoff point has an ascending-descending frequency distribution. Most cutoff points were set between 3.1 and 6.9 MPa. More important, only seven out of 106 stress range histograms had cutoff points that exceeded 25 percent of the maximum stress range.

Mean Stress Range Histogram

Despite the previously discussed differences in bar width, maximum stress range, $\sigma_{r\max}$, and cutoff points, the concavity of the frequency distribution curve from the peak frequency at about 25 percent of $\sigma_{r\max}$ to a low value at $\sigma_{r\max}$ is typical of all histograms. To preserve this characteristic shape, and to permit a meaningful comparison, all histograms were normalized with respect to the maximum stress range, $\sigma_{r\max}$, and the lowest quartile was deleted.

A uniform cutoff point at 25 percent $\sigma_{r\max}$ was selected for the following reasons:

1. Most histograms, 99 out of 106, extended to frequency distributions below the chosen cutoff point.
2. The peaks occurred near 25 percent $\sigma_{r\max}$.

3. Stress ranges smaller than 25 percent $\sigma_{r\,max}$ usually fell well below the constant amplitude endurance limit. These cycles would not contribute to fatigue crack propagation until the crack reached a size at which the fatigue life would be nearly exhausted.

4. Stress ranges induced by partial car lane loads were not recorded, although their magnitude would be comparable to those for very light trucks. If they had been recorded, the frequency curve would continue to rise with decreasing stress range, since there are about eleven times more cars on the road than trucks.

5. The insignificant low stress ranges are prevented from distorting the cumulative frequency distribution curve at the higher and significant stress ranges.

After the lowest quartile was deleted and the stress ranges nondimensionalized with respect to the maximum value, cumulative frequency distribution curves were computed for all 106 histograms and plotted in Fig. 4 together with the computed average. This average was redrawn in Fig. 5 as a histogram consisting of 15 bars. The corresponding frequency distribution function, computed by the least squares method, is given by Ref *14*

$$f(x) = 12.0\,(1.0 - x)^3 + 0.07 \quad \text{for} \quad 0.25 \leq x \leq 1.0 \tag{1}$$

where $x = \sigma_r/\sigma_{r\,max}$ is the normalized stress range. Note that the area under the function, $f(x)$, between $x = 0.25$ and $x = 1.0$, is equal to one. The stress range histogram predicted with Eq 1 is compared in Fig. 5 with the average of all 106 histograms. When Eq 1 is used for variable amplitude

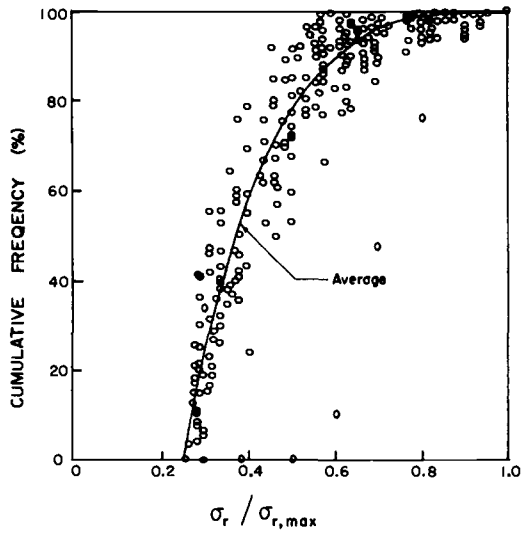

FIG. 4—*Cumulative frequency plot of 106 stress range histograms.*

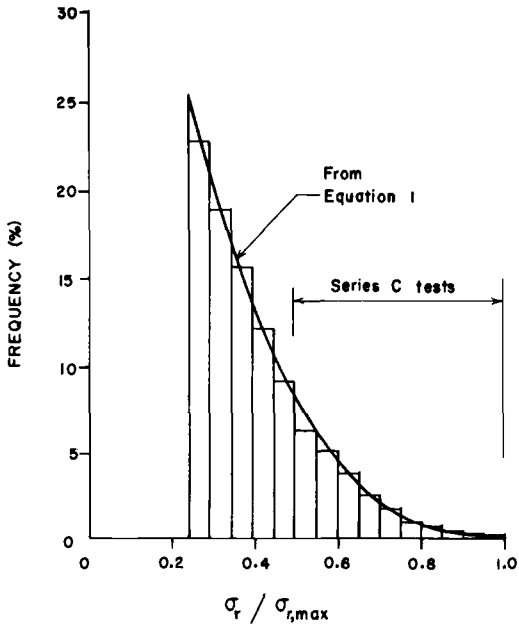

FIG. 5—*Mean stress range histogram and probability density function.*

fatigue design, the normalized stress ranges are multiplied by the maximum stress range that was computed for the given bridge girder detail. The average histogram accounts then for the actual live load variation.

Comments on Rayleigh Functions

Among the curves investigated for the purpose of best fitting the average cumulative frequency distribution, shown as a step function in Fig. 5, were Rayleigh functions. They were used in the past by others [*15,16*], presumably to match the ascending-descending shape of individual histograms for truck traffic such as those shown in Fig. 1. In this study, the results of the least square fit analysis revealed a significant lack of correlation for the Rayleigh curve. Its applicability appears to be questionable also for conceptual reasons. A Rayleigh curve would predict gradually vanishing frequencies at very low loads. But, in reality, the addition of stress ranges from single cars as well as from groups of cars capable of producing stress fluctuations comparable to those from very light trucks would yield a histogram similar to that shown in Fig. 5, but with a continuously rising curve as the normalized stress range approaches zero. During the year 1973 the average daily traffic at a representative point of I-695 (the Baltimore Beltway) ranged from 92 000 to 103 000 vehicles, of which 8 to 10 percent were trucks [*17*]. If events other than trucks were

added, the area under the curve in Fig. 5, bounded by $0 \leq \sigma_r/\sigma_{r\max} \leq 0.25$, would therefore be about 11 times larger than the area bounded by $0.25 \leq \sigma_r/\sigma_{r\max} \leq 1.0$ that corresponds to truck traffic. Hence, Rayleigh functions are not suitable. Further, retaining the very low stress ranges reduces the equivalent constant amplitude stress range, as discussed later, and leads to nonconservative estimates of variable amplitude fatigue life.

Experimental Work

Specimens

The tension specimens used in this study were saw-cut from a larger plate that had transverse stiffeners continuously welded by the automatic submerged-arc welding process. The specimen geometry, shown in Fig. 6, consisted of a main plate 10 by 26 mm and 330 mm long and two transverse plates 7 by 26 mm and 52 mm long. The weld size was 6 mm. The detail simulates the stress condition at transverse stiffeners and diaphragm gussets. It is classified in fatigue design specifications for buildings and bridges [*18,19*] under Stress Category C.

All steel conformed to the ASTM Specification for High-Strength Low-Alloy Structural Steel with 50 000 psi (345 MPa) Minimum Yield Point to 4 in. (100 mm) Thick (A 588-75). The measured yield strength and tensile strength were 420 and 570 MPa, respectively.

Block Loading

To shorten the testing time, only that portion corresponding to the upper 10 bars of the histogram shown in Fig. 5 was retained for the experimental work. These bars then were arranged in the random order plotted in Fig. 7 to form a basic load block. Each group of constant amplitude stress range cycles in Fig. 7 is defined by the stress range at the center of the bars in Fig. 5 and by the number of cycles computed by integration of Eq 1 be-

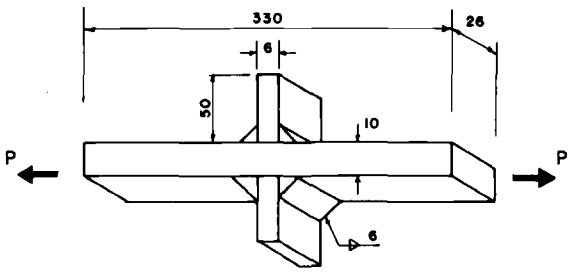

FIG. 6—*Test specimen.*

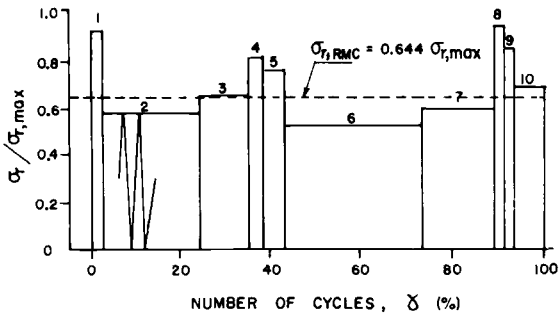

FIG. 7—*Basic loading block.*

tween the normalized stress range values which determine the bar width. The values that define each group of cycles are summarized in Table 1. The load block was applied repeatedly until the specimens failed.

Equivalent Constant Amplitude Stress Range

It is well known that a variable amplitude stress range history can be replaced by an equivalent constant amplitude stress range

$$\sigma_{r\,\text{equivalent}} = \left(\sum_{i=1}^{k} \gamma_i \, \sigma_{ri}{}^{n} \right)^{1/n} \tag{2}$$

that will cause the same amount of fatigue damage. In Eq 2, k is the number of stress range levels; γ_i and σ_{ri} are the frequency of occurrence and the level of the stress range, respectively. The exponent, n, is the slope of the crack growth equation

$$\frac{da}{dN} = C\,\Delta K^{n} \tag{3}$$

in a log-log plot of the crack growth rate, da/dN, versus the range of the stress intensity factor, ΔK. Because $n \cong 3$ for ferritic steels [*20*], the term $\sigma_{r\,\text{equiv}}$ in Eq 2 is herein called the root-mean-cube (RMC) stress range,

TABLE 1—*Data for loading block shown in Fig. 7.*

Sequence No.	1	2	3	4	5	6	7	8	9	10
$\sigma_r/\sigma_{r,\,max}$	0.925	0.575	0.675	0.825	0.775	0.525	0.625	0.975	0.875	0.725
No. of Cycles, %	1.7	22.3	10.8	3.1	4.7	30.6	15.9	1.6	2.1	7.2

$\sigma_{r\,RMC}$. The value of n is also equal to the slope of the mean regression line through fatigue test data for welded bridge details fabricated from ferritic steels.

It can be shown [*21*] that the equivalent stress range concept and Miner's cumulative damage criteria, when used in conjunction with well defined *S-N* plots, are special cases of the fracture mechanics approach that is based on Eq 3. All three give identical variable amplitude fatigue life predictions provided that: (1) the crack initiation phase is negligible, (2) the block size is sufficiently small to prevent interaction in high-low stress range sequences, (3) all stress ranges are above the constant amplitude fatigue limit, and (4) the inverse slope of the *S-N* curve and the slope of the crack growth rate curve are about equal, that is $n \cong 3$ for ferritic steels.

The loading block of Fig. 7 has a RMC stress range of

$$\sigma_{r\,RMC} = 0.644\ \sigma_{r\,max} \tag{4}$$

See also Column 3 in Table 2. Note that for load spectra with a narrow band width the value of the equivalent stress range in Eq 2 does not vary much with the exponent, n. For example, when $n = 2$, the equivalent stress range for the load block of Fig. 7 would be $\sigma_{r\,RMS} = 0.633\ \sigma_{r\,max}$. This root-mean-square stress range is only two percent smaller than the $\sigma_{r\,RMC}$ value given by Eq 4.

Experiment Design

The experiment design consisted of 36 specimens arranged in a two-way factorial with three levels of stress range, four levels of block size, and three replicates per cell. The three maximum stress range levels were 207, 304, and 386 MPa. The four levels of block size were 10^2, 10^3, 10^4, and 10^5 cycles. The values in columns two and four of Table 2, in conjunction with those in Table 1, define the loading block for each test. The minimum stress is not a significant variable. In this study it was held constant arbitrarily at 3 MPa.

About 52.9 percent of the stress range cycles applied to the first twelve specimens listed in Table 2 were below the constant amplitude fatigue limit, estimated from the results of additional tests not reported herein to fall at 124 MPa. All other cycles were above the fatigue limit.

Control specimens—A total of twelve control specimens of same geometry, material and fabrication technique were available from a previous study [*1*]. Three specimens each were subjected to constant amplitude stress ranges of 144, 177, 230, and 262 MPa. The minimum stress was also 3 MPa.

TABLE 2—*Fatigue test data.*

Specimen No.	Stress Range, σ_r, MPa	Root-Mean-Cube Stress Range, $\sigma_{r,RMC}$, MPa	Block Size, ΔN, cycles	Fatigue Life, N, kilocycles	Log Average Fatigue Life, kilocycles	N/N_{RMC}
C 101				2028	2162	0.69
C 102	103-207	133	10^2	2798		
C 103				1782		
C 111				2717		
C 112	103-207	133	10^3	2528	2595	0.82
C 113				2545		
C 121				2220		
C 122	103-207	133	10^4	3921	2856	0.91
C 123				2676		
C 131				8137		
C 132	103-207	133	10^5	4968	>7590	>2.41
C 133				10600[a]		
C 201				937		
C 202	152-304	196	10^2	504	612	0.98
C 203				485		
C 211				445		
C 212	152-304	196	10^3	556	508	0.81
C 213				530		
C 221				840		
C 222	152-304	196	10^4	849	736	1.18
C 223				560		
C 231				1252		
C 232	152-304	196	10^5	784	959	1.53
C 233				898		
C 301				153		
C 302	193-386	249	10^2	183	189	0.66
C 303				242		
C 311				239		
C 312	193-386	249	10^3	247	254	0.88
C 313				278		
C 321				326		
C 322	193-386	249	10^4	267	292	1.01
C 323				286		
C 331				426		
C 332	193-386	249	10^5	515	477	1.66
C 333				495		

[a] Runout.

Results

Crack Initiation and Propagation

All cracks initiated at one or more points along the weld toe line and then propagated through the thickness of the main plate in a direction perpendicular to the applied force. Eventual failure was caused by ductile rupture of the net ligament at average net section stresses close to the ultimate strength.

Figure 8*a* shows the fatigue crack surface of specimen C131 that was subjected to 103 to 207 MPa stress range blocks of 10^5 cycles. Its fatigue life was 8.137 million cycles. The beach marks on the crack surface formed as groups of high stress range cycles alternated with those of lower stress range.

While the main crack propagated to failure, another crack shown in Fig. 8*b* was growing in the second weld toe plane normal to the main plate. This crack was exposed, after the specimen failed, by saw-cutting from one

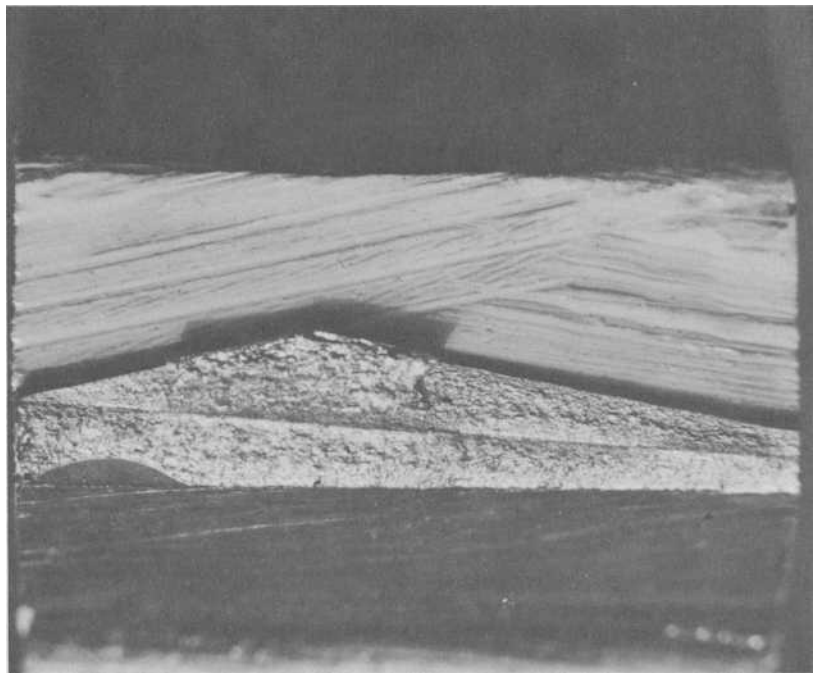

(*a*) Crack at failure section.

FIG. 8—*Fatigue crack surfaces in specimen C131.*

side of the plate and prying the remaining ligament open. Such secondary cracks were found in most specimens.

Constant Amplitude Test Data

The data for the 12 control specimens, tested under constant amplitude cycling during a previous study [*1*], is plotted in Fig. 9. The solid line represents the mean regression line computed by the least square method. It is given by

$$\log N = 13.1998 - 3.23 \log \sigma_r \tag{5}$$

The estimated standard deviation of the normal life distribution for log N was $\hat{S} = 0.1694$ and the coefficient of correlation was $r = 0.90$. The solid circles, connected by a dashed line, give the stress ranges allowed by the American Association of State Highway Transportation Officials (AASHTO) highway bridge specifications [*19*] for the detail employed in this study.

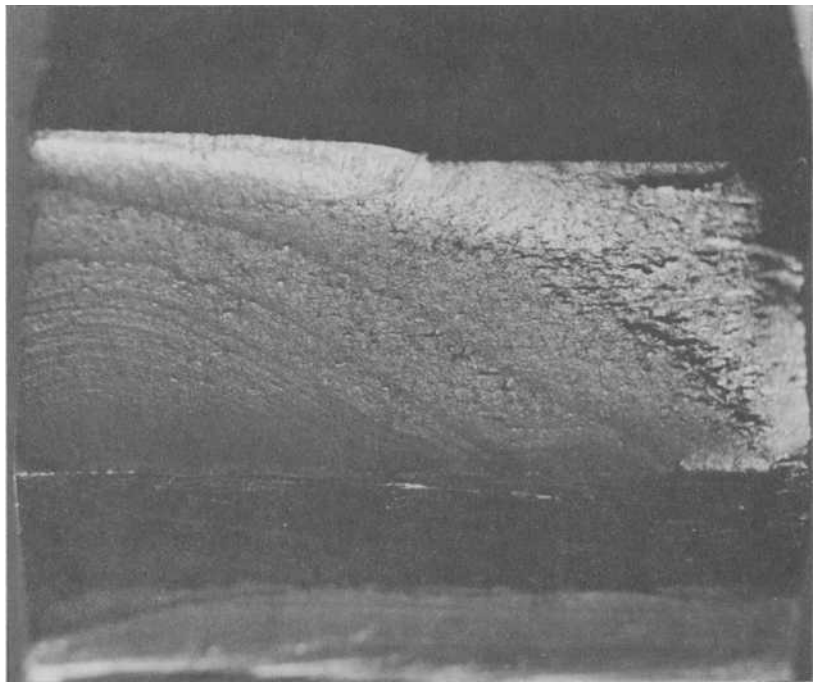

(*b*) Secondary crack.

FIG. 8—(*Continued.*)

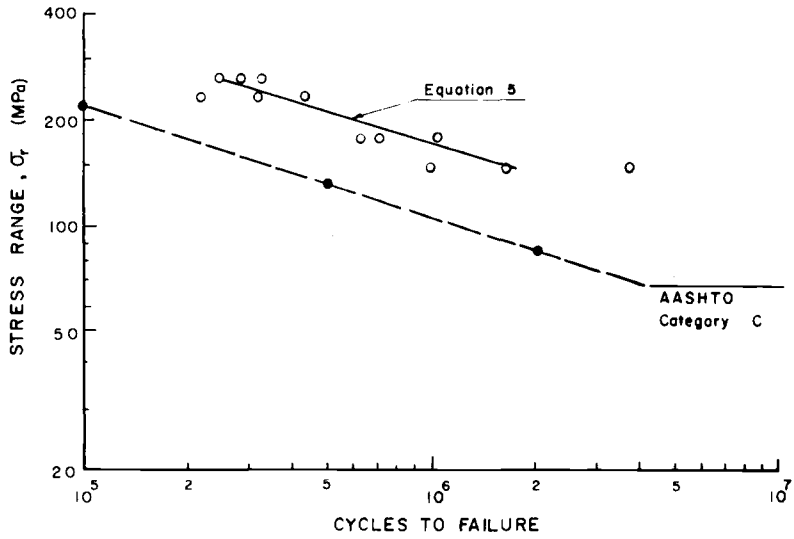

FIG. 9—S-N *plot for control specimens subjected to a constant amplitude stress cycling.*

Because of the excellent weld quality, the specimens exhibited a fatigue resistance greater than implied by the AASHTO Category C.

Variable Amplitude Test Data

The data for the 36 specimens subjected to the stress range blocks of variable amplitude are plotted in Fig. 10 and listed in Table 2. Also shown for ease of comparison are the mean for the control specimens. The fatigue lives were plotted, with symbols corresponding to the base 10 power of the block size, against the RMC stress range given by Eq 4.

Testing of Specimen C133, identified with an arrow in Fig. 10, was discontinued after 10.6 million cycles failed to produce any detectable fatigue cracking. The stress range then was increased to the next level of from 152 to 304 MPa, and testing continued with the same block size. The specimen failed after 808 000 cycles, a life that falls within the range observed for the comparable Specimens C231 through C233. Indeed, this indicates that no significant fatigue crack growth had taken place during the previous load history.

Expected Fatigue Lives

For the two levels of stress range in the experiment design that were entirely above the constant amplitude fatigue limit, the expected fatigue lives of N_{RMC} = 625 000 cycles and N_{RMC} = 288 000 cycles were obtained

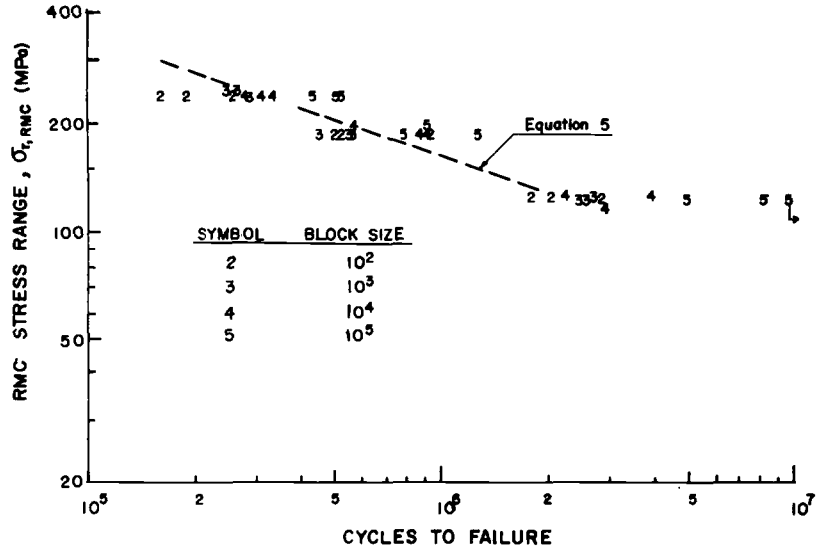

FIG. 10—S-N *plot for specimens subjected to variable amplitude block loading.*

by substituting the RMC stress range of 196 and 249 MPa, respectively, in Eq 5.

This procedure was modified for the lowest level of stress range, 103 to 207 MPa, because for that loading block the groups of cycles with sequence number 2 and 6 (see Fig. 7 and Table 1) fell below the fatigue limit of 124 MPa. The expected fatigue life was obtained as follows [*21*]:

(*a*) Equivalent stress range for cycles above the fatigue limit, from Eq 2

$$\sigma_{r\,\mathrm{RMC}} = 0.727\,\sigma_{r\,\max} = 0.727 \times 207 = 150\ \mathrm{MPa}$$

(*b*) Number of cycles corresponding to $\sigma_r = 150$ MPa, from Eq 5

$$N_P = 1\ 483\ 000\ \text{cycles}$$

(*c*) Expected fatigue life, including the cycles below the fatigue limit

$$N_{\mathrm{RMC}} = 1\ 483\ 000\ \frac{100}{100 - 22.3 - 30.6} = 3\ 148\ 000\ \text{cycles}$$

Note that the number of cycles that fell below the fatigue limit were, from Table 1, equal to 22.3 + 30.6 = 52.9 percent. It was tacitly assumed that cycles below the fatigue limit do not drive the crack. Admittedly, they

eventually will as the crack grows in size. But, by that time, a major portion of the life will have expired.

Effect of Block Size

The block size effect is illustrated in Fig. 11, where each data point represents the log average fatigue life of the three replicate specimens normalized by the expected fatigue life, N_{RMC}. The ratio N/N_{RMC} are also given in Table 2. The horizontal line, drawn at the unit value of the ordinate, corresponds to Eq 5, the mean regression line for the constant amplitude data. The deviation of the data points from the horizontal line is a measure of the amount of load interaction in the variable amplitude histogram. At a block size of 10^5 cycles the load interaction effects extend the fatigue life by at least 50 percent. At the small block sizes of 10^2 and 10^3 cycles, the variable amplitude fatigue life leveled out at about 85 percent of the constant amplitude fatigue life. About equal number of cycles to failure were obtained for constant and variable amplitude fatigue when the block size was 10^4 cycles. Except for the largest block size tested, the relative fatigue lives at all three stress range levels correlated well with block size.

Effect of Number of Blocks

Figure 12, which is similar to Fig. 11, shows the effect of the number of applied blocks on the fatigue life. The correlation between the three stress

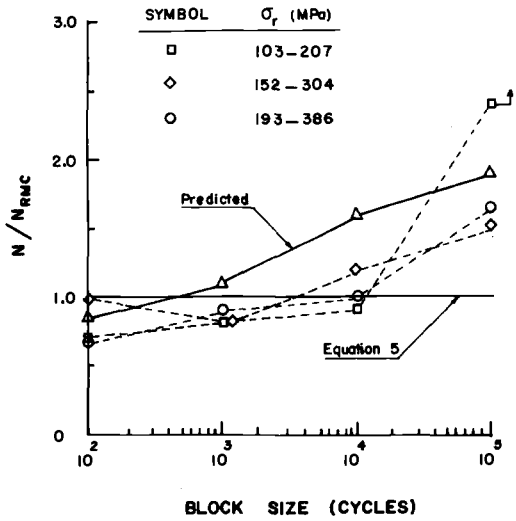

FIG. 11—*Effect of block size on fatigue life.*

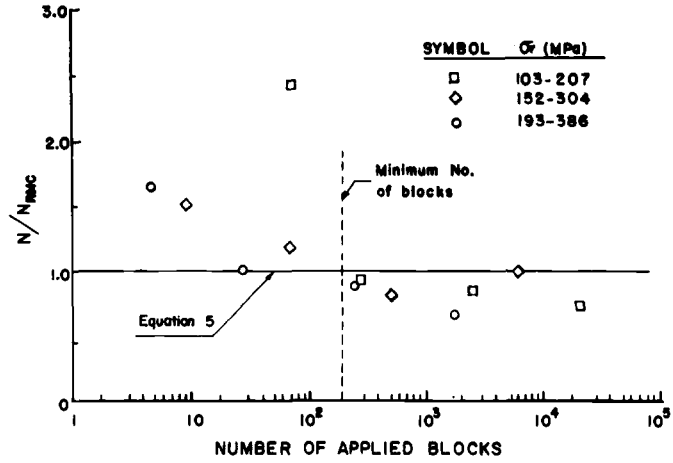

FIG. 12—*Effect of number of applied blocks on fatigue life.*

range levels is not as good as in Fig. 11. The largest deviation from the data trend occurred for the lowest stress range level and a block size of 10^5.

Significance of Results

The typical load history of a highway bridge consists of a sequence of random loads whose mean frequency distribution can be described by a function such as Eq 1. Random loading can be simulated in laboratory tests by load blocks of a size small enough so that the results are not affected significantly by load interaction effects. Based on the results of this study, it appears that random loading can be simulated with block sizes of 10^3 cycles or less. This finding was verified experimentally in this study for variable amplitude load histories of which up to 53 percent of the cycles fell below the constant amplitude fatigue limit. A semi-analytical method of predicting the maximum block size that will still ensure random load representation is explained in the following analysis section. It is based on known facts pertaining to overloads.

An experimental limiting criterion to ensure adequate random load simulation could also be based on the number of blocks applied. According to Fig. 12, the minimum number would be 200. This criterion is more difficult to apply because fatigue life estimates prior to testing may not be available.

Analysis

Experimental evidence with elastoplastic metals (steel, aluminum, titanium) which exhibit irrecoverable plastic deformations indicates that

prior high load excursions produce delays in fatigue crack growth during subsequent cycling. For a summary of previous work see Ref *1*. The delay effects increase with the stress range ratio in a high-to-low loading sequence. The rate of fatigue crack growth returns to a level free of load interaction when the leading edge of the crack has advanced through the prior overload plastic zone. At that time the clamping effect of the residual compressive stresses in the oversized plastic zone is no longer effective, and the crack opens again at about the same applied stress level as it did prior to the overload.

A typical example of delay effects is illustrated in Fig. 13. The open circles show the drop in growth rate, da/dN, following an overload. The data were measured by Von Euw [*22*] for an aluminum alloy tested under a quasi-constant value of stress intensity range, $\Delta K = 19.6$ MPa$\sqrt{m}$. The crack increment, Δa, in Fig. 13 was normalized with respect to the overload plastic zone size

$$2r_Y = \frac{1}{\pi}\left(\frac{K}{\sigma_Y}\right)^2 \tag{6}$$

where

r_Y = radius of the plastic zone,
K = maximum stress intensity factor, and
σ_Y = yield strength elevated by the degree of plane strain.

For the block loading shown in Fig. 7, potentially significant delays in crack growth may occur (*a*) while cycling at stress ranges labeled Nos. 2 and 3, following the high cycles No. 1, and (*b*) during cycle groups Nos. 6 and 7, following the high cycle groups Nos. 4 and 5. Crack growth delay after the ninth group of cycles would not be appreciable because of the small number of cycles in group No. 10.

The amount of delay in the aforementioned high-low sequences was estimated with the aid of data for specimens subjected to constant amplitude cycling with equally spaced periodic overloads [*1*] as shown in Fig. 13(*a*). The specimens were of identical geometry, material, and fabrication technique as those employed in this study. The pertinent data are summarized in Fig. 14, where the fatigue lives of the periodically overloaded specimens were normalized with respect to the fatigue life of the control specimens given in Fig. 9 and plotted against the number of cycles between overloads. Each data point represents the log average of three replicate specimens. The ratio between the overload stress range and the constant amplitude stress range was 1.67 for all specimens. Also drawn in Fig. 14 is the mean for all data. The only data excluded from the mean were the runout point at 144 MPa stress range and 10^4 cycles between overloads.

The following calculations were based on the assumptions that multiple

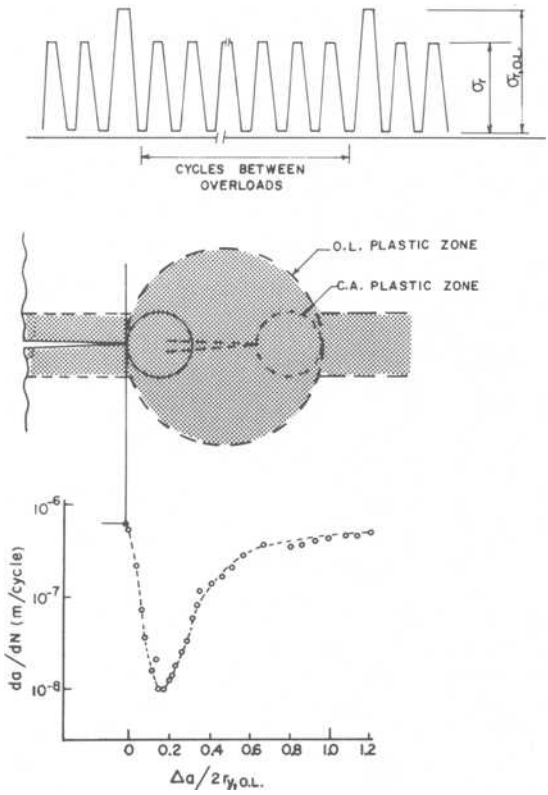

FIG. 13—*Illustration of crack growth delay after an overload.*

overloads cause the same amount of delay during subsequent low stress range cycling as a single overload, and that the delay factor decreases in proportion to the ratio of the high-to-low stress ranges. Accordingly, delay factors, N/N_{noOL}, for stress range ratios smaller than 1.67 can be obtained from Fig. 14 by linear interpolation between the mean line for the overload data and the horizontal line at $N/N_{noOL} = 1.0$ for which the stress range ratio is obviously 1.0.

A sample calculation for the block size of 10^3 cycles is summarized in Table 3. The delay effect was determined for the two major high-low sequences. The results for the first sequence was obtained as follows: (*a*) From Fig. 7 and Table 1: the stress ranges are 0.925 $\sigma_{r\ max}$ at the high level and an average of 1/2 (0.575 + 0.675) $\sigma_{r\ max}$ = 0.625 $\sigma_{r\ max}$ at the low level: (*b*) the corresponding stress range ratio is 0.925/0.625 = 1.48; (*c*) the number of cycles excluding delay is, from Table 1: 1000 (22.3 + 10.8) percent = 331; (*d*) the delay factor for 331 cycles and 1.48 stress range ratio is equal to 1.12 and was obtained by linear interpolation between

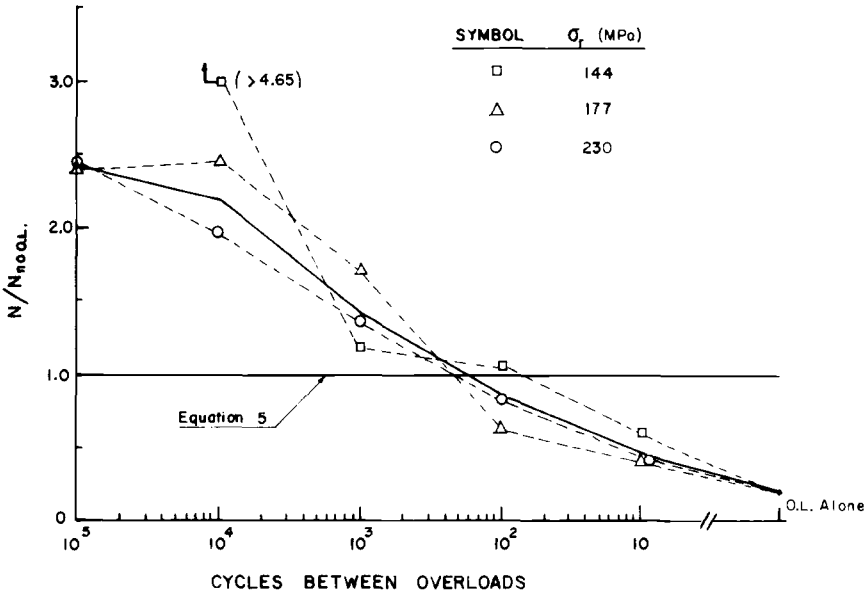

FIG. 14—*Effect of overload spacing on constant amplitude fatigue life.*

TABLE 3—*Fatigue life prediction for block size of 1000 cycles based on overload data.*

Cycle group no.	1	2 and 3	4 and 5	6 and 7	8, 9 and 10	Summation
Mean stress range $\sigma_r/\sigma_{r,\,max}$	0.925	0.625	0.800	0.575	...	
Stress range ratio	...	1.48	...	1.39	...	
Cycles excluding delay	17	331	78	465	109	$\Sigma = 1000$
Delay factor N/N_{noOL}	...	1.12	...	1.17	1.0	
Cycles including delay	17	371	78	544	109	$\Sigma = 1119$

NOTE—$N_{pred}/N_{RMC} = 1119/1000 \simeq 1.12$

the mean line (1.67) and the horizontal line (1.0) in Fig. 14; (*e*) the number of cycles at the low stress range level, including the delay, is then $331 \times 1.12 = 371$. Similar calculations give the number of cycles in the second high-low sequence. The last column in Table 3 shows the sum of the cycles in the block, both excluding and including the delay effect.

Next, it was assumed that the delay factor remains constant over the full life. The predicted life for specimens subjected to load blocks of 10^3 cycles is then

$$N_{pred} = (1119/1000)\, N_{RMC} = 1.12 \cdot N_{RMC} \tag{7}$$

where the life free of delay effects, N_{RMC}, is obtained by substituting the value of $\sigma_{r,\,RMC}$ for the given load block into Eq 5.

The calculations were repeated for all block sizes and the results plotted with a solid line in Fig. 11. Although the predicted values follow the trend of the data, they overestimate the observed delay. This discrepancy may be attributed to the fact that (*a*) multiple overloads can cause shorter delay effects than single overloads [*23*], (*b*) crack growth rates following a prior high load excursion were observed [*23*] to accelerate briefly before dropping as shown in Fig. 13, (*c*) delay factors could drop exponentially rather than in proportion to the overload ratio, and (*d*) multiple overloads could speed up crack initiation.

The preceding calculations also presume that the equivalent stress range concept gives an accurate estimate of variable amplitude fatigue life, N_{RMC}, when the block size is small. The specimens employed in this study had a long crack initiation life of about 40 percent of the total life [*1*], because the welds were of excellent quality. Consequently, the equivalent stress range concept no longer reduces to the fracture mechanics approach and N_{RMC} may not be an accurate estimate. In fact, Fig. 11 shows that for small block sizes the observed fatigue life approaches asymptotically a mean value of about 0.85 N_{RMC}. If the prediction had been normalized with respect to that value, the correlation at larger block sizes would have been excellent.

The concept of delay effects following a prior high load excursion are also useful for estimating the largest block size that still will ensure a random load simulation free of interaction. Rearranging the loading block shown in Fig. 7 for maximum interaction would have a high cycle group such as No. 1 followed by the four lowest, namely Nos. 2,3,6, and 7 which comprise 79.6 percent of the block size. The stress ranges are 0.925 $\sigma_{r,\,max}$ for No. 1 and an average of 0.6 $\sigma_{r,\,max}$ for the lower level. Delay effects are avoided if during the low stress cycling the crack front does not advance more than, say, 2 percent into the plastic zone created during the prior high load (see Fig. 13). Using Eq 3 and 6, this condition gives

$$\frac{\Delta a}{2r_Y} = \pi\, C\sigma_Y{}^2 \frac{\Delta K_{low}{}^n}{\Delta K_{high}{}^2} \Delta N_{low} \leq 0.02 \tag{8}$$

Assuming a plane strain corrected yield stress $\sigma_Y = \sqrt{3}\ \sigma_{ys}$, mean values of $C = 4.8 \times 10^{-12}$ and $n = 3$ for ferritic steels [*18*], and $\Delta K_{high} = 0.925/0.6\ \Delta K_{low}$, Eq 8 becomes

$$\frac{\Delta a}{2r_Y} = 3.36 \times 10^{-6}\ \Delta K_{low}\ \Delta N_{low} \leq 0.02 \tag{9}$$

Evidently, for the same number of low stress range cycles, ΔN_{low}, the crack front penetrates deeper into the high prior load plastic zone at larger values of ΔK_{low}, as the crack deepens; but most of the life is spent while ΔK is small. Recalling that ΔN_{low} is 79.6 percent of the block size, one

obtains from Eq 9 a maximum block size of 1500 cycles when $\Delta K_{low} = 5$ MPa$\sqrt{m}$ and 300 cycles when $\Delta K_{low} = 25$ MPa$\sqrt{m}$. Calculations of fatigue crack propagation showed that 99 percent of the life has elapsed by the time $\Delta K = 25$ MPa$\sqrt{m}$. Therefore, it is reasonable to choose a block size limit closer to the upper value, say 1200 cycles. Indeed, Fig. 11 shows that block sizes of 1000 cycles and less have no significant effect on fatigue life.

Conclusions

The following conclusions are based on the results of the experimental investigation.

1. When the number of cycles in the block was 1000 or less for all stress levels considered, the block size had no significant effect on the fatigue life. In this case, the root-mean-cube stress range provided a reasonable transfer function between block loading and constant amplitude cycling.

2. When the block size was larger than 1000 cycles, crack growth retardation in high-low stress range sequences increased significantly the number of cycles to failure.

3. When nondimensionalized with respect to N_{RMC}, the fatigue lives for all stress range levels considered correlated well with block size. The correlation with the number of blocks applied was poor.

4. Random loading can be simulated with loading blocks not exceeding 1000 cycles and which are subdivided into ten stress range groups. Under these conditions and given also that most of the stress range cycles were above the constant amplitude fatigue limit, the root-mean-cube stress range provided a reasonable transfer function between block loading and constant amplitude cycling.

References

[1] Albrecht, P., Abtahi, A., and Irwin, G. R., "Fatigue Strength of Overloaded Bridge Components," *Report No. FHWA-MD-R-76-7,* Department of Civil Engineering, University of Maryland, College Park, Md., Oct. 1975.

[2] Cudney, G. R., "The Effects of Loadings on Bridge Life," *Research Report No. R-638,* Michigan Department of State Highways, Sept. 1967.

[3] Douglas, T. R. and Karrh, J. B., "Fatigue Life of Bridges Under Repeated Highway Loading," *HPR Report No. 54,* Alabama Highway Research, April 1971.

[4] Heins, C. P. and Sartwell, A. D., "Tabulation of 24 Hours Dynamic Strain Data on Four Simple Span Girder-Slab Bridge Structures," *Progress Report No. 29,* Civil Engineering Department, University of Maryland, College Park, Md., June 1969.

[5] McKeel, W. T., Maddox, C. E., Kinnier, H. L. and Galambos, C. F., "A Loading History Study of Two Highway Bridges in Virginia," *Final Report No. 70-R48,* Virginia Highway Research Council, June 1971.

[6] Sartwell, D. C. and Heins, C. P., "Tabulation of Dynamic Strain Data on a Girder-Slab Bridge Structure During Seven Continuous Days," *Progress Report No. 31,* Civil Engineering Department, University of Maryland, College Park, Md., Sept. 1969.

[7] Sartwell, A. D. and Heins, C. P., "Tabulation of Dynamic Strain Data on a Three Span Continuous Bridge Structure," *Progress Report No. 33,* Civil Engineering Department, University of Maryland, College Park, Nov. 1969.

[8] Goodpasture, D. W., "Stress History of Highway Bridges," Department of Civil Engineering, University of Tennessee, Dec. 1972.

[9] Christiano, P. O. and Goodman L. E., "Bridge Stress Range History," *Highway Research Record No. 382,* 1972.

[10] Bowers, D. G., "Loading History Span No. 10 Yellow Mill Pond Bridge I-95, Bridgeport, Conn.," *Research Project HPR 175-332,* Connecticut, May 1972.

[11] Fisher, J. W., Yen, B. T., and Marchica, N. V., "Fatigue Damage in the Lehigh Canal Bridge," *Report No. 386.1,* Fritz Engineering Laboratory, Lehigh University, Bethlehem, Pa., Nov. 1974.

[12] Yamada, K. and Albrecht, P. A., "A Collection of Live Load Stress Histograms of U.S. Highway Bridges," *Civil Engineering Report,* University of Maryland, College Park, Md., 1975.

[13] Goble, C. G., Moses, F., and Pavia, A., "Field Measurements and Laboratory Testing of Bridge Components," *Report No. OHIO-DOT-08-74.* Case Western Reserve University, Cleveland, Ohio, Jan. 1974.

[14] Yamada, K., "Fatigue Behavior of Structural Components Subjected to Variable Amplitude Loading," Ph.D. Dissertation, University of Maryland, College Park, Md., 1975.

[15] Klippstein, K. H. and Schilling, C. G. in *Fatigue Crack Growth Under Spectrum Loads, ASTM STP 595,* American Society for Testing and Materials, 1976, pp. 203–216.

[16] Fisher, J. W., "Bridge Fatigue Guide, Design and Details," American Institute of Steel Construction, New York, N.Y., 1977.

[17] "Traffic Volume Data," Bureau of Traffic Engineering, Maryland State Highway Administration, Baltimore, Md., 1973.

[18] "Specification for the Design, Fabrication and Erection of Structural Steel for Buildings," American Institute of Steel Construction, New York, N.Y., 1969.

[19] "Standard Specifications for Highway Bridges," American Association of State Highway and Transportation Officials, Washington, D.C., 1977.

[20] Barsom, J. M., "Fatigue Crack Propagation in Steels of Various Yield Strength," presented at the 1st National Conference on Pressure Vessels and Piping, San Francisco, Calif., May 1971.

[21] Yamada, K. and Albrecht, P., "Fatigue Design of Welded Bridge Details for Service Stresses," *TRR No. 607,* Transportation Research Board, National Academy of Sciences, Washington, D.C., 1976, pp. 25–30.

[22] Von Euw, E. F. G., "Effect of Overload Cycle(s) on Subsequent Crack Propagation in 2024-T3 Aluminum Alloy," Ph.D. Dissertation, Lehigh University, Bethlehem, Pa., 1971.

[23] Gardner, F. H. and Stephens, R. I., "Subcritical Crack Growth Under Single and Multiple Periodic Overloads in Cold-Rolled Steel," 7th National Symposium on Fracture Mechanics, University of Maryland, College Park, Md., Aug. 1973.

Summary

Summary

The assurance of a minimum level of durability is the paramount goal of the designer, builder, and user of a given structure. In order to assure that durability economically, considerable interdependence is necessary between the people who define the "loads environment" the structure will operate within and those who design the structure to withstand that usage durably. In the development of a compendium of terms and definitions associated with fatigue load spectra, it was demonstrated graphically that several of the key terms used in describing load histories had different definitions in the structural durability community than in the service loads monitoring community. The Symposium on Service Fatigue Loads: Monitoring, Analysis, and Simulation was developed to foster a dialog between these two communities to help in the assurance of structural durability.

This special technical publication presents an excellent state of the art of the service fatigue loads technology. This technology encompasses a number of processes for measuring, recording, and characterizing the "loads environment" of a structure and relating it to durability. The loads environment can be defined as a measure of continuing load, stress, strain, displacement, etc. history that a structure experiences during its operation. Although some parameter other than "load" (such as displacement) is often of interest, the term service loads is used to describe the process generically.

The papers in this publication are divided into two sections: (1) Service Loads Monitoring and Analysis and (2) Service Spectrum Generation and Simulation. The reader will notice that there is considerable overlap in any one of these areas of interest but this is to be expected in this sort of interrelated technology.

The technology of service loads monitoring and analysis covers the processes of gathering the data concerning the structures' load environment and characterizing its content. The type of structure, loads environment, and reason for gathering the data help in defining the number of load parameters to be monitored and the required accuracy and frequency of the measurement.

The paper by Buxbaum presents an evaluation of methods used to characterize load histories. In the paper, he concludes that much data important to service load characterization can be lost by simple counting methods. He describes problems associated with many of the currently

used methods and effectively builds a case for characterization of service loads by time and frequency domain analyses.

Clay et al present an excellent state of the art in monitoring procedures with special emphasis on the types of recording equipment used. The paper also indicates the cost and data requirements for typical aircraft loads monitoring systems.

Berens' paper provides an excellent background on the type and amount of data to record to ensure the proper characterization of the load environment. The amount of data that must be monitored to characterize the service loads is controlled by the structural application and the degree of variation in the potential loads environment over its service life.

de Jonge and Spiekhout describe the complete process of service loads data collection and analysis using a simple magnetic recorder on a commercial aircraft. They present the data obtained in terms of usage variation with aircraft type, route flown, and season of the year.

The paper by Stone et al presents an example of a monitoring system for a large complex aircraft structure. The paper indicates the scale of the recording program and those purposes besides durability analysis for which the data are required. In this program, data from over 50 transducers are monitored and recorded at data rates ranging from once to twenty times per second. The data proved valuable in defining the actual loads environment of the structure and was responsible for changes in criteria and analysis methodology.

Morcock provides an overview of a service life monitoring program for a large aircraft structure. This paper shows many similarities as well as differences with the service loads recording program described by Stone et al. Among the differences are the number of channels of data monitored and the purposes for which the data are obtained.

Ashbaugh and Grandt present detailed information concerning a metal gage that can be mounted on a structure to give an advanced indication of the crack growth potential of a structure. This crack growth gage can provide a direct measure of the crack growth behavior potential of the structure to which it is attached since they both experience an identical load environment. If a proper transfer function can be determined, the crack growth in a structure can be monitored based on the behavior of the crack growth gage.

The service loads spectrum generation and simulation technology encompasses those approaches that are used to create a service loads usage from an actual or projected loads environment and simulate that history in the laboratory. One must often simulate the load intensity environment at structural locations remote from the point of application of load in order to evaluate the structures durability. For small, simple load path structures the process of spectrum generation involves a direct application of data

obtained in the monitoring phase. For larger structures with multiple independent paths for load application, the technology of spectrum generation becomes more complicated.

The paper by Marchica et al describes the creation of a usage spectrum for simulation testing of a scale model structure. In this case, the model is bigger than most structures tested, being 26 m long, scaled down from an aluminum ship. The paper discusses the full spectrum of data acquisition requirements, data analysis, and the development of an accelerated load history to apply in durability testing of the structural model.

Sandlin describes the development of stress spectra for different locations on a fighter aircraft wing, tail, and fuselage. Complicated transfer functions are derived, and the load spectrum at a given location is given as a summation of the inputs from several sources.

Denyer demonstrates the development of flight-by-flight load spectra from a flight segment approach. In this approach the load history is determined by summing the expected load histories from each of several logical segments of a flight; following "takeoff" of an aircraft, there is an "ascent" segment through an atmosphere containing a typically decreasing gust environment. The structure then performs a "cruise" segment of level flight through an atmosphere with little gust load input. The assembly of a load history is accomplished by adding many segments, each with their own load severity and conditions. Complicated load transfer function are utilized as in Sandlin's paper to obtain the load environment at a specific structural location.

Wilson and Garrett describe procedures for structural stress spectra prediction based around data from load sources in the structure. These included wing stresses, lateral and vertical acceleration, control surface motions and landing gear loads as well as gross weight, Mach number, and altitude. These additional data allow a better characterization of the stress environment of the actual structure under projected usage.

Kaplan et al describe a procedure for the development of flight-by-flight stress histories in fighter aircraft. They use random load simulation with randomized mission sequences to create a load history for durability analysis or test. The procedure incorporated a complicated mission segment analysis that considered vehicle velocity, altitude, weight, and load factor.

Weiss measured the service stress environment of an overhead traveling bridge crane beam. From these data, a simulation using beta distributed loads was created. The simulation then was used to evaluate the fatigue life of existing structures and develop design codes for cranes.

Gassner and Lipp present data on long duration random fatigue tests with comparison to accelerated testing. Their conclusions are that results from accelerated testing can be misleading due to a reduction in environ-

mental corrosion and load history effects. They also report that the simple eight-step block program loading gives a very high overestimation of fatigue life.

Jeans and Trimble developed service loads histories based on the use of power spectral density (PSD) concepts. They then tested graphite-epoxy composite coupon specimens to these load histories, noting the failure behavior with variations in the PSD shape. He concluded that PSD shape is of significance to the structural lifetime of these composite coupons.

Yamada and Albrecht present service load data from 29 bridges in eight states. They created blocked load histories based on this data and reported the results of an experimental verification test of a welded bridge structural element.

P. R. Abelkis

Douglas Aircraft Co. Long Beach, Calif. 90846. Symposium cochairman and co-editor.

J. M. Potter

AFFDL/FBE, Wright-Patterson Air Force Base, Ohio 45433; Symposium cochairman and coeditor.

Index

A

Aircraft Integrated Data System (AIDS), 50
Aircraft loads, 21
Aircraft Structural Integrity Program (ASIP), 68, 86, 145
Aircraft Structural Integrity Management Information System (ASIMIS), 89
Aluminum, 222
Atmospheric turbulence, 48
Automobiles, 224
A-7D, 145

B

Bridges, 255
Block size, 270
B-1, 161
B-747, 49

C

Composite materials, 240
Costs, 33
Counting methods, 9, 12
Crack growth, 90, 97, 213, 266
Crack growth gage, 94
Crane beam, 208
C-5, 67
C-141, 84

D

Damage index, 24
Data recording, 21, 67
Design limit load, 22

E

Economic life, 92
Elevator, 90

F

Fatigue damage, 36
Fatigue life prediction, 7, 233
Fighter aircraft, 144, 193, 240
Flap, 90
Flight-by-flight, 24, 53, 155, 158, 193, 240
Flight test, 21

G

GAG cycle, 207
Gusts, 57, 64, 80, 165, 176

I

Individual Aircraft Tracking (IAT), 24, 32, 144

L

Landing rollout, 81
Laser-interferometer, 101
Load factor spectrum, 62
Loads/Environmental Spectra Survey (L/ESS), 23, 32, 144
Load monitoring, 48

M

Maneuver, 81, 163, 197
Mechanical Strain Recorder (MSR), 25

Mission profile, 195
Monitoring systems, 27, 87

O

Operational loads, 22
Operational usage, 36
Ordering, 155, 205, 216

P

Power Spectral Density (PSD), 15, 240
Programmed Depot Maintenance (PDM), 23
Processing of data, 52, 178

R

Rain-flow counting method, 13
Random load analysis, 8
Range-pair counting method, 13
Rudder, 90
Regression analysis, 146

S

Sample size, 36, 40
Sequence, 155, 216
Service life, 67, 84
Service Loads Recording Program (SLRP), 70
Ship, 121
Spoiler, 90
Stationary process, 16
Statistics, 38, 56, 79, 222
Steel, 222, 255
Stochastic process, 16
Strain counter, 26
Strain monitoring, 26
Stratified sampling, 42
Stress-time history, 7
Stress spectrum, 130, 155

T

Take-off, 81
Taxi, 31
Terrain following, 165
Testing, 8, 121
Test spectrum, 121, 129, 172
Touch and go, 81

V

VGH recorder, 28

W

Wave heights, 133